



Micro- and macroencapsulation technologies for advanced β -cell replacement in Type 1 Diabetes Mellitus

Albert Espona Noguera
NanoBioCel Group, Laboratory of Pharmaceutics
University of the Basque Country UPV/EHU
Faculty of Pharmacy
Vitoria-Gasteiz 2019



NanoBioCel
Grupo de Micro y Nano Technologies,
Biomateriales y Células

AKNOWLEDGEMENTS

Tres años y medio. Este es el tiempo que ha pasado desde que llegué a Vitoria. Vine con una mano delante y otra detrás, sin conocer a nadie, sin haber pisado nunca el País Vasco, pero con muchas ganas e ilusión para empezar un nuevo proyecto académico y personal, la tesis doctoral. Muchos amigos de la carrera que estaban trabajando en su tesis me decían que lo pensara bien porque la investigación es un trabajo duro, sacrificado y que genera mucha frustración. Esta descripción no hacía más que motivarme, ya que para mí los retos más difíciles son los más satisfactorios cuando los consigues. De hecho, años atrás ya se me había planteado un reto con unas perspectivas similares, jugar en un equipo de alto rendimiento de balonmano. Durante esa etapa, el trabajo, el sacrificio y la frustración fueron muy presentes, los cuales me hicieron valorar mucho más los logros conseguidos. Una vez pasadas ambas experiencias, tanto en el balonmano como en la tesis doctoral, he detectado un engranaje de personajes comunes que han girado alrededor de mí como jugador e investigador, que fueron clave para ganar campeonatos y también han sido clave para llegar hasta este momento, el final de la tesis doctoral.

Para empezar, en el equipo de balonmano había una figura muy importante, el entrenador. Esta persona nos enseñaba este deporte, nos guiaba, nos daba toques de atención cuando los necesitábamos y en definitiva nos ayudaba a ser mejores jugadores. En este sentido, mis directores de la tesis Jose Luis y Laura habéis hecho de entrenadores dándome la confianza y las herramientas para que poco a poco yo fuera siendo mejor científico y pudiera ir consiguiendo los objetivos de la tesis. Por otro lado, no hay que olvidar la figura del segundo entrenador, una persona que se encuentra en un segundo plano, pero que también te guía para conseguir los objetivos. En este caso, Jesús has sido esta figura y tus consejos me han ayudado a madurar como persona y como científico. A los tres, ¡gracias!

Por otro lado, los compañeros de equipo fueron imprescindibles para poder ganar partidos, pero sobretodo, para que yo pudiera crecer como jugador. Día a día, en cada entrenamiento nos ayudábamos entre todos para potenciar nuestros puntos débiles y perfeccionar los puntos fuertes, y de esta manera poder progresar. Aquí entran en juego todos y cada uno de compañeros del laboratorio, que en menor o mayor medida han contribuido en que yo pudiera ir avanzando a lo largo de estos años de tesis. Pero entre todos los compañeros de balonmano, había unos pocos con los que tenía mayor complicidad, y que en el terreno de juego, con un solo gesto o mirada ya sabíamos lo que iba a hacer el otro para hacer una jugada. Haritz, Alberto y Bea habéis sido este tipo de compañeros; trabajar codo con codo con vosotros durante esta etapa ha sido un placer. ¡Gracias!

Para acabar, en los partidos había otro factor muy importante, la afición. Esa gente

que venía a ver los partidos para animarme, aunque no le gustara el balonmano o incluso sin saber de qué iba este deporte. De la misma manera, durante estos años también he tenido una “afición” que me ha ido siguiendo y apoyando. Als meus pares i a la tieta Victòria pel suport incondicional en totes les decisions i projectes de la meva vida. A la Glòria per aguantar-me i estar al meu costat malgrat la distancia. A Miguel y Paula por acogerme desde el primer minuto cuando llegué a Vitoria y a Gorka por toda la tontería que llevamos en casa que hace olvidar cualquier mal día. Por todo esto, gràcies! ¡gracias! eta eskerrik asko!

Albert Espona Noguera

ACKNOWLEDGMENT FOR THE FINANCIAL SUPPORT

This thesis has been partially supported by the Basque Government (Consolidated Groups, IT-407-07) and the University of the Basque Country UPV/EHU. The intellectual and technical assistance from the ICTS “NANBIOSIS”, more specifically, by the Drug Formulation Unit (U10) of the CIBER in Bioengineering, Biomaterials & Nanomedicine (CIBER-BBN) at the University of the Basque Country UPV/EHU is acknowledged. Albert Espona Noguera gratefully acknowledges the funding and support provided by the DRIVE project consortium.

ACKNOWLEDGMENT TO THE EDITORIALS

Authors would like to thank the editorials for granting permission to reuse their previously published articles in this thesis.

A. Espona-Noguera et al. *International Journal of Biological Macromolecules*. 107 (2018) 1261 - 1269. DOI: 10.1016/j.ijbiomac.2017.09.103

A. Espona-Noguera et al. *International Journal of Pharmaceutics*. 2019; 560:65-77. DOI: 10.1016/j.ijpharm.2019.01.058

A. Espona-Noguera et al. *International Journal of Pharmaceutics*. 2019; S0378-5173(19)30453-3. DOI: 10.1016/j.ijpharm.2019.06.009

A. Espona-Noguera et al. “Immobilization of Enzymes and Cells: Methods and Protocols” Series: *Methods in Molecular Biology* of Springer Nature.

ACKNOWLEDGMENT TO RESEARCH GROUPS

Authors would like to thank the Group of Applied Mechanics and Bioengineering (AMB) of the Aragón Institute of Engineering Research (I3A) at the University of Zaragoza, the MICROFLUIDICS Cluster of the University of the Basque Country UPV/EHU and the Instituto de Microelectrónica de Barcelona (IMB-CNM,CSIC) for their contribution to this work. Authors also acknowledge the CRCINA/University of Nantes, Grup 9: Apoptosis and Tumor Progression research group for the intellectual and technical support to Albert Espona Noguera during his stay in their lab.

GLOSSARY

A: Alginate

AFM: Atomic Force Microscopy

APA: Alginate-Poly-L-lysine-Alginate

BSA: Bovine Serum Albumin

CaCl₂: Calcium chloride

CAM: Chicken chorioallantoic membrane

CaO₂: Calcium peroxide

CaSO₄·2H₂O: Calcium sulphate dihydrate

CCK-8: Cell Counting Kit-8

DM: Diabetes Mellitus

DMEM: Dulbecco's Modified Eagle's Medium

DPBS: Dulbecco's Phosphate Buffered Saline

D1: Device 1

D2: Device 2

D1-MSCs: D1 mouse mesenchymal stem cells

D1-MSCs-GFP: D1-MSCs to express the green fluorescence protein (GFP)

ECM: Extracellular matrix

EMEM: Eagle's Minimum Essential Medium

EPCs: Endothelial Progenitor Cells

Es: Young's modulus

FBS: Fetal Bovine Serum

FCS: Fetal Calf Serum

FDM: Fused Deposition Modelling

G: Gularonic acid

G[?]: Elastic modulus

G^{''}: Viscous modulus

GLP: Good Laboratory Practice

GSA: Glucose Signal Amplifying enzymes

GSIS: Glucose-Stimulated Insulin Secretion assay

GTT: Glucose Tolerance Test

Ha: Aggregated modulus

hPSC: Human Pluripotent Stem Cells

IEQ: Islet equivalent

KCl: Potassium chloride

KRB: Krebs-Ringer Bicarbonate buffer
LDH: Lactate dehydrogenase
M: Manuroric acid
MgCl₂: Magnesium chloride
MRI: Magnetic Resonance Imaging
MTT: 3-(4,5-dimethylthiazol-2-yl)-2,5-diphenyltetrazoliumbromid
MW: Molecular Weight
NaCl: Sodium chloride
Na₂HPO₄·2H₂O: Di-sodium hydrogen phosphate dyhydrate
NPs: Nanoparticles
NVP: N-vinylpyrrolidone
OH: Hydroxyl group
PA: Polyamide
PBS: Phosphate Buffered Saline
PCL: Poly(ε-caprolactona)
PEG: Polyethylene glycol
PEI: Poly(ethyleneimine)
PEO: Polyethylene oxide
PET: Polyethylene terephthalate
Phil-D1: Hydrophilic device 1
Phil-D2: Hydrophilic device 2
Phob-D1: Hydrophobic device 1
Phob-D2: Hydrophobic device 2
PLA: Polylactic acid
PLL: Poly-L-Lysine hydrobromide
PLO: Poly-L-Ornithine
PPCs: Pancreatic Progenitor Cells
P/S/G: Penicillin/Streptomycin/Glutamine
RGD: Arginine–glycine–aspartate
RPMI: Roswell Park Memorial Institute
SEM: Scanning Electron Microscopy
SLS: Selective Laser Sintering
SPIONs: Superparamagnetic Iron Oxide Nanoparticles
SR: Swelling ratio
STZ: Streptozotocin
T1DM: Type I Diabetes Mellitus

TEA: Triethanolamine

TMV: Tobacco Mosaic Virus

TNF: Tumor Necrosis Factor

VEGF: Vascular Endothelial Growth Factor

Wc: Water content

Wd: Dried weight

Ws: Wet weight

W/V: Weight/Volume

3D: Three dimensional

μ -CT: Micro-computed tomography

θ_w : Contact angle

Index

Chapter 1: Introduction

Advanced-hydrogel based cell encapsulation systems for insulin delivery in Type 1 Diabetes Mellitus.....3

Chapter 2: Objectives.....45

Chapter 3:

Type 1 Diabetes Mellitus reversal via implantation of magnetically purified microencapsulated pseudoislets.....51

Chapter 4:

Tunable injectable alginate-based hydrogel for cell therapy in Type 1 Diabetes Mellitus....83

Chapter 5:

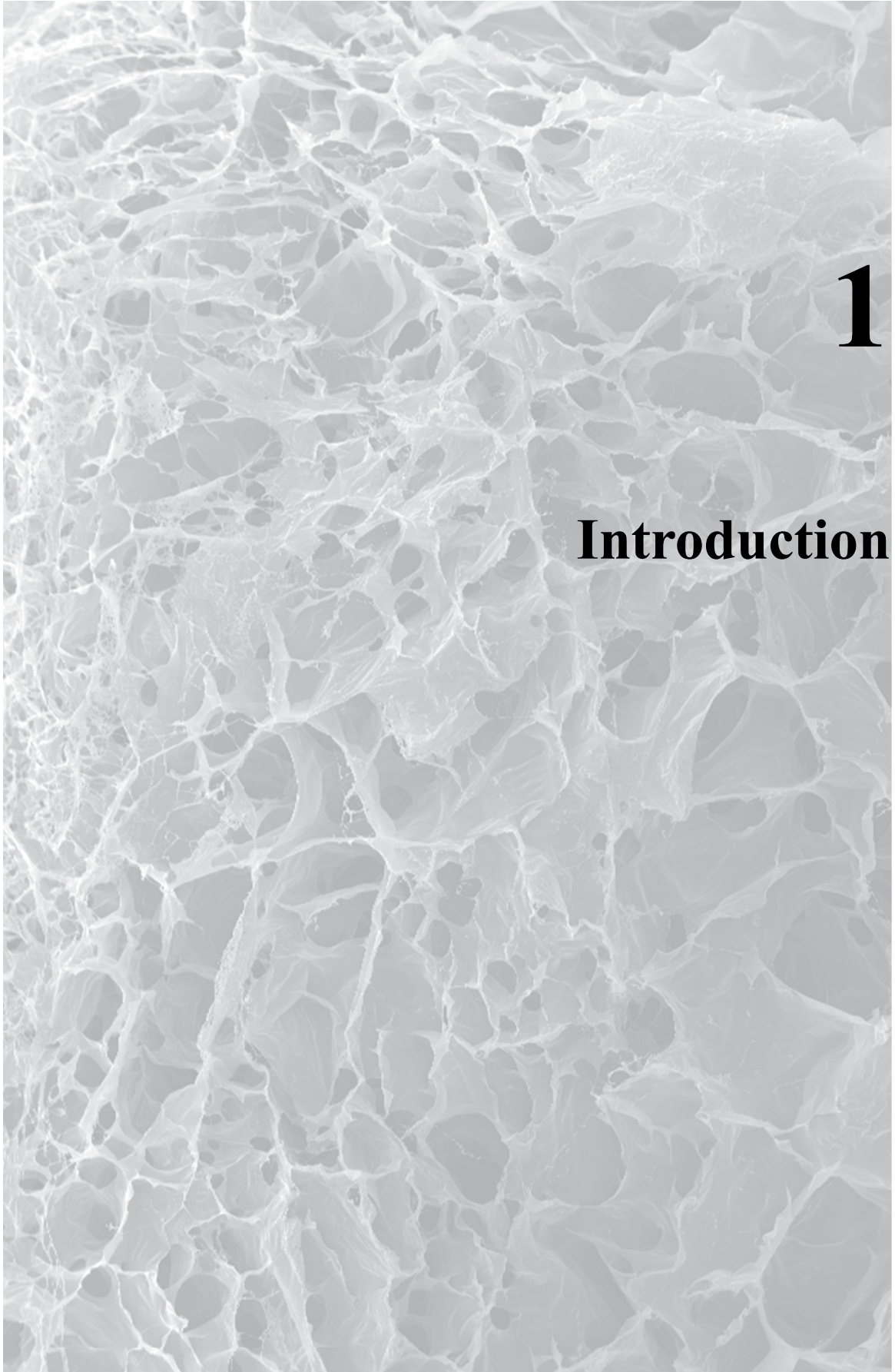
3D printed polyamide macroencapsulation devices combined with alginate hydrogels for insulin-producing cell-based therapies.....105

Chapter 6: Discussion.....133

Chapter 7: Conclusions.....161

Annex I:

Immobilization of INS1E insulin-producing cells within injectable alginate hydrogels....165



1

Introduction

Advanced hydrogel-based cell encapsulation systems for insulin delivery in Type 1 Diabetes Mellitus

A. Espona-Noguera^{1,2}, J. Ciriza^{1,2}, A. Cañibano-Hernández^{1,2}, G. Orive^{1,2,3,4}, Rosa M. Hernández^{1,2}, L. Saenz del Burgo^{1,2*}, J.L. Pedraz^{1,2*}

¹NanoBioCel Group, Laboratory of Pharmaceutics, School of Pharmacy, University of the Basque Country UP/EHU, Paseo de la Universidad 7, 01006, Vitoria-Gasteiz, Spain.

²Biomedical Research Networking Center in Bioengineering, Biomaterials and Nanomedicine (CIBER-BBN), Vitoria-Gasteiz, Spain.

³University Institute for Regenerative Medicine and Oral Implantology - UIRMI (UPV/EHU-Fundación Eduardo Anitua), Vitoria, Spain.

⁴Singapore Eye Research Institute, The Academia, 20 College Road, Discovery Tower, Singapore.

NanoBioCel Group, Laboratory of Pharmacy and Pharmaceutical Technology, Faculty of Pharmacy, University of the Basque Country UPV/EHU, Vitoria-Gasteiz, Spain

* Corresponding authors

ABSTRACT

Type 1 Diabetes Mellitus (T1DM) is an autoimmune disease resulting from the destruction of insulin-producing β -cells in the pancreatic islets. In this regard, whole pancreas and isolated pancreatic islets aim for the replacement of the damaged β -cells in Type 1 diabetic patients. However, pancreatic islets transplantation appears to be the most suitable strategy for blood glucose homeostasis restoration, since this approach avoids complications associated with daily insulin administrations and reduce the surgical risks involved in whole pancreas transplantation. Unfortunately, this procedure still has limitations for its widespread clinical application. The most relevant drawbacks include the lack of cadaveric donor pancreas, the loss of a large percentage of islets after transplantation and the need of long-term immunosuppressive treatments. To overcome the aforementioned issues, islets can be encapsulated within hydrogel-like biomaterials, thereby allowing a localized implantation and diminishing the loss of islets, while permitting a physical separation from the host immune system by a permselective membrane resulting in a reduction or elimination of immunosuppression regimes and enabling the use of other insulin-producing cells sources. This review aims to provide an update on the different islet and β -cells hydrogel-based encapsulation strategies, highlighting the advantages and drawbacks for a successful clinical application.

Keywords: Type 1 Diabetes Mellitus, hydrogels, nanoencapsulation, microencapsulation, macroencapsulation, bioprinting

INTRODUCTION

Diabetes mellitus (DM) is currently affecting almost 422 million people worldwide and the global incidence rate is predicted to increase to 552 million by 2030, thereby its increasing prevalence throughout the world has led to the consideration of DM as an epidemic of the 21st century [1]. Type 1 Diabetes Mellitus (T1DM) contributes to 10 % of the total cases of DM worldwide mostly in young people and, it is seen as an increasing health hazard [2]. T1DM is characterized by an autoimmune destruction of pancreatic islets, resulting in severe insulin deficiency and, subsequent elevation of blood glucose levels. The high blood glucose levels (hyperglycemia) lead to devastating microvascular and macrovascular complications in diabetic patients, including cardiovascular disease, retinopathy, nephropathy and neuropathy [3, 4].

Currently, exogenous insulin therapy is the primary treatment in Type 1 diabetic patients. Managing T1DM requires significant patient compliance with multiple daily blood glucose measurements and, subcutaneous exogenous insulin administrations for the rest of their lives [5]. However, this treatment does not mimic the real-time secretory pattern of pancreatic β -cells, and therefore, it is difficult to maintain a stringent control of blood glucose levels [6]. In consequence, any carelessness can result in episodes of hyperglycemia, but also it is often associated with an increased risk of acute low blood glucose levels episodes (hypoglycemia) [7]. These episodes can lead to cognitive impairment, seizures, coma and even death. Additionally, the quality of life is lower even for patients with well-regulated blood glucose [7, 8].

Alternatively, there are other approaches based on the replacement of the damaged β -cells in T1DM patients. The first approach, that was developed and successfully applied in the clinics, was the whole organ pancreas transplant [9]. This treatment aims to reestablish normoglycemia by the replenishment of the depleted pancreatic islets reserve, thus avoiding issues related with daily exogenous insulin injections [10]. The first clinical pancreas transplant was performed at the University of Minnesota in 1966 [11]. Initial results showed immediate blood-glucose levels restoration, but the procedure displayed very poor graft survival rates; as less than 8 % of transplanted pancreas survived after six months. Nowadays, according to the International Pancreas Transplant Registry, with the advances made in surgical technique, immunosuppression treatments, and post-transplant monitoring, approximately the 80 % of transplanted patients achieve a three years survival rate, defined as insulin independence [9]. However, although whole pancreas transplantation offers the above advantages, it still comes with many drawbacks such as the scarcity of pancreas donors, the need of long-term immunosuppressive therapy and the increased risk of surgical complications such as graft

thrombosis, peritonitis, graft pancreatitis, among others [12]. The high risk of morbidity caused by the surgical complications and the strong immunosuppressive regimen, hard look at alternative methods of β -cell replacement.

Interestingly, the pancreatic islets mass represents only the 2 % of the whole pancreas, and therefore, pancreatic islets transplantation appears to be a promising alternative for blood glucose levels restoration in Type 1 diabetic patients, as it avoids complications associated with daily insulin administrations and reduce the surgical risks associated with whole pancreas transplantation [13]. The first successful results of islets transplantation were described in 2000, when a research group at University of Alberta (Edmonton, Canada) achieved insulin independence for an average of 1 year in seven patients with T1DM, that were transplanted with 800.000 allogeneic pancreatic islets into the hepatic portal vein under a steroid-free immunosuppressive treatment [14]. This procedure is universally known as the “Edmonton protocol” and, it represented a turning point in the field, provoking a significant increase in islet transplantation research [15]. Currently, after advances in the islet isolation techniques and in the immunosuppressive treatments, pancreatic islets transplantation represents the best option for T1DM cure, improving the metabolic glucose control and the quality of life in T1DM patients without side effects [14, 15]. However, although the short-term survival of the grafts is up to 80 %, less than 20 % of the grafted patients remain insulin-independent after 5 years, because pancreatic islet transplantation based on the Edmonton protocol still possesses limitations that hamper the widespread clinical application [16]. The most relevant obstacles include the scarcity of cadaveric donor pancreas, the low islet extraction yield from whole pancreas and, the loss of a large percentage of the transplanted islets (> 60 %) after the intraportal islet infusion [17, 18]. Besides, the survival of the transplanted islets is jeopardized due to the poor vascularization at the implantation site that supposes low nutrients supply and hypoxia during the first period after transplantation, thus leading to a potential graft failure [13, 14]. Therefore, until these deficiencies are not overcome, islet transplantation will remain as a treatment available only for carefully selected cases of severe T1DM.

In this regard, recent approaches seek to mitigate these issues by means of cell encapsulation techniques [19]. This technology aims to encapsulate therapeutic cells, such as pancreatic islets, within biocompatible materials, with the objective of providing a support structure to the islets that replicates the native islet micro- and macro-environment and offers immunoisolation once implanted [16, 19]. Therefore, encapsulation of pancreatic islets prior to transplantation could potentially address some of these problems, overcoming the shortage of human donors since it may allow for xenografting and transplanting other insulin producing cell phenotypes, providing a delimited structured scaffold that prevents the islets

loss after implantation and eliminating the need for long-term immunosuppression [16, 19]. Among all the different types of biocompatible materials, biomaterials with the ability to form hydrogels have received significant attention for pancreatic islet encapsulation [20].

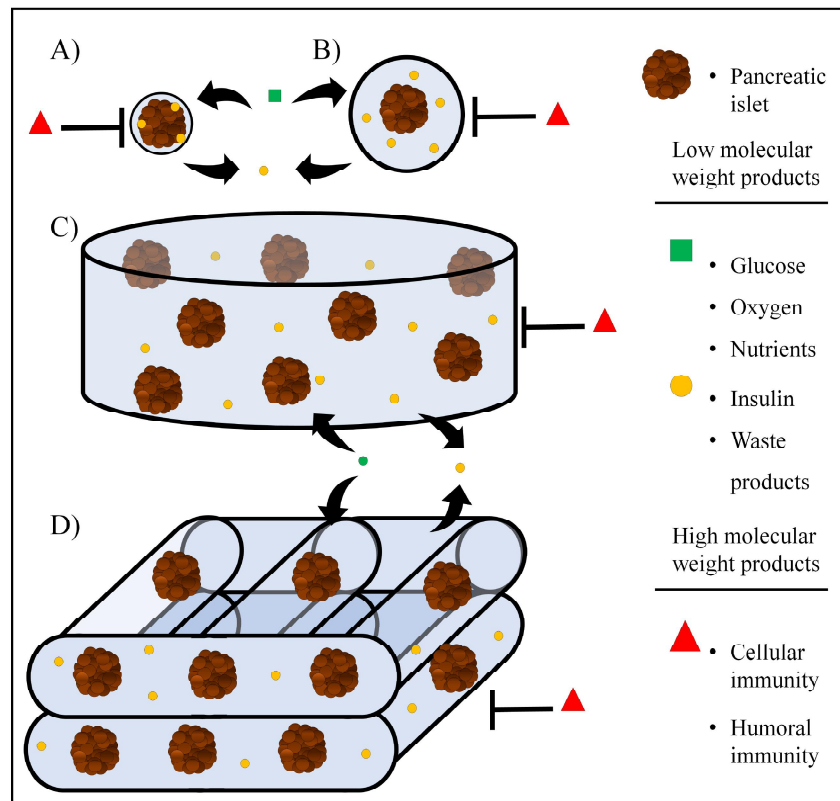


Figure 1. Current hydrogel-based approaches for pancreatic islet encapsulation. A) Nanoencapsulation, B) microencapsulation, C) macroencapsulation, and D) 3D bioprinting.

Hydrogels have been defined as two or multicomponent systems consisting of a three-dimensional (3D) network of polymer chains and water that fills the space between macromolecules [21]. Hydrogel-like biomaterials have demonstrated to be good candidates for pancreatic islet encapsulation because of their high-water content, good biocompatibility, structural and mechanical similarities with the native pancreatic extracellular matrix (ECM) and their permselectivity to low and high molecular weight components, which provides protection against immune cells and high molecular weight cytotoxic molecules, while allows the active diffusion of oxygen, nutrients and hormones such as insulin [22]. As a consequence of better understanding the physiological requirements for encapsulation of pancreatic islets and other insulin producing cell phenotypes, new approaches and strategies are constantly developed into the field, that can be classified into four categories: a) nanoencapsulation, by placing thin hydrogel films around individual islets (Figure 1A), b) microencapsulation of individual islets, small groups of islets or other insulin-producing cells within spherically

shaped hydrogel microcapsules (Figure 1B), c) macroencapsulation of islets or other insulin-producing cells within bulk hydrogels that can be shaped and molded within encapsulating devices (Figure 1C) and d) 3D bioprinted hydrogel-like scaffolds with embedded islets or other insulin-producing cells (Figure 1D) [22-25].

In this regard, this review aims to provide an update on the pancreatic islet encapsulation within the different aforementioned hydrogel-based approaches for T1DM treatment. Analyzing several variables that still need to be optimized prior to their large-scale clinical application. Our basic contention in this article will be the currently available islet and β -cells encapsulation strategies, highlighting the advantages and drawbacks for a successful clinical application.

NANOENCAPSULATION

Nanoencapsulation is a technique where hydrogel films are applied to the surface of a pancreatic islet or other cell aggregate by interfacial polymerization [26]. The final cross-linked hydrogel film results in a nanometric conformal coating placed around the surface of each individual islet or cell aggregate [27]. Thereby, graft survival is improved since islets are protected against the host's immune system and the reduced nanocapsules size decreases the diffusion distance for the oxygen and nutrients to reach the islet core from the nanocapsules surface [28]. This type of islet encapsulation can be achieved using conformal coatings.

Conformal coating

The most common hydrogel-based technique for conformal coating of islet is carried out by light-mediated interfacial polymerization of acrylate-based macromers, being the acrylated polyethylene glycol (PEG) the most used biomaterial [29]. The islet nanoencapsulation technology using acrylated PEG was invented by *Jeff Hubbell* at the University of Texas, and patented by Neocrin Inc. that posteriorly was transferred to Novocell Inc.[30]. Briefly, for the islets nanoencapsulation, the photoinitiator eosin Y is incubated with islets, resulting in islet-bonded eosin Y on their surfaces. Next, a mixture of acrylated PEG and n-vinylpyrrolidone (NVP) monomers are mixed with the polymerizing accelerant triethanolamine (TEA) and added to the islets, and finally, islets are exposed to UV light thus cross-linking the acrylates and NVP to form a hydrogel film binding to the eosin Y at the islet surface (Figure 2A) [31]. The cross-linking propagates outward from the surface to a controllable distance producing an interfacially cross-linked hydrogel conformally around each islet [31].

***In vivo* approaches**

The first *in vivo* study with nanoencapsulated islets was carried out by Neocrin Inc., where they explored the feasibility of islet xenotransplantation of PEG nanoencapsulated porcine islets in diabetic rat models [32]. Results showed that 5000-8000 nanoencapsulated porcine islets decreased blood glucose levels within the normoglycemic range (< 200mg/dL) when implanted into diabetic rats. However, animals returned to hyperglycemia 60-70 days after implantation [32]. When these studies were attempted to be translated to non-human primates, nanoencapsulated islets did not succeed in restoring normoglycemia [33]. The islet viability was compromised due to the cytotoxic effects of the co-initiator TEA exposure, required in the polymerization [34], and importantly, due to the aggressive immune reaction from animals to the PEG coatings and the xenotransplanted islets that were incompletely coated leaving them partially exposed [35].

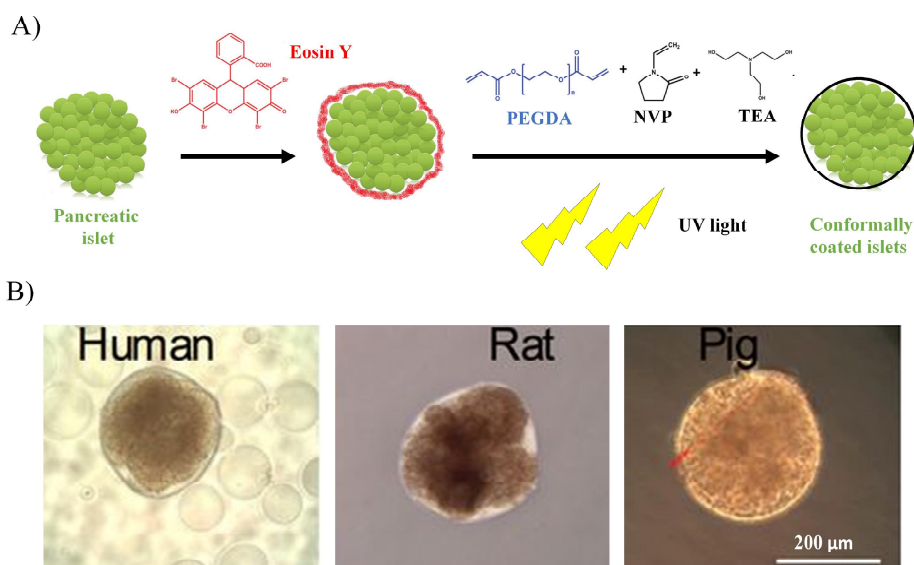


Figure 2. A) Schematic of pancreatic islet nanoencapsulation with polyethylene glycol diacrylate (PEGDA), eosin Y, triethanolamine (TEA), N-vinylpyrrolidone (NVP) by UV light-mediated interfacial photopolymerization. B) Bright-field images of conformally coated human, rat, and pig islets. Scale bar: 200 μm . Adapted from [42].

For these reasons, the islet nanoencapsulation technology was improved to obtain completely coated encapsulated islets with better biocompatibility and higher immunoprotection. In this regard, the company Novocell, Inc. with the attempt to improve the PEG-coating formulations, modified the PEG component to enhance binding to photo-initiators and to accelerate the cross-linking reaction in order to be less immunoreactive in large animals and achieve more uniform and full coatings. The company carried out a pre-clinical non-human primate study by implanting nanoencapsulated allogeneic islets into the

subcutaneous tissue of the abdomen in five diabetic baboons. Results demonstrated allograft function with complete insulin independence up to 20 months in three of the implanted recipients. The other two implanted animals in this group of 5 had partial function and did not achieved insulin independence [30].

Clinical trials

Encouraged by the successful results in non-human primates, Novocell launched a phase I/II clinical trial in USA with human patients with T1DM. The study was approved by the FDA for 12 patients, but only 2 patients of 25-30 years were approved by Novocell following the inclusion and exclusion criteria to start the study [36]. The implant procedure involved nanoencapsulated allogeneic islets injected in subcutaneous sites of the abdomen and the back, without the use of long-term immunosuppression. Although the recipients did not show evidence of allograft immune rejection and experienced a decrease in the number of hyperglycemic (> 300 mg/dl) and hypoglycemic (< 70 mg/dL) episodes, none of the patients achieved insulin independence during the first 6 and 4 months post-implantation [30]. For this reason, no more patients were implanted with nanoencapsulated islets and the clinical trial was terminated (Table 1).

Advantages and limitations of nanoencapsulation

In clinical pancreatic islets transplantation programs, the Edmonton protocol is the most standardized approach, where islets are infused into the liver through the hepatic intraportal vein, which is the clinically preferred site for islet transplantation [14]. Despite encouraging early results of islet transplantation through the Edmonton protocol, capsules of higher diameter than the islets themselves and large graft volumes may plug narrower blood vessels potentially resulting in severe thrombosis of the liver [37-39]. In this sense, nanoencapsulation provides a very reduced nanocapsule diameter by an ultrathin hydrogel film, and besides, allows to minimize the graft volume, thereby enabling a successful transplantation through the portal veins following the Edmonton procedure without clogging the portal veins [40]. Another point to take into account is that pancreatic islets are highly variable in size [41]. Nanoencapsulation technology allows the standardization of the capsule thickness on each islet independently of its size, as the capsule conforms to the shape and size of the islets, resulting in nanocapsules uniform in thickness (Figure 2B) [42]. Moreover, the reduced capsule thickness has a direct impact on its diffusion properties because of the very short diffusion distance between the islet core and the capsule surface. Therefore, it facilitates that oxygen and nutrients reach the islet core, as well as a robust response to

Table 1. Overview of clinical trials based on transplantation of encapsulated islets.

Investigator or company	Type of encapsulation	Hydrogel-like biomaterial	Islet source	Implantation site	Dose	Immunosuppression	Country
Novocell, In. (Viacyte, Inc.)	Nanoencapsulation	PEG	Allogeneic	Subcutaneous	Undetermined	No	USA
<i>Soon-Shiong et al.</i>	Microencapsulation	Alginate-Poly-L-Lysine	Allogeneic	Peritoneum	104000 islets equivalents/patient	Yes	USA
<i>Calafiore et al.</i>	Microencapsulation	Alginate-Poly-L-Ornithine	Allogeneic	Peritoneum	400000-600000 islets equivalents/patient	No	Italy
<i>Tuch et al.</i>	Microencapsulation	Barium cross-linked alginate	Allogeneic	Peritoneum	178000 islets equivalents/ patient	No	Australia
Living Cell Technologies (LCT)	Microencapsulation	Alginate-Poly-L-Ornithine	Xenogeneic-porcine insulin-producing cells	Peritoneum	5000-10000 islets equivalents/kg body weight	No	Australia
<i>Dufrane et al.</i>	Macroencapsulation-Monolayer Cellular Device	Collagen/Alginate	Allogeneic	Subcutaneous space	Undetermined	Undetermined	Belgium
Beta-O2 Technologies	Macroencapsulation- β -Air device	Alginate	Allogeneic	Peritoneum	2100 islets equivalents/kg body weight	No	Germany
<i>Alejandro Rodolfo et al.</i>	Macroencapsulation-BioHub	Thrombin/patient's own plasma	Allogeneic	Omentum	600000 islets equivalents/patient	Yes	USA

physiological stimulation, leading to great glucose sensitivity and a rate of insulin release in response to glucose [43]. Although nanoencapsulation offers many advantages in the field of islet transplantation in comparison with the other encapsulation strategies, this approach has some limitations that difficult its clinical application.

The main issue that shows the nanoencapsulation technology is that islets sometimes are not completely coated leaving them exposed, which can trigger the host's immune system leading to graft failure [35]. Although huge advances have been achieved in the nanoencapsulation procedure to fully coat pancreatic islets, some compounds used for the interfacial hydrogel-film cross-linking such as TEA, as well as the UV light used in the cross-linking still have a cytotoxic effect on islets viability [34]. Moreover, PEG may infiltrate and interact with the islets, causing necrosis [44]. Therefore, further investigation is required in developing less immunoreactive formulations that will not jeopardize the islet survival and that could facilitate the reconstruction of the microenvironment (e.g. provide extracellular matrix support), as well as satisfy the biological and physical demands of islet grafts [45].

From the point of view of the graft biosafety, the implantation strategy of nanoencapsulated islets up to date still has limitations. Potential adverse events of the transplantation of nanoencapsulated islets following the Edmonton protocol might be direct consequences of the surgical procedure (for example, hemorrhage or thrombosis from through-the-skin access to the portal vein) [46]. Moreover, this approach does not allow an easy removal of the transplanted islets, since there is no control over the location of every single nanoencapsulated islet [47]. For this reason, new approaches must be developed to allow a simple and safe graft implanting/removal operation.

MICROENCAPSULATION

Microencapsulation technology consists of embedding single-cells or micro tissues within non-toxic and biocompatible hydrogel-like polymers in a spherical shape that constitute permselective protection from the host immune attack [30]. The goal of the microencapsulation technology is to exclude large molecular weight immune system constituents such as antibodies and immune cells, while, at the same time, allowing the exchange of beneficial molecules such as low molecular weight oxygen, glucose, insulin, nutrients, and hormones to pass through the microcapsule (Figure 3A) [48, 49].

A major challenge that affects the applicability of microencapsulation for islet transplantation is the biocompatibility of the encapsulation material [50]. Biocompatibility determines the performance of microcapsules for immunoprotection while remaining free from fibrotic overgrowth, which allow long-term pancreatic islet survival [51]. A wide range

of biocompatible polymers that can form hydrogels have been used in microencapsulation applications such as agarose, chitosan, collagen, gelatin, cellulose, PEG, poly-methyl methacrylates and 2-hydroxyethylmethacrylate; but with low performance in islet encapsulation [23, 52].

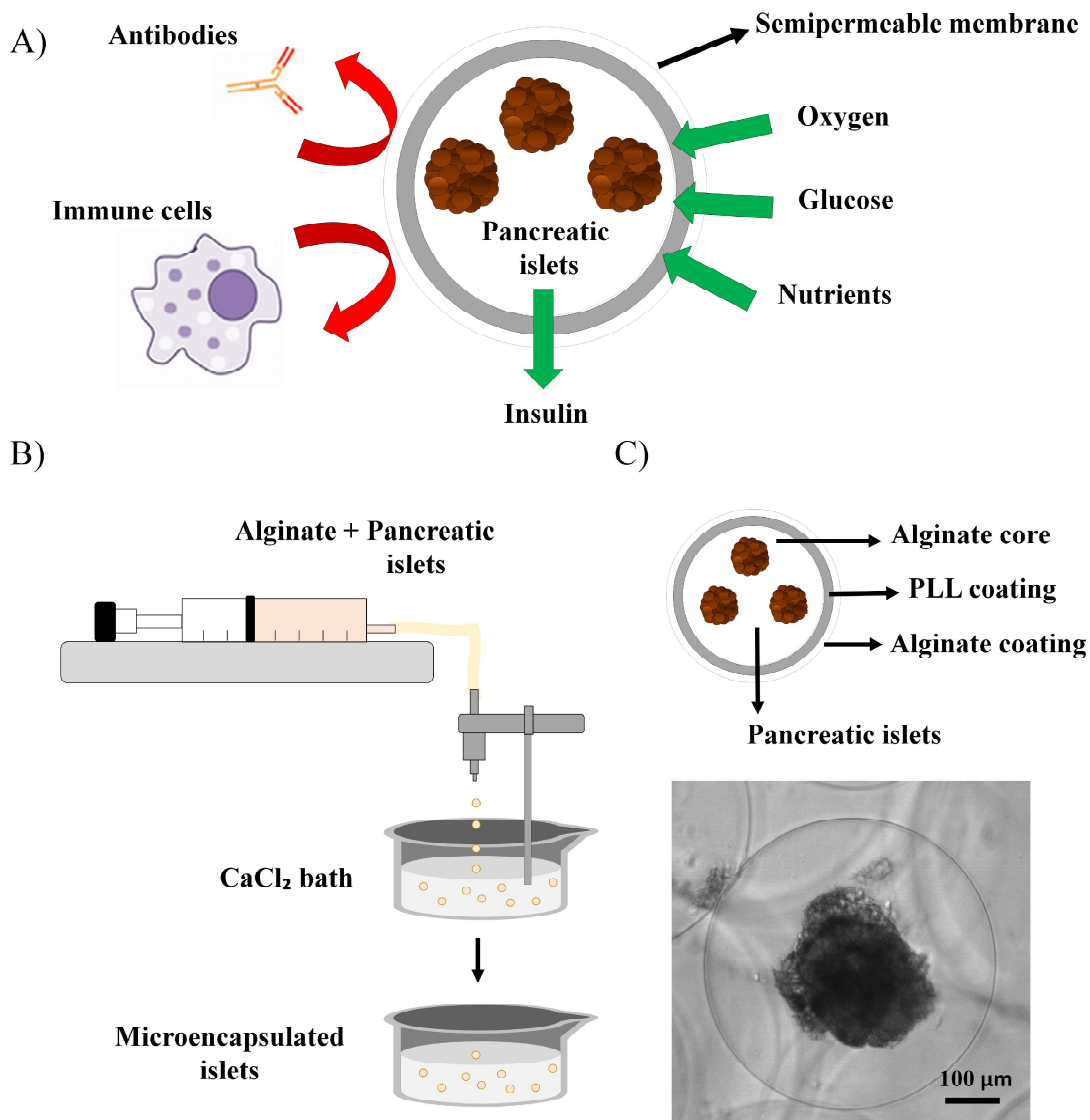


Figure 3. A) Principle of immunoisolation by a microcapsule. The semipermeable membrane allows the diffusion of molecules such as nutrients, glucose, oxygen, and insulin while providing protection against macromolecules and cells of the immune system of the host. B) Schematic of pancreatic islet microencapsulation within alginate microcapsules obtained by ionic cross-linking in a CaCl_2 bath where droplets that are generated by an electrostatic droplet generator are gelled. C) Layers structure of an alginate-poly-L-lysine-alginate (APA) microcapsule and, Brightfield image of a microencapsulated pseudoislet generated from the rat insulinoma INS1E cell line. Scale bar: 100 μm .

Among the materials used for microencapsulation, alginate is the most used hydrogel-like biomaterial for pancreatic islets microencapsulation, as it displays high

biocompatibility for both the cells in the microenvironment at the implantation site and for the cells inside the microcapsules, not interfering with cellular function [53]. This biomaterial is a natural anionic polymer extracted from brown sea weeds that consists of linear blocks of (1,4)-linked β -D-mannuronate (M) and α -L-guluronate (G) residues. The most common method to prepare alginate hydrogels as microcapsules is the ionic cross-linking [54]. Briefly, the islet-containing alginate solution is dropped through a nozzle into a solution with divalent cations such as calcium or barium ions, where microcapsules of 250-1000 μm in diameter are finally gelled, thereby entrapping one or more pancreatic islets (Figure 3B) [55]. The great biocompatibility and the easy formation process of microcapsules under physiological conditions without the need of cytotoxic chemicals and without affecting the islet viability and function, makes this biomaterial an excellent candidate for pancreatic islet microencapsulation, that has been already successfully applied in *in vivo* studies and clinical trials [56].

***In vivo* approaches**

The application of alginate-based microcapsules in the T1DM treatment has shown great promise, since many studies have demonstrated the successful entrapment of viable pancreatic islets in alginate microcapsules, which are able to restore glucose homeostasis *in vivo* in diabetic animal models [57]. In 1980, *Lim and Sun* described for the first time success in reversing diabetes by transplantation of islets within alginate microcapsules [56]. After implantation into diabetic rats, blood glucose levels decreased to normoglycemia for a period of three weeks, thereby confirming the potential treatment for diabetes using microencapsulated islets to create an artificial immune-privileged site for islets [23]. Since then, alginate microencapsulation gained progressive popularity, and research focused on improving microencapsulation material formulations to achieve appropriate immunoprotection, biocompatibility and mechanical stability for pancreatic islet transplant purposes.

In this regard, many studies aiming diabetes reversal used alginate microcapsules for islet microencapsulation coated by a polycation thin layer, such as poly-L-lysine (PLL), poly(allylamine), poly(vinylamine) or poly-L-ornithine (PLO), to obtain better control of diffusion and permselectivity, as well as to enhance the mechanical stability of the microcapsule system [30]. However, some of those polycations display cytotoxic and proinflammatory effects. For example, PLL coatings on microcapsules at higher concentrations than 0.05 % are toxic to several cell types such as β -cells, T-lymphocytes and monocytes. Besides, PLL may enhance the fibrotic and inflammatory responses against the microcapsules when

implanted into Balb/c mice through the induction of proinflammatory cytokines such as the Tumor Necrosis Factor (TNF) [58]. For this reason, another external alginate coating is often added to the microcapsules to hide the polycation layer. Thus a typical tri-layer alginate microcapsule comprises an alginate core surrounded by a semipermeable polycationic layer and an alginate outer shell [59], thereby improving the biocompatibility of the whole microcapsule, while maintaining the advantages of the polycation coating (Figure 3C) [60]. Several in vivo studies in large animals have been carried out using alginate–poly-L-lysine–alginate (APA) microcapsules. Sun et al., transplanted APA microencapsulated pig islets into diabetic *Cynomologus* monkey recipients without immunosuppression. After transplantation, the general condition of all animals improved substantially, and became insulin independent for periods ranging from 120 to 804 days with blood glucose levels in the normoglycemic range [61]. Despite these encouraging results, the main factor that seemed to lead to graft failure with APA microcapsules was islet necrosis caused by low oxygenation, high fibrotic response against the microcapsules and the PLL degradation over time [62].

To overcome the problems associated with PLL in APA microcapsules, *Elliott et al.*, modified the microcapsule composition with a PLO coating instead of PLL, and transplanted PLO microencapsulated neonatal porcine islets diabetic *Cynomologus* primates [63]. Six of the eight recipients achieved normoglycemia, and after retrieving the implanted PLO microcapsules, pig islets remained viable denoting high graft survival [63]. Other authors directly used polycation coating-free microcapsules, to avoid the potential cytotoxic and proinflammatory effects of polycations, by cross-linking the alginate microcapsules with barium ions [47]. These barium-cross-linked microcapsules have shown higher strength and less permeability to high molecular weight immune components such as IgG in comparison with calcium-cross-linked microcapsules [64]. Thereby, the absence of polycations in the microcapsules formulation makes these barium-cross-linked alginate microcapsules more biocompatible compared to APA microcapsules [65]. However, even in the absence of polycations, the barium alginate microcapsules still are susceptible to fibrotic overgrowth [47].

Overall, the fibrotic and inflammatory response against the microencapsulated islets, or the microcapsule material itself, mostly determine the success of the grafted microcapsules. However, this reaction is still poorly understood. In fact, in addition to the use of polycations in the microcapsules formulation, there are more factors that can be involved in the immune response such as the alginate purity, the biocompatibility of the materials conforming the microcapsule, the alginate chemical composition (guluronic/mannuronic ratio) and the size of the microcapsules [24, 66, 67].

Clinical trials

In 1996 Soon-Shiong et al., conducted the first successful clinical trial with APA microencapsulated allogeneic islets (15000 islets equivalents (IEQ)/Kg body weight) transplanted into the peritoneal cavity of a type 1 diabetic patient under immunosuppression treatment (Table 1) [68]. Results demonstrated glycemic control and insulin independence for 9 months. Following this initial trial, *Calafiore et al.*, transplanted intraperitoneally alginate-PLO microencapsulated human islets (400000-600000 IEQ/patient) without immunosuppression. Several weeks after transplantation, patients decreased the exogenous insulin requirements, approximately to half of the pre-transplantation insulin consumption levels and, no side effects of the grafting procedure, nor evidence of immune sensitization were detected (Table 1) [69]. Later, *Tuch et al.*, transplanted four diabetic patients intraperitoneally with allogeneic islets microencapsulated in barium-alginate without the use of immunosuppression, resulting in a decrease in blood glucose levels, but not enough to reduce the insulin requirements (Table 1) [70].

Although initial clinical trials mainly focused on the use of human pancreatic islets, the permselective immunobarrier of microcapsules allows the safe and efficacious use of xenogeneic islets for transplantation, thereby offering an alternative source of insulin producing cells that can help to overcome the shortage of pancreas donors. In this regard, transplantation of microencapsulated xenogeneic islets, especially porcine islets, commenced in patients with T1DM, as they are physiologically compatible and there is high homology between porcine and human insulin [36]. In 2007, Living Cell Technologies (LCT) Company performed a larger clinical study using commercial alginate-PLO microencapsulated pig islets called “Diabecell”, where eight patients received varying islet doses (5000 to 10000 IEQ/kg body weight), with some patients receiving multiple transplants (Table 1). Six patients demonstrated a reduced exogenous insulin requirement for up to 8 months [71]. Although no clinical trials involving porcine tissue have resulted in excellent metabolic control to date, these initial studies have demonstrated the potential use of this technology as a safe and effective treatment option for T1DM.

Advantages and limitations of microencapsulation

In most tissues it has been shown that maximum diffusion distance for effective oxygen and nutrient diffusion from blood capillary to cells is about 200 μm [72]. Higher diffusion distances induce a nutrient gradient from the cell encapsulation system surface to the center of the cells, which may affect cell function and survival [72]. In this sense, the reduced diameter and the large surface area-to-volume ratio of microcapsules result in

improved diffusion, thereby making this encapsulation system preferable over others, such as macroencapsulation, where longer diffusion distances hardly compromise oxygen and nutrients diffusion [23]. This fact also has a direct impact in the graft function as the response of microencapsulated islets to glucose changes in bloodstream is faster and more effective than in the macroencapsulation systems [24]. Another advantage of microencapsulation is that each microencapsulated islet is independently protected from the host immune attack, thereby if one microcapsule breaks or is attacked by the immune system due to any fabrication defect, the whole graft is not lost [23]. In contrast, if there is a small graft failure of islets encapsulated in a macroencapsulation device, the entire load of islets is at risk for destruction by the host immune cells since they are contained in a single volume [30]. Further, the microcapsules can be implanted using a minimally invasive procedure and the smooth spherical geometry minimizes foreign body reaction as opposed to host inflammatory reactions seen against rough surfaces [47].

In contrast, the major limitation to translate the microencapsulated islet technology to the clinics is the lack of large-scale microcapsules production systems. Current available microencapsulation devices are unable of efficiently encapsulating large numbers of islets in a reasonable amount of time, which may result in hypoxic stress and loss of islet viability or function [73]. Moreover, this technology has another technical obstacle that relies on the large therapeutic graft volume that may enhance the host immune reaction after implantation; this occurs due to two factors: the predominant volume made up of the encapsulating hydrogel with only a very small volume being the encapsulated islets and the high number of empty microcapsules generated during the islet microencapsulation process [74, 75]. In this regard, aiming to reduce microcapsules graft volume, separation of microencapsulated islets from empty microcapsules is usually accomplished by hand selection; however, the manual separation procedure is tedious, slow, and complicates its reproducibility [74, 75]. Recently, a novel microcapsule sorting system allows for the separation of magnetically labelled microencapsulated islets from empty microcapsules [57]. This purification system is based on a magnetic separation through a microfluidic device containing magnets, which guide the magnetized microencapsulated islets towards an output channel, while the empty microcapsules are eliminated through a different output channel. This technology allows high purification yields, while enabling the monitorization of the process, and avoids manual steps, thus, minimizing technical errors and improving the reproducibility of the purification process. Overall, the too high graft volume and the large microcapsules diameter impide the transplantation of microencapsulated islets into the liver following the standard Edmonton procedure, as it would suppose high risk of thrombosis. Alternatively, microcapsules containing islets have been transplanted into the peritoneal cavity in most of clinical trials,

where large volume of microcapsules can be implanted without clogging the vascular system [69-71]. However, the indirect access to blood within the peritoneum leads to lower availability of nutrients and oxygen, which can compromise the islets survival, thereby reducing the probability of success [76]. In addition, with the use of microencapsulated islets, as it happens with nanoencapsulated islets, there is no control over the location of every microencapsulated islet and, subsequently, microcapsules are difficult, if not impossible, to retrieve completely after implantation, thereby affecting negatively to the biosafety of this approach [70, 77, 78].

MACROENCAPSULATION

Hydrogel-based macroencapsulation systems are macroscopic encapsulation devices (> 1 mm) that involve a biocompatible hydrogel-like matrix containing large number of pancreatic islets or insulin-producing cells, thereby allowing the delivery of a curative β -cell dose within only one or very few devices [23]. These devices have been considered as a safeguard to reduce the perceived risk of islets exposure to the host's immune system and the risk associated to the use of insulin-producing cells derived from pluripotent stem cells [79]. Moreover, macroencapsulation provides the ability to retrieve the cells in the case of loss of function, adverse effects, or malignant transformation, which is an additional advantage in terms of clinical safety [6]. The described hydrogel-based macroencapsulation system to date are extravascular devices, so they are placed outside the vasculature usually in the peritoneal cavity, in the omentum, or at a subcutaneous site. In this sense, the major drawback of extravascular approaches is the limited oxygen diffusion and nutrient transport at those implantation sites, which tends to result in impaired viability, dysfunction, or even central necrosis in the islets [80]. Research on macroencapsulation systems focuses on the development of strategies and device configurations that can provide sufficient oxygen and nutrients to transplanted islets or insulin-producing cells.

***In vivo* approaches**

Macroencapsulation systems involving hydrogels are mostly circular or planar devices consisting of islets embedded in hydrogels placed within two circular or rectangular semipermeable flat sheets fastened to make a sealed chamber. This encapsulation system is designed to prevent cell clustering inside the device while protecting the cells from mechanical stress after implantation [81, 82].

Islet Sheet is one example of the planar flat sheet devices designed by Islet Sheet Medical; which involved a multilayered construct of alginate composed of a central alginate

layer containing islets, and two external acellular alginate layers covering the central layer for immunoprotection. This device demonstrated to provide excellent graft survival in allogeneic islet transplantation in diabetic dogs, achieving normoglycemia for 12 weeks. However, the Islet Sheet devices are yet to be tested in clinical trials for their safety and efficacy [83]. More recently, *Dufrane et al.*, developed a planar flat sheet device called Monolayer Cellular Device consisting on a monolayer of collagen matrix where islets are embedded, and two alginate layers covering both sides of the collagen matrix [84]. Encapsulated porcine islets within this device were implanted subcutaneously and demonstrated to correct hyperglycemia for up to 6 months in diabetic monkeys without immunosuppression. Although a strong immune response was detected after transplantation, a total impermeability of alginate layers to IgG was demonstrated up to 20 weeks [84].

The major disadvantage with macroencapsulation devices is the poor oxygen diffusion throughout the outer semipermeable membrane compromising the viability of the implanted islets, thereby limiting their ability to secrete insulin and leading to graft failure. This issue was addressed by another macroencapsulation system, an oxygen-refueled device called β -Air, which was developed by Beta-O₂ Technologies Ltd [85]. This device consists of a semipermeable chamber containing islets embedded within an alginate hydrogel and, an additional compartment that enables daily oxygen supply through an external tubing system (Figure 4A). Preliminary studies with the β -Air implanted in diabetic rats and pigs showed that the function of encapsulated allogeneic islets was preserved, and blood glucose levels were decreased to normal values for several months [86, 87]. Regarding the oxygen supply strategy, perfluorocarbons and calcium peroxide (CaO₂) as source of oxygen has been added within hydrogel formulations containing β -cells in in vitro experiments, having a considerable impact on cells with high oxygen uptake rates and enhanced cell viability and metabolic activity [88, 89]. In this sense, inclusion of these sort of oxygen carriers in the encapsulation matrix could be a useful strategy for overcoming the oxygen limitations, ensuring cell viability and functionality of β -cells within macroencapsulation devices.

In attempt to address the low oxygen supply from another point of view, BioHub macroencapsulation system was developed at the Diabetes Research Institute of Miami aiming a high graft vascularization [59]. The novelty of this technology is the use of an injectable biomaterial for islet encapsulation, which consists of a hydrogel-like matrix made with thrombin and the patient's own plasma. This hydrogel degrades over time, leaving the islets intact, while new blood vessels are formed to supply oxygen and nutrients to the islets, thereby supporting their survival and function [90]. After achieving good results in small animals, further studies were performed in diabetic *Cynomolgus* monkeys. On this matter, allogeneic islets were injected using BioHub system in the omentum of diabetic monkeys

under immunosuppressive treatment. A few weeks after implantation, recipients showed progressive reduction of exogenous insulin requirements. After retrieving the grafts 49 days post-implantation, histopathologic analysis demonstrated well-preserved islet morphology with abundant internal and external vascularization [90].

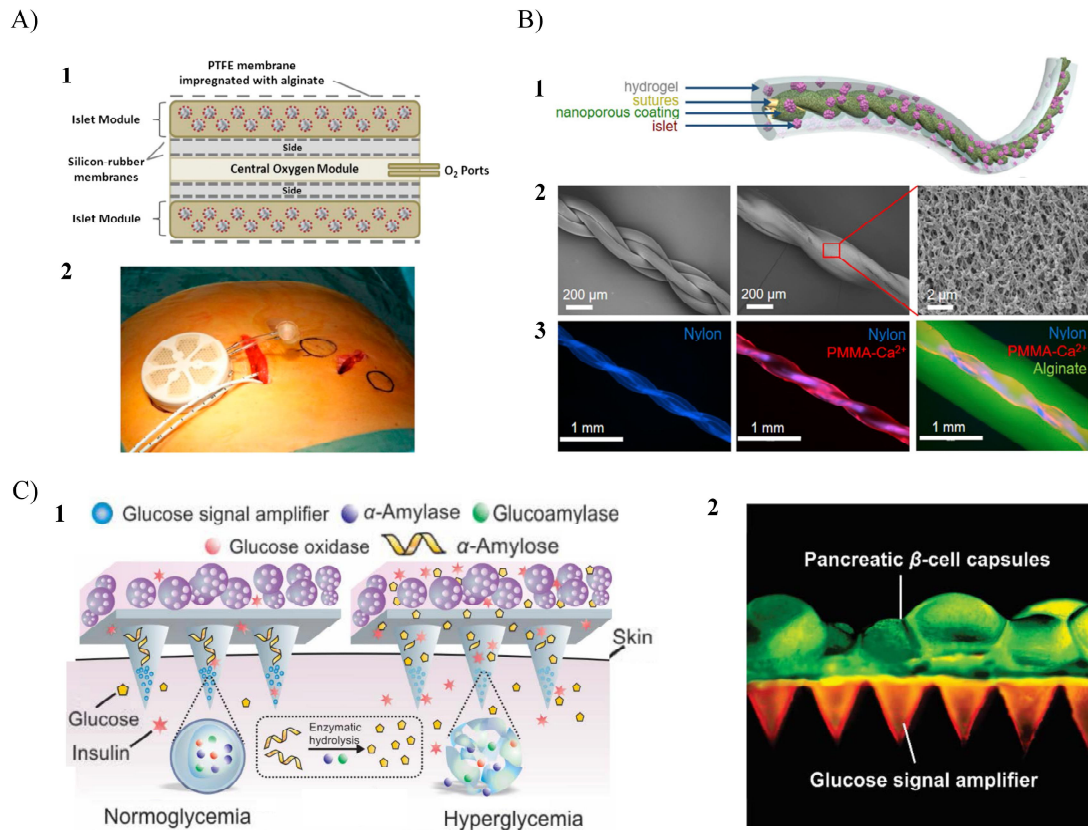


Figure 4. A) β -Air macroencapsulation system for islet encapsulation. 1) Schematic view of the chamber system. The core of the device has a gas module, connected to access ports for exogenous oxygen refilling. Separated by gas permeable membranes, two compartments surround the gas module that houses pancreatic islets immobilized within alginate, 2) Chamber system with integrated human islet graft with connected access ports before implantation. Adapted from [85]. B) TRAFFIC islet macroencapsulation device. 1) Schematic illustration of the design of TRAFFIC. 2) SEM images of the thread and the uniform nanoporous surface modifications. 3) Fluorescent microscopic images of the thread, modified thread, and the complete TRAFFIC device. Adapted from [91]. C) Microneedle patch system with integrated pancreatic cells and synthetic glucose-signal amplifiers. 1) Schematic of the glucose responsive system functioning of the microneedle patch where glucose signal amplifiers (GSA) promote insulin release triggered by a hyperglycemia state. 2) Fluorescence microscopy image of the microneedle patch: patch was loaded with rhodamine-labeled GSA and calcium AM-stained pancreatic β -cells were positioned on the back of the patch. Scale bar: 500 μ m. Adapted from [92].

Recently, other macroencapsulation devices geometries have been developed to enhance the diffusion properties and, to improve their retrievability and replaceability. For example, the thread-reinforced alginate fiber for islets encapsulation (TRAFFIC) device, which involves an alginate hydrogel layer with controllable thickness containing islets placed around a nanoporous calcium-releasing central nylon thread (Figure 4B) [91]. The device can

be extended to meters long allowing to scale-up the system to large animals and, still be entirely retrievable through a minimally invasive surgery. In vivo studies in mice showed that TRAFFIC encapsulating rat islets restored normoglycemia in diabetic mice while providing immune protection for up to 3 months. Additionally, no significant tissue damage, fibrosis, or cellular overgrowth was noted on the device or peritoneum of these mice. Similarly, the TRAFFIC device scalability and retrievability was also demonstrated in dogs [91].

Other authors have developed another novel β -cell encapsulation device that is placed externally onto the skin, thereby eliminating the immune response caused in more invasive implantation procedures and avoiding the use of immunosuppression [92]. This system involves a microneedle patch composed by hyaluronic acid hydrogel housing β -cells and glucose signal amplifying enzymes (GSA) (Figure 4C). With this device, in a hyperglycemic state, glucose diffuses inside the microneedles and, next, the glucose signal is amplified through GSA thus stimulating the insulin secretion from encapsulated β -cells, which is secreted through the microneedles in a minimally invasive manner. In in vivo studies with diabetic mice, a microneedle patch responded rapidly to hyperglycemia leading to stabilization of blood glucose levels for 10 hours [92]. This macroencapsulation device displayed a promising alternative to pancreatic β -cells internal implantation for glucose homeostasis regulation, but further work is required for improving the glucose diffusion and the viability of encapsulated cells.

Clinical trials

There has been only limited clinical testing of macroencapsulated islet products in a small number of patients using some of the abovementioned macroencapsulated islet or β -cells products. In addition, only Beta-O₂ company has published clinical results with β -Air device, while other researchers evaluating other macroencapsulation devices had made oral presentations at public meetings.

For example, in 2000 *Dufrane et al.*, encouraged by the results obtained in the preclinical studies in diabetic monkeys [84], implanted subcutaneously the Monolayer Cellular Device containing allogeneic islets in a 74-year-old type 1 diabetic patient (Table 1) [93]. Blood glucose levels were controlled for 361 days after transplantation, along with a notable reduction of hypoglycemic episodes. Implant retrieval after a year revealed the macroscopic integrity of the device without signs of inflammation and immunization against the donor cells. No more details of this clinical trial have been published.

Later, in 2012, a pilot clinical trial was carried out with allogeneic islets (2100 IEQ/kg body weight) encapsulated in β -Air device that were implanted in a 63-years old

patient. In this study, graft function was achieved for 10 months with controlled blood glucose and insulin secretion regulation, while preserving the islet morphology and function without immunosuppression (Table 1) [85]. Encouraged by the good results in terms of glucose metabolism control and safety signals without serious adverse effects of β -Air device implantation, another clinical trial has been conducted to continue evaluating the safety and efficacy of this system into type 1 diabetic human patients [94]. In this study, four patients were implanted with 1800–4600 islet equivalents per kg/ body weight and were monitored for 3-6 months. Results reinforced the preliminary results where implantation of β -Air device was safe and successfully prevented immunization and rejection of the transplanted islets. However, although this device can support survival of allogeneic islets for several months, it cannot achieve long-term insulin independence due to limited function of transplanted islets. More recently, the mentioned BioHub macroencapsulation system has been evaluated in an ongoing clinical trial, with the objective to demonstrate the safety and long-term feasibility of this approach (Table 1) [80]. In such study, a 43-year-old diabetic woman was implanted in the omentum with approximately a total dose of 600000 allogeneic IEQ encapsulated within the BioHub system [95]. This approach demonstrated promising results, as the patient experienced a restoration of glucose homeostasis with insulin independence for 12 months. Although this strategy requires the administration of immunosuppressive treatments, it demonstrates that the omentum is a good site for islet transplantation with the BioHub approach.

Advantages and limitations

The main advantage of pancreatic islet macroencapsulation technology over nano- and microencapsulation is the control of confining the islets in a precise location of the body in one single device without cell spreading and the possibility to retrieve the device in case of graft failure or other complications [6]. A key factor of macroencapsulation device retrievability is that most of them are designed to be implanted in the subcutaneous or omentum space, thus facilitating the device implantation and retrieval, resulting in a reduction of surgical risks [84, 94]. In addition, the wide flexibility of designing, developing and fabricating macroencapsulation devices allows optimizing the devices configuration to facilitate their retrieval by minimal invasive surgical procedures, as it was demonstrated with the mentioned TRAFFIC device [91]. The microneedle patch explored the skin as a new implantation site, thereby reducing the inflammatory and immune response derived from more invasive implantation procedures [92].

From another point of view, because of their large size, macroencapsulation devices

can support high number of islets within a reduced graft volume, thus minimizing the host's immune reaction compared to microcapsules where higher implant volumes are required to correct diabetes disease. Although there are other types of macroencapsulation devices that do not involve hydrogels and can also hold high amounts of islets [79], in most cases islets are freely floating inside the encapsulation chamber, resulting in aggregation of islets that negatively affects islet structure, limits the nutrients and oxygen diffusion, and leads to loss of islet function, apoptosis and death [76]. In contrast, macroencapsulation devices embedding islets within hydrogels provide a physical separation of the islets preventing aggregation, maintaining the islet's rounded morphology, improving the oxygen and nutrients supply to all encapsulated islets thereby enhancing their viability and survival [81, 82]. Moreover, as BioHub device demonstrated, engineering the macroencapsulating hydrogels, can also improve the viability and functionality of the islets [80]. However, some hydrogels are fragile and not stable enough to support the transplanted islets over a long period and, therefore, the long-term islet survival cannot be guaranteed [6]. For this reason, introducing hydrogel-islets biosystems within macroencapsulation devices, like in the β -Air device, has become a promising strategy that confines hydrogel-islets structures, conferring a strong mechanical protection that results in improved integrity of the inner hydrogel [85, 96].

Although interesting benefits come from using macroencapsulation approaches, additional issues must be addressed before the macroencapsulation technology can emerge as a practical clinical option for the treatment of T1DM. As islets exhibit elevated oxygen consumption rates compared to other cell types [97, 98], the primary limitation of the macroencapsulation devices compared to nano- and microencapsulation is the reduced islet oxygenation due to larger diffusional distances between the encapsulated islets and the outside of the macroencapsulation device [80]. In this sense, the diminished diffusional properties to the transport of oxygen, and to other essential substances such as nutrients, metabolites and hormones like insulin, is the main reason for compromised islet viability, leading to eventual graft failure [80]. These type of macroscopic devices are usually implanted in the subcutaneous space, which presents low vascularization and demonstrates relatively poor capacity for vascular enhancement, and subsequent low glycemic control [99]. In this regard, different strategies to address this limitation include oxygen-perfused approaches such as β -Air device that require daily replenishment [85], bioactive hydrogels like BioHub that promote vascularization around and inside the device [80], and/or the infusion of vasculogenic factors such as the Vascular Endothelial Growth Factor (VEGF) to stimulate greater vascularization at the device surface [100, 101]. However, further investigation is required for adequate oxygenation and nutrient supply to achieve long-term islet survival.

Other problems also limit the success of macroencapsulation devices such as the

fibrotic response and cellular adherence to the outer wall membrane. In this regard, the way that an implantable device interacts with the host's biological environment and immune system at the implantation site determines the success of the graft [102]. This fact depends on the device size, geometry and configuration and most importantly, depends on the surface properties, such as roughness, morphology, pore size, surface hydrophilicity and chemical composition. However, it is still not well known how they influence on the inflammatory and fibrotic response [103]. In this sense, it is essential to explore macrodevice designs and surface properties to achieve a successful and functional graft during the short and long-term after implantation.

BIOPRINTING

Bioprinting is an innovative approach based on the automated additive manufacturing, that offers the potential to assembly tissue-like structures by the controlled positioning of cells, biomaterials, and cell-laden biomaterials individually or in tandem, in a stacking layer by layer at a desire location [104, 105]. In addition, biologically active components can be also added and precisely patterned, such as proteins, genes and drugs, to better guide tissue generation and/or formation [106]. Thereby, bioprinting technology has great potential to address the increasing demand for organs transplants, thus being a key technology to step forward in the field of tissue engineering and regenerative medicine for organ repair and organ replacement [107].

Hydrogel-based biomaterials used in bioprinting are called bioinks and can be loaded with cells or any biological component. Bioinks must possess enough viscoelastic properties to enable its precise layer by layer deposition, thus achieving high fidelity 3D printed constructs [108]. After the printing process, depending on the bioink cross-linking method, 3D structures can be solidified through three different mechanisms: physical (temperature and light) [109], enzymatic [110], and chemical (pH and ionic compound) [111] cross-linking. As the other cell encapsulation techniques, bioinks employ hydrogel-like polymers that provide a biocompatible protective matrix to the embedded islets or β -cells and, a specific biochemical and physical environment to ensure the integrity of the printed structure and an appropriate cell development [112]. In addition, the accuracy of bioprinting technology and the possibility for multi-bioink fabrication may allow the creation of pancreatic tissue-like structures, were pancreatic islets and other cells present in the pancreas could be included and positioned in the tissue construct similarly to physiological conditions [112]. Currently, β -cell and islet bioprinting has been studied using two different bioprinting systems, inkjet- and extrusion-based printing techniques.

Bioprinting technology fundamentals

Inkjet bioprinting

Inkjet-based bioprinting is an electronically controlled cartesian bioprinting process that utilizes thermal- or piezoelectric-driven mechanisms to dispose picoliter-sized droplets of bioinks with high resolution [113]. Such bioinks can contain single-cells and/or other biological compounds like proteins, drugs, etc. which are deposited through a nozzle or multi-nozzle system in a high-throughput manner with positional accuracy on the microscale [107]. Thermal and piezoelectric inkjet printing are shown schematically in Figure 5A. This printing process enables fast fabrication speeds over a large area at high shear rates (10^5 - 10^6 s⁻¹) maintaining high cell viabilities (80-90 %). However, this approach is restricted to low viscosity bioinks (< 10 mPa/s), since the more viscous is the bioink greater the force required to eject droplets from the printing nozzle, thereby limiting its applicability [114, 115]. In addition, in some cases, cell densities applicable in this technology may be lower than physiologically relevant numbers (< 10^6 cells/mL) due to the possible nozzle clogging problems [113]. Another limitation of this approach is that uses bioinks that possess relatively weak mechanical properties, thus limiting the printing of structures requiring higher mechanical properties [116].

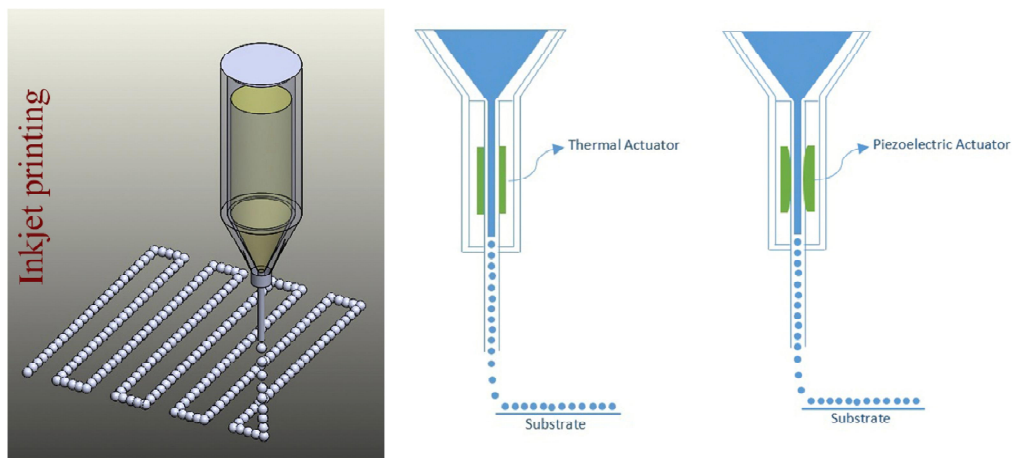
Inkjet printing application in 3D bioprinting has been limited compared to extrusion-based studies. The main reason for that is the inherent inability of the printing head to provide a continuous flow which limits its application in bioprinting.

Extrusion bioprinting

Currently, most of the commercially available bioprinters are extrusion-based, with bioinks driven through a single or multiple nozzle by pneumatic (air-pressure or mechanical (screw/piston-driven) dispensing system [117]. In pneumatic dispensing, air pressure provides the required driving force to deposit the bioink, while in mechanical systems with piston and screw-driven dispensing, vertical and rotational forces enable the printing process (Figure 5B) [113]. This approach is a combination of fluid-dispensing system and an automated robotic cartesian system for extrusion and bioprinting, where bioinks are spatially disposed under computer-controlled motion, resulting in the precise deposition of cells encapsulated within the bioink as micrometric cylindrical filaments allowing desired 3D custom-shaped structures [117]. This rapid fabrication technique provides better structural integrity compared to inkjet bioprinted constructs due to the continuous deposition of filaments. In addition, the extrusion-based technique enables the use of bioinks with a wider range of viscosity (from 0.1 to 30×10^7 mPa/s), incorporating higher working cell densities and/or

other biological compounds, and even the incorporation of larger cellular structures such as cell pellets, tissue spheroids, and tissue strands [114, 118]. Further comparison with inkjet bioprinting, although the extrusion-based bioprinting technique displays great printing speed, this fabrication speed is lower than in the inkjet printing. In addition, the printing resolution is also lower ($> 200 \mu\text{m}$). Besides, depending on the size of the nozzle diameter and pressure of extrusion, cell viability values may be lower than that obtained with inkjet printers (40-80 %) [116, 119]. Overall, extrusion-based bioprinting can be regarded as the most promising, as this technology allows the fabrication of multicomponent organized structures of clinically relevant sizes within a realistic time frame.

A)



B)

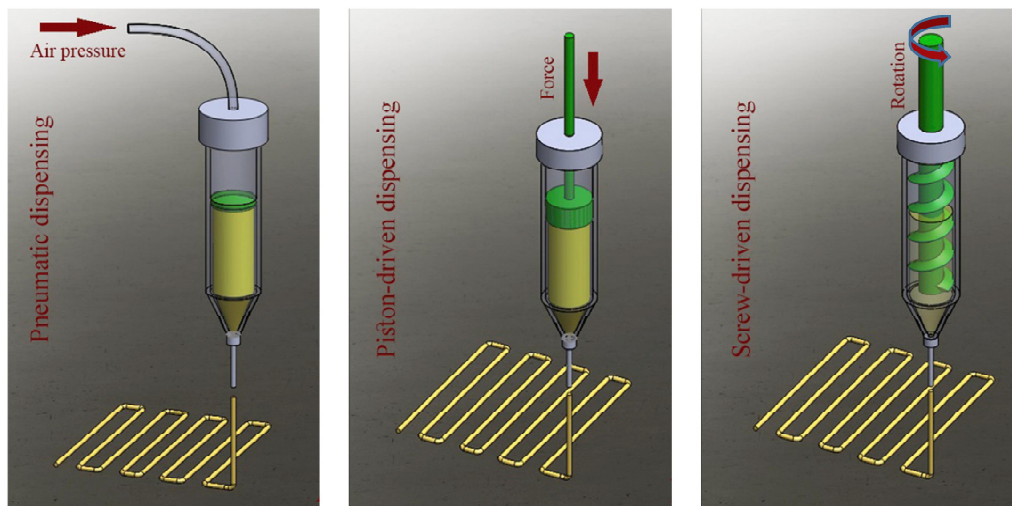


Figure 5. A) Diagram of common extrusion-based bioprinting methods: pneumatic, piston-driven, and screw-driven dispensing method. B) Diagram of inkjet-based printing method using thermal and piezoelectric actuators. Figures A and B as originally published in Derakhshanfar S, Mbeleck R, Xu K, et al. 3D bioprinting for biomedical devices and tissue engineering: A review of recent trends and advances. *Bioactive Materials* 2018, licensed under CC BY-NC-ND 4.0 license (<https://creativecommons.org/licenses/by-nc-nd/4.0/>).

Bioink properties

The development of bioink materials allows to manipulate the biological environment as well as living cells to create complex biological tissue-like constructs. However, although wide range of biomaterials have been developed for tissue engineering and regenerative medicine, most of them are not compatible with existing bioprinting technologies [120]. In this regard, the bioink viscosity, defined by its rheological properties, is the most important factor for successful 3D structures fabrication through bioprinting [108]. In this sense, depending on the bioprinting process mechanism (inkjet- or extrusion-based modalities), bioinks must possess different rheological requirements.

Bioinks used in inkjet bioprinting must have low viscosity and a nanofibrous nature, thereby they can easily flow through the tubing system and nozzle without clogging problems [116]. For appropriate inkjet bioprinting, bioinks must display a rheopectic behavior, a dilatant behavior that enables the droplets formation during the bioink ejection due to a viscosity increase after the shear stress application in the nozzle. Further, the bioink should also have appropriate surface tension and wettability to travel through the bioprinting system without leaking out, thus avoiding flooding of the print head and wetting of the exterior of the nozzle tip [121]. Finally, an important post-printing characteristic is that bioink ejected droplets should solidify immediately after landing onto the plate to allow the 3D structure formation [116].

On the other hand, bioinks in extrusion-based bioprinting must hold different requirements, being the viscosity one of the most important factors to take into account. Viscosity of the bioink exerts influence on cell bioprinting having a direct impact on the printing efficiency and shape fidelity of the 3D construct [108]. While high viscosity bioinks are expected to maintain optimal printability and structural fidelity after printing, their biocompatibility may get affected in the process, since nutrient diffusion is compromised and the required high shear force for extrusion can diminish cell viability. On the other hand, low viscosity bioinks are more likely to require lower shear forces for extrusion allowing higher cell viabilities. However, the printed structures may spread in situ due to weak mechanical properties losing the 3D shape modelled in the digital design, thereby supposing poor printing fidelity [108, 113]. In this regard, bioinks showing thixotropic shear thinning rheological behavior are the most suitable in maintaining high printing fidelity, while showing high cell viabilities after the printing process [113]. In shear thinning behavior, the application of pneumatic or mechanical shear forces during the extrusion align the random polymer chains in a favorable direction reducing the viscosity of the bioinks and thereby making them extrudable. But in thixotropic shear thinning rheological behavior, in addition to exhibit low

viscosity during the extrusion process, bioinks also assume a high viscosity stable form at rest in the printing cartridge, which is regained after the extrusion process thus allowing the formation of 3D structures [119]. In this sense, bioinks showing thixotropy enable extrusion of filaments at low shear forces, thereby protecting cells from physical stress and then reform to achieve high fidelity printed structures. Moreover, bioinks should possess low adhesion and surface tension characteristics to eliminate their attachment on the surface of the nozzle tip, thus enabling successful bioink filament extrusion [105, 119, 121].

Bioprinting process stages

The complete bioprinting process to generate tissue constructs principally involves the three key stages from the 3D design phase to post-bioprinting steps: pre-bioprinting, bioprinting and post-bioprinting (Figure 6) [122].

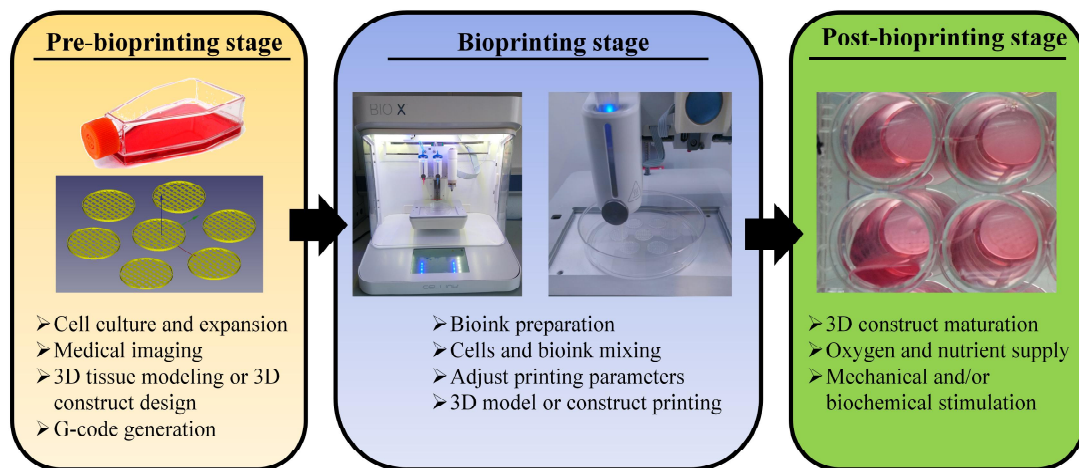


Figure 6. Stages in the 3D bioprinting process: pre-bioprinting, bioprinting and post-bioprinting with their most important steps.

The pre-bioprinting step plays a crucial role in determining the properties of the final bioprinted structure, as in this stage, the main task resides in the creation of a computer-aided 3D design model suitable for bioprinting [116]. In this regard, the 3D construct designs can be generated de novo using 3D design softwares or, they can be obtained from biomedical diagnostic image acquisition techniques that allow precise tissue 3D modelling directly from patient's anatomy, such as 3D laser scanning, micro-computed tomography (μ -CT) and magnetic resonance imaging (MRI) [116, 123]. After obtaining the 3D construct design, such design must be converted to G-code, the language consisting of commands that have an assigned movement or action that allow the bioprinter to move the printing system through the X, Y and Z axes to fabricate the 3D structure layer-by-layer [124]. Because there

are hundreds or thousands of movements involved in producing a 3D structure, the G-code contains information that can be hundreds of pages long of commands. For this reason, usually G-code is automatically generated by slicing softwares that slices the 3D structure into layers that are rapidly converted to the G-code containing all the necessary information for the layer-by-layer printing [125].

Once the G-code is obtained, the fabrication process begins in the bioprinting which involves three elements: the bioink, the bioprinter and the bioprinting process [122]. First, the bioink/s used for the tissue construct printing must be defined and characterized to ensure that they possess the abovementioned properties, such as biocompatibility, non-toxicity and optimal viscoelastic characteristics, required for adequate printability in the different bioprinting modalities [126]. In addition, tissue-specific cells that will be included within the bioink must be obtained in enough quantity and robustness. To that end, cells must be isolated and/or differentiated, and expanded in culture before mixing with the bioink [116]. In this sense, clinical application becomes more feasible if cells are obtained from patients by biopsies through minimally-invasive surgical procedures and if the protocols followed for the expansion of cells are cost effective and achievable under good laboratory practice (GLP) conditions [122]. After obtaining the cell-laden bioink, bioprinting parameters require strict optimization to achieve great printing resolution for successful construct fabrication, which are mainly defined by the bioprinter characteristics and bioink printability [127]. The most important parameters to take into account are the Z axis precision that defines the layer height, the availability to use nozzles with different diameters demarking the filament or droplet resolution in the X and Y axes. In addition, the printing pressure range to dispense the bioink that will limit the minimum and maximum bioink viscosity for appropriate printing and the printing speed that is closely related to the bioink viscosity, which must be adjusted alongside the working pressure to obtain a uniform filament or droplet with the desired resolution for bioprinting. Otherwise, the printing process can fail due to the lack of bioink deposition or the dispensing of too large amounts of bioink that impede the printing of the desired shape [108, 114, 128, 129]. Once all these parameters are optimized for the specific bioink and bioprinter, the bioink is placed in the bioprinter cartridge and layer-by-layer deposition takes place based on the G-code to obtain the tissue-like 3D construct.

Finally, the bioprinted tissue structure is required to become mature in suitable bioreactors. This step occurs in the post-bioprinting stage where tissue-like constructs are cultured under controlled conditions, where cells are recovered from the stress suffered during the printing process and, besides, cells are biochemically and/or mechanically stimulated to promote cell-cell and cell-bioink matrix interactions, thereby achieving the desired biological tissue-like characteristics [122].

Early approaches

Nowadays, the development of a tissue-like pancreas containing pancreatic islets using 3D bioprinting is still an early stage and, limited in vitro and in vivo work has been performed until date.

Duin et al., developed a bioink composed of 3 % alginate and 9 % methylcellulose to be used for pancreatic islets encapsulation within mesh pattern obtained through extrusion-based bioprinting (Figure 7A) [130]. In this study, pancreatic islets from Wistar rats were successfully embedded within bioprinted constructs without affecting their morphology, while preventing their aggregation. Cell viability and biological function was also evaluated showing viability values around 80 % and glucose responsiveness for up to 7 days in culture. More recently, researchers from the University of Wollongong in Australia, also used an alginate/gelatin bioink for pancreatic islet extrusion-based bioprinting, but with a step forward. They developed a more advanced 3D construct design to enhance islet immunoprotection and promote vascularization [131]. In this work, the printed structure consisted of a multicellular construct accommodating mouse pancreatic islets and endothelial progenitor cells (EPCs). Both cells were successfully disposed forming an inner core containing functional islets that was covered with an outer protecting shell with embedded EPCs (Figure 7B). In this approach, the outer shell seeks to provide immunoprotection to the islets improving immunoisolation, while it simultaneously contains supporting cells, such as EPCs, that can promote the vascularization of the graft.

Currently, the inkjet-based bioprinting technology is also being developed for patterning β -cell in different construct designs. For example, *Yang, et al.*, used this technology to pattern spots composed of anisotropic tobacco mosaic virus (TMV) particles conjugated with RGD (arginine–glycine–aspartate) that support and control the formation of pancreatic progenitor cells (PPCs) clusters [132]. With this approach, author aimed a novel PPCs expansion and differentiation method for the generation of insulin-producing β -cells through a high-throughput production of size-controlled clusters of PPCs. Results showed that PPCs were able to adhere onto the multiple printed cell-adhesive spots and form cell aggregates in uniform size and shape, thereby obtaining a robust and reproducible PPCs-cluster patch (Figure 7C). Due to the early stage of inkjet-based bioprinting for diabetes treatment application, no more studies have been described to date.

However, some hydrogel are fragile and not stable enough to guarantee the long-term islet survival [6]. For this reason, bioprinted constructs with hydrogel-based bioinks can be combined with more stable and stiffer macroencapsulation structures that can be printed simultaneously through another 3D printing modality called Fused Deposition Modelling

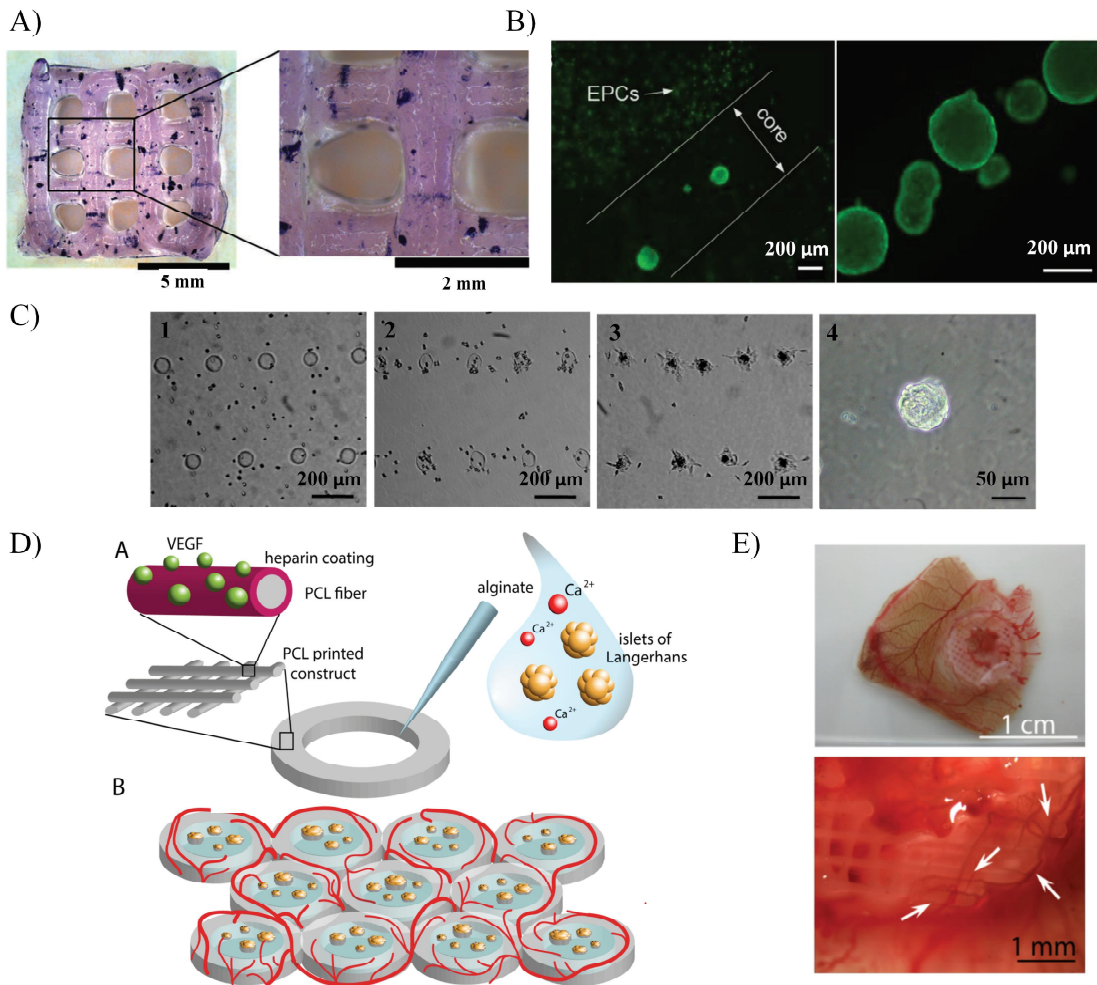


Figure 7. A) Bioprinted scaffold by extrusion-based printing with a bioink composed of alginate and methylcellulose were islets are stained for metabolic activity with MTT 1 day after bioprinting. Scale bars: 5 mm and 2 mm. Adapted from [130]. B) A coaxial printed construct with encapsulated islets in the core and endothelial progenitor cells (EPCs) in the outer shell. Scale bar: 200 μ m. Adapted from [131]. C) Microscopic images illustrating the formation of pancreatic progenitor cells (PPC) clusters on anisotropic tobacco mosaic virus (TMV) particles conjugated with RGD (arginine–glycine–aspartate) patterned spots at 0 h (1), 3 h (2), 24 h (3), and 3 days (4) after seeding. The scale bars of 1–3 and 4 are 200 μ m and 50 μ m, respectively. D) Schematic of the hybrid polycaprolactone (PCL)/alginate scaffold concept. 3D plotted PCL rings were covalently functionalized with a heparin layer. Heparin was used as an active linker to bind VEGF and protect it from degradation. Islets were encapsulated in the inner part of the structure using alginate hydrogel. Multiple constructs can be printed one next to the other in a honeycomb configuration increasing the available surface for islets embedding and revascularization of the scaffold. Adapted from [138]. E) CAM assay performed with heparin coated PCL scaffolds loaded with VEGF. Scaffold with 200 ng load VEGF induce blood vessels formation, with normal morphology (Arrows indicate the blood vessel formation). Adapted from [138]. C) Reprinted (adapted) with permission from Yang J, Zhou F, Xing R, et al. Development of large-scale size-controlled adult pancreatic progenitor cell clusters by an inkjet-printing technique. *ACS Appl Mater Interfaces* 2015. DOI:10.1021/acsami.5b02676. Copyright (2019) American Chemical Society.

(FDM) [133]. This modality is based on the extrusion of heated plastic filaments through a nozzle tip to deposit layers onto the printing platform to build 3D objects layer by layer directly from the digital model [134]. The materials used in FDM cannot be mixed with cells, but some of these materials are biocompatible and can be combined with hydrogel-based structures containing cells, thereby obtaining hybrid constructs with enhanced mechanical properties that improve the integrity and stability of the hydrogel cell-laden printed part [135, 136]. For example, researcher from the Washington University School of Medicine created a novel 3D printed human pluripotent stem cells (hPSC)-derived β -cell clusters encapsulation device based on polylactic acid (PLA) and a fibrin hydrogel [137]. After validating good cell viability and insulin production in vitro, such constructs were subcutaneously implanted in mice under immunosuppression. In this study, glucose responsiveness of the implanted cells was demonstrated detecting the according human insulin levels after performing an intraperitoneal glucose tolerance test 12 days after implantation. Moreover, the constructs maintained their structural integrity and were easily retrieved without risk of deformation. Another hybrid bioprinted construct based on polycaprolactone (PCL) and alginate hydrogels was developed to promote quick vascularization after implantation [138]. The construct consisted in a 3D ring-shaped PCL structure with heparinized surface to electrostatically bind VEGF, surrounding an alginate hydrogel core where pancreatic islets were embedded. Thereby, the whole construct was designed to easily implant islets within a mechanically reinforced hydrogel matrix, while actively promoting graft vascularization (Figure 7D). In this study, human pancreatic islet within the bioprinted construct demonstrated to remain viable and functional after the printing process. Besides, such constructs were implanted in a chicken chorioallantoic membrane (CAM) and vasculogenic potential was confirmed with the observation of new blood vessels formation in the tissue surrounding the graft and even on the surface on the construct (Figure 7E).

Advantages and limitations

The main advantage of the bioprinting technology is that it offers a unique role in the pancreatic tissue-like constructs fabrication, through its potential in recreating complex morphologies and multicellular environments. In addition, this technology overcomes the limitations of the conventional islet encapsulation technology, such as the hypoxia state, the lack of vascularization, the diffusion properties of the encapsulation system, etc. [139]. To that end, pancreatic islets could be strategically positioned to mitigate the autoimmune response while enhancing the islets biological function. In this regard, islets may be immunoprotected inside the hydrogel-like bioinks and further inclusion of immunosuppressive or immunomodulatory

factors into the bioink formulation may prevent rejection [131]. Besides, aiming to mimic tissue-specific biological cues, some groups have incorporated decellularized matrices within bioinks, which have been extracted from natural tissues such as adipose, cartilage and heart [140]. In this sense, including decellularized matrices of pancreas within bioinks, closer biomimetic environments could be achieved to enhance the islet viability and biological function.

From another point of view, bioprinting also may permit for the coordinated fabrication of a vascularized encapsulated islet. Multiple print heads could be used for the precise positioning of the bioinks, thus generating an intricate vasculature inside the bioprinted construct to overcome the poor oxygenation and nutrients supply that characterize the islet macroencapsulation [105]. In this regard, sacrificial materials as bioinks, such as pluronic [141] and gelatin [142], in combination with hydrogel-based bioinks have been used in generating these microchannels through inkjet- and extrusion-based bioprinting. To that end, printing sacrificial bioinks, forming precise structures inside the construct, artificial vasculature can be generated after removing the sacrificial material from the construct, thus leaving empty microstructures mimicking an intricate perfusable vascular network [139]. In addition, bioinks may also incorporate endothelial cells and/or slow releasing compounds such as VEGF to promote angiogenesis surrounding the bioprinted structure [138]. Overall, this technology would allow for the embedded islets long-term survival inside the bioprinted graft, while mimicking a functional pancreas.

However, although the bioprinting approach is a revolutionary technology with high potential for the study and treatment of T1DM, the use of this technique for artificial pancreas fabrication is in the horizon and, for this reason, it still has several limitations due to the early stages of its development. The main technological barrier is that, currently, the choice of bioink materials is limited by the stringent printing conditions. Moreover, there are few available standard or commercial bioinks with good biocompatibility and the appropriate biological and physicochemical properties, such as optimal degree of hydrophilicity, pH neutrality, functional groups, stiffness, elasticity and porosity, that can mimic the natural pancreatic tissue and achieve the islet physiological function [143]. Additionally, with the current bioprinting technology, human scale tissues and organs would require too prolonged time for the printing process, thereby affecting the cell viability of the printed cells [116]. However, as printing technology and biomaterial science applied to this technique develop, artificial tissues more similar to organs will be created to finally obtain functional 3D printed constructs with better therapeutic capacity.

CONCLUSIONS

Islet encapsulation technologies involving nano-, micro-, macroencapsulation and bioprinting represent promising approaches for T1DM treatment, as they provide means to transplant islets without immunosuppressive agents and enable the use of alternative islets or β -cells donor sources. However, there are still limitations in each encapsulation modality that hamper their widespread clinical application. The ability to retrieve implanted cells, if needed or desired, is an important biosafety consideration for successful therapy. In this sense, in nano- and microencapsulation approaches, the implanted capsules cannot be contained in a precise location and, consequently, if requiring cell replenishment or in case of graft failure, they cannot be easily and completely removed from the patient, thus supposing a poor degree of biosafety. In contrast, macroencapsulation modality has a high degree of biosafety, as islets are implanted in one single device that can be easily retrieved. However, in these larger configurations, diffusional problems that lead to poor diffusion of oxygen, dramatically affect the islets viability impeding long-term functioning of the transplanted islets. In this sense, bioprinting technology is an emerging technology that has the potential to overcome all the mentioned issues by generating artificial pancreatic tissues with vascular structures that would enhance the diffusional issues of macroencapsulation approaches. However, this technology is still in early stages of development and requires more research in biomaterial science to allow this advanced artificial pancreas fabrication. Overall, advances in biomaterial science, fabrication technologies, safer implantation strategies, angiogenesis inducement and cell biology, together with progress in regulatory pathways, may allow the translation of these cell encapsulation technologies into medical reality.

ACKNOWLEDGEMENTS

Authors thank the support to research on cell microencapsulation from the University of the Basque Country UPV/EHU (EHUa16/06 to LSB) and the Basque Country Government (Grupos Consolidados, No ref: IT907-16 to JLP). Authors also thank to ICTS “NANBIOSIS”, specifically by the Drug Formulation Unit (U10) of the CIBER in Bioengineering, Biomaterials & Nanomedicine (CIBER-BBN) at the University of the Basque Country UPV/EHU in Vitoria-Gasteiz.

REFERENCES

- [1] Vieira A, Druelle N, Avolio F, et al. beta-Cell Replacement Strategies: The Increasing Need for a “beta-Cell Dogma”. *Front Genet* 2017.
- [2] Yoon JW and Jun HS. Autoimmune destruction of pancreatic beta cells. *Am J Ther* 2005.

- [3] Montanya E. Islet- and stem-cell-based tissue engineering in diabetes. *Curr Opin Biotechnol* 2004.
- [4] Amer LD, Mahoney MJ and Bryant SJ. Tissue engineering approaches to cell-based type 1 diabetes therapy. *Tissue Eng Part B Rev* 2014.
- [5] Li W, Zhao R, Liu J, et al. Small islets transplantation superiority to large ones: implications from islet microcirculation and revascularization. *J Diabetes Res* 2014.
- [6] Skrzypek K, Groot Nibbelink M, van Lente J, et al. Pancreatic islet macroencapsulation using microwell porous membranes. *Sci Rep* 2017.
- [7] Cooke DW and Plotnick L. Type 1 diabetes mellitus in pediatrics. *Pediatr Rev* 2008.
- [8] Harlan DM, Kenyon NS, Korsgren O, et al. Current advances and travails in islet transplantation. *Diabetes* 2009.
- [9] Gruessner AC and Sutherland DE. Analysis of United States (US) and non-US pancreas transplants as reported to the International Pancreas Transplant Registry (IPTR) and to the United Network for Organ Sharing (UNOS). *Clin Transpl* 1998.
- [10] Sutherland DE, Gruessner RW, Dunn DL, et al. Lessons learned from more than 1,000 pancreas transplants at a single institution. *Ann Surg* 2001.
- [11] Sutherland DER, Gores PF, Farney AC, et al. Evolution of kidney, pancreas, and islet transplantation for patients with diabetes at the University of Minnesota. *The American Journal of Surgery* 1993.
- [12] Beck J, Angus R, Madsen B, et al. Islet encapsulation: strategies to enhance islet cell functions. *Tissue Eng* 2007.
- [13] Figliuzzi M, Bonandrini B, Silvani S, et al. Mesenchymal stem cells help pancreatic islet transplantation to control type 1 diabetes. *World J Stem Cells* 2014.
- [14] Moore SJ, Gala-Lopez BL, Pepper AR, et al. Bioengineered stem cells as an alternative for islet cell transplantation. *World J Transplant* 2015.
- [15] Bottino R, Knoll MF, Knoll CA, et al. The Future of Islet Transplantation Is Now. *Front Med (Lausanne)* 2018.
- [16] Desai T and Shea LD. Advances in islet encapsulation technologies. *Nat Rev Drug Discov* 2017.
- [17] Sakata N, Tan A, Chan N, et al. Efficacy comparison between intraportal and subcapsular islet transplants in a murine diabetic model. *Transplant Proc* 2009.
- [18] Schuetz C, Anazawa T, Cross SE, et al. beta Cell Replacement Therapy: The Next 10 Years. *Transplantation* 2018.
- [19] Korsgren O. Islet encapsulation: Physiological possibilities and limitations. *Diabetes* 2017; 66: 1748-1754.
- [20] Burcu Kepsutlu, Caner Nazli, Tugba Bal Bal, et al. Design of Bioartificial Pancreas with Functional Micro/Nano-Based Encapsulation of Islets. *Current Pharmaceutical Biotechnology* 2014.
- [21] Ahmed EM. Hydrogel: Preparation, characterization, and applications: A review. *J Adv Res* 2015.
- [22] Knobloch T, Abadi SEM, Bruns J, et al. Injectable Polyethylene Glycol Hydrogel for Islet Encapsulation: an in vitro and in vivo Characterization. *Biomed Phys Eng Express* 2017.
- [23] Krishnan R, Alexander M, Robles L, et al. Islet and stem cell encapsulation for clinical transplantation. *Rev Diabet Stud* 2014.
- [24] Sakata N, Sumi S, Yoshimatsu G, et al. Encapsulated islets transplantation: Past, present and future. *World J Gastrointest Pathophysiol* 2012.
- [25] Ravnic DJ, Leberfinger AN and Ozbolat IT. Bioprinting and Cellular Therapies for Type 1 Diabetes. *Trends Biotechnol* 2017.
- [26] Zhi ZL, Khan F and Pickup JC. Multilayer nanoencapsulation: a nanomedicine technology for diabetes research and management. *Diabetes Res Clin Pract* 2013.
- [27] Kozlovskaya V, Zavgorodnya O, Chen Y, et al. Ultrathin polymeric coatings based on hydrogen-bonded polyphenol for protection of pancreatic islet cells. *Adv Funct Mater* 2012.
- [28] Krol S, del Guerra S, Grupillo M, et al. Multilayer nanoencapsulation. New approach for immune protection of human pancreatic islets. *Nano Lett* 2006.
- [29] Shih H, Mirmira RG and Lin CC. Visible light-initiated interfacial thiol-norbornene photopolymerization for forming islet surface conformal coating. *J Mater Chem B* 2015.

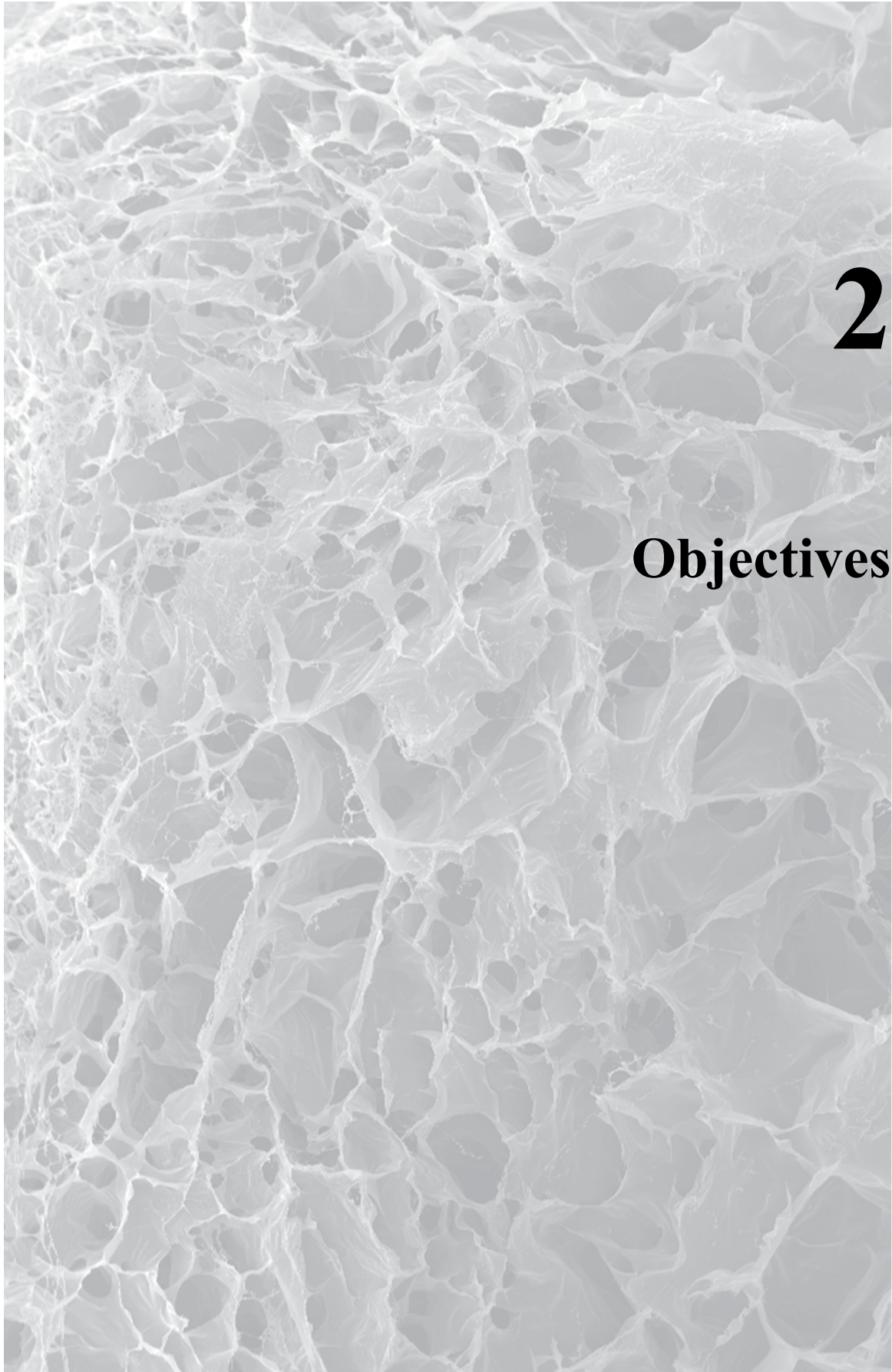
- [30] Scharp DW and Marchetti P. Encapsulated islets for diabetes therapy: History, current progress, and critical issues requiring solution. *Advanced Drug Delivery Reviews* 2014.
- [31] Teramura Y and Iwata H. Bioartificial pancreas microencapsulation and conformal coating of islet of Langerhans. *Adv Drug Deliv Rev* 2010.
- [32] Hill RS, Cruise GM, Hager SR, et al. Immunoisolation of adult porcine islets for the treatment of diabetes mellitus. The use of photopolymerizable polyethylene glycol in the conformal coating of mass-isolated porcine islets. *Ann N Y Acad Sci* 1997.
- [33] W. Scharp D. Encapsulated human islet allografts: Providing safety with efficacy. In: *Anonymous Cellular Transplantation: Elsevier Inc, 2007, p.135.*
- [34] Phelps EA, Enemchukwu NO, Fiore VF, et al. Maleimide cross-linked bioactive PEG hydrogel exhibits improved reaction kinetics and cross-linking for cell encapsulation and in situ delivery. *Adv Mater* 2012.
- [35] Wilson JT, Cui W and Chaikof EL. Layer-by-layer assembly of a conformal nanothin PEG coating for intraportal islet transplantation. *Nano Lett* 2008.
- [36] Meirigeng Qi. Transplantation of Encapsulated Pancreatic Islets as a Treatment for Patients with Type 1 Diabetes Mellitus. *Advances in medicine* 2014.
- [37] Dufrane D and Gianello P. Macro- or microencapsulation of pig islets to cure type 1 diabetes. *World J Gastroenterol* 2012.
- [38] Calafiore R, Basta G, Luca G, et al. Alginate/Polyaminoacidic Coherent Microcapsules for Pancreatic Islet Graft Immunoisolation in Diabetic Recipients. *Annals of the New York Academy of Sciences* 1997; 831: 313-322.
- [39] Leblond FA, Simard G, Henley N, et al. Studies on Smaller (~315 μ M) Microcapsules: IV. Feasibility and Safety of Intrahepatic Implantations of Small Alginate Poly-L-Lysine Microcapsules. *Cell Transplantation* 1999.
- [40] Seda Kizilel, Andrew Scavone, Xiang Liu, et al. Encapsulation of pancreatic islets within nano-thin functional polyethylene glycol coatings for enhanced insulin secretion. *Tissue Engineering Part A* 2010; 16: 2217-2228.
- [41] Zorzi D, Phan T, Sequi M, et al. Impact of islet size on pancreatic islet transplantation and potential interventions to improve outcome. *Cell Transplant* 2015.
- [42] Tomei AA, Manzoli V, Fraker CA, et al. Device design and materials optimization of conformal coating for islets of Langerhans. *Proc Natl Acad Sci U S A* 2014.
- [43] Yang HK and Yoon KH. Current status of encapsulated islet transplantation. *J Diabetes Complications* 2015.
- [44] Hwang PT, Shah DK, Garcia JA, et al. Progress and challenges of the bioartificial pancreas. *Nano Converg* 2016.
- [45] Zhu H, Lu L, Liu X, et al. Treatment of diabetes with encapsulated pig islets: an update on current developments. *J Zhejiang Univ Sci B* 2015.
- [46] O'Sullivan ES, Vegas A, Anderson DG, et al. Islets Transplanted in Immunoisolation Devices: A Review of the Progress and the Challenges that Remain. *Endocrine Reviews* 2011.
- [47] Vaithilingam V, Bal S and Tuch BE. Encapsulated Islet Transplantation: Where Do We Stand?. *Rev Diabet Stud* 2017.
- [48] Pérez-Luna VH and González-Reynoso O. Encapsulation of Biological Agents in Hydrogels for Therapeutic Applications. *Gels* (Basel, Switzerland) 2018.
- [49] Lim GJ, Lee SJ and Atala A. Cell-Based Drug Delivery. In: *Anonymous Principles of Regenerative Medicine: Academic Press, p.954.*
- [50] Vaithilingam V and Tuch BE. Islet Transplantation and Encapsulation: An Update on Recent Developments. *The review of diabetic studies : RDS* 2011.
- [51] Zekorn TD, Horcher A, Mellert J, et al. Biocompatibility and Immunology in the Encapsulation of Islets of Langerhans (Bioartificial Pancreas). *The International journal of artificial organs* 1996.
- [52] Gasperini L, Mano JF and Reis RL. Natural polymers for the microencapsulation of cells. *J R Soc Interface* 2014.
- [53] de Vos P, Faas MM, Strand B, et al. Alginate-based microcapsules for immunoisolation of pancreatic islets. *Biomaterials* 2006.

- [54] Ertesvåg H and Valla S. Biosynthesis and applications of alginates. *Polymer Degradation and Stability* 1998.
- [55] Omami M, McGarrigle JJ, Reedy M, et al. Islet Microencapsulation: Strategies and Clinical Status in Diabetes. *Curr Diab Rep* 2017.
- [56] Cappai A, Petruzzo P, Ruiu G, et al. Evaluation of new small barium alginate microcapsules. *The International journal of artificial organs* 1995.
- [57] Espona-Noguera A, Etxebarria-Elezgarai J, Saenz Del Burgo L, et al. Type 1 Diabetes Mellitus reversal via implantation of magnetically purified microencapsulated pseudoislets. *Int J Pharm* 2019.
- [58] Strand BL, Ryan L, Veld PI, et al. Poly-L-Lysine Induces Fibrosis on Alginate Microcapsules via the Induction of Cytokines. *Cell Transplantation* 2001.
- [59] Farina M, Alexander JF, Thekkedath U, et al. Cell encapsulation: Overcoming barriers in cell transplantation in diabetes and beyond. *Adv Drug Deliv Rev* 2018.
- [60] Kleinberger RM, Burke NAD, Dalnoki-Veress K, et al. Systematic study of alginate-based microcapsules by micropipette aspiration and confocal fluorescence microscopy. *Materials Science & Engineering C* 2013.
- [61] Sun Y, Ma X, Zhou D, et al. Normalization of diabetes in spontaneously diabetic cynomolgus monkeys by xenografts of microencapsulated porcine islets without immunosuppression. *J Clin Invest* 1996.
- [62] Duvivier-Kali VF, Omer A, Parent RJ, et al. Complete protection of islets against allo rejection and autoimmunity by a simple barium-alginate membrane. *Diabetes* 2001.
- [63] Elliott RB, Escobar L, Tan PL, et al. Intraperitoneal alginate-encapsulated neonatal porcine islets in a placebo-controlled study with 16 diabetic cynomolgus primates. *Transplant Proc* 2005.
- [64] Morch YA, Donati I, Strand BL, et al. Effect of Ca²⁺, Ba²⁺, and Sr²⁺ on alginate microbeads. *Biomacromolecules* 2006.
- [65] Abdulkadir Omer, Valérie F. Duvivier-Kali, Nitin Trivedi, et al. Survival and Maturation of Microencapsulated Porcine Neonatal Pancreatic Cell Clusters Transplanted into Immunocompetent Diabetic Mice. *Diabetes* 2003.
- [66] Pia Montanucci, Silvia Terenzi, Claudio Santi, et al. Insights in Behavior of Variably Formulated Alginate-Based Microcapsules for Cell Transplantation. *BioMed Research International* 2015.
- [67] Orive G, Ponce S, Hernández RM, et al. Biocompatibility of microcapsules for cell immobilization elaborated with different type of alginates. *Biomaterials* 2002.
- [68] Soon-Shiong P, Heintz RE, Merideth N, et al. Insulin independence in a type 1 diabetic patient after encapsulated islet transplantation. *Lancet* 1994.
- [69] Calafiore R, Basta G, Luca G, et al. Microencapsulated Pancreatic Islet Allografts Into Nonimmunosuppressed Patients With Type 1 Diabetes: First two cases. *Diabetes care* 2006.
- [70] Bernard E. Tuch, Gregory W. Keogh, Lindy J. Williams, et al. Safety and Viability of Microencapsulated Human Islets Transplanted Into Diabetic Humans. *Diabetes Care* 2009.
- [71] Tan PL. Company Profile: Tissue regeneration for diabetes and neurological diseases at Living Cell Technologies. *Regenerative Medicine* 2010.
- [72] Lovett M, Lee K, Edwards A, et al. Vascularization strategies for tissue engineering. *Tissue Eng Part B Rev* 2009.
- [73] Opara EC and Kendall WF. Immunoisolation techniques for islet cell transplantation. *Expert Opin Biol Ther* 2002.
- [74] Buder B, Alexander M, Krishnan R, et al. Encapsulated islet transplantation: strategies and clinical trials. *Immune Netw* 2013.
- [75] Lee KY and Mooney DJ. Alginate: properties and biomedical applications. *Prog Polym Sci* 2012.
- [76] Schweicher J, Nyitray C and Desai TA. Membranes to achieve immunoprotection of transplanted islets. *Front Biosci (Landmark Ed)* 2014.
- [77] Jacobs-Tulleneers-Thevissen D, Chintinne M, Ling Z, et al. Sustained function of alginate-encapsulated human islet cell implants in the peritoneal cavity of mice leading to a pilot study in a type 1 diabetic patient. *Diabetologia* 2013.

- [78] Weir GC and Bonner-Weir S. Scientific and Political Impediments to Successful Islet Transplantation. *Diabetes* 1997.
- [79] Barkai U, Rotem A and de Vos P. Survival of encapsulated islets: More than a membrane story. *World Journal of Transplantation* 2016.
- [80] Alejandro R. Allogeneic Islet Cells Transplanted Onto the Omentum 2014.
- [81] Desai T and Shea LD. Advances in islet encapsulation technologies. *Nature reviews. Drug discovery* 2017.
- [82] Silva AI, de Matos AN, Brons IG, et al. An overview on the development of a bio-artificial pancreas as a treatment of insulin-dependent diabetes mellitus. *Med Res Rev* 2006.
- [83] STORRS R, DORIAN R, KING SR, et al. Preclinical Development of the Islet Sheet. *Annals of the New York Academy of Sciences* 2001.
- [84] Dufrane D, Goebbels R and Gianello P. Alginate Macroencapsulation of Pig Islets Allows Correction of Streptozotocin-Induced Diabetes in Primates up to 6 Months Without Immunosuppression. *Transplantation* 2010.
- [85] Barbara Ludwig, Andreas Reichel, Anja Steffen, et al. Transplantation of human islets without immunosuppression. *Proceedings of the National Academy of Sciences of the United States of America* 2013.
- [86] Barbara Ludwig, Avi Rotem, Janine Schmid, et al. Improvement of islet function in a bioartificial pancreas by enhanced oxygen supply and growth hormone releasing hormone agonist. *Proceedings of the National Academy of Sciences of the United States of America* 2012.
- [87] Neufeld T, Ludwig B, Barkai U, et al. The Efficacy of an Immunoisolating Membrane System for Islet Xenotransplantation in Minipigs. *PLoS ONE* 2013.
- [88] Chin K, Khattak SF, Bhatia SR, et al. Hydrogel-Perfluorocarbon Composite Scaffold Promotes Oxygen Transport to Immobilized Cells. *Biotechnology progress* 2008.
- [89] Gholipourmalekabadi, Mazaher|Zhao, Susan|Harrison, Benjamin S.|Mozafari, Masoud|Seifalian, Alexander M. Oxygen-Generating Biomaterials: A New, Viable Paradigm for Tissue Engineering?. *Trends in Biotechnology* 2016.
- [90] Berman DM, Molano RD, Fotino C, et al. Bioengineering the Endocrine Pancreas: Intraomental Islet Transplantation Within a Biologic Resorbable Scaffold. *Diabetes* 2016.
- [91] An D, Chiu A, Flanders JA, et al. Designing a retrievable and scalable cell encapsulation device for potential treatment of type 1 diabetes. *Proc Natl Acad Sci U S A* 2018.
- [92] Ye Y, Yu J, Wang C, et al. Microneedles Integrated with Pancreatic Cells and Synthetic Glucose-Signal Amplifiers for Smart Insulin Delivery. *Adv Mater* 2016.
- [93] Dufrane D, Mourad M, Goffin E, et al. A Simple and Safe Clinical Procedure for Human Encapsulated Islet Transplantation in the Subcutaneous Tissue for Diabetes Treatment. *Transplantation* 2013.
- [94] Carlsson PO, Espes D, Sedigh A, et al. Transplantation of macroencapsulated human islets within the bioartificial pancreas betaAir to patients with type 1 diabetes mellitus. *Am J Transplant* 2018.
- [95] Baidal DA, Ricordi C, Berman DM, et al. Bioengineering of an Intraabdominal Endocrine Pancreas. *N Engl J Med* 2017.
- [96] Kepsutlu B, Nazli C, Bal T, et al. Design of bioartificial pancreas with functional micro/nano-based encapsulation of islets. *Curr Pharm Biotechnol* 2014.
- [97] Dionne KE, Colton CK and Lyarmush M. Effect of Hypoxia on Insulin Secretion by Isolated Rat and Canine Islets of Langerhans. *Diabetes* 1993.
- [98] Sato Y, Endo H, Okuyama H, et al. Cellular hypoxia of pancreatic beta-cells due to high levels of oxygen consumption for insulin secretion in vitro. *The Journal of biological chemistry* 2011.
- [99] Weaver JD, Headen DM, Aquart J, et al. Vasculogenic hydrogel enhances islet survival, engraftment, and function in leading extrahepatic sites. *Sci Adv* 2017.
- [100] Trivedi N, Steil GM, Colton CK, et al. Improved Vascularization of Planar Membrane Diffusion Devices following Continuous Infusion of Vascular Endothelial Growth Factor. *Cell Transplantation* 2000.
- [101] Weaver JD, Headen DM, Hunckler MD, et al. Design of a vascularized synthetic poly(ethylene glycol) macroencapsulation device for islet transplantation. *Biomaterials* 2018.

- [102] Chandorkar Y, K R and Basu B. The Foreign Body Response Demystified. ACS Biomaterials Science & Engineering 2019.
- [103] Liping Tang, Paul Thevenot and Wenjing Hu. Surface Chemistry Influences Implant Biocompatibility. Current Topics in Medicinal Chemistry 2008.
- [104] Kačarević ŽP, Rider PM, Alkildani S, et al. An Introduction to 3D Bioprinting: Possibilities, Challenges and Future Aspects. Materials (Basel, Switzerland) 2018.
- [105] Rider P, Kačarević ŽP, Alkildani S, et al. Bioprinting of tissue engineering scaffolds. Journal of tissue engineering 2018.
- [106] Boyd-Moss M, Fox K, Brandt M, et al. Bioprinting and Biofabrication with Peptide and Protein Biomaterials. Advances in experimental medicine and biology 2017.
- [107] Cui H, Nowicki M, Fisher JP, et al. 3D Bioprinting for Organ Regeneration. Adv Healthc Mater 2017.
- [108] Gopinathan J and Noh I. Recent trends in bioinks for 3D printing. Biomater Res 2018.
- [109] Kim SH, Yeon YK, Lee JM, et al. Precisely printable and biocompatible silk fibroin bioink for digital light processing 3D printing. Nat Commun 2018.
- [110] Petta D, Armiento AR, Grijpma D, et al. 3D bioprinting of a hyaluronan bioink through enzymatic-and visible light-crosslinking. Biofabrication 2018.
- [111] Rutz AL, Hyland KE, Jakus AE, et al. A multimaterial bioink method for 3D printing tunable, cell-compatible hydrogels. Adv Mater 2015.
- [112] Yue Z, Liu X, Coates PT, et al. Advances in printing biomaterials and living cells: implications for islet cell transplantation. Current opinion in organ transplantation 2016.
- [113] Derakhshanfar S, Mbeleck R, Xu K, et al. 3D bioprinting for biomedical devices and tissue engineering: A review of recent trends and advances. Bioactive Materials 2018.
- [114] Hölzl K, Lin S, Tytgat L, et al. Bioink properties before, during and after 3D bioprinting. Biofabrication 2016.
- [115] Ozbolat IT and Yin Yu. Bioprinting Toward Organ Fabrication: Challenges and Future Trends. TBME 2013.
- [116] Bishop ES, Mostafa S, Pakvasa M, et al. 3-D bioprinting technologies in tissue engineering and regenerative medicine: Current and future trends. Genes & Diseases 2017.
- [117] Kirchmajer DM, Gorkin III R and in het Panhuis M. An overview of the suitability of hydrogel-forming polymers for extrusion-based 3D-printing 2015.
- [118] Sarker MD, Naghieh S, Sharma NK, et al. 3D biofabrication of vascular networks for tissue regeneration: A report on recent advances. Journal of Pharmaceutical Analysis 2018.
- [119] Mandrycky C, Wang Z, Kim K, et al. 3D bioprinting for engineering complex tissues. Biotechnol Adv 2016.
- [120] Varkey M, Visscher DO, van Zuijlen, P P M, et al. Skin bioprinting: the future of burn wound reconstruction?. Burns Trauma 2019.
- [121] Ozbolat IT. 3D Bioprinting: Fundamentals, Principles and Applications. San Diego, CA, USA: Elsevier Science, 2016.
- [122] Datta P, Barui A, Wu Y, et al. Essential steps in bioprinting: From pre- to post-bioprinting. Biotechnology Advances 2018.
- [123] Ballyns JJ and Bonassar LJ. Image-guided tissue engineering. Journal of Cellular and Molecular Medicine 2009.
- [124] Sodupe-Ortega E, Sanz-Garcia A, Pernia-Espinoza A, et al. Accurate Calibration in Multi-Material 3D Bioprinting for Tissue Engineering. Materials (Basel, Switzerland) 2018.
- [125] McElheny C, Hayes D and Devireddy R. Design and Fabrication of a Low-Cost Three-Dimensional Bioprinter. Journal of Medical Devices 2017.
- [126] Berg J, Hiller T, Kissner MS, et al. Optimization of cell-laden bioinks for 3D bioprinting and efficient infection with influenza A virus. Scientific Reports 2018.
- [127] Li Z, Huang S, Liu Y, et al. Tuning Alginate-Gelatin Bioink Properties by Varying Solvent and Their Impact on Stem Cell Behavior. Scientific reports 2018.

- [128] Blaeser A, Duarte Campos DF, Puster U, et al. Controlling Shear Stress in 3D Bioprinting is a Key Factor to Balance Printing Resolution and Stem Cell Integrity. *Advanced Healthcare Materials* 2016.
- [129] Lee JM and Yeong WY. Design and Printing Strategies in 3D Bioprinting of Cell-Hydrogels: A Review. *Advanced Healthcare Materials* 2016.
- [130] Duin S, Schütz K, Ahlfeld T, et al. 3D Bioprinting of Functional Islets of Langerhans in an Alginate/Methylcellulose Hydrogel Blend. *Advanced Healthcare Materials* 2019.
- [131] Liu X, Carter SD, Renes MJ, et al. Development of a Coaxial 3D Printing Platform for Biofabrication of Implantable Islet-Containing Constructs. *Adv Healthc Mater* 2019.
- [132] Yang J, Zhou F, Xing R, et al. Development of large-scale size-controlled adult pancreatic progenitor cell clusters by an inkjet-printing technique. *ACS Appl Mater Interfaces* 2015.
- [133] Ji S and Guvendiren M. Recent Advances in Bioink Design for 3D Bioprinting of Tissues and Organs. *Front Bioeng Biotechnol* 2017.
- [134] Chia HN and Wu BM. Recent advances in 3D printing of biomaterials. *J Biol Eng* 2015.
- [135] Tappa K and Jammalamadaka U. Novel Biomaterials Used in Medical 3D Printing Techniques. *J Funct Biomater* 2018.
- [136] Kolan K, Liu Y, Baldrige J, et al. Solvent Based 3D Printing of Biopolymer/Bioactive Glass Composite and Hydrogel for Tissue Engineering Applications. *Procedia CIRP* 2017.
- [137] Song J and Millman JR. Economic 3D-printing approach for transplantation of human stem cell-derived beta-like cells. *Biofabrication* 2016.
- [138] Marchioli G, Di Luca A, de Koning E, et al. Hybrid Polycaprolactone/Alginate Scaffolds Functionalized with VEGF to Promote de Novo Vessel Formation for the Transplantation of Islets of Langerhans. *Advanced Healthcare Materials* 2016.
- [139] Lee SJ, Lee JB, Park Y, et al. 3D Bioprinting for Artificial Pancreas Organ. *Advances in experimental medicine and biology* 2018.
- [140] Pati F and Cho D. Bioprinting of 3D Tissue Models Using Decellularized Extracellular Matrix Bioink. *Methods in molecular biology (Clifton, N.J.)* 2017.
- [141] Suntornnond R, Tan EYS, An J, et al. A highly printable and biocompatible hydrogel composite for direct printing of soft and perfusable vasculature-like structures. *Scientific reports* 2017.
- [142] Hinton TJ, Jallerat Q, Palchesko RN, et al. Three-dimensional printing of complex biological structures by freeform reversible embedding of suspended hydrogels. *Sci Adv* 2015.
- [143] Jipeng Li, Mingjiao Chen, Xianqun Fan, et al. Recent advances in bioprinting techniques: approaches, applications and future prospects. *Journal of Translational Medicine* 2016.



2

Objectives

2. OBJECTIVES

Currently, micro- and macroencapsulation technologies for pancreatic islets encapsulation are the most studied cell-based therapies with several successful clinical trials in restoring the insulin secretory function in Type 1 diabetic patients. In both approaches, hydrogel-like biomaterials are widely employed because of their high-water content, good biocompatibility, structural and mechanical similarities with the native pancreatic extracellular matrix (ECM), and their permselectivity to low and high molecular weight components, which provides immunoprotection while allowing the diffusion of oxygen, nutrients and hormones such as insulin. On this regard, alginate has been extensively used in islet micro- and macroencapsulation because of its high biocompatibility, low toxicity and its fast and easy gelation under mild conditions. However, aspects of both types of encapsulation approaches using alginate as encapsulating biomaterial have some issues that should be optimized for the future translation to widespread clinical application.

On the one hand, in the microencapsulation approach, one crucial problem to be considered is the high number of empty microcapsules that are generated during the islet microencapsulation process, thereby leading to a high graft volume, which can enhance the host immune reaction after implantation. Nowadays, the reduction of the graft volume is accomplished by separating the microencapsulated islets from the empty microcapsules by hand selection. This manual procedure is tedious, slow, and complicates its reproducibility.

On the other hand, in the macroencapsulation approach, the fast and poorly controlled gelation of alginate hydrogels forces to make them in a mold outside the body, and to implant the final gelled product by invasive surgical procedure, instead of by simple injection into the patient's body or by molding within a device that is ease to implant and retrieve. In this sense, the lack of control over the gelation rate restricts the practical use of alginate macroscopic hydrogels in the clinics. Moreover, in this approach, alginate hydrogels are fragile and not stable enough to support the transplanted islets over a long period and, therefore, the long-term islet survival cannot be guaranteed. Thus, in order to give a boost to pancreatic islet micro- and macroencapsulation we intended to address the abovementioned limitations with the following specific goals.

1. To develop and validate an automatized microcapsules magnetic sorting system that can be monitored with the aim of eliminating the empty microcapsules generated during the microencapsulation process, thereby reducing the therapeutic graft volume of microcapsules used in Type 1 Diabetes Mellitus treatment.

1.1. To validate a microfluidic system for the magnetic separation of microcapsules containing Fe_3O_4 nanoparticles-labeled D1-MSK and D1-MSK-GFP cells.

1.2. To assess the cytotoxicity of Fe_3O_4 nanoparticles on islet-like cell aggregates (pseudoislets) generated from rat insulinoma INS1E β -cells.

1.3. To evaluate the purification yield, cell behavior and biological function of microencapsulated islets after magnetic separation.

1.4. To determine the capacity to reestablish the blood-glucose levels of magnetically purified versus non-purified microcapsules in a diabetic rat model.

2. To modulate the alginate gelation process by adding phosphate salts-based retardant agents in order to slow down the alginate gelling reaction, and achieve a tunable hydrogel with a better control over its gelation rate and physicochemical properties, thus facilitating the alginate hydrogels manipulation.

2.1. To characterize the gelation time and physicochemical properties of different alginate hydrogel formulations containing increasing concentrations of retardant agent (Na_2HPO_4).

2.2. To evaluate the biocompatibility of all different alginate formulations by studying the cell behavior and biological function of encapsulated rat insulinoma INS1E β -cells.

3. To develop a biocompatible, permeable and retrievable macroencapsulation device to confine the alginate hydrogel-islets scaffolds and achieve a strong mechanical protection, thereby improving the long-term integrity of the inner alginate hydrogel.

3.1. To generate several macroencapsulation devices with different external pore sizes and surface hydrophilicity/hydrophobicity degrees.

3.2. To evaluate the biocompatibility of the different microencapsulation devices following the ISO 10993-5, which set entails a series of standards for evaluating the biocompatibility of medical devices.

3.3. To determine which are the most suitable devices for rat insulinoma INS1E single- β -cells encapsulation through the evaluation of the cell behavior and biological function.

3.4. To evaluate the suitability of the selected devices (3.3. objective) to encapsulate islet-like cell aggregates (pseudoislets), generated from rat insulinoma INS1E β -cells, through the assessment of the cell behavior and biological function.



3

**Type 1 Diabetes Mellitus reversal
via implantation of magnetically
purified microencapsulated
pseudoislets**



Type 1 Diabetes Mellitus reversal via implantation of magnetically purified microencapsulated pseudoislets

A. Espona-Noguera^{1,2†}, J. Etxebarria-Elezgarai^{4†}, L. Saenz del Burgo^{1,2}, A. Cañibano-Hernández^{1,2}, H. Gurruchaga^{1,2}, F.J. Blanco^{7,8}, G. Orive^{1,2,3}, Rosa M. Hernández^{1,2}, F. Benito-Lopez⁵, J. Ciriza^{1,2}, L. Basabe-Desmonts^{4,6*} and J.L. Pedraz^{1,2*}

¹ NanoBioCel Group, Laboratory of Pharmaceutics, School of Pharmacy, University of the Basque Country UPV/EHU, Paseo de la Universidad 7, 01006, Vitoria-Gasteiz, Spain.

² Biomedical Research Networking Center in Bioengineering, Biomaterials, and Nanomedicine (CIBER-BBN), Vitoria-Gasteiz, Spain.

³ University Institute for Regenerative Medicine and Oral Implantology - UIRMI (UPV/EHU-Fundación Eduardo Anitua); BTI Biotechnology Institute, Vitoria-Gasteiz, Spain.

⁴ BIOMICS-microfluidics Research Group, Microfluidics Cluster UPV/EHU, University of the Basque Country, Spain.

⁵ AMMa LOAC Research Group, Microfluidics Cluster UPV/EHU, University of the Basque Country, Spain

⁶ Basque Foundation of Science, IKERBASQUE, Spain

⁷ INIBIC-Hospital Universitario La Coruña, La Coruña, Spain

⁸ Biomedical Research Networking Center in Bioengineering, Biomaterials and Nanomedicine (CIBER-BBN), La Coruña, Spain

[†] These authors contributed equally to this work

* Corresponding authors

ABSTRACT

Microencapsulation of pancreatic islets for the treatment of Type I Diabetes Mellitus (T1DM) generates a high quantity of empty microcapsules, resulting in high therapeutic graft volumes that can enhance the host's immune response. We report a 3D printed microfluidic magnetic sorting device for microcapsules purification with the objective to reduce the number of empty microcapsules prior transplantation. In this study, INS1E pseudoislets were microencapsulated within alginate (A) and alginate-poly-L-lysine-alginate (APA) microcapsules and purified through the microfluidic device. APA microcapsules demonstrated higher mechanical integrity and stability than A microcapsules, showing better pseudoislets viability and biological function. Importantly, we obtained a reduction of the graft volume of 77.5 % for A microcapsules and 78.6 % for APA microcapsules. After subcutaneous implantation of induced diabetic Wistar rats with magnetically purified APA microencapsulated pseudoislets, blood glucose levels were

restored into normoglycemia (< 200 mg/dL) for almost 17 weeks. In conclusion, our described microfluidic magnetic sorting device represents a great alternative approach for the graft volume reduction of microencapsulated pseudoislets and its application in T1DM disease.

Keywords: microcapsule sorting, alginate, superparamagnetic iron oxide nanoparticles, microfluidics, Type I Diabetes Mellitus

International Journal of Pharmaceutics. 2019 Apr 5;560:65-77

1. INTRODUCTION

Type 1 Diabetes Mellitus (T1DM) is a metabolic disorder characterized by the autoimmune destruction of the pancreatic β -cells and, subsequently, an absolute deficiency of insulin to maintain blood-glucose homeostasis [1, 2]. Currently, exogenous insulin injection is widely implemented being the most effective therapy. However, administration of insulin is onerous for the patients, since it is difficult for these formulations to avoid both hyperglycemia and hypoglycemia episodes, which can lead to diabetic complications [3,4]. Alternatively, the Edmonton protocol emerged as a promising method to restore the endogenous β -cell function, thus, normalizing the glucose metabolic control in patients with T1DM [5]. This procedure is based on the transplantation of isolated cadaveric pancreatic islets, thus providing a new β -cell source capable of assessing blood-glucose levels and secrete insulin in a glucose-dependent manner in T1DM patients. Although great successes have been achieved in the glucose homeostasis restoration, there are still several issues to overcome before the widespread clinical application. One of the main obstacle of islet transplantation is the long-term use of immunosuppressants to avoid the immune rejection of transplanted islets [4, 6, 7]. In order to circumvent this problem, pancreatic islets can be immunoisolated by microencapsulation techniques within a biocompatible matrix [8, 9].

The microencapsulation technology provides a physical barrier between the therapeutic cells and the host immune system, thus avoiding the entrance of high molecular weight immune components such as immunoglobulins and immune cells [10]. Moreover, the structure of the microcapsule permits the diffusion of nutrients and oxygen between the environment and the core of the microcapsule, while allowing the release of the therapeutic molecules produced by the embedded cells, as for example, insulin [11]. Among different biomaterials, such as poly(hydroxyethyl methacrylate-methyl methacrylate), agarose, chitosan, and polyethylene glycol (PEG); alginate is the most commonly used biomaterial in pancreatic islet microencapsulation [12]. This natural polymer has excellent properties for biomedical applications as it demonstrates high biocompatibility and low toxicity [13, 14]. Moreover, alginate microcapsules can be modified to tune their physical properties, like their mechanical and diffusion properties, which are critical to ensure their integrity and to allow the release of therapeutic molecules produced by the encapsulated cells, respectively [15, 16]. However, this technology has several technical obstacles that difficult its clinical application. One crucial problem is the high number of empty microcapsules generated during the islet microencapsulation process, leading to a high graft volume, which can enhance the host immune reaction after implantation [17]. Although the reduction of the graft volume is nowadays still being accomplished by separating the microencapsulated islets

from the empty microcapsules by hand selection, the manual procedure is tedious, slow, and complicates its reproducibility [8, 18-20]. On this regard, many microfluidic techniques for cell sorting have been proposed over the last decade, including active and passive sorting; the former being mostly employed [21, 22]. Active sorting can be categorized, according to the actuation mechanism, as electric, acoustic, magnetic, pneumatic and thermal sorting [21,23-25]. Among all, magnetic actuation is the most commonly used method in many applications [21, 22]. Different applications in which magnetic separation techniques and microfluidic devices have been implemented, in macro or mesoscale systems, including the extraction and concentration of magnetized porcine pancreatic islets from the digested pancreas that are previously magnetized *in vivo* [26], or the microencapsulation of pancreatic islets or other cells within microfluidic devices [27]. However, this application has not been used yet for the magnetic purification of magnetized microencapsulated islets from empty microcapsules. Overall, microfluidics systems constitute microscale platforms that enable the automatization and monitorization of the purification process. Importantly, these systems also minimize technical errors improving the reproducibility of the purification process. Moreover, as described by Temiz et al., the 3D printing technology enables the fabrication of complex microfluidic devices in a single-step, and allows the prototyping and low volume production of monolithic LOC devices for microfluidic applications, that do not require an additional sealing or microfluidic port integration step [28]. This facilitates the design conformation for the inlet/outlet connectors, as well as the integration of other components (e.g., magnets) with no need of any external packaging. Furthermore, 3D printing enables easy modifications of design features, accelerating the optimization stage of the microfluidic performance.

In this manuscript, with the aim of reducing the therapeutic graft volume in T1DM, we report a 3D printed magnetic sorting microfluidic device for the purification of microencapsulated pseudoislets. To this end, we combined the superparamagnetic iron oxide nanoparticles (SPIONs) and the microfluidic technologies. On the one hand, SPIONs provide magnetic properties to the pseudoislet-containing microcapsules that allow their separation, and, on the other hand, microfluidics offers the creation of a platform at microscale level that enables the purification process, its automatization and monitorization. For the validation of the device, we generated a pancreatic islet-like cell aggregates from the INS1E rat insulinoma cell line. After purifying the microencapsulated pseudoislets through the microfluidic device, different parameters were evaluated *in vitro* such as the viability, metabolic activity, insulin production and mechanical integrity of the purified and non-purified microcapsules. Then, the therapeutic potential of purified microencapsulated rat pancreatic pseudoislets was investigated in Wistar rats with induced T1DM.

2. MATERIAL AND METHODS

2.1. Materials and reagents

Ultrapure low-viscosity high guluronic acid sodium alginate (G/M ratio ≥ 1.5) with a molecular weight of 75–200 kDa was purchased from FMC Biopolymer (Sandvika, Norway), penicillin/streptomycin/glutamine (P/S/G) from Invitrogen (Carlsbad, United States), HEPES buffer from Lonza (Basilea, Switzerland), trisodium citrate dihydrate and sodium chloride (NaCl) from Panreac (Castellar del Vallès, Spain), and Rat Insulin ELISA kit from Mercodia (Uppsala, Sweden). Poly-L-lysine hydrobromide (PLL, 15–30 kDa), poly(ethyleneimine) solution (PEI), sodium pyruvate, β -mercaptoethanol, citric acid solution, the Cell Counting Kit 8 (CKK-8), potassium chloride (KCl), magnesium chloride ($MgCl_2$), calcium chloride ($CaCl_2$), bovine serum albumin (BSA), streptozotocin (STZ) and D-glucose were purchased from Sigma-Aldrich (San Luis, United States). Dulbecco's Modified Eagle's Medium (DMEM), Roswell Park Memorial Institute (RPMI) medium 1640, fetal bovine serum (FBS), penicillin-streptomycin (P/S) and LIVE/DEAD® Viability/Cytotoxicity Kit were purchased from Life Technologies (Carlsbad, United States).

2.2. Cell culture and INS1E pseudoislets formation

D1 mouse mesenchymal stem cells (D1-MSCs) (ATCC, USA) and engineered D1-MSCs to express the green fluorescence protein (GFP) (D1-MSCs-GFP) were grown in DMEM high glucose medium supplemented with 10 % FBS and 1 % of P/S as previously described [29]. Rat insulinoma INS1E cells provided by the University of Geneva Medical Center [30], were cultured in complete medium consisting of RPMI 1640 supplemented with 10 % FBS, 1 % P/S/G, 1 % sodium pyruvate 100 mM, 1 M HEPES buffer and 0.1 % mercaptoethanol. The INS1E cell line was used for pseudoislets formation by the hanging-drop method. Briefly, cells were trypsinized to obtain a cell suspension of 2.5×10^4 cells/mL, and 20 μ L droplets, containing 500 cells/droplet, were applied onto the lid of a 245x245 mm cell culture dish (Corning Incorporated, New York, United States). The lid was carefully flipped and placed onto the dish, which had been previously filled with distilled water to maintain humidity. Cells were cultured for five days to allow pseudoislet formation. Next, pseudoislets were harvested and transferred into a non-adherent 60mm culture dish (Corning Incorporated, New York, United States). All cells and pseudoislets were cultured in a humidified atmosphere containing 5 % CO_2 at 37 °C.

2.3. Synthesis of SPIONs and cell magnetization

The SPIONs used in this study were nanoparticles (NPs) of Fe_3O_4 /PEI that were

prepared by chemical co-precipitation as described by *Munoz de Escalona, et al.* [31]. Briefly, Fe_3O_4 NPs were re-dispersed in a 0.1 N citric acid solution, sonicated for 40 minutes and, finally, the dispersion was adjusted to pH 7 with 0.5 M NaOH. After that, SPIONs were coated by adding a PEI aqueous solution drop-wise to the iron oxide aqueous dispersion (3:4 ratio of PEI: Fe_3O_4) under mechanical stirring (2000 rpm). Then, the dispersion was neutralized again to pH 7 with 0.5 M HCl, and the NPs were magnetically washed by repeated separation from the liquid medium by a permanent 0.4 T magnet. Finally, NPs were resuspended in distilled water.

D1-MSCs-GFP were magnetized as described by *Megías, et al.* [29]. Briefly, NPs were diluted in complete culture medium and 10 mL added to a confluent T75 flask at a 11 μg of NPs/ 10^5 cells ratio. Then, the flask was placed onto a 0.4 T magnet for 15 minutes. Next, cells were detached and microencapsulated. On the other hand, INS1E pseudoislets in suspension were placed in a 60 mm culture dish with complete medium containing optimal NPs concentration and incubated for 24 hours to magnetize the pseudoislets.

2.4. Microencapsulation

For microencapsulation, sterile 1.5 % (w/v) sodium alginate solution was prepared in a 1 % (w/v) mannitol solution. Then, it was filtered through a 0.22 μm pore Minisart Syringe Filter (Sartorius, Gotinga, Germany). Afterward, cells were suspended in the alginate solution at a cell density of 5×10^6 cells/mL or 2000 pseudoislets/mL. These suspensions were extruded in an electrostatic droplet generator (Nisco Engineering, Duluth, United States) through a 0.17 mm inner diameter needle using a 10 mL sterile syringe with a peristaltic pump at 5.9 mL/h flow rate. Microcapsules were collected in a 55 mM CaCl_2 bath and maintained in agitation for 10 minutes to obtain the alginate (A) microcapsules. Next, microcapsules were chemically crosslinked with 0.05 % (w/v) PLL for 5 minutes, and then, they were coated with 0.1 % (w/v) alginate for 5 minutes, giving rise to alginate-poly-L-lysine-alginate (APA) microcapsules. All procedures were performed at room temperature, under aseptic conditions. Microcapsules were cultured in the correspondent complete medium at 37 °C in a 5 % CO_2 atmosphere.

2.5. Fabrication of the cell sorting microfluidic device

The magnetic purification device was designed using PTC Creo Parametric 3D modeling Software and manufactured in a Formlab stereolithography 3D printer (Formlabs, Somerville, United States) using an optically clear acrylic material, Clear resin FLGP CL02 (Formlabs, Somerville, United States), and a 50 μm printing resolution. The printed

parts were rinsed in an isopropanol bath for 4min to eliminate the excess of uncured resin, and subsequently, post-cured under 365 nm UV light for 15 minutes to ensure complete polymerization and reach the highest strength and stability for the parts. Supports were removed using a snip, and the parts were gently sand polished to assure transparent and high-quality polymeric parts. Finally, the chip was finalized by covering the top channel with a pressure sensitive PSA AR-MH-92712 adhesive (Adhesive Research, Limerick, Ireland). Figure 2a exhibits the finalized microfluidic magnetic cell sorting device for purification of the magnetized-microcapsules. The device integrates commercial neodymium magnets of 1.3 T (Supermagnete, Gottmadingen, Germany) with a magnetic clamping force of 10.8 N for the 5 mm x 5 mm magnet, and 6.86 N for the 5 mm diameter x 3 mm height magnet. Thereby, while the magnetized capsules are envisioned to move to the upper channel due to the magnetic field, the empty capsules will be divided equally between both channels, leading to a separation of non-magnetized capsules that allows recovery of highly concentrated magnetized samples in the upper outlet.

2.6. Setup for microfluidic microcapsules sorting

The characterization of microcapsules purification was carried out with A microencapsulated non-magnetized D1-MSCs (non-mag-D1-MSCs) and magnetized D1-MSCs-GFP (mag-D1-MSCs-GFP). Both types of microcapsules were mixed at different mag-D1-MSCs-GFP/non-mag-D1-MSCs ratios (5/95, 10/90, 25/75, 50/50, 75/25) to evaluate the purification performance at each condition. The setup for the characterization of the purification involved: 1) a positive pressure flow controller (Fluigent MFCSTM FLEX) to drive the liquid through the microfluidic device; 2) a microscope and 3) a fluorescent reader (FluoroReader®, Elveflow) to analyze the distribution of the mag-D1-MSCs-GFP microcapsules in situ (Figure 1A). Fluorescence at the outlet of the channels was displayed in real time in order to monitor the deviation of mag-D1-MSCs-GFP from the purification channel. Additionally, the purification efficiency for different conditions was quantified by flow cytometry. Briefly, non-purified and purified microcapsules from each condition were dissolved in 1 % trisodium citrate dihydrate. Then, cells were collected by centrifugation, rinsed with DPBS, and transferred to a FACS tube. The proportion of mag-D1-MSCs-GFP and non-mag-D1-MSCs after purification was analyzed for all samples using the BD FACS Calibur flow cytometer (BD Bioscience, Franklin Lakes, United States). Three independent experiments, with three replicates each one, were conducted.

The purification of A and APA microencapsulated INS1E pseudoislets was carried out under sterile conditions by placing the setup within a laminar flow cabinet after ethanol

and UV light sterilization. The setup was similar than the one used in the separation of non-mag-D1-MSCs and mag-D1-MSCs-GFP; but instead of a fluorescent reader, a microscope with an integrated camera (ISH500 Tucsen Photonics) and a TCapture software application (ISCapture, Tucsen Photonics) were used for real-time monitorization of the purification process (Figure 1B).

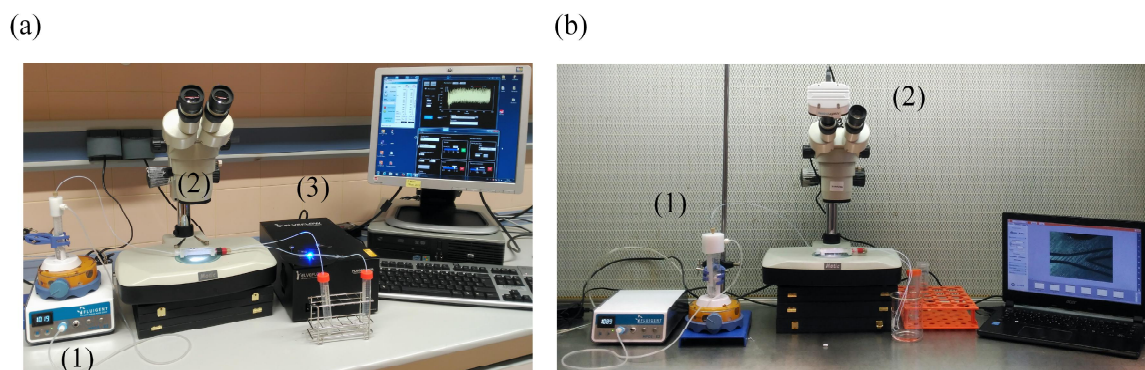


Figure 1. (a) Experimental setup for the optimization of microfluidic magnetic cell sorting flow conditions comprised of a positive pressure flow controller (1), a microscope with an integrated camera (2) and a fluorescent reader (3). (b) Experimental setup for microfluidic magnetic purification of INS1E, in sterile conditions, comprised of a positive pressure flow controller (1) and a microscope with an integrated camera (2).

Also, the purification efficiency after separation was determined by measuring the 24 hours secreted insulin from the non-purified and purified samples. Briefly, 50 μL of microcapsules from each sample were rinsed twice with medium, resuspended in 0.5 mL of medium, and incubated for 24 h at 37 $^{\circ}\text{C}$ and 5 % CO_2 . The insulin content of collected supernatants was quantified with the Rat Insulin ELISA kit following the manufacturer's recommendations. Three independent experiments, with three replicates each one, were conducted.

2.7. Cell metabolic activity and viability determination

Metabolic activity was determined using the Cell Counting Kit 8 (CCK-8). During the optimization of the pseudoislets magnetization process, 50 magnetized pseudoislets were harvest after 24 hours of incubation with different NPs concentrations (5, 10, 20, 40, 80, 160, 320 and 640 μg of NPs/mL), and resuspended in 500 μL of complete medium containing 50 μL of CCK-8 reagent, placed in a 500 μL conical tube and incubated in a shaker for 4 hours at 37 $^{\circ}\text{C}$ into the incubator. The supernatants were collected, transferred into a 96 well-plate, and the absorbance was read out on an Infinite M200 TECAN plate reader (TECAN Trading AG, Männedorf, Switzerland) at 450 nm with a reference wavelength set at 650 nm. Control tests were carried out similarly incubating the pseudoislets in complete medium without NPs.

To study the metabolic activity of the purified microencapsulated pseudoislets, 50 μL of microcapsules were resuspended in 150 μL of complete medium with 15 μL of CCK-8 reagent, plated in a 96-well plate, incubated, and the absorbance was read following the same procedure previously described. Non-purified encapsulated pseudoislets were used as controls. Three independent tests were conducted for each condition.

On the other hand, cell viability was determined by fluorescence microscopy, and structural integrity of the microcapsules was determined by bright field microscopy. With this aim, 25 μL of purified encapsulated pseudoislets were stained with the LIVE/DEAD® Viability/Cytotoxicity Kit. First, the microcapsules were washed twice with DPBS. Then, they were resuspended in 200 μL of 0.5 μM calcein AM, and 0.5 μM ethidium homodimer-1 in DPBS and, finally, microcapsules were transferred into 96-well plates and incubated at room temperature for 40 minutes in the dark. Next, samples were observed under a Nikon TMS microscope with the excitation/emission settings for calcein AM staining (495/515nm) and ethidium homodimer staining (495/635nm). The images of fluorescence and brightfield microscopy were acquired with a Nikon Eclipse TE2000-Scamera (Nikon, Amsterdam, Netherlands), which was controlled by the EclipseNet software version 1.20.0, and at least three independent experiments were analyzed.

2.8. Glucose-Stimulated Insulin Secretion

In order to assess the microencapsulated pseudoislets insulin secretory capacity, the Glucose-Stimulated Insulin Secretion assay (GSIS) was performed 24 hours after magnetic purification. 50 μL of purified and non-purified microcapsules were washed four times with Krebs-Ringer bicarbonate (KRB) buffer composed of 125 mM NaCl, 3 mM KCl, 0.85 mM CaCl_2 , 1.3 mM MgCl_2 , 0.1 % BSA and 25 mM HEPES buffer. After washing, microcapsules were incubated at 37 °C in the incubator in KRB buffer for 1 hour with shaking. Next, KRB buffer was replaced with KRB containing 3.3 mM glucose and incubated for 2 hours (low glucose condition). Supernatants were collected, and the samples were washed with KRB four times again. Next, they were incubated for 2 hours in KRB containing 16.6 mM glucose (high glucose condition), and supernatants were collected. The insulin secretion for 24 hours from culture supernatants was determined at days 1, 7, 21 and 28 after magnetic separation. At each timepoint, 50 μL of microcapsules were rinsed twice with medium, resuspended in 0.5 mL of medium, and incubated for 24 h at 37 °C and 5 % CO_2 . Then, supernatants were collected. The insulin content of collected supernatants was quantified with the Rat Insulin ELISA kit following the manufacturer's recommendations. Three independent experiments, with three replicates each one, were conducted.

2.9. Induction of Diabetes *in vivo* and implantation of pseudoislets-containing microcapsules

Male Wistar rats of 150-200 g from ENVIGO (Sant Feliu de Codines, Spain) were housed with sterile food and autoclaved water. Six days before implantation of microencapsulated pseudoislets, diabetes was induced by a single intravenous injection of 80 mg/kg body weight of STZ diluted in 50 mM sodium citrate buffer. Animals were considered diabetic if blood glucose exceeded 20 mmol/L (> 360 mg/dL) for at least two consecutive measurements. Then, diabetic rats were divided into 4 groups. The first group was implanted subcutaneously with 0.4mL from the purified microcapsules pool, containing 3000 microencapsulated equivalent pseudoislets/rat, suspended in 1mL PBS using an 18-gauge catheter; the second group was implanted with the same volume of microcapsules from the non-purified pool; the third group received the same volume of empty microcapsules (without cells), and in the fourth group (negative control) diabetic animals were not implanted. Non-diabetic rats were monitored in parallel as controls of glycemia too. During implantation, animals were maintained under anesthesia by isoflurane inhalation. Blood samples were collected from the tail vein to measure blood glucose levels with a glucometer (Abbott Laboratories, Chicago, United States), during the first week every 24 h and afterward, weekly. Animals were also weighted daily during the first week after implantation, then twice per week and, at the end of the study, weekly. All the experimental procedures were performed in compliance with protocols approved by the institutional animal care and use committee of the University of Basque Country UPV/EHU (Permit Number: M20_2016_082_CIRIZA ASTRAIN).

2.10. Glucose tolerance test

A glucose tolerance test (GTT) was performed two months after microcapsules implantation. A dose of 2 g glucose/kg bodyweight was administered intraperitoneally to rats after 12 hours fasting, and blood glucose levels were measured at 0, 0.5, 1, 1.5, 2, 2.5, 3, 4, 5, 6 and 7 h after glucose challenge using a glucometer.

2.11. Immunohistochemistry

Animals from each group were sacrificed by CO₂ inhalation and, the implants were retrieved and fixed with 4 % formaldehyde (Panreac, Castellar del Vallès, Spain) for histological analyses. Serial horizontal cryostat sections (14 µm) were processed for hematoxylin and eosin or Masson's trichrome (H&E) staining. Photographic images were

taken using a Nikon D-60. Microscopy sections were examined by an expert pathologist blinded to the treatments. The presence and distribution of infiltrating cells, and preservation of the tissue along with the extension of fibrosis were evaluated.

2.12. Statistical analysis

Statistical analysis was performed with SPSS software, version 21.00.1. Data were expressed as means \pm standard deviation, and differences were considered significant for comparison of groups using ANOVA, Tukey's Post Hoc Test when $p < 0.05$ after assessing their normal distribution. Kaplan-Meier cumulative survival analysis was used to determine the animal survival of each group of study after transplantation.

3. RESULTS AND DISCUSSION

3.1. Optimization of microfluidic device design and flow conditions for microcapsules purification

The microfluidic pathway within the device consisted in a "Y" shape configuration, a main channel 36 mm long which split in two channels 37 mm long. The design integrated commercial neodymium magnets located in parallel to the main channel close to the bifurcation in order to trigger the movement of the magnetized capsules to the upper channel due to the magnetic field. The empty capsules were expected to be divided equally between both channels, leading to a separation of non-magnetized capsules that allows recovery of highly concentrated magnetized samples in the upper outlet (Figure 2A-B).

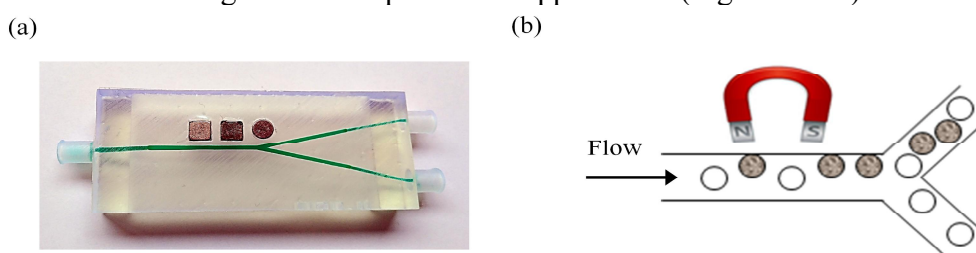


Figure 2. (a) 3D printed microfluidic chip sealed with a pressure sensitive adhesive, integrating commercial magnets. The chip has been filled with green-colored solution to highlight the internal channels. (b) Working principle of the magnetic separation of the microcapsules: while the magnetized-microcapsules move to the upper channel due to the force generated by the magnet, the empty capsules divide equally between both channels.

For setting up the magnetic sorting device and the purification performance, D1-MSCs-GFP cells were magnetized (mag-D1-MSCs-GFP), while D1-MSCs cells were not magnetized (non-mag-D1-MSCs), next generating microcapsules from both populations, representing microcapsules containing islets and empty microcapsules.

Different parameters were studied, such as distinct device architectures and magnet configurations. Variations on the microfluidic channel dimensions and the position of the connectors for the inlet and outlet tubings were analyzed, as well as the magnets configuration, the use of different fluid pressure conditions and distinct microcapsules concentrations. Initially, the connectors and tubings were arranged perpendicularly to the main microfluidic channel (Figure 3A), which resulted in changes in the direction of the flow due to elbows inside the microchannels, that influenced on the local resistance and generated sudden local velocity decrease, decelerating and accumulating the microcapsules at a certain point, and causing clogging issues. This problem was resolved when the connectors were arranged in parallel to the main fluidic channel (Figure 3B). Similar effects were observed by *Li et al.* [32], who investigated the flow performance of a cell suspension near the chip inlet area and compared the different performances when using vertical and parallel inlet connectors. Vertical inlet connectors comprised larger dead volumes and initial impact driven by the vertical direction of hydrodynamic force, resulting in flow irregularities near the inlet area and formation of cell blockages, which is especially detrimental to experiments that require recovery of purified cells. In contrast, parallel inlets alleviated channel blockage caused by large dead volume and irregular flow directions [32]. The parallel configuration of the connectors was possible due to the fabrication flexibility provided by the 3D printing technique in comparison with more traditional fabrication techniques to generate microfluidic devices such as photolithography or PDMS casting [33].

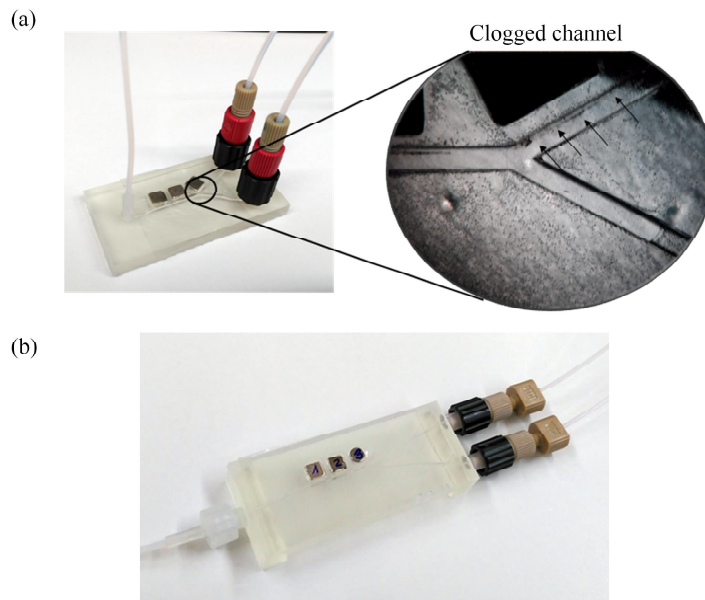

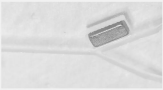



Figure 3. Optimization of the design and architecture of the magnetic separation device. (a) Image of a microfluidic sorting device prototype with perpendicular inlets and outlets connectors clogged by microcapsules. (b) Final 3D printed microfluidic sorting device with the optimal inlets and outlets connectors design, magnets positioning and configuration avoiding microcapsules clogging. Black arrows: microcapsules clogging the microchannel.

Regarding the dimensions of the microchannels, the best flow containing microcapsules through the microfluidic device, with no clogging issues, was obtained when using the main channel of 1 mm x 1 mm cross-section, which splits in two channels of 750 μm x 750 μm cross section (Table 1). In this way, alginate microcapsules with an average diameter of 450 μm were satisfactorily driven through the microchannels. In addition, a balance between the magnetic field and the flow velocity inside the microchannels was essential to provide a high-throughput purification system and increase the purification efficiency and yield. Different shapes and number of magnets were analyzed for various fluidic pressures (Table 1).

Table 1. Experimental results obtained during the optimization of the purification system design and operation conditions.

Architecture / Design			
Microchannels dimensions	Purification Result		Comments
Main channel: 700 μm x 700 μm Bifurcated channels: 575 μm x 575 μm	✗		Channels clogged due to a high ratio of the particle to the channel size
Main channel: 1 mm x 1 mm Bifurcated channels: 750 μm x 750 μm	✓		Appropriate particle to channel size ratio
Inlet/outlet connectors conformation	Purification Result		Comments
Vertical connectors	✗		Clogging of the channels near inlet and outlet connectors
Parallel connectors	✓		-
Magnetic Force / Flow conditions			
Magnets Configuration	Flow rate ($\mu\text{L}/\text{min}$)	Purification Result	Comments
5 x 5 x 5 mm (3 units) 	50-100	✗	Too high magnetic force for the employed flow rates. Retention of microcapsules near magnets, leading to clogging.
	200	✗	Too high flow rate. Clogging occurs in the constriction of the outlet channels
10 x 3.5 x 2.25 mm (1 unit) 	50-60	✗	Appropriate separation of microcapsules, but too low flow rates. Clogging in bifurcated channels.
	75-100	✗	Poor balance between magnetic force and flow rate. High loss of magnetized microcapsules
5 x 5 x 5 mm (2 units) D=5 mm, H=3 mm (1 unit) 	50-75	✗	Too low flow rate, occasionally clogging occurs
	100	✓	Successful purification Optimal ratio of magnetic force to flow rate
	200	✗	Too high flow rate. Clogging occurs in the construction of the outlet channels

On the one hand, employing inappropriate balances of too high magnetic forces and too low fluid velocities, in general, led to the retention of the magnetized microcapsules near the bifurcation of the split channels, clogging the outlet channel and the whole purification. On the other hand, low magnetic forces required low flow rates to ensure successful separation of magnetized microcapsules, but this led to a reduced movement of the microcapsules after the bifurcation, clogging the microchannels. For this reason, the optimal configuration consisted of three magnets; two with rectangular shape (5 mm x 5 mm x 5 mm) and a smaller circular magnet (5 mm diameter and 3 mm height), generating a total magnetic clamping force of around 28.5 N. For this magnetic force, fluid velocities at 50, 60, and 75 mbar fluidic pressures, led to the retention of the magnetized microcapsules near bifurcation of the split channels, while higher fluidic pressures (200 mbar) resulted in accumulation of the capsules in the constriction of the outlet channels, again clogging the whole microfluidic system, resulting 100 mbar the optimal fluidic pressure.

When the design of the microfluidic device was optimized, we proceeded to optimize the particle concentration for its purification through the device. According to Dresaire et al., the clogging dynamic is controlled by the concentration of large particles and the flow rate in the channel. In case of high flow rates, for example, clogging of a channel can be caused by the simultaneous arrival of particles that plug the cross-section of the channel, typically at the inlet/outlet or at a constriction. The clogging probability increases with the particle concentration, with the flow rate and with the ratio of the particle to the channel size [34].

Different microcapsules suspensions were prepared diluting different amounts of microcapsules suspensions in 30mL of cell culture media. Dilutions of 5, 2, 1, 0.5 mL of microcapsules/30mL of media were prepared, resulting in final capsules concentrations of $465 \cdot 10^3$, $186 \cdot 10^3$, $93 \cdot 10^3$ and $46 \cdot 10^3$ microcapsules/mL respectively. Those samples were processed through the microfluidic device and then analyzed. Microcapsules concentrations higher than $93 \cdot 10^3$ microcapsules/mL resulted in the accumulation of microcapsules in the inlets of the microfluidic device, thus blocking the sample flow. However, at 1/30 and 0.5/30 mL of microcapsules/mL of media, microcapsules were able to flow through the microfluidic channels while the generated magnetic field promoted the separation of the mag-D1-MSCs-GFP from non-mag-D1-MSCs microcapsules, attracting the mag-D1-MSCs-GFP microcapsules towards the top outlet channel, while splitting equally towards both outlet channels the non-mag-D1-MSCs or empty microcapsules (supplementary material, Video 1 and 2).

Hence, the final microfluidic device design consisted in a main channel of 1 mm x 1mm cross-section, which split in two channels of 750 μ m x 750 μ m cross section where the inlet and outlet connectors were arranged in parallel to main fluidic channel; a magnet

configuration of three magnets strategically placed alongside the main microfluidic channel, two with rectangular shape (5 mm x 5 mm x 5 mm) and an smaller circular magnet (5 mm diameter and 3 mm height) placed near the bifurcation; and using a pressure of 100 mbar imposed across the whole system, which generated a flow rate of 1.3 mL/min with a microcapsules dilution of 1 mL of microcapsules/30 mL of media.

3.2. Characterization of the magnetic purification performance

Once the optimal device design and working conditions were determined, the performance of the purification system depending on the ratio of the magnetized microcapsules respect to the non-magnetized was studied. Different mag-D1-MSCs-GFP/non-mag-D1-MSCs ratios were evaluated (5/95, 10/90, 25/75, 50/50, 75/25) with special attention to the lower ratios 5/95 and 10/90, which are similar to the pancreatic islets-containing microcapsules/empty microcapsules proportion after microencapsulation of real islets in preclinical studies.

First, the green fluorescence from mag-D1-MSCs-GFP microcapsules at the outlet of the channels was displayed, in situ and in real-time, monitoring the loss of magnetized-microcapsules that diverted from the purification channel. The fluorescent readouts from both outlet channels showed that most of the mag-D1-MSCs-GFP microcapsules were attracted towards the magnets and driven through the top channel (Figure 4A), and a few of them were diverted towards the bottom channel (Figure 4B).

Second, the non-purified samples and the purified microcapsules collected from the magnet channel were quantified by flow cytometry, for each concentration ratio, in order to determine the efficiency of the purification. Flow cytometry results showed that, after the purification, the concentration of the mag-D1-MSCs-GFP microcapsules increased for all the suspensions isolated from the top channel in comparison with the non-purified samples (Figure 4C). The increase in the mag-D1-MSCs-GFP concentration in the different mag-D1-MSCs-GFP/non-mag-D1-MSCs ratios relies on the elimination of the non-mag-D1-MSCs microcapsules during the purification step. Thereby, the concentration of the mag-D1-MSCs-GFP microcapsules was highly increased for the lowest ratios, due to a larger amount of empty microcapsules, achieving an increase of mag-D1-MSCs-GFP percentage from $5.1 \pm 0.36\%$ to $8.6 \pm 1.02\%$, which supposed a purification yield of $80 \pm 7.1 \%$ for the 5/95 ratio sample. In contrast, the concentration increase was not so prominent for high initial ratios, obtaining a purification yield of $33.3 \pm 3.95 \%$ for the 75/25 ratio sample.

Finally, a sample with an initial ratio of 5/95 mag-D1-MSCs-GFP/non-mag-D1-MSCs microcapsules, envisioned to mimic a real scenario of pancreatic islets-containing

microcapsules together with a huge number of empty microcapsules, was successively circularized three times through the magnetic sorting device. The mag-D1-MSCs-GFP concentration was considerably increased, from $5.14 \pm 1.01\%$ to $35.23 \pm 3.4\%$, thus obtaining a highly concentrated mag-D1-MSCs-GFP microcapsules pool with 6.91 ± 0.55 times more presence of mag-GFP-D1-MSCs in the purified sample compared to the non-purified sample (Figure 4D). Therefore, in this case, a theoretical implantation volume of 10 mL on microcapsules could be reduced 6.91 times to a final implantation volume of 1.48 mL, which would mean an implantation volume reduction of 85.2 %.

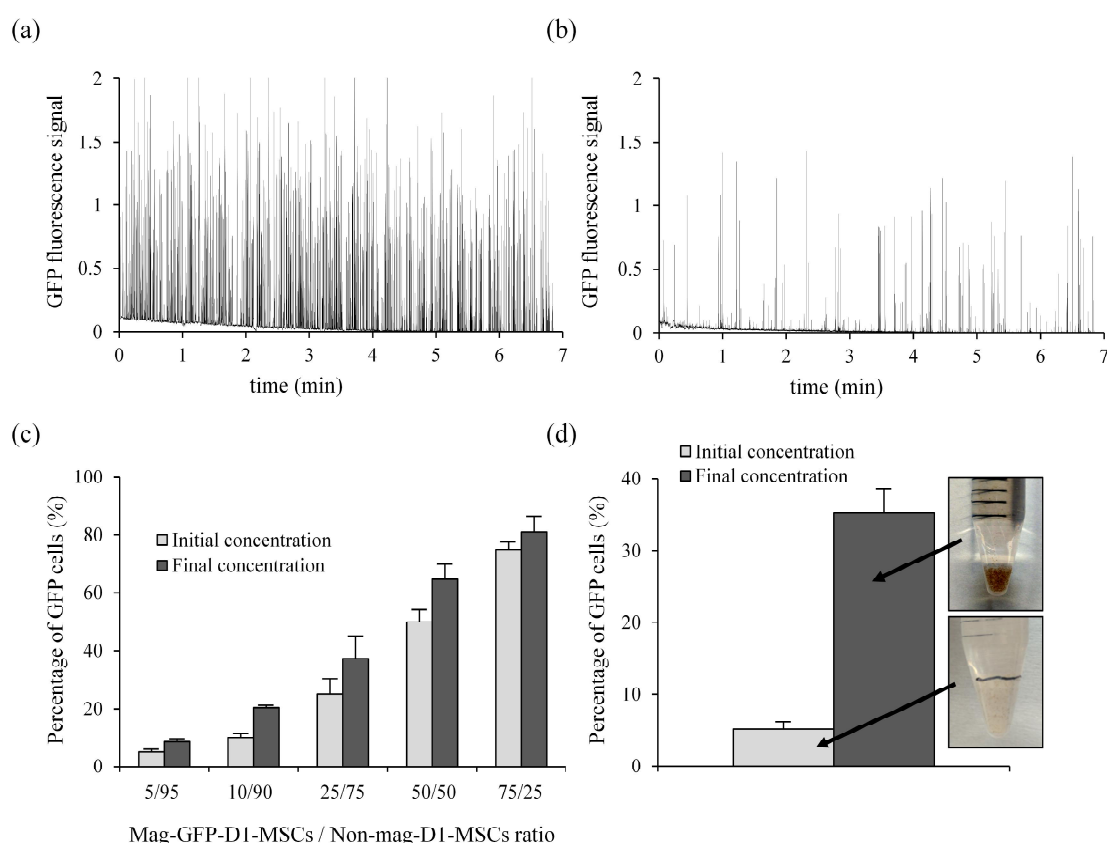


Figure 4. Optimization of the purification flow conditions for the microfluidic magnetic cell sorting, using mag- D1-MSCs-GFP and non-Mag-D1-MSCs microcapsules. (a) Fluorescent readouts obtained for the top and, (b) bottom outlet tubings. (c) Flow cytometry analysis of non-purified and purified microcapsules from different samples mixtures at different mag-D1-MSCs-GFP/non-mag-D1-MSCs ratios. (d) Flow cytometry analysis of the non-purified and purified microcapsules after 3cycles through the sorting device, for a sample with a 5/95 mag-D1-MSCs-GFP/non-mag-D1-MSCs ratio.

3.3. Determination of the optimal conditions for pseudoislets magnetization

The preservation of pseudoislet viability and the conferring of magnetic motion after magnetization are crucial factors for future *in vivo* studies and clinical applications. For that reason, we evaluated the toxic and motion effect of $\text{Fe}_3\text{O}_4/\text{PEI}$ NPs concentration on

INS1E pseudoislets after magnetization. To that end, pseudoislets were exposed to different Fe₃O₄/PEI NPs concentrations (0, 5, 10, 20, 40, 80, 160, 320 and 640 µg/mL) for 24 h. No significant influence on pseudoislet metabolic activity was detected after exposing to 5, 10, 20, 40 and 80 µg Fe₃O₄/PEI NPs/mL conditions, compared to non-magnetized pseudoislets used as controls (Figure 5). However, at higher concentrations, a dose-dependent cytotoxicity was observed with a significant reduction in the metabolic activity of pseudoislets of 30.9 % for 160 µg Fe₃O₄/PEI NPs/mL, 80.6 % for 320 µg Fe₃O₄/PEI NPs/mL and, 87.5 % for 640 µg Fe₃O₄/PEI NPs/mL ($p < 0.001$). Cell viability of different cell types, such as A3 human T lymphocytes and Sprague-Dawley rat smooth muscle cells, are also not affected after 24 hours incubation at low magnetic NPs concentrations (5-100µg magnetic NPs/mL), with reduced viability at higher concentrations [35, 36]. Hence, due to this detected dose-dependent cytotoxicity, higher concentrations than 80 µg Fe₃O₄/PEI NPs/mL were not used in the following experiments.

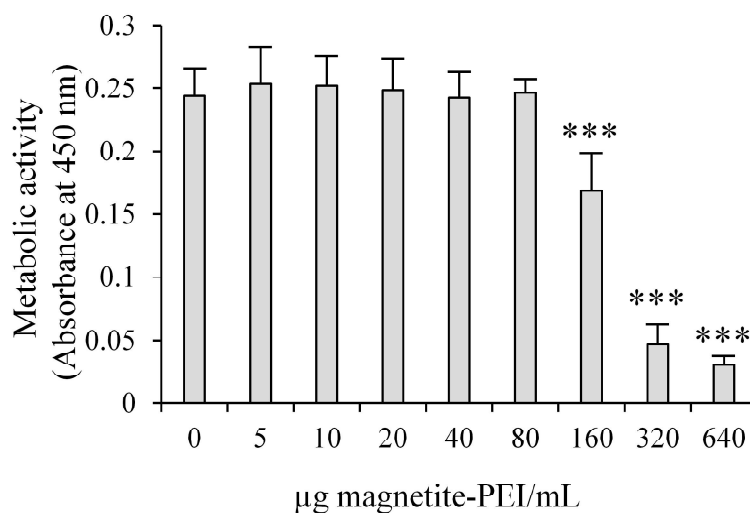


Figure 5. Metabolic activity of INS1E pseudoislets after incubation with different concentrations of Fe₃O₄/PEI nanoparticles for 24 h. Values represent mean \pm SD. ***: $p < 0.001$ compared to control incubated without Fe₃O₄/PEI nanoparticles.

The magnetic NPs concentration used in the magnetization step should be enough to give the pseudoislets sufficient magnetic properties to allow the displacement of the microcapsules during the purification process. Using 40 and 80 µg Fe₃O₄/PEI NPs/mL, appropriate magnetic properties were provided to pseudoislets, since motion was detected when a magnetic field was applied, by placing a magnet next to the petri dish, with higher mobility of the pseudoislets that had been incubated with 80 µg Fe₃O₄/PEI NPs/mL. Likewise, in other studies, porcine pancreatic islets have been magnetized with 100 µg magnetic NPs/mL without affecting their viability and being magnetically directed as desired when a

magnetic field was applied. Also, they had been imaged and tracked when implanted *in vivo* by magnetic resonance imaging (MRI) [26, 37]. In our studies, both 40 and 80 $\mu\text{g Fe}_3\text{O}_4/\text{PEI}$ NPs/mL concentrations were able to confer magnetic motion to the pseudoislets. However, after microencapsulation, the magnetized pseudoislets should be able to displace the whole microcapsule through the microfluidic device towards the magnetic channel. Regarding the biosafety of the use of SPIONs, it is well known that, at appropriate concentrations, they do not display cytotoxic effects; besides, magnetic nanoparticles are metabolized in the lysosomes after intracellular uptake and used in the production of hemoglobin and transferrin becoming part of the normal iron metabolism pathway of the body [38]. Therefore, in our approach, the magnetic nanoparticles inside the microcapsules will not have any contact with the surrounding tissue at the implantation site and will be metabolized by the encapsulated pseudoislets, thereby ensuring great biosafety.

Overall, since the 80 $\mu\text{g Fe}_3\text{O}_4/\text{PEI}$ NPs/mL concentration demonstrated to provide higher mobility to the pseudoislets, this concentration was chosen for the subsequent pseudoislets magnetization and purification processes.

3.4. *In vitro* evaluation of microencapsulated pseudoislets after microfluidic purification

Two different types of microcapsules for encapsulated magnetized pseudoislets were studied: alginate microcapsules (A) and alginate-poly-L-lysine-alginate (APA) microcapsules. Both types of microcapsules display different key physical properties, mechanical strength, and macromolecules diffusion, which are crucial for the microcapsules integrity during the magnetic sorting and the pseudoislet insulin release after purification. A microcapsules provide higher diffusion rates than APA microcapsules, since the PLL coating reduce the porosity of the microcapsule surface, thus potentially affecting the diffusion of the therapeutic molecules secreted by the microencapsulated cells such as insulin. However, the PLL coating in APA microcapsules confers higher mechanical strength [39, 40], a crucial characteristic that they need to fulfill in order to avoid their breakage during the high mechanical stress generated in the magnetic purification process. Hence, A microcapsules are good candidates for pseudoislets microencapsulation in terms of better insulin diffusion, while APA microcapsules are good candidates in terms of higher mechanical stability.

After pseudoislets microencapsulation at a density of 2000 pseudoislets/mL of alginate, we performed the magnetic purification with three recircularization steps, collecting microcapsules from the magnetic channel (purified microcapsules). Samples from the non-purified and purified microcapsules were evaluated under the brightfield microscope (Figure 6A-B). Many empty microcapsules were observed in the non-purified sample (Figure 6A),

with a higher presence of microencapsulated pseudoislets in the purified sample (Figure 6B). It was evidenced that the pseudoislets featured the expected magnetic properties and enabled the motion of the microcapsules towards the magnets placed on the microfluidic device, allowing their purification. Besides, microcapsules endured the mechanical stress suffered during the purification process, keeping their spherical shape while maintaining intact the pseudoislets.

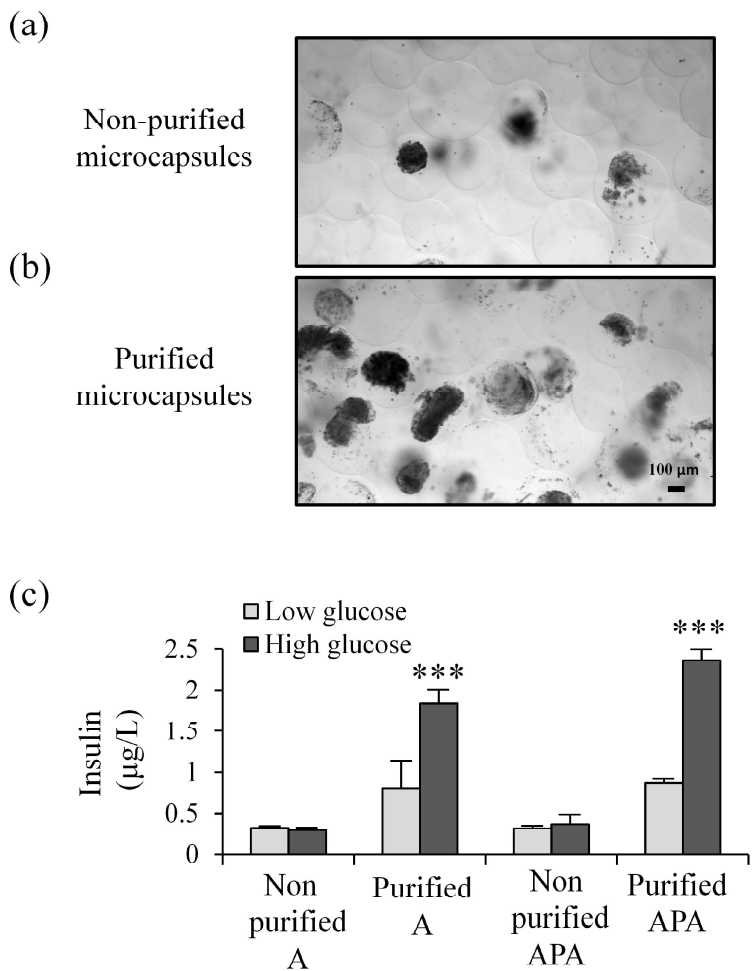


Figure 6. (a) Representative brightfield microphotographs of microencapsulated pseudoislets directly after encapsulation (non-purified microcapsules) and (b) after 3 recircularized magnetic separations (purified microcapsules). (c) Glucose-stimulated insulin secretion of A and APA microencapsulated INS1E pseudoislets before and after 3 recircularized magnetic separations. Values represent mean \pm SD ***: $p < 0.001$ compared to low glucose condition.

Next, the biological function of A and APA microencapsulated pseudoislets after purification was analyzed. For this purpose, the insulin secretory response to glucose challenges was evaluated after exposing non-purified and purified A and APA microcapsules to low and high glucose concentrations (3.3 mM and 16.7 mM, respectively) (Figure 6C). For the non-purified samples, insulin levels were almost below the lower detection limit, and no

significant differences were observed between low and high glucose conditions, probably due to the very low presence of microencapsulated pseudoislets. However, purified A and APA samples showed higher insulin levels. These results evidenced the capacity of both types of microcapsules for insulin production and release. Regarding the glucose responsiveness of the encapsulated pseudoislets, the secretion of insulin at high-glucose stimulus increased significantly compared to low-glucose stimulus ($p < 0.001$) both in A and APA purified samples, with similar insulin folding between high and low conditions: 2.52 ± 0.52 and 2.71 ± 0.16 times more insulin secreted in high glucose than in low glucose conditions, for A and APA microcapsules, respectively. Therefore, purified $\text{Fe}_3\text{O}_4/\text{PEI}$ NPs-conjugated pseudoislets maintained their capacity to secrete insulin as well as the glucose responsiveness within both A and APA microcapsules after the purification process.

We also quantified the insulin secretion from purified and non-purified A and APA microcapsules over the time, which allowed to estimate the purification efficiency just after purifying and assess the evolution of insulin production over time for 28 days. The insulin secretion ratio (purified/non-purified samples) of each time point were compared between A and APA microencapsulated pseudoislets (Figure 7A). Comparing these ratios, at day 1, similar insulin folding for A and APA microcapsules were obtained, 4.43 ± 0.59 and 4.67 ± 0.9 respectively, which entails a volume reduction of 77.5 % for A microcapsules and, 78.6 % for APA microcapsules with respect to each non-purified sample. The values for APA microcapsules remained stable with average insulin secretion ratio values between 4.2-4.6 during the length of the study, but the insulin ratio from A microcapsules decreased during the first three weeks compared to APA microcapsules; from initial average insulin ratios of 4.4 to final values of 3.2. Comparing both groups, we detected statistically significant differences at the end of the study, when the ratio values from A microcapsules were lower than those from APA microcapsules ($p < 0.01$, at day 20, and $p < 0.05$, at day 28). These differences between purified/non-purified A and APA microcapsules insulin ratios correlated with their metabolic activity, where purified A microcapsules showed significant lower metabolic activity values at day 28 compared to APA microcapsules ($p < 0.01$) (Figure 7B). To explain these results, microcapsules physical integrity and cell viability of A and APA purified samples were analyzed over time under brightfield and fluorescence microscope (Figure 7C). Pseudoislets from both types of microcapsules showed cell death at day 1 on the surface of the pseudoislets due to the mechanical stress suffered during the microencapsulation process. The analysis of A microcapsules under brightfield displayed some unencapsulated small cell aggregates at day 1, which were more abundant at the end of the study (day 21 and 28 after purification). Moreover, the microscopy analysis unveiled that the pseudoislets growth inside A microcapsules provoked an excessive internal mechanical stress that led

to the progressive breakage of these microcapsules. This progressive A microcapsules rupture released pseudoislets and, subsequently, the unprotected pseudoislets fragmented into smaller cell aggregates due to the mechanical stress when manipulated for microscopy analysis. Increasing amounts of fragmented pseudoislets were observed from day 1 till the end of the study.

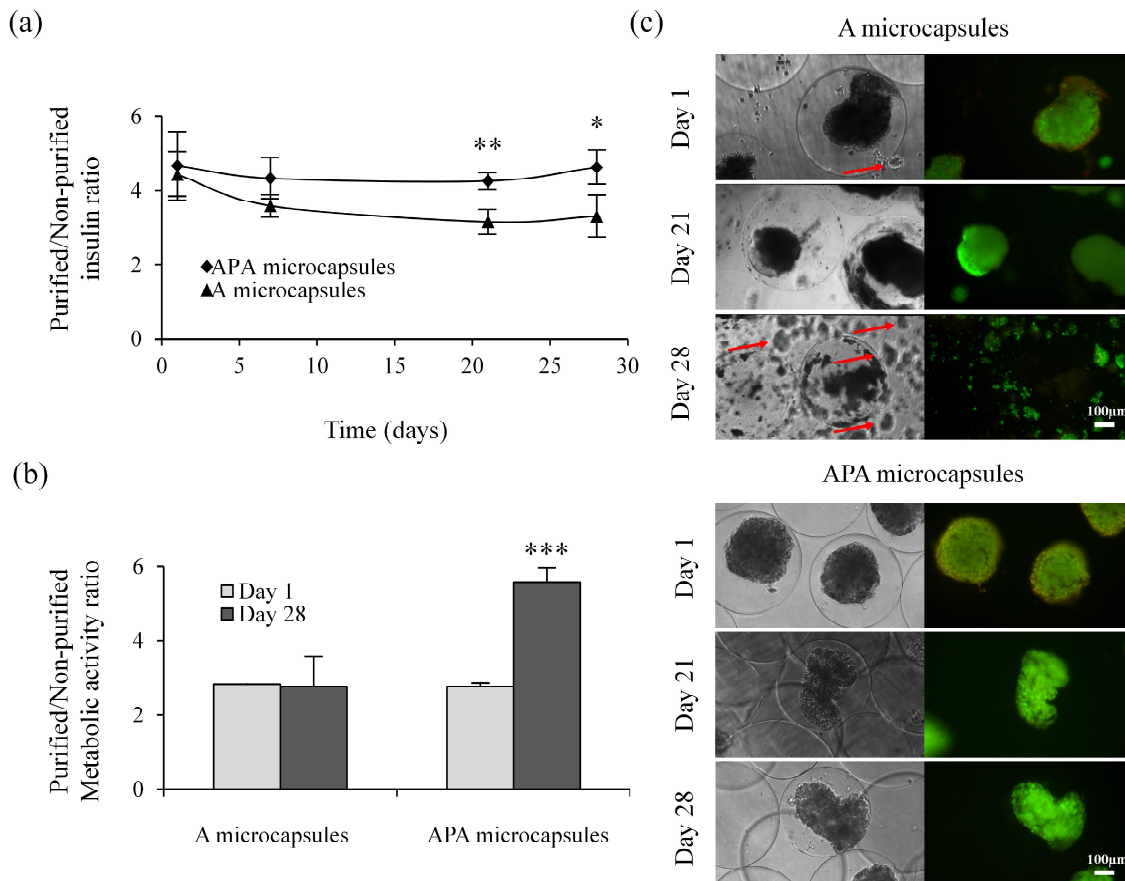


Figure 7. Purified/non-purified ratios of (a) insulin production and (b) metabolic activity of A and APA microencapsulated INS1E pseudoislets before and after magnetic separation. Values represent mean \pm SD: * $p < 0.05$, **: $p < 0.01$ and ***: $p < 0.001$. (c) Brightfield microphotographs and fluorescence microscopy images of purified A and APA microencapsulated INS1E pseudoislets (green fluorescence for live cells and red for dead cells). Red arrows identify fragmented INS1E cell aggregates. Scale bar: 100 μ m.

In contrast, in APA microcapsules samples, aggregates were not detected in the media; instead, all pseudoislets remained microencapsulated and, importantly, no evidence of microcapsules breakage was observed all over time. The higher mechanical strength of APA microcapsules, therefore, allowed restricting the pseudoislets growth, maintaining the pseudoislets within the matrix, thus improving the biosafety of the graft. The reduced mechanical integrity of A microcapsules can be attributed to the poor stability of the reversible ionic crosslinking of the sodium alginate macromolecules with a divalent ion, such as for

example Ca^{2+} ions. In fact, the gelled alginate can exchange Ca^{2+} ions with the Na^+ present in the media, leading to a progressive degradation of the alginate hydrogels, which is an interesting property for cell delivery applications, where cells are required to escape from the microcapsule [40]. In contrast, APA microcapsules are protected against osmosis by the PLL coating, which strengthens the microcapsule, preventing its swelling and loss of stiffness [39, 40]. Therefore, the decrease of the purified/non-purified insulin release and metabolic activity ratios for the A microcapsules compared to the APA microcapsules might occur due to the differences on their mechanical integrity that led to the loss of A microencapsulated pseudoislets. Importantly, for in vivo application in T1DM reversal, microcapsules need to hold physical and osmotic stress to avoid any cell exposure [41, 42], since the breakage of the microcapsules may trigger the host's immune rejection against the exposed pseudoislets, implying the graft failure. Based on these results, APA microcapsules were selected in order to perform the implantation of pseudoislets into STZ-induced diabetic Wistar rats.

3.5. Normoglycemia restoration of STZ-induced diabetic Wistar rats

Blood glucose levels of all studied groups (see 3.9 section for details of animal groups) were monitored for 142 days after STZ injection (Figure 8A). During the first 11 days after implantation of 0.4 mL of microcapsules from purified, non-purified and empty microcapsules pools, rats from all STZ-treated groups remained diabetic, with blood glucose levels between 350-500 mg/dL, with no significant differences among groups. In contrast, non-diabetic control rats maintained their blood glucose levels around 100 mg/dL. During the whole study, rats from the diabetic group and those implanted with non-purified microcapsules and empty microcapsules maintained high glucose levels, between 400-500 mg/dL, with no significant differences among them. However, 19 days after implantation, blood glucose levels of rats implanted with purified microcapsules significantly decreased, reaching values between 140-200 mg/dL, which are comprised within the normal glycemic range (< 200 mg/dL), very close to the non-diabetic control levels. These results correlated with the bodyweight gain and cumulative survival analysis data (Figure 8B-C). Diabetic control animals did not gain weight during the first weeks, begun to show discomfort 22 days after implantation and, subsequently, were sacrificed. Similarly, rats implanted with non-purified and empty microcapsules did not gain weight during the first weeks either, but discomfort appeared later, from day 44 to 66 after implantation. In contrast, rats implanted with purified microencapsulated pseudoislets began to gain weight 2 days after implantation, showing statistically significant higher body weight values during all the study compared to the rest of the diabetic groups ($p < 0.001$). Non-diabetic control rats also gained weight

during the study always showing statistically significant higher values than the rats implanted with purified microcapsules ($p < 0.001$), and all the animals survived the whole procedure, as expected.

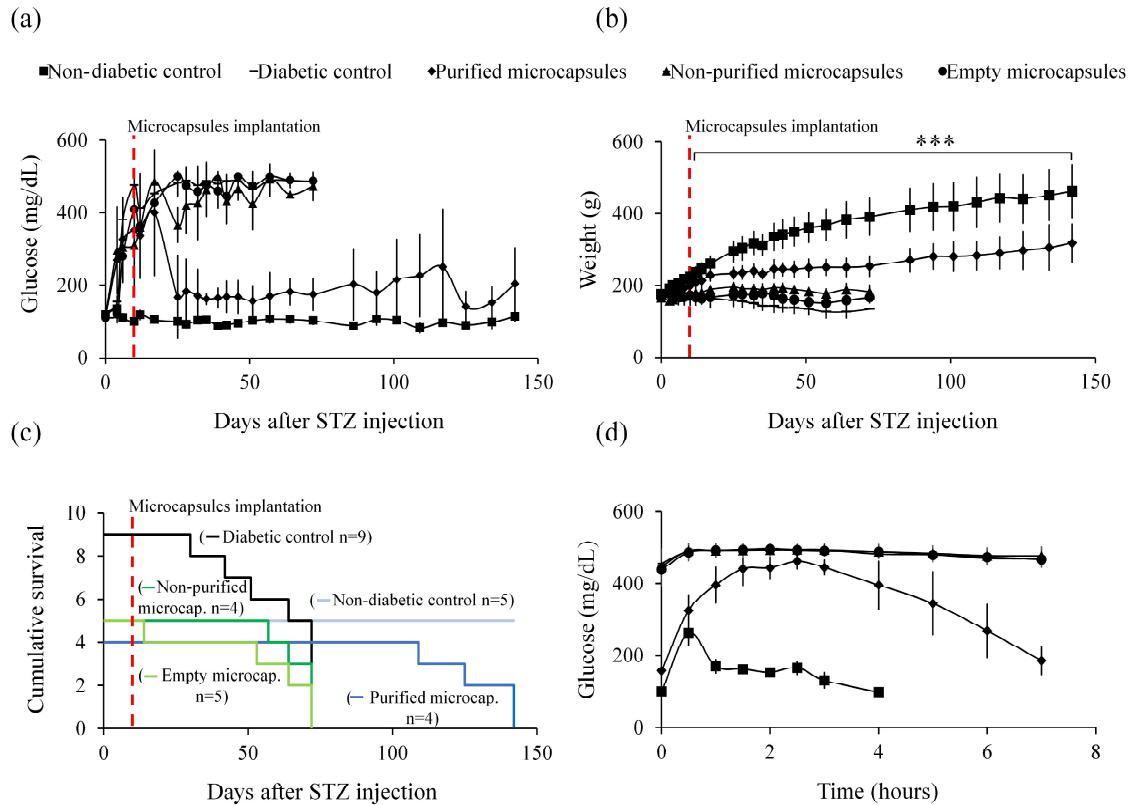


Figure 8. Long-term monitoring of blood glucose levels (a) and body weights (b) of STZ-induced diabetic Wistar rats implanted with empty microcapsules, non-purified and purified microcapsules containing INS1E pseudoislets. Non-diabetic and non-implanted diabetic rats were used as controls. (c) Intraperitoneal glucose tolerance test two months after microcapsules implantation. (d) Kaplan-Meier analysis of rats from different groups. Dotted red lines identify the microcapsules implantation time point. ***: $p < 0.001$ compared to rats implanted with purified microencapsulated pseudoislets.

Focusing on the animals implanted with purified microcapsules, symptoms of graft failure were noticed on day 104 after implantation, being the last graft failure on day 136 post implantation. Similarly, Albino Oxford (AO) rats implanted with 2-2.5 mL of non-purified APA microencapsulated allogeneic Lewis-islets become normoglycemic within 5 days after implantation and, remained normoglycemic, with blood glucose levels below 200 mg/dL. However, some animals began to show symptoms of graft failure 42 days after implantation [43]. Therefore, although the initial therapeutic effect of our purified microencapsulated pseudoislets was detected later than in the study by *de Vos and cols* [43], our implants demonstrated better results in terms of normoglycemia maintenance. In fact, AO rats showed the first symptoms of graft failure just 42 days after implantation, and in our study, the first graft failure was detected on day 104. Hence, these data demonstrate that

implantation of 0.4 mL of purified microencapsulated pseudoislets is able to restore blood glucose levels within the normoglycemic range. In contrast, in other studies, implantation volumes of microencapsulated allogeneic pancreatic islets have been ranged between 2-2.5 mL per animal in order to achieve normoglycemia in STZ-induced diabetic AO rats [43, 44]. Therefore, we have achieved blood glucose levels restoration into the normoglycemic range with a 5 to 6.25 times reduction in the implant volume. Undoubtedly, this is a highly relevant achievement for reducing the host's immune response against the graft [18].

In order to evaluate the capacity of the different animal groups to respond to glucose stimuli, we performed a glucose tolerance test two months after implantation (Figure 8D). As expected, results for the diabetic control animals and those implanted with non-purified and empty microcapsules showed no response to glucose stimulus, with high blood glucose levels around 500 mg/dL. In contrast, in rats implanted with purified microcapsules, which showed initial blood glucose levels under 200 mg/dL, glucose values increased up to 420-450 mg/dL, smoothly decreasing to final values around 200 mg/dL 7 hours after the glucose administration. Non-diabetic control rats showed a stronger response to glucose stimulus with lower peak values (around 230 mg/dL), requiring less time for normoglycemic glucose values restoration, which occurred 2 hours after glucose administration. Similarly to our results, AO rats implanted with microencapsulated allogeneic Lewis-islets show higher initial blood glucose levels than non-diabetic control in the glucose tolerance test. However, in that study, animals are able to diminish blood glucose levels faster than our rats implanted with purified microcapsules [43]. This difference might be due to graft implantation site. In fact, in type I diabetes mellitus patients, insulin is detected faster in the bloodstream when it is administrated through intraperitoneal injection than when it is administered subcutaneously, with ranges between 60-150 minutes and 150-300 minutes, respectively [45]. This occurs due to the different degree of vascularization of the implantation site; the high vascularization of the peritoneal cavity promotes faster insulin absorption, while the subcutaneous tissue is not that highly vascularized, limiting the diffusion of insulin towards the bloodstream [46, 47]. This could have been the reason why in our subcutaneously implanted rats we noticed a delayed glucose response and slower restoration of normoglycemia. Nevertheless, although the implantation of microencapsulated islets in the peritoneum cavity has shown faster glucose response in AO rats, this location has several disadvantages that make it not suitable for clinical application. One important one is that the implantation of microcapsules in this location goes through an invasive surgical technique which provokes a strong inflammatory response in the implantation site [44, 48]. In addition, the high vascularization of the peritoneum facilitates the easy access of the host's immune cells, which transforms the acute inflammatory reaction into a chronic process that leads to the graft failure [48]. Finally, in the

peritoneum, microencapsulated islets are freely floating, which would difficult the removal of the whole graft if required, compromising the biosafety of the implant. Unfortunately, this situation would force the use of more invasive techniques such as peritoneum lavage [43, 44].

Lastly, we performed a histological evaluation by hematoxylin and eosin and Masson's trichrome staining in order to examine the retrieved microcapsules and to evaluate the inflammatory response (Figure 9A-B). Collagen-like surrounding tissue was detected, indicating the presence of fibrotic tissue in all the samples, with no differences among the different grafts, independently of the implanted microcapsules (Figure 9A).

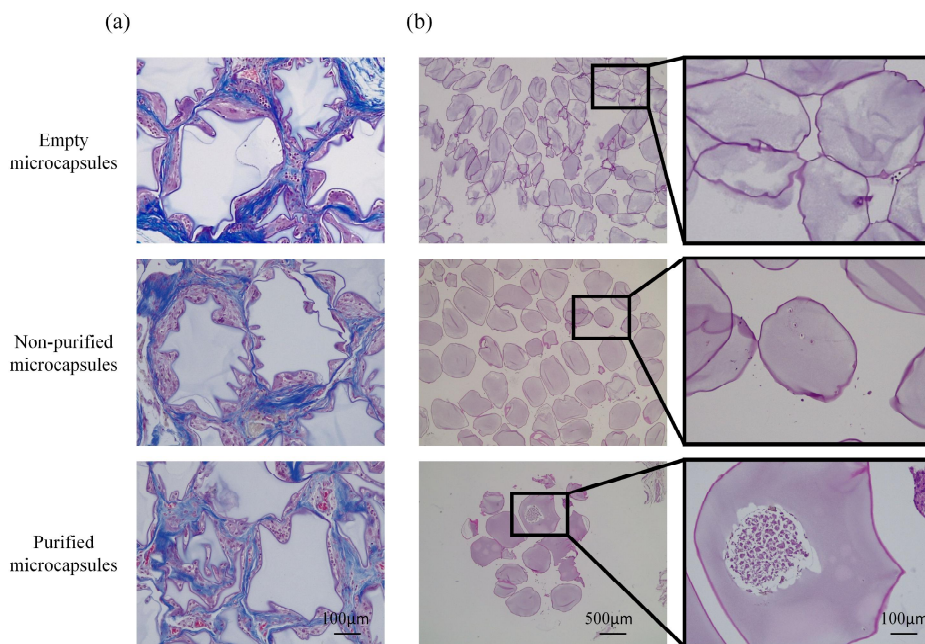


Figure 9. Foreign body reaction analysis of subcutaneously implanted empty microcapsules, non-purified and purified microencapsulated INS1E pseudoislets in STZ-induced diabetic Wistar rats. (a) Representative photographic images of Masson's trichrome staining of explanted grafts. (b) Representative images of hematoxylin-eosin staining of explanted grafts. Scale bars: 100 μm or 500 μm .

Also, no differences among groups were detected on the surrounding inflammatory response with the presence of some infiltrating lymphocyte and neutrophil cells. Regarding the microcapsules, in the empty and non-purified microcapsules samples, we mainly observed empty microcapsules, while in the purified sample, we observed a higher presence of microencapsulated pseudoislets without cell protruding (Figure 9B). Importantly, although the purified sample contained higher quantities of pseudoislets, the inflammatory response was similar to the empty and non-purified microcapsules samples, since the pseudoislets from the purified group remained encapsulated and did not trigger higher host's immune response.

4. CONCLUSIONS

The combination of 3D printing, microfluidics, magnetic sorting, and magnetic cell labeling technologies, enabled the production of a magnetic sorting device for the purification of magnetically labeled encapsulated pseudoislets. While these implants showed the capacity to normalize glucose blood levels in diabetic rats, a considerable reduction of the graft volume has been accomplished (higher than 75 %), compared to previously reported works. Our microfluidic device provides high purification yields, enables the monitorization of the process and avoids manual steps, thus, minimizing technical errors and improving the reproducibility of the purification process. Moreover, the miniaturized nature of the approach facilitates the parallelization of processes, the multiplexing capabilities, and high-throughput screening. Therefore, this technology will improve the efficacy of therapeutic strategies that include the use of microencapsulated pancreatic islets for the Type 1 Diabetes Mellitus clinical management. In this sense, future directions for its widespread clinical application should focus on scaling-up the procedure. On this regard, further investigations on the development of a technology that is able to perform the microencapsulation and the sorting processes in one single step would suppose a step forward in the optimization and reduction of the costs of this approach, bringing this technology closer to the clinics.

ACKNOWLEDGMENTS

Authors thank the support to research from the University of the Basque Country UPV/EHU (EHUa16/06 to LSB, and ESPOC 16/65), the Basque Country Government (Grupos Consolidados with Grant N° IT907-16 to JLP, Elkartek with Grant N° KK-2017/0000088 and RIS3 with Grant N° 307616FKA4) and the Spanish Government (RYC-2012-10796). Authors also wish to thank the intellectual and technical assistance from the ICTS “NANBIOSIS”, more specifically by the Drug Formulation Unit (U10) of the CIBER in Bioengineering, Biomaterials & Nanomedicine (CIBER-BBN) at the University of the Basque Country UPV/EHU, Prof. Maechler from the University of Geneva Medical Center for providing the INS1E cell line, Adhesive Research for providing PSA sheets and Prof. Martínez de Pancorbo for her laboratory facilities at University of the Basque Country UPV/EHU.

REFERENCES

- [1] de Groot M, Schuurs TA and van Schilfgaarde R. Causes of limited survival of microencapsulated pancreatic islet grafts. *Journal of Surgical Research* 2004.
- [2] Yun Lee D, Hee Nam J and Byun Y. Functional and histological evaluation of transplanted pancreatic islets immunoprotected by PEGylation and cyclosporine for 1 year. *Biomaterials* 2007.

- [3] Skrzypek K, Groot Nibbelink M, Lente Jv, et al. Pancreatic islet macroencapsulation using microwell porous membranes. *Scientific Reports* 2017.
- [4] Wenjuan Li, Ruxing Zhao, Jidong Liu, et al. Small Islets Transplantation Superiority to Large Ones: Implications from Islet Microcirculation and Revascularization. *Journal of diabetes research* 2014.
- [5] Street CN, Lakey JRT, Shapiro AMJ, et al. Islet graft assessment in the Edmonton Protocol: implications for predicting long-term clinical outcome. *Diabetes* 2004.
- [6] Ryan EA, Lakey JRT, Paty BW, et al. Successful islet transplantation: continued insulin reserve provides long-term glycemic control. *Diabetes* 2002.
- [7] Edmond A. Ryan, Jonathan R.T. Lakey, Ray V. Rajotte, et al. Clinical Outcomes and Insulin Secretion After Islet Transplantation With the Edmonton Protocol. *Diabetes* 2001.
- [8] Brian Buder, Michael Alexander, Rahul Krishnan, et al. Encapsulated Islet Transplantation: Strategies and Clinical Trials. *Immune Network* 2013.
- [9] de Vos P and Marchetti P. Encapsulation of pancreatic islets for transplantation in diabetes: the untouchable islets. *Trends in Molecular Medicine* 2002.
- [10] El-Sherbiny IM and Yacoub MH. Hydrogel scaffolds for tissue engineering: Progress and challenges. *Glob Cardiol Sci Pract* 2013.
- [11] Yang HK and Yoon KH. Current status of encapsulated islet transplantation. *J Diabetes Complications* 2015.
- [12] Borg DJ and Bonifacio E. The use of biomaterials in islet transplantation. *Curr Diab Rep* 2011.
- [13] Lee KY and Mooney DJ. Alginate: Properties and biomedical applications. *Progress in Polymer Science* 2011.
- [14] Sakata N, Sumi S, Yoshimatsu G, et al. Encapsulated islets transplantation: Past, present and future. *World J Gastrointest Pathophysiol* 2012.
- [15] Smidsrod O and Skjak-Braek G. Alginate as immobilization matrix for cells. *Trends Biotechnol* 1990.
- [16] Strand BL, Ryan TL, In't Veld P, et al. Poly-L-Lysine induces fibrosis on alginate microcapsules via the induction of cytokines. *Cell Transplant* 2001.
- [17] Kobayashi T, Aomatsu Y, Iwata H, et al. Survival of Microencapsulated Islets at 400 Days Posttransplantation in the Omental Pouch of NOD Mice. *Cell Transplantation* 2006.
- [18] King A. Microencapsulation of islets of Langerhans: impact of cellular overgrowth. *Ups J Med Sci* 2001.
- [19] Park H, Lee HJ, An H, et al. Alginate hydrogels modified with low molecular weight hyaluronate for cartilage regeneration. *Carbohydrate Polymers* 2017.
- [20] Wanyu Chen, Mark Lisowski, Gamal Khalil, et al. Microencapsulated 3-Dimensional Sensor for the Measurement of Oxygen in Single Isolated Pancreatic Islets. *PLoS One* 2012.
- [21] Wyatt Shields IV C, Reyes CD and López GP. Microfluidic cell sorting: a review of the advances in the separation of cells from debulking to rare cell isolation. *Lab on a chip* 2015.
- [22] Xi H, Zheng H, Guo W, et al. Active droplet sorting in microfluidics: a review. *Lab Chip* 2017.
- [23] Ahne Myklatun, Michele Cappetta, Michael Winklhofer, et al. Microfluidic sorting of intrinsically magnetic cells under visual control. *Scientific Reports (Nature Publisher Group)* 2017.
- [24] Adeyemi AH. Microfluidic Devices for the Characterization and Manipulation of Encapsulated Cells in Agarose Microcapsules Using Dielectrophoresis and Electrophoresis. Thesis. Faculty of Engineering. UNIVERSITY OF OTTAWA. 2017.
- [25] Girault M, Kim H, Arakawa H, et al. An on-chip imaging droplet-sorting system: a real-time shape recognition method to screen target cells in droplets with single cell resolution. *Scientific Reports* 2017.
- [26] Kennedy DJ, Todd P, Logan S, et al. Engineering quadrupole magnetic flow sorting for the isolation of pancreatic islets. *Journal of Magnetism and Magnetic Materials* 2007; 311: 388-395.
- [27] Tendulkar S, Mirmalek-Sani SH, Childers C, et al. A three-dimensional microfluidic approach to scaling up microencapsulation of cells. *Biomed Microdevices* 2012.
- [28] Temiz Y, Lovchik RD, Kaigala GV, et al. Lab-on-a-chip devices: How to close and plug the lab. *Microelectronic Engineering* 2015; 132: 156-175.

- [29] Megías R, Arco M, Ciriza J, et al. Design and characterization of a magnetite/PEI multifunctional nanohybrid as non-viral vector and cell isolation system. *International Journal of Pharmaceutics* 2017.
- [30] Merglen A, Theander S, Rubi B, et al. Glucose Sensitivity and Metabolism-Secretion Coupling Studied during Two-Year Continuous Culture in INS-1E Insulinoma Cells. *Endocrinology* 2004.
- [31] Muñoz de Escalona M, Sáez-Fernández E, Prados JC, et al. Magnetic solid lipid nanoparticles in hyperthermia against colon cancer. *International Journal of Pharmaceutics* 2016.
- [32] Li P, Tian Y and Pappas D. Comparison of inlet geometry in microfluidic cell affinity chromatography. *Anal Chem* 2011.
- [33] Ho CM, Ng SH, Li KH, et al. 3D printed microfluidics for biological applications. *Lab Chip* 2015.
- [34] Dressaire E and Sauret A. Clogging of microfluidic systems. *Soft Matter* 2016.
- [35] Ying E and Hwang H. In vitro evaluation of the cytotoxicity of iron oxide nanoparticles with different coatings and different sizes in A3 human T lymphocytes. *Science of The Total Environment* 2010; 408: 4475-4481.
- [36] Zhang S, Chen X, Gu C, et al. The Effect of Iron Oxide Magnetic Nanoparticles on Smooth Muscle Cells. *Nanoscale Research Letters* 2008.
- [37] Kim HS, Kim H, Park KS, et al. Evaluation of porcine pancreatic islets transplanted in the kidney capsules of diabetic mice using a clinically approved superparamagnetic iron oxide (SPIO) and a 1.5T MR scanner. *Korean J Radiol* 2010.
- [38] Thakor AS, Jokerst JV, Ghanouni P, et al. Clinically Approved Nanoparticle Imaging Agents. *J Nucl Med* 2016.
- [39] Shen F, Mazumder MA, Burke NA, et al. Mechanically enhanced microcapsules for cellular gene therapy. *J Biomed Mater Res B Appl Biomater* 2009.
- [40] Wilson JL, Najia MA, Saeed R, et al. Alginate encapsulation parameters influence the differentiation of microencapsulated embryonic stem cell aggregates. *Biotechnol Bioeng* 2014.
- [41] Opara EC, Mirmalek-Sani SH, Khanna O, et al. Design of a bioartificial pancreas(+). *J Investig Med* 2010.
- [42] Vaithilingam V and Tuch BE. Islet transplantation and encapsulation: an update on recent developments. *Rev Diabet Stud* 2011.
- [43] de Vos P, van Hoogmoed CG, van Zanten J, et al. Long-term biocompatibility, chemistry, and function of microencapsulated pancreatic islets. *Biomaterials* 2003; 24: 305-312.
- [44] De Vos P, Van Straaten JF, Nieuwenhuizen AG, et al. Why do microencapsulated islet grafts fail in the absence of fibrotic overgrowth?. *Diabetes* 1999.
- [45] Giacca A, Caumo A, Galimberti G, et al. Peritoneal and subcutaneous absorption of insulin in type I diabetic subjects. *J Clin Endocrinol Metab* 1993.
- [46] Figliuzzi M, Cornolti R, Plati T, et al. Subcutaneous xenotransplantation of bovine pancreatic islets. *Biomaterials* 2005; 26: 5640-5647.
- [47] Burnett DR, Huyett LM, Zisser HC, et al. Glucose sensing in the peritoneal space offers faster kinetics than sensing in the subcutaneous space. *Diabetes* 2014.
- [48] Robitaille R, Dusseault J, Henley N, et al. Inflammatory response to peritoneal implantation of alginate-poly-L-lysine microcapsules. *Biomaterials* 2005; 26: 4119-4127.

The background of the slide is a grayscale scanning electron micrograph (SEM) showing a highly porous, interconnected network of fibers. The fibers form a complex, web-like structure with irregular, interconnected pores of varying sizes. The overall appearance is that of a porous hydrogel scaffold.

4

**Tunable injectable alginate-based
hydrogel for cell therapy in Type 1
Diabetes Mellitus**



Tunable injectable alginate-based hydrogel for cell therapy in Type 1 Diabetes Mellitus

A. Espona-Noguera^{1,2}, J. Ciriza^{1,2}, A. Cañibano-Hernández^{1,2}, L. Fernandez^{3,4,5}, I. Ochoa^{3,4,5}, L. Saenz del Burgo^{1,2*}, J.L. Pedraz^{1,2*}

¹ NanoBioCel Group, Laboratory of Pharmacy and Pharmaceutical Technology, Faculty of Pharmacy, University of the Basque Country, UPV/EHU, Vitoria-Gasteiz, Spain

² Biomedical Research Networking Center in Bioengineering, Biomaterials and Nanomedicine, CIBER-BBN, Vitoria-Gasteiz, Spain

³ Group of Applied Mechanics and Bioengineering (AMB), Aragón Institute of Engineering Research (I3A), University of Zaragoza, Zaragoza, Spain

⁴ Biomedical Research Networking Center in Bioengineering, Biomaterials and Nanomedicine (CIBER-BBN), Zaragoza, Spain

⁵ Aragon Institute of Biomedical Research (IIS Aragón) Instituto de Salud Carlos III, Zaragoza, Spain

* Corresponding authors

ABSTRACT

Islet transplantation has the potential of reestablishing naturally-regulated insulin production in Type 1 diabetic patients. Nevertheless, this procedure is limited due to the low islet survival after transplantation and the lifelong immunosuppression to avoid rejection. Islet embedding within a biocompatible matrix provides mechanical protection and a physical barrier against the immune system thus, increasing islet survival. Alginate is the preferred biomaterial used for embedding insulin-producing cells because of its biocompatibility, low toxicity and ease of gelation. However, alginate gelation is poorly controlled, affecting its physicochemical properties as an injectable biomaterial. Including different concentrations of the phosphate salt Na_2HPO_4 in alginate hydrogels, we can modulate their gelation time, tuning their physicochemical properties like stiffness and porosity while maintaining an appropriate injectability. Moreover, these hydrogels showed good biocompatibility when embedding a rat insulinoma cell line, especially at low Na_2HPO_4 concentrations, indicating that these hydrogels have potential as injectable biomaterials for Type 1 Diabetes Mellitus treatment.

Keywords: alginate, hydrogel, insulin, diabetes

International Journal of Biological Macromolecules. 107 (2018) 1261 - 1269

1. INTRODUCTION

Type 1 Diabetes Mellitus (T1DM) is a metabolic disorder characterized by an autoimmune response that promotes the destruction of β -cells within the pancreatic islets, resulting in a lifelong inadequate insulin secretion [1]. The most used therapy is the subcutaneous administration of exogenous insulin. Although maintaining physiologic blood glucose levels is the key in T1DM treatment, exogenous insulin injections fail to provide constant metabolic control leading to hypoglycaemia and diabetic complications [2]. Alternatively, pancreatic islet transplantation has the potential of reestablishing naturally-regulated insulin production thus, restoring the physiologic metabolic glucose control in T1DM patients. Nevertheless, there are some issues that make this treatment strategy difficult such as the low islet survival after transplantation and the lifelong immunosuppression to avoid rejection [2 3]. One of the strategies developed to overcome this bottleneck is the islet embedding within a biocompatible matrix [4]. The matrix provides mechanical protection and also acts as a physical barrier keeping high molecular weight immune system components out, while allowing the diffusion of oxygen, nutrients and therapeutic factors like insulin. In this way, islets survival is increased and the required number of pancreatic islets per patient can be optimized [3 5].

Hydrogels are three-dimensional networks composed of cross-linked polymers that possess many interesting properties for biomedical applications such as high water content, biocompatibility and mechanical properties mimicking the structural and mechanical properties of extracellular matrices [6]. Furthermore, a great advantage of hydrogel-based cell therapies is that they allow a minimally invasive cell delivery by means of hydrogel injection in the transplant site [7]. All these properties have converted hydrogels into a biomaterial extensively used in tissue engineering applications [8-12]. One of the most used materials is alginate [10]. This is a natural polymer isolated from brown algae that can form hydrogels. Besides, it shows great properties like biocompatibility, low toxicity and ease of gelation [13]. Among all its biomedical applications, alginate has been commonly used in pancreatic islets embedding [14 15].

The most commonly used method for alginate hydrogel preparation is the ionic cross-linking, where the aqueous alginate solution is combined with ionic cross-linking agents such as divalent cations. The modification of the internal hydrogel structure leads to changes both on the swelling behavior and the mechanical properties and, therefore, its stiffness, which has been described as an important conditioner for the differentiation of stem cells towards mature cells [16-18]. For example, in alginate capsules with stiffness lower than 10 KPa, human Embryonic Stem Cells are able to grow and promote pancreatic

differentiation, while in capsules in the range of 22-73 KPa of stiffness cell proliferation is restricted and pancreatic progenitors induction is strongly suppressed [19]. However, gelation is usually poorly controlled which limits effectiveness as an injectable biomaterial for tissue engineering applications [20-21]. The ideal gelation process of a therapeutically useful hydrogel should be quite fast, in the order of seconds to minutes and, at the same time, the hydrogel should remain in a viscous state long enough to facilitate its manipulation and injection [20-22]. On this regard, alginate gelation process has been modulated by modifying the alginate and/or the Ca^{2+} ions source, achieving, therefore, different ranges of physicochemical properties [20-23]. The modulation of alginate has also been described by adding cholic acid from bile acids improving the physicochemical properties, the stability of the alginate hydrogels and the viability of the embedded cells [24-25]. The lack of injectability forces to make the hydrogel in a mold outside the body and implanting the final gelled product by invasive surgical procedure instead of by simple injection. Thus, the practical use of hydrogel-based therapies in the clinic is significantly restricted [22]. Alternatively, retarding agents can be added slowing down the alginate gelling reaction and achieving a better control over the gelation rate and a wider working time [13]. Phosphate salts act as retarding agents due to the ability of phosphate groups to interact with the Ca^{2+} source producing calcium phosphate. This prevents Ca^{2+} ions from reacting with sodium alginate to form the alginate hydrogel. Once the phosphate compound is depleted, alginate can form the hydrogel [13-21]. These properties of alginate have been shown, for example, in dental material impressions and orthodontic models [26], where sodium phosphate is added to delay the gelation time of the hydrogel, providing longer working times when loading in alginate impressions [21-27] as well as their biocompatibility with the rat insulinoma cell line INS1E. Hydrogels that gellify too fast, force clinicians to manage this technology very quick under stressful daily work conditions. Seeing that fast alginate gelation supposes a restriction when it is used as a injectable biomaterial, we have explored the effect of a phosphate salt Na_2HPO_4 as a retardant agent in order to improve its gelation for cell therapy application in T1DM treatment. To that end, we have characterized the physicochemical properties of the different alginate hydrogels containing Na_2HPO_4 . The novelty of this research resides in the alginate hydrogel gelation delay without affecting their injectability, helping, therefore, to their translation from bench to the clinic. On this regard, hydrogels with a delayed gelation time would add more flexibility to the application of these scaffolds in hospitals.

2. MATERIAL AND METHODS

2.1. Materials

Ultrapure sodium alginate with molecular weight of 75-200 KDa and Guluronate/Mannuronate ratio ≥ 1.5 was purchased from FMC Biopolymer. Calcium sulphate dihydrate ($\text{CaSO}_4 \cdot 2\text{H}_2\text{O}$), FITC apoptosis Detection Kit, Cell Counter Kit-8 (CCK-8) and the *In Vitro* Toxicology LDH based Assay were purchased from Sigma-Aldrich. Di-Sodium Hydrogen Phosphate dyhydrate ($\text{Na}_2\text{HPO}_4 \cdot 2\text{H}_2\text{O}$) was purchased from Panreac. LIVE/DEAD[®] Viability/Cytotoxicity Kit was purchased from Life Technologies, Rat Insulin ELISA kit from Mercodia and the Pierce[®] BCA Protein Assay from Thermo Scientific. In this study, a rat insulinoma cell line called INS1E [28] which has been provided by the University of Geneva Medical Center has been used.

2.2. Characterization of alginate hydrogels containing Na_2HPO_4

2.2.1. Alginate hydrogel preparation

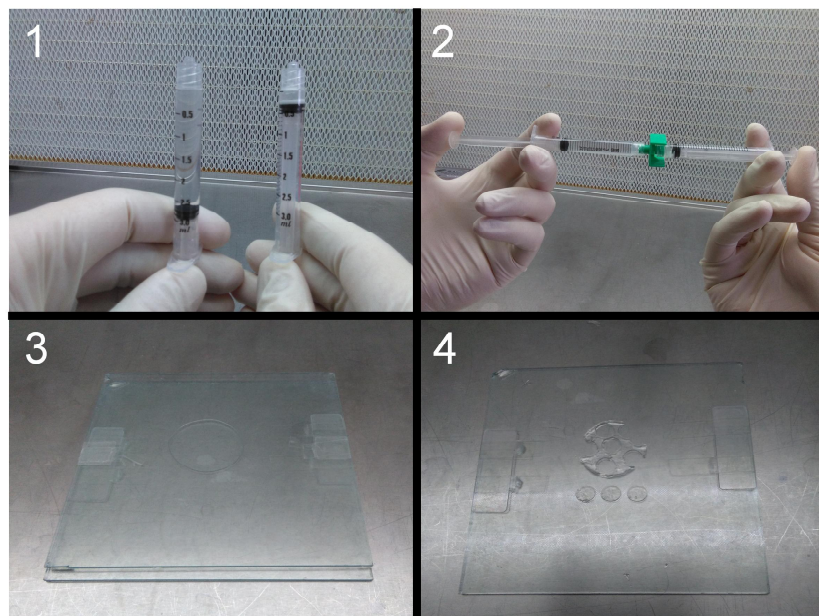
Ultrapure sodium alginate (FMC Biopolymer), was dissolved in 1 % D-mannitol (Sigma-Aldrich) at a concentration of 1.5 %. Then, it was filtered through a 0.22 μm pore Minisart Syringe Filter (Sartorius). For gelation, 2.7 mL of 1.5 % alginate were mixed with 60 μL of 1.22 M $\text{CaSO}_4 \cdot 2\text{H}_2\text{O}$ (Sigma-Aldrich) diluted in 240 μL of distilled water through two LuerLock syringe (BS Syringe) connected with a Fluid Dispensing Connector (Braun). Alginate and $\text{CaSO}_4 \cdot 2\text{H}_2\text{O}$ were mixed 15 times until complete homogenization. For retardation gelation time, 60 μL of $\text{Na}_2\text{HPO}_4 \cdot 2\text{H}_2\text{O}$ (Panreac) were added in the cross-linking reaction from the following solutions 0.1 M, 0.3 M, 0.5 M, 0.6 M and 0.9 M. Hydrogels were molded between two glass plates with 2 mm spacers, obtaining 6, 10 or 14 mm diameter discs with a circular punch (Figure 1A).

2.2.2. Rheology and injectability

Rheological properties of all hydrogels were measured on the rheometer AR1000 (TA instruments. New Castle, United States) with flat plate geometry and compared to alginate hydrogels formed without Na_2HPO_4 . Oscillatory shear measurements were conducted at 20°C to obtain the gelation time, the elastic modulus (G') and the viscous modulus (G''). These were determined via time sweep, by dosing 4 drops of 100 μL of 1.5 % alginate solution and 8 smaller drops of 5 μL of $\text{CaSO}_4/\text{Na}_2\text{HPO}_4$ mixture on the rheometer platform. Next, all conditions were set with a gap at 400 μm , a delay time of 3 seconds, a displacement of 1e^{-3} rad and an angular frequency of 1 Hz. Then, a pre-shear of 2000 1/s was

applied to initiate alginate gelation and immediately G' and G'' moduli measurements were performed as a function of time and gelation time was considered as the value of the G' modulus plateau (Figure 1B). Three independent experiments, with three replicates each one, were conducted. Injectability of hydrogels was assessed by passing the hydrogel through a syringe at 25 °C with gauges from 25 to 30. Three independent experiments, with three replicates each one, were conducted.

A)



B)

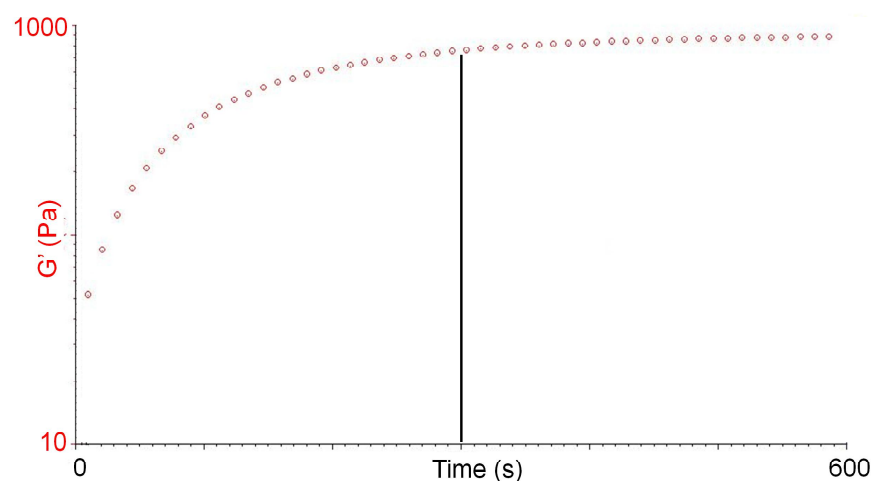


Figure 1. A) Detailed procedure of alginate hydrogels preparation. 1.- 1.5 % Alginate solution and, CaSO_4 - Na_2HPO_4 placed in independent syringes. 2.- Syringes connected and content mixed. 3.- The resultant mixture spread between two glasses with 2 mm spacer. 4.- Disk punched from the hydrogel. B) Elastic modulus (G') through time and gelation time determination from rheological measurements.

2.2.3. Homogeneity

To evaluate homogeneity of all different alginate hydrogels, five discs of 10 mm in diameter of each hydrogel were weighted (wet weight). Discs were dried at 70 °C in a drying oven (J.P. Selecta. Abrera, Spain) for 1 hour and weighed again (dry weight). Dry/wet ratios were calculated in three independent experiments with three replicates each one.

2.2.4. Swelling and water content

To evaluate swelling behavior and water content, discs of 10 mm in diameter were punched and weighted (wet weight: W_s). Then, all discs were lyophilized (Telstar cryodos Freeze Dryer. Terrassa, Spain) and reweighed (dried weight: W_d). Water content (W_c) was calculated as: $W_c = W_s - W_d$. Afterwards, the dried alginate discs were placed in DPBS with Ca^{2+} and Mg^{2+} to estimate their swelling capacity. At selected time points, discs were removed from DPBS and wiped using filter paper, and then weighed and returned to DPBS until the swelling ratio reached the equilibrium. Swelling ratio (SR) was determined in every time point using the following formulae: $SR = (W_s - W_d) / W_d$. Three independent experiments, with three replicates each one, were conducted.

2.2.5. Compressive properties

Uniaxial unconfined and confined compression were performed to measure the compressive properties, Young's (E_s) and aggregated (H_a) moduli and Poisson coefficient of all different alginate hydrogels. Young's modulus is a measurement of the elasticity of a material that has been subjected to opposite forces along an axis and the aggregated modulus defines the stiffness of a material. Discs of 6 mm in diameter were punched from each hydrogel and evaluated following the protocol described by Acosta Santamaría [29]. An Instron MicroTester 5548 machine (Instron. Massachusetts, United States) was used with a precision of 0.0001 N and 0.001 mm in force and displacement, respectively. A monotonic ramp at 1 mm/min cross-head velocity was carried out with a 50 N load cell. From the unconfined compression test data, E_s modulus was obtained from the slope of the linear region in the stress–strain curve using the initial cross-section area. From the confined compression test data, the H_a modulus was obtained following the same procedure. Poisson coefficient is a constant of a material describing the lateral expansion during axial compression, and is defined as the ratio of lateral and axial strains and directly deduced from E_s and H_a . Three independent experiments, with six replicates each one, were conducted.

2.2.6. Pore morphology

Scanning electron microscopy (SEM) images of all different alginate hydrogels were acquired. Samples were frozen in liquid nitrogen and subsequently lyophilized (Telstar cryodos Freeze Dryer, Terrassa, Spain) for at least 24 hours. Finally, samples were coated with a Gold / Palladium thin film and examined with an SEM Inspect™ F50 (FEI Company, Hillsboro, United States).

2.3. Biocompatibility of alginate hydrogels formed with Na₂HPO₄ containing INS1E

2.3.1. Cell culture conditions in alginate hydrogels

Rat insulinoma INS1E cells were cultured in complete medium (RPMI 1640 supplemented with 10 % Fetal Bovine Serum (Gibco), 1 % penicillin/streptomycin / glutamine (Invitrogen), 1 % sodium pyruvate 100 mM (Sigma), 1 M HEPES (Lonza) and 0.1 % mercaptoethanol (Sigma). 1.5 % alginate was mixed with 5x10⁶ cells/mL and hydrogels were formed following the procedure mentioned above. Once alginate had gelled, 14 mm flat discs were punched and cultured in a 24 well-plate with complete medium in a humidified incubator at 37 °C and 5 % CO₂. The entire procedure was performed under sterile conditions.

2.3.2 Flow cytometry viability and apoptosis assays

Viability and apoptosis of INS1E cells embedded within all different alginate hydrogels were evaluated. At selected time points, medium was removed and hydrogels were dissolved in 1 % trisodium citrate dihydrate. Then, cells were collected and stained using the LIVE/DEAD® Viability/Cytotoxicity Kit (Life Technologies), and the Annexin-V-FITC apoptosis Detection Kit (Sigma-Aldrich). All samples were analyzed using the BD FACS Calibur flow cytometer (BD Company, Franklin Lakes, United States). Unstained cells and cells stained with calcein or ethidium were established as controls in the cell viability assay. Unstained cells and cells stained with annexin or propidium iodide were established as controls in the apoptosis assay. Three independent experiments, with three replicates each one, were conducted.

2.3.3 Metabolic activity and cell membrane activity assay

These assays were determined using the Cell Counter Kit-8 (CCK-8) (Sigma) and the *In Vitro* Toxicology LDH based Assay (Sigma-Aldrich) respectively. In the CCK-8 assay the absorbance was recorded using the Infinite M200 microplate reader (TECAN Trading AG, Männedorf, Switzerland) at 450 nm with reference wavelength set at 650 nm. In the

LDH assay the absorbance was read at 490 nm, with 690 nm measurement as background. Membrane damage values from the samples were relativized to hydrogels formed without the retardant agent. Three independent experiments were conducted with three replicates each.

2.3.4 Glucose-Stimulated Insulin Secretion (GSIS) assay

To assess the INS1E cells glucose response, GSIS assay was performed 7 days after cell embedding within all different alginate hydrogels. Discs were washed and incubated with Krebs-Ringer bicarbonate (KRB) for 30 minutes. Next, KRB was replaced with KRB containing 3.3 mM glucose and incubated for 2 hours. Then, supernatants were collected and discs were washed and incubated for 2 hours in KRB containing 16.6 mM glucose. Final supernatants were collected. The insulin content of collected supernatants was quantified with the Rat Insulin ELISA (Mercodia). Insulin concentration was normalized to total protein content determined with the Pierce® BCA Protein Assay (Thermo Scientific). Three independent experiments, with three replicates each one, were conducted.

2.3.5 Statistical analysis

Statistical analysis was performed with SPSS software, version 21.00.1. Data were expressed as means \pm standard deviation and differences were considered significant, for comparison of groups using ANOVA, Tukey's Post Hoc Test when $p < 0.05$.

3. RESULTS

3.1 Characterization of alginate hydrogels containing Na_2HPO_4

3.1.1 Na_2HPO_4 effect on hydrogels rheological and injectability properties

The influence of Na_2HPO_4 on the alginate hydrogels formation was studied by oscillatory shear measurements. Elastic modulus (G') and viscous modulus (G'') were measured as a time function in order to characterize the gelation process. G' modulus values were higher than G'' modulus values among alginate hydrogels (Table 1), indicating an elastic solid-like behavior. G' values of hydrogels with 0.1 M and 0.3 M Na_2HPO_4 were significantly higher than controls ($p < 0.05$), while in alginate hydrogels with higher Na_2HPO_4 concentrations, the final G' modulus diminished significantly ($p < 0.05$), demonstrating lower elastic properties. G'' moduli were all statistically different than hydrogel without Na_2HPO_4 ($p < 0.05$), except for the hydrogel containing 0.1 M Na_2HPO_4 . G' modulus stabilized when hydrogels solidified, establishing the gelation time when the G' modulus reached the plateau. The obtained gelation times differed considerably among the different conditions tested

(Table 1). The gelation of alginate hydrogels without Na_2HPO_4 was around 4 minutes (4.2 ± 0.2 minutes), while the presence of higher concentrations of Na_2HPO_4 (0.5 M, 0.6 M and 0.9 M) slowed down the gelation process significantly ($p < 0.01$). Finally, when injectability was assessed, all hydrogels passed through all needles in less than a minute (data not shown).

Table 1. Rheological properties (G' and G'' moduli) and gelation time of alginate hydrogels containing different concentrations of Na_2HPO_4 and control without Na_2HPO_4 . Values represent mean \pm SD. *: $p < 0.05$, **: $p < 0.01$ compared to control hydrogel.

	[Na_2HPO_4]					
	Control	0.1 M	0.3 M	0.5 M	0.6 M	0.9 M
Elastic modulus G' (Pa)	853.2 \pm 110.2	1165.5 \pm 177.8(*)	1445.6 \pm 55.3(*)	468.6 \pm 73.9(*)	483.8 \pm 97.2(*)	27.9 \pm 6.4(*)
Viscous modulus G'' (Pa)	87.4\pm9.1	108.1\pm15.7	120.9\pm4.5(*)	31.2\pm2.8(*)	30.5\pm4.8(*)	6.8\pm1.2(*)
Gelation time (min)	4.2\pm0.2	7.7\pm 0.4(**)	9.9\pm 0.2(**)	73.3\pm 7.6(**)	148.5\pm 13.1(**)	253.3\pm 25.2(**)

3.1.2 Hydrogel homogeneity

The homogeneity was determined by comparing the hydration degree of five punched discs equidistantly distributed in each alginate hydrogel. Discs were weighted in the swollen state (W_s), dried and reweighted (W_d). Homogeneity was calculated as the average of the W_d / W_s ratios (Table 2) of the different discs of each hydrogel containing different concentrations of Na_2HPO_4 . No statistical differences among hydrogels were detected, indicating that Na_2HPO_4 does not affect the homogeneity of hydrogels. concentrations of Na_2HPO_4 on water content and swelling properties of alginate hydrogels was assessed. All the hydrogels contained a high percentage of water (around 97 %) with no significant differences among them (Table 2).

Table 2. Homogeneity and water content of alginate hydrogels containing different concentrations of Na_2HPO_4 and control without Na_2HPO_4 . Values represent mean \pm SD.

	[Na_2HPO_4]					
	Control	0.1 M	0.3 M	0.5 M	0.6 M	0.9 M
Homogeneity	0.3\pm0.014	0.3\pm0.007	0.3\pm0.014	0.3\pm0.002	0.3\pm0.014	0.3\pm 0.010
Water content (%)	97.2\pm0.7	97.5\pm0.7	97.2\pm0.5	97.1\pm0.6	97.5\pm0.1	96.1\pm0.5

Next, all lyophilized alginate discs were immersed in DPBS in order to calculate the swelling ratio at different time points. Water uptake by the hydrogels increased over the time until they reached the equilibrium (Figure 2). Hydrogels containing 0.5 M, 0.6 M and 0.9 M

Na_2HPO_4 reached the equilibrium within 100-200 minutes, while the rest of the hydrogels needed 2 days, indicating that the Na_2HPO_4 content affects the water uptake rate. The final stable swelling ratio of all hydrogels was similar (Figure 2).

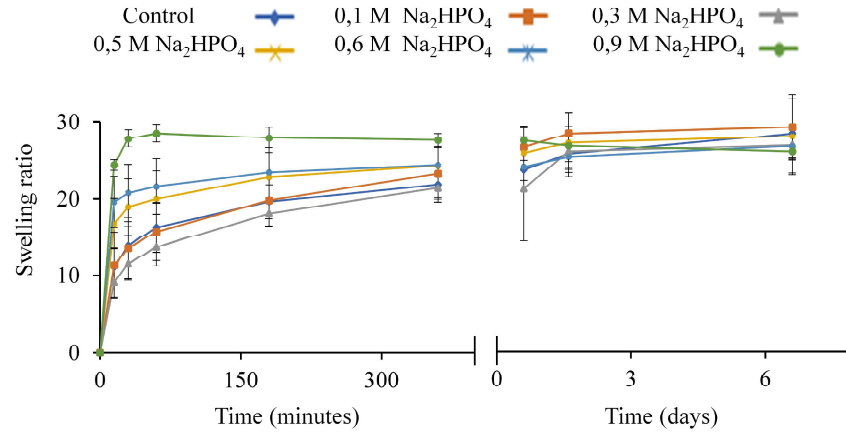


Figure 2. Swelling ratio profile of alginate hydrogels containing different concentrations of Na_2HPO_4 and control without Na_2HPO_4 .

3.1.4 Compressive properties

Compressive properties of hydrogels by Young (Es) and Aggregate (Ha) moduli were determined by Uniaxial unconfined and confined compression respectively, allowing the calculation of Poisson coefficient. All hydrogels followed a similar tendency with higher Ha than Es values which was in accordance with the need of applying a higher force to deform the hydrogel, because in the unconfined compression test, the hydrogel can generate a lateral deformation when a load is applied; while in the confined compression test the lateral hydrogel deformation is constrained because the discs are placed in a confined space [30]. No statistical differences among hydrogels without Na_2HPO_4 and 0.1 and 0.3 M Na_2HPO_4 hydrogels were appreciated (Table 3). In contrast, the presence of 0.5 M, 0.6 M and 0.9 M Na_2HPO_4 showed lower Es and Ha values than hydrogel without Na_2HPO_4 ($p < 0.001$). Poisson coefficient values did not change among all the hydrogels (Table 3).

Table 3. Compressive properties (Young and Aggregate moduli) and Poisson's coefficient of alginate hydrogels containing different concentrations of Na_2HPO_4 and control without Na_2HPO_4 . Values represent mean \pm SD. ***: $p < 0.001$ compared to control hydrogel.

	[Na_2HPO_4]					
	Control	0.1 M	0.3 M	0.5 M	0.6 M	0.9 M
Young modulus (KPa)	10.1 \pm 1.3	9.8 \pm 1.0	11.7 \pm 2.0	7.6 \pm 0.7 (***)	7.9 \pm 0.9 (***)	5.4 \pm 1.2 (***)
Aggregate modulus (KPa)	1092.7 \pm 110.4	1150.3 \pm 96.8	1183.4 \pm 57.6	741.4 \pm 109.8 (***)	724.8 \pm 86.8 (***)	785.5 \pm 119.2 (***)
Poisson's coefficient	0.4984 \pm 0.0002	0.4986 \pm 0.0001	0.4989 \pm 0.001	0.4983 \pm 0.0002	0.4981 \pm 0.0001	0.4986 \pm 0.0006

3.1.5 Pore morphology

The effect of Na_2HPO_4 on the internal structure of all hydrogels was examined by SEM. Hydrogels showed a microporous internal structure and the degree of alginate cross-linking and pore size were similar among hydrogels without Na_2HPO_4 and with 0.1 and 0.3 M Na_2HPO_4 (Figure 3A-C). However, hydrogels with 0.5 M, 0.6 M and 0.9 M Na_2HPO_4 showed lower degree of cross-linking leading to an increase of their pore size (Figure 3D-F).

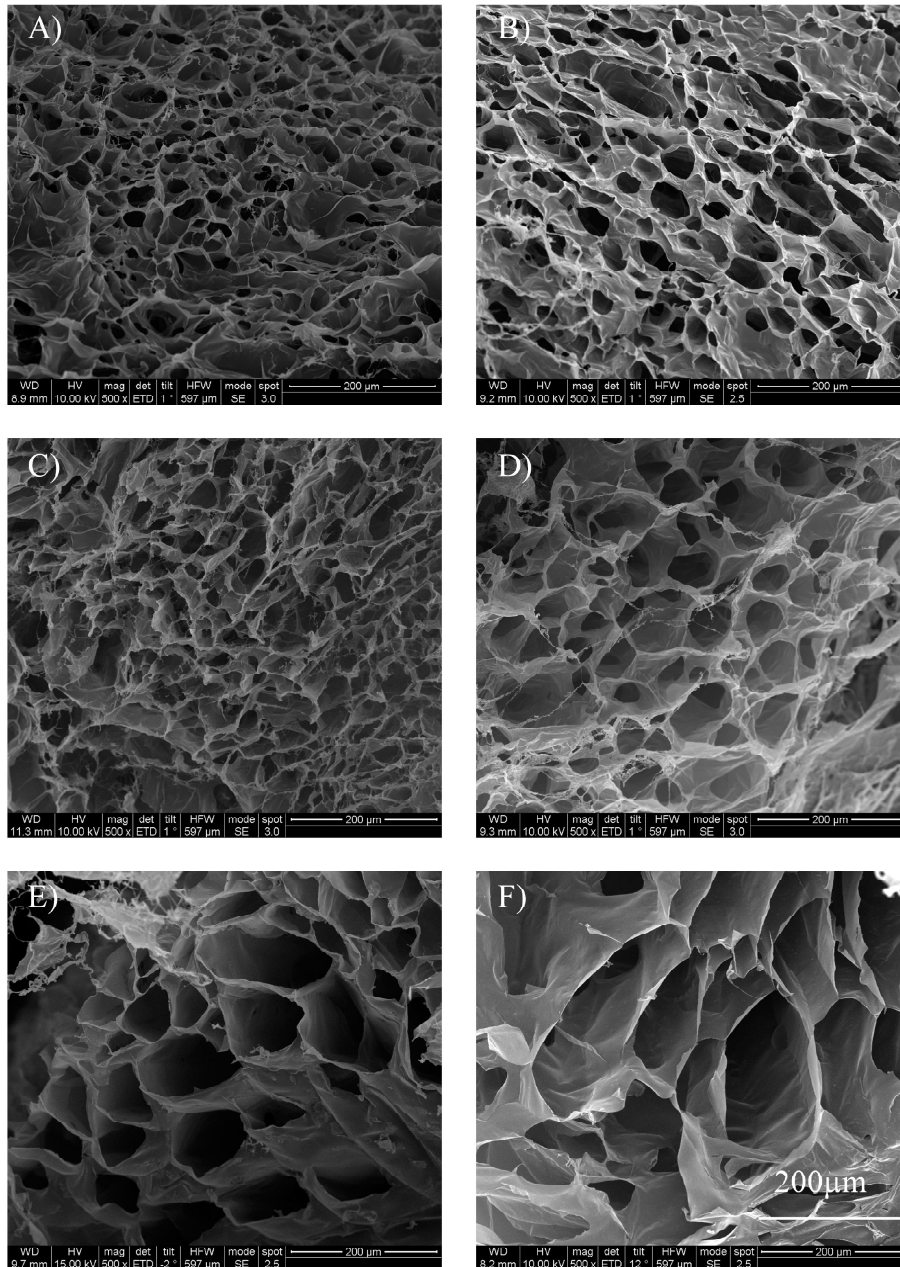


Figure 3. Scanning electron microscopy (SEM) images from the cross-section of alginate hydrogels. A) Control hydrogel without Na_2HPO_4 . Alginate hydrogels containing different Na_2HPO_4 concentrations: B) 0.1 M, C) 0.3 M, D) 0.5 M, E) 0.6 M and F) 0.9 M.

3.2. Biocompatibility of alginate hydrogels containing Na₂HPO₄ with INS1E

After physicochemical characterization, the biocompatibility of alginate hydrogels containing Na₂HPO₄ was assessed.

3.2.1 INS1E cell viability and apoptosis

We quantified the viability of INS1E cells within the different hydrogels by flow cytometry. At day 1 after cell embedding, the percentage of dead cells in all the hydrogels was higher than at the rest of the time points (Figure 4A). Hydrogels with 0.5 M, 0.6 M and 0.9 M Na₂HPO₄ at day 1 showed significantly higher dead cell percentages than the control hydrogel ($p < 0.05$). 7 days after hydrogel formation cell death percentages decreased drastically, keeping below 1% until the end of the assay with no statistical differences among hydrogels. Hence, solely the highest concentrations of Na₂HPO₄ (over 0.5 M) affected cell viability at day 1 after hydrogel formation. We also quantified the percentage of apoptotic cells within the hydrogels. Apoptosis correlated with cell viability with a dramatical reduction of apoptotic cell percentages at day 7 in all the hydrogels, and no statistical differences were detected among the samples at any time point (Figure 4B). Hence, different Na₂HPO₄ concentrations neither promote nor reduce the early apoptotic percentage of INS1E cells within alginate hydrogels.

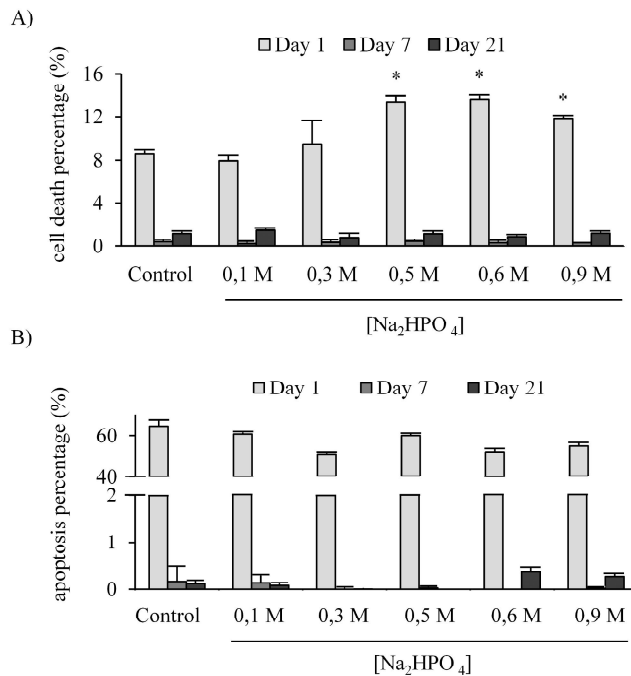


Figure 4. Effect of different Na₂HPO₄ concentrations on the viability of INS1E embedded within different alginate hydrogels compared to control without Na₂HPO₄. A) Live/dead analysis and B) early apoptosis analysis, assessed by flow cytometry. Values represent mean \pm SD. *: $p < 0.05$ compared to control hydrogel.

3.2.2 INS1E cell metabolic activity and membrane integrity

Next, the effect of Na_2HPO_4 on the cell metabolic activity over three weeks was quantified. The highest metabolic activity of embedded INS1E cells was achieved a week after hydrogel formation and, afterwards, it remained stable in alginate hydrogels with low concentrations of Na_2HPO_4 . The different Na_2HPO_4 concentrations did not affect the metabolic activity of the embedded cells at day 1, except at 0.9 M concentration that showed significantly higher metabolic activity than the control ($p < 0.001$) (Figure 5A). At day 7, only hydrogels with 0.6 M and 0.9 M Na_2HPO_4 showed a significant reduction on the INS1E cell metabolic activity compared to control ($p < 0.001$). At day 21, only hydrogels formed with 0.1 and 0.3 M Na_2HPO_4 remained with similar metabolic activity levels than control. The rest of the hydrogels showed a significant metabolic activity reduction which was more notorious when the amount of Na_2HPO_4 was higher ($p < 0.001$). The effect of Na_2HPO_4 on INS1E cell membrane integrity was also assessed. No significant differences over three weeks were detected among all the hydrogels, except for hydrogels with 0.9 M Na_2HPO_4 , which demonstrated significantly higher membrane damage comparing to the control at day 1 ($p < 0.05$), day 7 and 21 (both, $p < 0.01$) (Figure 5B).

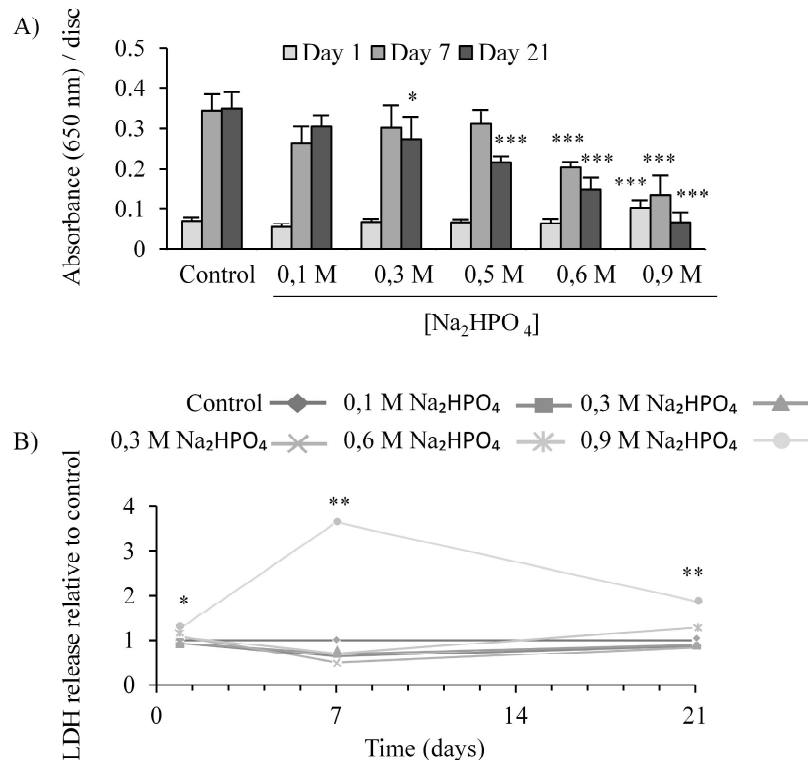


Figure 5. Effect of Na_2HPO_4 on the metabolic activity and membrane damage of INS1E embedded within different alginate hydrogels compared to control without Na_2HPO_4 . A) Metabolic activity and B) membrane damage analysis. Values represent mean \pm SD. *: $p < 0.05$ compared to control hydrogel.

3.2.3 INS1E cell glucose response

We finally evaluated the insulin secretory response to different concentration of glucose to test the application of these hydrogels in the treatment of T1DM. At day 7, when embedded cells showed the highest viability, INS1E cells produced and released insulin (Figure 6), responding to glucose stimuli in all the studied alginate hydrogels. There were no significant differences in glucose-stimulated insulin secretion assay among hydrogels, except for the hydrogel with 0.9 M Na_2HPO_4 that showed significantly lower insulin response after exposure to 16.6 mM glucose ($p < 0.001$).

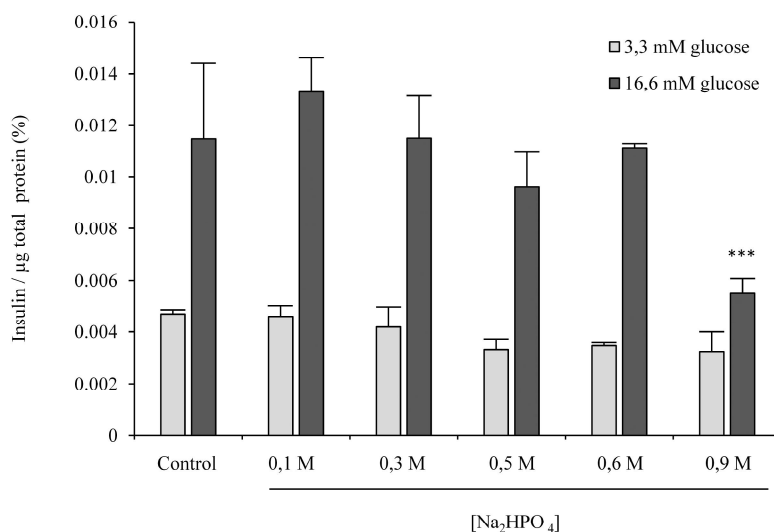


Figure 6. Effect of Na_2HPO_4 on the insulin secretion of INS1E embedded within alginate matrices compared to control without Na_2HPO_4 by glucose-stimulated insulin secretion assay. Values represent mean \pm SD. *: $p < 0.05$ compared to control hydrogel.

4. DISCUSSION

4.1 Characterization of alginate hydrogels containing Na_2HPO_4

We have characterized and compared distinct alginate hydrogels formed with varying concentrations of Na_2HPO_4 , which allows modulating the gelation time and tuning the physicochemical properties of the resultant hydrogels. We have been able to establish the most adequate physicochemical properties of an injectable biomaterial that could be used as a scaffold for insulin-secreting cells. The rheological results showed a stronger elastic behavior, which is characteristic of a predominantly solid-like behavior, an important factor for the attachment of therapeutic cells [31]. A higher final elastic modulus was observed in hydrogels with 0.1 and 0.3 M Na_2HPO_4 than in the control hydrogel, due to the slower release of Ca^{2+} in the presence of HPO_4^{2-} , resulting in a more uniform dispersion of calcium throughout the hydrogel before the cross-linking occurs [20]. However, when the Na_2HPO_4 concentration

increased, the elastic properties of the resultant hydrogels diminished significantly. We hypothesize that at high Na_2HPO_4 concentrations, a part of Ca^{2+} ions are retained as CaHPO_4 , resulting in a lower degree of cross-linking between Ca^{2+} and sodium alginate, leading to a reduction of the elastic properties. This hypothesis based on the Ca^{2+} ions availability is also reflected on the gelation time, since hydrogels with higher elastic properties (low Na_2HPO_4 concentrations) showed shorter gelation times, while hydrogels with lower elastic properties (high Na_2HPO_4 concentrations) demonstrated longer gelation times. Hence, based on their gelation characteristics, alginate hydrogels containing low Na_2HPO_4 concentrations, in the order of 0.1 - 0.3 M, could be good candidates as injectable biomaterials.

Swelling properties are also very useful for studying hydrogels behavior, since it depends on the inner morphological structure of the scaffold, and it is related to the elastic and mechanical properties of the hydrogel [32-34]. Our results showed that Na_2HPO_4 affects the water uptake rate of alginate hydrogels. Hydrogels containing high Na_2HPO_4 concentrations showed faster water uptake rate which inversely correlated with their elastic properties, as hydrogels with faster water uptake rates demonstrated lower elastic modulus. Regarding the compressive properties, the tendency of both E_s and H_a moduli also correlated with the swelling behavior and the elastic properties. Alginate hydrogels containing 0.1 and 0.3 M Na_2HPO_4 demonstrated the highest stiffness, with E_s and H_a values around 9-11 KPa, while hydrogels with higher Na_2HPO_4 concentrations were softer, around 5-7 KPa. Importantly, all tested alginate hydrogels ranged within the described native soft tissues E_s values, validating the studied alginate hydrogels as 3D matrixes able to mimic the characteristics of native soft tissues (0.1 KPa to 40 KPa) [35 36].

SEM analysis provided visual proof of the changes promoted by Na_2HPO_4 on the internal hydrogel structure. Hydrogels with absence of Na_2HPO_4 or with 0.1 and 0.3 M Na_2HPO_4 showed a similar degree of cross-linking as well as similar small pore size, which can explain their similar mechanical properties and slower water uptake rate. On the contrary, alginate hydrogels containing higher Na_2HPO_4 concentrations demonstrated lower degree of cross-linking and, consequently, a higher pore size. These results confirm the hypothesis that Ca^{2+} ions remain as CaHPO_4 providing a lower cross-linking degree. Moreover, hydrogels with a bigger pore size showed softer mechanical properties and an increased permeability reflected on the higher water uptake rate. Similarly, poly-L-lactic acid hydrogels with big pores have shown an enhancement of their permeability and a decrease of their mechanical properties [30].

4.2. Biocompatibility of alginate hydrogels containing Na_2HPO_4 with INS1E

Cell viability and apoptosis assays showed correlation at day 1, when the percentage

of dead cells and apoptosis were as high as almost 10 % and 60 % respectively, as a consequence of the embedding process itself that generates a huge stress on cells [37]. Cell viability was higher in hydrogels containing low Na_2HPO_4 concentrations (0.1 M and 0.3 M) due to their physicochemical properties. In fact, although the porosity of these hydrogels was lower, it did not compromise the nutrient and oxygen diffusion through the hydrogel. Also, these scaffolds provided appropriate mechanical signals to promote cell proliferation and functionality [30]. Importantly, at day 7, dead cells percentages were significantly reduced, cell metabolic activity was the highest and the membrane damage level was the lowest over the whole study.

Focusing on the effect of mechanical properties and porosity over cell behavior, it has been described that INS1E cells within stiffer hydrogels are not able to proliferate [37]. It can be explained by the high alginate concentration that increases the stiffness of the scaffold and reduces the pore size causing higher mechanical cell constrain and nutrient diffusion problems [38]. All our hydrogels contain 1.5 % of alginate, and, consequently, their stiffness is lower and show higher porosity than 4 % alginate hydrogels. Thus, the mechanical stimuli on the cells and nutrient diffusion capacity are different. This fact would explain the differences of INS1E cells behavior between 1.5 % and 4 % alginate hydrogels with higher cell viability and metabolic activity in our scaffolds.

Finally, cells within alginate hydrogels were able to secrete insulin after low and high concentrations of glucose stimulation, similarly to INS1E cells in polyacrylamide gels with stiffness around 13.4 KPa [39]. Cells within all hydrogels demonstrated similar secreted insulin levels, except hydrogels containing 0.9 M Na_2HPO_4 , which showed lower secreted insulin in accordance to its lower metabolic activity. Insulin diffusion through the scaffolds was not affected by the smaller pore size of alginate hydrogels with low Na_2HPO_4 (0.1 M and 0.3 M) as the hydrogel with higher pore size (0.9 M Na_2HPO_4) showed lower amount of secreted insulin. Hence, based on our data, it can be concluded that 1.5 % alginate hydrogels containing 0.1 and 0.3 M Na_2HPO_4 , besides having great injectability properties and an adequate gelation time, provide the best mechanical properties and porosity for INS1E cell support and recovery after hydrogel formation.

5. CONCLUSION

The present study widely deepens on the modulation of alginate gels properties by the inclusion of Na_2HPO_4 as a retardant agent, demonstrating that its addition in the alginate hydrogel forming reaction slows down its gelation time, changes its mechanical properties as well as its porosity, which are very important parameters for cell survival, proliferation

and functionality. Hydrogels containing 0.1 and 0.3 M Na₂HPO₄ showed the ideal injectable properties for their application in the clinic, as well as a good biocompatibility with the preservation of the functionality of INS1E cells. Hence, these scaffolds are excellent candidates to be used as injectable biomaterials.

ACKNOWLEDGMENTS

We thank the ICTS “NANBIOSIS”, specifically by the Drug Formulation Unit (U10) of the CIBER-BBN at the University of the Basque Country UPV/EHU in Vitoria-Gasteiz, the Tissue & Scaffold Characterization Unit (U13) of the CIBER-BBN at the University of Zaragoza, and Professor Maechler from the University of Geneva Medical Center for providing the INS1E cell line.

REFERENCES

- [1] Corritore E, Lee YS, Sokal EM, Lysy PA. Beta-Cell Replacement Sources for Type 1 Diabetes: a Focus on Pancreatic Ductal Cells. *Ther Adv Endocrinol Metab* 2016 Aug;7(4):182-199
- [2] Mettler E, Trenkler A, Feilen PJ, Wiegand F, Fottner C, Ehrhart F, et al. Magnetic separation of encapsulated islet cells labeled with superparamagnetic iron oxide nano particles. *Xenotransplantation* 2013;20(4):219-226
- [3] Yang HK, Yoon K. Current status of encapsulated islet transplantation. *J Diabetes Complications* 2015;29(5):737-743
- [4] Fotino N, Fotino C, Pileggi A. Re-engineering islet cell transplantation. *Pharmacol Res* 2015 Aug;98:76-85
- [5] Krishnan R, Alexander M, Robles L, Foster CE, 3rd, Lakey JR. Islet and stem cell encapsulation for clinical transplantation. *Rev Diabet Stud* 2014;11(1):84-101
- [6] El-Sherbiny IM, Yacoub MH. Hydrogel scaffolds for tissue engineering: Progress and challenges. *Glob Cardiol Sci Pract* 2013 Nov 1;2013(3):316-342
- [7] Lee KY, Mooney DJ. Hydrogels for tissue engineering. *Chem Rev* 2001 Jul;101(7):1869-1879
- [8] Heo EY, Ko NR, Bae MS, Lee SJ, Choi B, Kim JH, et al. Novel 3D printed alginate–BFP1 hybrid scaffolds for enhanced bone regeneration. *Journal of Industrial and Engineering Chemistry* 2017;45:61-67
- [9] Nih LR, Moshayedi P, Llorente IL, Berg AR, Cinkornpumin J, Lowry WE, et al. Engineered HA hydrogel for stem cell transplantation in the brain: Biocompatibility data using a design of experiment approach. *Data in Brief* 2017;10:202-209
- [10] Park H, Lee HJ, An H, Lee KY. Alginate hydrogels modified with low molecular weight hyaluronate for cartilage regeneration. *Carbohydr Polym* 2017;162:100-107
- [11] Riahi N, Liberelle B, Henry O, De Crescenzo G. Impact of RGD amount in dextran-based hydrogels for cell delivery. *Carbohydr Polym* 2017;161:219-227
- [12] Rocca DGD, Willenberg BJ, Qi Y, Simmons CS, Rubiano A, Ferreira LF, et al. An injectable capillary-like microstructured alginate hydrogel improves left ventricular function after myocardial infarction in rats. *Int J Cardiol* 2016;220:149-154
- [13] Lee KY, Mooney DJ. Alginate: Properties and biomedical applications. *Progress in Polymer Science* 2012;37(1):106-126
- [14] Witkowski P, Sondermeijer H, Hardy MA, Woodland DC, Lee K, Bhagat G, et al. Islet grafting and imaging in a bioengineered intramuscular space. *Transplantation* 2009 Nov 15;88(9):1065-1074
- [15] de Vos P, Faas MM, Strand B, Calafiore R. Alginate-based microcapsules for immunoisolation of pancreatic islets. *Biomaterials* 2006;27(32):5603-5617

- [16] Byrne DP, Lacroix D, Planell JA, Kelly DJ, Prendergast PJ. Simulation of tissue differentiation in a scaffold as a function of porosity, Young's modulus and dissolution rate: Application of mechanobiological models in tissue engineering. *Biomaterials* 2007;28(36):5544-5554
- [17] Park JS, Chu JS, Tsou AD, Diop R, Tang Z, Wang A, et al. The effect of matrix stiffness on the differentiation of mesenchymal stem cells in response to TGF- β . *Biomaterials* 2011;32(16):3921-3930
- [18] Tse JR, Engler AJ. Stiffness gradients mimicking in vivo tissue variation regulate mesenchymal stem cell fate. *PloS one* 2011;6(1):e15978
- [19] Richardson T, Barner S, Candiello J, Kumta PN, Banerjee I. Capsule stiffness regulates the efficiency of pancreatic differentiation of human embryonic stem cells. *Acta Biomaterialia* 2016 Apr 15;35:153-165
- [20] Kuo CK, Ma PX. Ionically crosslinked alginate hydrogels as scaffolds for tissue engineering: part 1. Structure, gelation rate and mechanical properties. *Biomaterials* 2001 Mar;22(6):511-521
- [21] Nandini VV, Venkatesh KV, Nair KC. Alginate impressions: A practical perspective. *J Conserv Dent* 2008 January 01;11(1):37-41
- [22] Hoare TR, Kohane DS. Hydrogels in drug delivery: Progress and challenges. *Polymer* 2008;49(8):1993-2007
- [23] Kaklamani G, Cheneler D, Grover LM, Adams MJ, Bowen J. Mechanical properties of alginate hydrogels manufactured using external gelation. *Journal of the mechanical behavior of biomedical materials* 2014 Aug;36:135-142
- [24] Mooranian A, Negrulj R, Takechi R, Jamieson E, Morahan G, Al-Salami H. New Biotechnological Microencapsulating Methodology Utilizing Individualized Gradient-Screened Jet Laminar Flow Techniques for Pancreatic beta-Cell Delivery: Bile Acids Support Cell Energy-Generating Mechanisms. *Mol Pharm* 2017 August 07;14(8):2711-2718
- [25] Mooranian A, Negrulj R, Arfuso F, Al-Salami H. Multicompartmental, multilayered probucol microcapsules for diabetes mellitus: Formulation characterization and effects on production of insulin and inflammation in a pancreatic β -cell line. *Artificial cells, nanomedicine, and biotechnology* 2016 Nov;44(7):1642-1653
- [26] Ashley M, McCullagh A, Sweet C. Making a good impression: (a 'how to' paper on dental alginate). *Dent Update* 2005 April 01;32(3):5
- [27] Anusavice KJ, Phillips RW. *Phillips' science of dental materials*. 11. ed. ed. Philadelphia, Pa. [u.a.]: Saunders; 2003
- [28] Merglen A, Theander S, Rubi B, Chaffard G, Wollheim CB, Maechler P. Glucose Sensitivity and Metabolism-Secretion Coupling Studied during Two-Year Continuous Culture in INS-1E Insulinoma Cells. *Endocrinology* 2004 Feb;145(2):667-678
- [29] Acosta Santamaría V, García Aznar J, Ochoa I, Doblare M. Effect of Sample Pre-Contact on the Experimental Evaluation of Cartilage Mechanical Properties. *Exp Mech* 2013 Jul;53(6):911-917
- [30] Santamaría VA, Deplaine H, Marigió D, Villanueva-Molines AR, García-Aznar JM, Ribelles JLG, et al. Influence of the macro and micro-porous structure on the mechanical behavior of poly(l-lactic acid) scaffolds. *Journal of Non-Crystalline Solids* 2012 Dec;358(23):3141-3149
- [31] Bashir S, Teo YY, Ramesh K, Ramesh S. Synthesis, characterization, properties of N-succinyl chitosan-g-poly (methacrylic acid) hydrogels and in vitro release of theophylline. *Polymer* 2016 Jun 1;92:36-49
- [32] Li W, Kang J, Yuan Y, Xiao F, Yao H, Liu S, et al. Preparation and characterization of PVA-PEEK/PVA- β -TCP bilayered hydrogels for articular cartilage tissue repair. *Composites Science and Technology* 2016 May 18;128:58-64
- [33] Xiao Y, He L, Che J. An effective approach for the fabrication of reinforced composite hydrogel engineered with SWNTs, polypyrrole and PEGDA hydrogel. *Journal of Materials Chemistry* 2012 Mar 27;22(16):876-882
- [34] Yu F, Cao X, Li Y, Zeng L, Zhu J, Wang G, et al. Diels-Alder crosslinked HA/PEG hydrogels with high elasticity and fatigue resistance for cell encapsulation and articular cartilage tissue repair. *Polymer Chemistry* 2014;5(17):5116

- [35] Huang G, Wang L, Wang S, Han Y, Wu J, Zhang Q, et al. Engineering three-dimensional cell mechanical microenvironment with hydrogels. *Biofabrication* 2012 Dec;4(4):042001
- [36] Tibbitt MW, Anseth KS. Hydrogels as extracellular matrix mimics for 3D cell culture. *Biotechnology and bioengineering* 2009 Jul 1;103(4):655-663
- [37] Marchioli G, Gurb v, L, Krieken v, P.P, Stamatialis D, Engelse M, Blitterswijk v, C.A, et al. Fabrication of three-dimensional bioplotting hydrogel scaffolds for islets of Langerhans transplantation. *Biofabrication* 2015;7(2):025009
- [38] Khavari A, Nydén M, Weitz DA, Ehrlicher AJ. Composite alginate gels for tunable cellular microenvironment mechanics. *Scientific reports* 2016;6:30854
- [39] Naujok O, Bandou Y, Shikama Y, Funaki M, Lenzen S. Effect of substrate rigidity in tissue culture on the function of insulin-secreting INS-1E cells. *Journal of Tissue Engineering and Regenerative Medicine* 2017

The background of the slide is a grayscale scanning electron micrograph (SEM) showing a highly porous, interconnected network of fibers. The structure consists of thin, irregularly shaped fibers that form a complex, web-like mesh with numerous small, irregular pores. The overall appearance is that of a highly porous, three-dimensional hydrogel structure.

5

**3D printed macroencapsulation
device combined with tunable
alginate hydrogels represents a
promising approach in Diabetes
Mellitus treatment**



3D printed polyamide macroencapsulation devices combined with alginate hydrogels for insulin-producing cell-based therapies

A. Espona-Noguera^{1,2,†}, J. Ciriza^{1,2,†}, A. Cañibano-Hernández^{1,2}, R. Villa^{2,3}, L. Saenz del Burgo^{1,2*}, M. Alvarez^{2,3}, J.L. Pedraz^{1,2*}

¹NanoBioCel Group, Laboratory of Pharmaceutics, School of Pharmacy, University of the Basque Country (UPV/EHU), Paseo de la Universidad 7, 01006, Vitoria-Gasteiz, Spain.

²Biomedical Research Networking Center in Bioengineering, Biomaterials, and Nanomedicine (CIBER-BBN), Spain.

³Instituto de Microelectrónica de Barcelona (IMB-CNM,CSIC). Campus UAB, 08193 Bellaterra, Barcelona, Spain.

[†]These authors contributed equally to this work

* Corresponding authors

ABSTRACT

Cell macroencapsulation has shown a great potential overcoming the low survival of the transplanted pancreatic islets in the Type 1 Diabetes Mellitus (T1DM) treatment, as it avoids the need for lifelong immunosuppression. It is still not completely known how these devices interact with the host immune system when implanted. However, their surface properties seem to be crucial factors for a successful implant. In this context, the hydrophilicity and porosity of the surface of the macrocapsules are two of the most important properties that can affect the functionality of the graft; hydrophilicity defines the interactions with the host's immune cells, while the porosity determines the biosafety of the device while conditioning the oxygen, nutrients and insulin diffusion. Here, we report a novel β -cell macroencapsulation system that combines an injectable alginate hydrogel with an external 3D-printed implantable device. This external macrocapsule protects the inner hydrogel containing cells, while allowing the precise location of the implant in the body. In addition, it would allow the easy extraction of the grafted cells in the case the implant fails or the renewal of the therapeutic cells is required.

This study evaluates the biological effect of the macroencapsulation devices' surface properties (hydrophilicity and porosity). We studied two different pore sizes and hydrophilicities in four different devices containing rat INS1E β -cells embedded in alginate hydrogels. All the devices showed great biocompatibility, although the hydrophilic ones exhibited higher fibroblast adhesion, which could potentially enhance the fibrotic response when implanted. Importantly, INS1E cells did not escape from the devices, denoting high

biosafety. Cells grown within all devices and maintained their insulin secretory function. However, the hydrophobic device with a smaller pore size showed better cell viability values and, therefore, it might be the best candidate for the development of a safe β -cell replacement therapy in T1DM.

Keywords: Type 1 Diabetes Mellitus, alginate, hydrogel, macroencapsulation.

International Journal of Pharmaceutics. 2019 Jun 5; S0378-5173(19)30453-3

1. INTRODUCTION

Type 1 Diabetes Mellitus (T1DM) is a chronic autoimmune disease characterized by an insulin deficiency caused by the specific pancreatic β -cell destruction, that leads to high blood glucose levels [1]. Daily exogenous insulin injections are an effective therapy to regulate blood glucose levels. Unfortunately, it lacks the capacity to precisely control the glucose homeostasis, which often results in hypoglycemia and hyperglycemia events that can lead to several complications such as cardiovascular diseases, nephropathy, and retinopathy [2,3]. Pancreatic islet transplantation is a promising therapy for reestablishing naturally-regulated insulin production and restoring β -cell function in diabetic patients [4]. However, several obstacles precludes its clinical application, such as the necessity of life-long immunosuppression and the reduction of the islet viability after implantation due to the lack of vascularization and the immune response against the implant [5]. Thus, it is essential the development of protecting systems that assure the long-term islet survival and achieve a physiological insulin production [6].

In this regard, cell encapsulation has emerged as a promising approach to overcome transplantation issues by eliminating the need for immunosuppression, due to the introduction of a physical barrier between the implanted β -cells and the recipient [7]. The most common strategy for pancreatic islet encapsulation involves embedding islets within hydrogel-like biomaterials, which offer immunoprotection and provide similar physicochemical properties to natural soft tissues, such as high-water content, flexibility and stiffness [8,9]. In a previous work, we studied the modulation of the physicochemical properties of alginate-based hydrogels by adding Na_2HPO_4 and its effect on embedded rat INS1E β -cells. Alginate formulations containing 0.3M Na_2HPO_4 provided a feasible gelation time around 8-10 minutes, which facilitates the alginate manipulation when it is required to inject it directly into the body or introduce in any kind of mold or device. Moreover, the mechanical properties of this alginate hydrogel, like stiffness and elasticity, were the most suitable ones for providing great biocompatibility, while maintaining the biological function of the embedded INS1E cells [10]. However, in most cases, hydrogels are fragile and unstable to support the transplanted islets over a long period and, therefore, the long-term islet survival cannot be guaranteed [11]. In this sense, introducing hydrogel-islets biosystems within macroencapsulation devices has become a promising strategy to confer a stronger mechanical protection that results in an improved integrity of the inner hydrogel [12].

Another benefit of using encapsulation approaches, as the one that we have developed in this study, is that the transplanted islets will remain in the specific location where they were first implanted, avoiding their dissemination. In fact, traditional non-

encapsulated pancreatic islet transplantation is performed into the portal vein where many islets can be lost. Thus, islets are usually tracked by radiological imaging techniques [13]. However, macroencapsulation devices would avoid the loss of islets, while permitting an easy graft retrieval and islet replenishment if required [4].

These macroencapsulation approaches are typically based on extravascular chambers that include porous membranes with pore sizes smaller than $1\ \mu\text{m}$ to block the immune agents. The entrance of sufficient oxygen to the cells inside this type of devices requires diffusion from the surrounding blood vessels to the device across the membrane and, next, through the interior of the device to the cells. The required small pore size combined with the large scale of the device can lead to insufficient oxygen diffusion; therefore, limiting the macrocapsule configuration [14]. We previously demonstrated the suitability of a 3D printed polyamide (PA) macrocapsule device with large micropores, with the objective of promoting easier vascularization and increasing the nutrients and oxygen supply. Moreover, with this approach we opened the range of cost-effective rapid prototyping available fabrication techniques, including 3D printing techniques, and the access to a large variety of materials (i.e. naturals and synthetic polymers) [15].

Synthetic polymers are especially interesting for the fabrication of implantable devices due to the capacity to control their physical and chemical properties based on the monomer units, polymerization reaction, and formation of co-polymers of different components at adjustable concentrations. Polyamides, additionally, consist of units linked by amide bonds, similarly to natural proteins (i.e. collagen or silk fibroin), that have demonstrated high biocompatibility [16]. The most common form of PA used in biomedical implants and devices is nylon, which better prevents bacterial transmission in comparison to other materials [17]. However, PA presents low hydrophilicity and high crystallinity. Thus, for the preparation of membranes, it might require additional modifications [18], in order to improve its water permeability and/or antifouling properties. Grafting hydrophilic polymers, including polyethylene glycol (PEG), polyethylene oxide (PEO), and zwitterionic polymers, onto PA surfaces has proved to enhance the antifouling performance [19]. PEG is an uncharged, highly water-soluble, and flexible long chain polymer that is well known for its exceptional ability to resist protein adsorption. The resistance of PEG-coated surfaces rises with increasing density and length of the chains in the surface-grafted film [20]. The grafted hydrophilic polymers are believed to form a hydration layer, through hydrogen bonding or ionic solvation, that serves as a steric repulsive barrier that prevents the attachment of foulants (proteins, cells, biofilm, etc.) on the membrane surface [21]. The way that an implantable device interacts with the biological environment in the implantation site determines the success of the graft. This fact depends on the surface properties, such as

roughness, morphology, pore size, surface hydrophilicity and chemical composition [22,23].

Here, we report a retrievable and straightforward β -cell encapsulation system, which involves the mentioned tunable alginate-based hydrogel and the previously described 3D printed semipermeable macroencapsulation device. In this system, the alginate hydrogel provides an immunoprotecting supportive matrix where the β -cells remain embedded, while the semipermeable macroencapsulation device confers mechanical protection, as well as easy handling and retrieval. We evaluated two of the above-mentioned surface properties in the macroencapsulation device: surface hydrophilicity and porosity. Our aim was to achieve a non-degradable macroencapsulation device, with a functional and biocompatible surface, able to stabilize the inner alginate hydrogel ensuring the biosafety of the system, while providing immunoprotection. Besides, the double encapsulation system should assure the appropriate oxygen, nutrients and insulin diffusion, while maintaining the viability and biological function of the encapsulated β -cells.

2. MATERIAL AND METHODS

2.1. Materials and reagents

Ultrapure low-viscosity high guluronic acid alginate (G/M ratio \geq 1.5) with molecular weight (MW) of 75–200 kDa was purchased from FMC Biopolymer (Norway). Penicillin/streptomycin/glutamine (P/S/G) from Invitrogen (United States), HEPES buffer and dulbecco's phosphate-buffered Saline (DPBS) from Lonza (Switzerland), disodium phosphate dihydrate ($\text{Na}_2\text{HPO}_4 \cdot 2\text{H}_2\text{O}$), trisodium citrate dihydrate, sodium chloride (NaCl) from Panreac (Spain), rat insulin ELISA kit from Mercodia (Sweden), and eagle's minimum essential medium (EMEM) from ATCC (United States). Fetal calf serum (FCS), L-glutamine, bovine serum albumin (BSA), 3-(4,5-dimethylthiazol-2-yl)-2,5-diphenyltetrazoliumbromid (MTT) *in vitro* toxicology assay kit, magnesium chloride (MgCl_2), calcium sulphate dihydrate ($\text{CaSO}_4 \cdot 2\text{H}_2\text{O}$), sodium pyruvate 100 mM, β -mercaptoethanol, potassium chloride (KCl), calcium chloride (CaCl_2), D-mannitol, D-glucose and Polyethylene glycol (PEG) (MW:400KDa) were purchased from Sigma-Aldrich (United States). Roswell park memorial institute (RPMI) medium 1640, fetal bovine serum (FBS), penicillin-streptomycin (P/S), *in vitro* toxicology LDH based assay kit and LIVE/DEAD® viability/cytotoxicity kit were purchased from Life technologies (United States). Polyamide (PA) powder (PA2200, non-filled powder on basis of PA12) was purchased from EOS GmbH (Germany). The mouse fibroblast L929 cell line from ATCC (United States) and the INS1E rat insulinoma cell line [24], provided by the University of Geneva medical center, were used for *in vitro* studies.

2.2. Devices fabrication by laser sintering

Macroencapsulation hydrophobic devices were fabricated as previously described [15]. Briefly, devices were designed with a disc shape of 22 mm external diameter, 20 mm internal diameter and interior cavity of 1.5 mm height. A central pillar was included to reduce the membranes deformation by external pressure. Devices were fabricated by laser sintering (Formiga P100 from EOS GmbH) using a CO₂ laser (10.6 μm wavelength, < 0.5 mm spot size, and 440 mm focus distance) with a power of 25 W and maximum scanning speed up to 5 m/s. Two different groups of devices, with varying sizes of pore and pitch, were fabricated: Device 1 (D1), based on the fabrication of continuous sintered layer with no pattern; and Device 2 (D2), based on a design pattern of square pores of 300x300 μm, with a pitch of 300 μm.

2.3. Hydrophilic treatment

A two steps surface coating process was followed to modify the hydrophobic properties of the fabricated devices. A hydrophilic surface was achieved by exposure of both sides of the devices to an O₂ plasma treatment (200 W, 30 s, 50 ml/min oxygen flow) to generate reactive hydroxyl groups (-OH), followed by immersion into an aqueous PEG solution (1:2) during 4 h. The devices were cleaned with ethanol under ultrasonic bath and dried with nitrogen before and after the plasma treatment. Then we obtained 4 different devices, two non-treated hydrophobic D1 and D2 devices (Phob-D1 and Phob-D2) and, two treated hydrophilic D1 and D2 devices (Phil-D1 and Phil-D2).

2.4. Surface evaluation and pore size determination

The surface morphology and pore size were characterized by scanning electron microscopy (SEM) (Auriga-40 microscope from Carl Zeiss, with an accelerating voltage of 1-2 kV) and optical microscopy. The fabricated devices were cut and both the interior and exterior sides of the membranes were evaluated before and after the surface treatment. The surface hydrophobicity was evaluated by measuring the contact angle of 2 μl water droplets deposited over the devices by using ImageJ analysis software (United States).

2.5. Biocompatibility evaluation of devices surface

Cytotoxicity of the devices was evaluated following the ISO 10993-5. L929 fibroblasts were used to perform the indirect and direct contact tests and the adhesion assay. Cells were cultured in EMEM media supplemented with 10 % FCS, 1 % P/S and 4 mM

L-glutamine at 37 °C in humidified 5 % CO₂ atmosphere. In all the experiments, cells were seeded at a cell density of $3.123 \cdot 10^4$ cells/cm².

In the indirect contact assay, devices were exposed to complete media for 24 h obtaining conditioned media. Next, cells were grown for 24 h, and then exposed to conditioned media for 24 h. In the direct contact test, cells were also cultured for 24 h and exposed directly to the devices by placing them onto the cell monolayer for 24 h. After that, cell viability was measured in both studies using the MTT in vitro toxicology assay kit following manufacturer's recommendations. In both direct and indirect tests, cells with no device exposure were used as controls. In the adhesion assay, cells were seeded onto the devices and, after 4 h, cell viability was measured using following the same MTT procedure. In this adhesion assay, cells seeded directly onto the culture plate were used as control.

In all the assays, the absorbance was recorded using an Infinite M200 microplate reader (TECAN Trading AG, Switzerland) at 570 nm with a reference wavelength set at 650 nm. Four independent experiments were conducted with three replicates each. Cell viability was calculated using the following equation:

$$\text{Cell viability} = (\text{testing sample OD570}/\text{untreated blank OD570}) \times 100.$$

2.6. INS1E cell culture and pseudoislets formation

INS1E cells were cultured in RPMI medium 1640 supplemented with 10 % FBS, 1 % P/S/G, 1 % sodium pyruvate 100 mM, 1M HEPES buffer and 0.1 % β-mercaptoethanol, at 37 °C in a humidified atmosphere containing 5 % CO₂. INS1E pseudoislets were formed by the hanging-drop method. Briefly, 20 μL droplets containing 500 cells/droplet were applied onto the lid of a petri dish and next, the lid was carefully flipped and placed onto the dish. After 5 days, pseudoislets were formed, harvested and immediately used for experimentation.

2.7. Alginate hydrogel preparation

Sodium alginate was dissolved at a concentration of 1.5 % (w/v), sterilized by filtration through a 0.22 μm pore Minisart Syringe Filter (Sartorius, Germany) and mixed with 5×10^6 cells/mL or 2000 pseudoislets/mL. Next, 2.7 mL of alginate-cell suspension were transferred to a LuerLock syringe (BD Syringe, United States); in parallel, another syringe was filled with 60 μL of 1.22 M CaSO₄·2H₂O, 60 μL of 0.3 M Na₂HPO₄·2H₂O and 180 μL of 1 % D-mannitol. The content of both syringes was mixed using Fluid Dispensing Connector (Braun, Germany). The final mixture was loaded into macroencapsulation devices by injection through the inlet. After 10 minutes alginate hydrogels were gelled, and devices

were maintained in complete culture media in a humidified atmosphere containing 5 % CO₂ at 37 °C. Unencapsulated alginate hydrogels were formed in a 12-well plate (same dimensions than the devices) and were used as controls in all biological experiments.

2.8. Cell membrane integrity assay

At day 1 and 21 after encapsulation, alginate hydrogels were removed from devices and, alongside the controls, were incubated with 500 µL of complete medium for 24 h. Supernatants were collected to determine the amount of released LDH using the in vitro toxicology LDH based assay kit. Simultaneously, samples with same conditions were treated with a lysis buffer to determine the total LDH amount. All supernatants were collected and processed following the manufacturer's recommendations. Finally, the absorbance was read on the Infinite M200 microplate reader at 490 nm, with 690 nm measurement as background. Membrane damage values from the samples were relativized to control (unencapsulated alginate hydrogels). Three independent experiments were conducted with three replicates each.

2.9. Viability quantification by flow cytometry

After 1 and 21 days post-encapsulation, alginate hydrogels were removed from the devices, and next all samples and controls were dissolved in 1 % trisodium citrate dihydrate. Then, cells were collected, rinsed with DPBS and stained using the LIVE/DEAD® Viability/Cytotoxicity Kit following the manufacturer's instructions. All samples were analyzed using the BD FACS Calibur flow cytometer (BD Bioscience, United States). Unstained cells and cells stained with calcein or ethidium were established as controls in the cell viability assay. Three independent experiments, with three replicates each one, were conducted.

2.10. Cell viability evaluation by fluorescence microscopy

For INS1E single-cells and pseudoislets viability evaluation, alginate hydrogels were removed from the devices and were stained with the LIVE/DEAD® Viability/Cytotoxicity Kit following manufacturer's indications. Samples were observed under a Nikon TMS microscope with the excitation/emission settings for calcein AM 495/515 nm and ethidium homodimer 495/635 nm. The images of fluorescence microscopy were acquired with a Nikon Eclipse TE2000-Scamera (Nikon, Netherlands), which was controlled by the EclipseNet software version 1.20.0. At least three independent experiments were analyzed.

2.11. Insulin secretion quantification and Glucose-Stimulated Insulin Secretion (GSIS) assay

For insulin secretion quantification at day 7 and 21 after encapsulation, all samples and controls were incubated with complete media for 24 h, next collecting supernatants.

For GSIS assay, 7 days after alginate hydrogels encapsulation, all samples and controls were washed with Krebs-Ringer bicarbonate (KRB) buffer composed of 125 mM NaCl, 3 mM KCl, 0.85 mM CaCl₂, 1.3 mM MgCl₂, 0.1 % BSA and 25 mM HEPES buffer. Next, samples were incubated with KRB containing 3.3 mM and 16.7 mM glucose for 2 hours. Supernatants were collected after each incubation.

The insulin content of collected supernatants was quantified with the Rat Insulin ELISA kit. Three independent experiments, with three replicates each one, were conducted, on both studies.

2.12. Statistical analysis

Statistical analysis was performed with IBM SPSS Statistics software, version 21.00.1. Data were expressed as means±standard deviation and differences were considered significant, for comparison of groups using ANOVA and the Tukey's Post Hoc Test, when $p < 0.05$.

3. RESULTS AND DISCUSSION

3.1. Macroencapsulation device fabrication, surface evaluation and pore size determination

In comparison to other polymers (e.g. polylactic acid and polycaprolactone), polyamides show significant advantages as biomaterial such as their unique combination of mechanical strength, flexibility, toughness, structural similarity to peptides (amide bonds) and resistance, while keeping the ability to be modified. The selected polyamide, on basis of PA12, is a polymer made of repeating molecules with 12 carbon atoms and the repeating amide group $[-C(=O)-NH-]$.

Macrocapsule devices with two different pore sizes were fabricated in polyamide by SLS (Figure 1A-B): D1 devices, based on the fabrication of continuous sintered layer with no pattern; D2 devices, based on a design pattern of square pores of 300 x 300 μm , with a pitch of 300 μm . The final porosity achieved in each device was checked by optical microscopy (Figure 1C-D). Images showed an evident increase in the pore size and pore density between D1 to D2 devices. The obtained mean length of the pores, calculated by

optical image analysis, was of $12 \pm 4 \mu\text{m}$ for D1 devices (maximum length of $30 \mu\text{m}$), and $40 \pm 26 \mu\text{m}$ for D2 devices (maximum length of $170 \mu\text{m}$). Although the mean length is quite similar in both cases, the density of large pores is higher in the D2 device, as shown in the pore size histogram in Fig. 1C-D. Increasing the size of the pore pattern or the pitch during the sintering process, permits to control and tune the macrocapsule porosity.

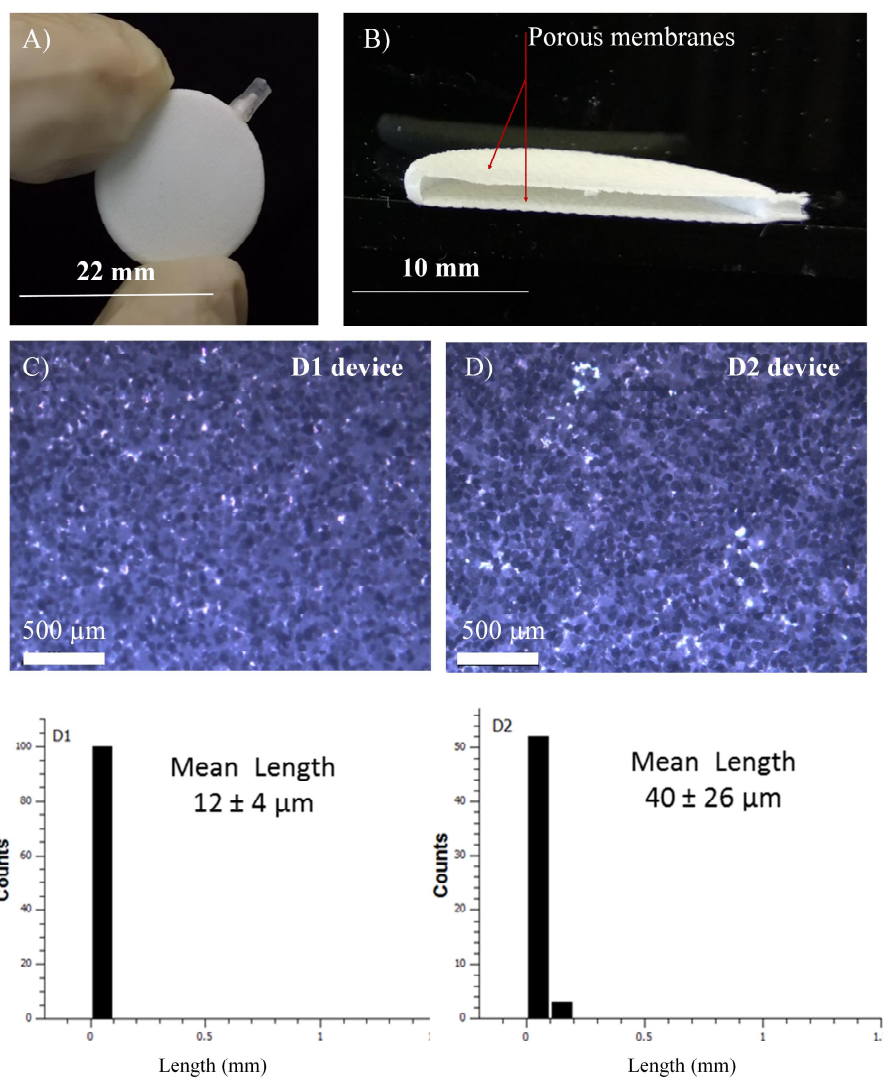


Figure 1. A) Photographs of the macrocapsule device, and B) half cut device showing the interior cavity between the two porous membranes: scale bar 10 mm. C) Optical images of devices D1 and D2 surface with their corresponding pore length histogram. scale bar $500 \mu\text{m}$.

In general, PAs are hydrophilic; however, the hydrophilicity decreases with the number of methylene groups in the polymer backbone, and the roughness of the material surface. The PA surfaces can be easily modified to achieve highly hydrophilic surfaces by using a two-step protocol [18]. Oxygen plasma treatment is widely used to introduce hydroxyl or carbonyl functional groups on material surface, including polyamides [25]. However,

the effects of plasma treatment on surface energy and chemistry are transient. To achieve a permanent hydrophilicity, the macrocapsule devices were immersed into a PEG solution after the plasma treatment. The -OH groups from the PEG react with the carboxyl groups created on the device surface (Figure 2A). PEG was selected for the surface coating because its hydrophilic and anti-fouling properties and its demonstrated biocompatibility [26].

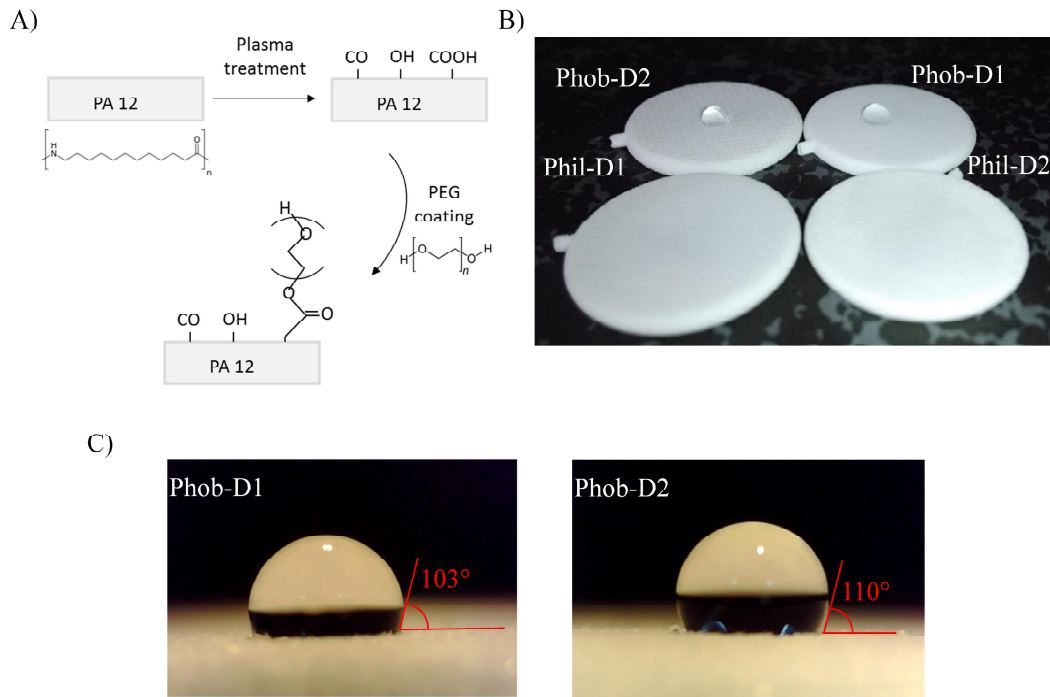


Figure 2. A) Scheme of the chemical reaction during the PA coating with PEG. B) Photograph of the hydrophobic and hydrophilic devices with a water drop on top. C) Close view of the water droplet on top of the Phob-D1 and Phob-D2 devices.

To characterize the PA surface wettability, we evaluated the contact angle (θ_w), formed by a water droplet on top of each device surface (Figure 2B). According to the equation defined by Thomas Young [27], a hydrophobic surface (i.e., $\theta_w > 90^\circ$) is less wettable as a consequence of the higher free energy of its solid–water interface compared to a hydrophilic surface ($\theta_w < 90^\circ$). The water droplet can only be observed on top of the uncoated devices, demonstrating the suitability of the treatment to increase the devices hydrophilicity. The untreated fabricated devices showed a high hydrophobicity, with a contact angle of $103 \pm 3^\circ$ for Phob-D1 devices and $110 \pm 3^\circ$ for Phob-D2 devices, as shown in Figure 2C. The measured contact angle of bare PA surface is in accordance with other reported values, depending on the sintering conditions during the fabrication process (i.e. laser power, speed, number of layers, etc.) and the final roughness [28,29]. After the surface coating, both types of hydrophilic

devices (Phil-D1 and Phil-D2) showed a reduction of the surface hydrophobicity, with a contact angle below 5° (water spread into the surface), similar to other coating approaches [30]. In aqueous solution, PEG has a molecular conformation where uncharged hydrophilic groups are exposed, and shows very high surface mobility (steric exclusion) [21].

The devices morphology was characterized by SEM, before and after the hydrophilic treatment (Figure 3).

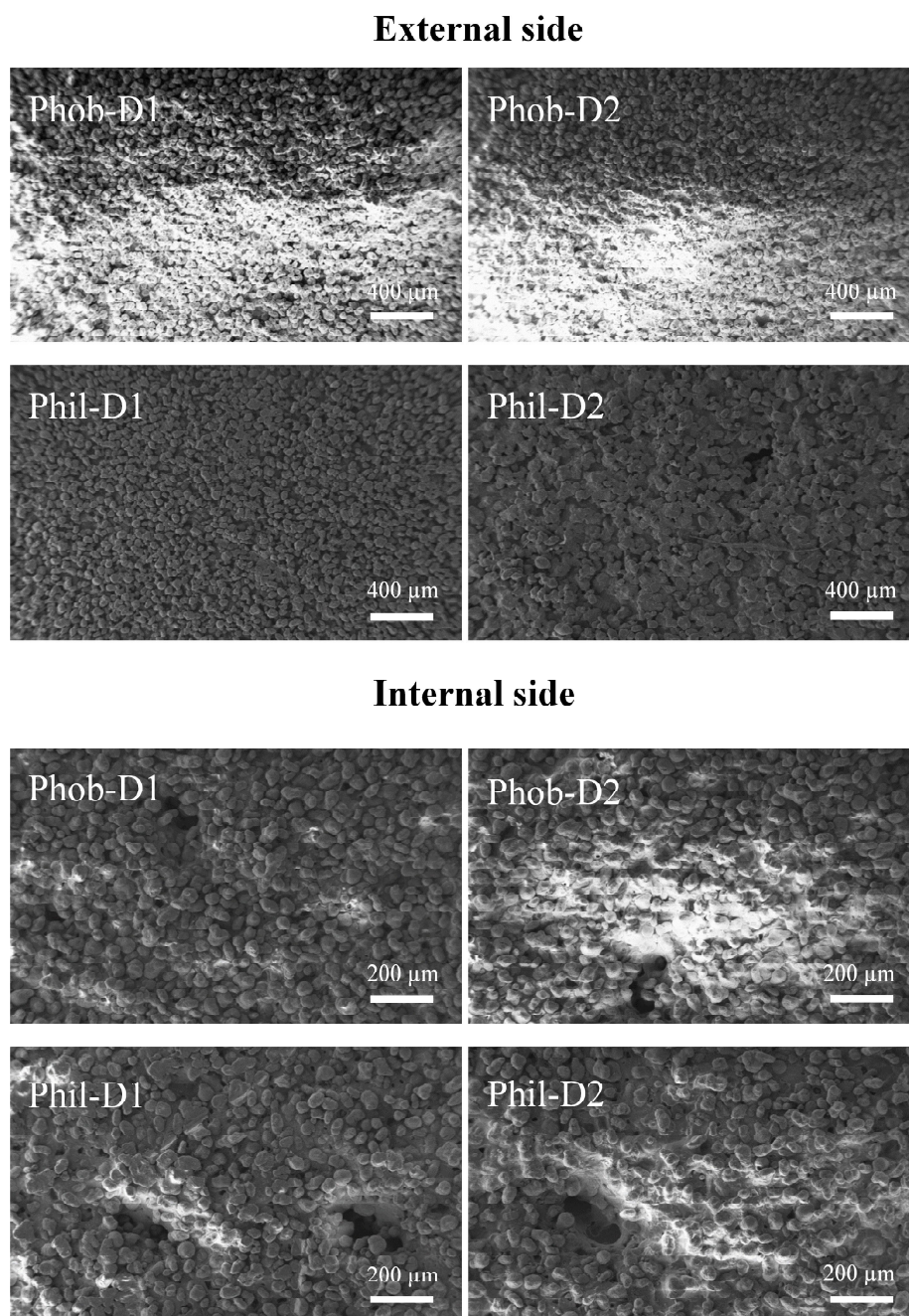


Figure 3. Comparative SEM images showing the morphology of the hydrophobic and hydrophilic devices surfaces: A) external side (scale bar $400\ \mu\text{m}$), and B) internal side of the membrane (scale bar $200\ \mu\text{m}$).

The PA devices showed high roughness due to the sintering conditions (laser power, single layer and high speed) [28], which would contribute to a high density of PEG chains grafted into the PA surface, accordingly to the high hydrophilicity achieved. After the hydrophilic coating, the devices showed flattened and softness of the surface roughness, probably due to a surface etching during the plasma treatment and the following covering with PEG [30], especially in the outer side of the devices while still being this roughness very high.

3.2. Devices surface biocompatibility

Before clinical application, the biocompatibility of an implantable device must be certified by the ISO 10993-5, which recommends three “Tests for in vitro cytotoxicity”: indirect contact, adhesion, and direct contact. The indirect contact test is applied to detect toxins leached from exposed surfaces, while adhesion and direct contact tests are able to detect weak cytotoxicity [31].

Indirect contact results showed a high percentage of viable cells, near 100 %, with no significant differences among all different devices (Figure 4A). However, in the adhesion assay, both hydrophilic devices demonstrated significantly higher ($p < 0.001$) cell adhesion values (approximately 150 %) compared to hydrophobic devices (Figure 4B). In accordance with ISO 10993-5, viability values under 70 % are associated with a potential cytotoxic effect of the tested material [31]. Therefore, none of the studied devices released cytotoxic leachable substances and, demonstrated a high cell adhesion onto the surface with significantly higher values for both hydrophilic devices.

Cell adhesion is a critical factor in the success of an implant [32]. Although the influence of material surface properties (i.e. chemistry, wettability, domain composition and morphology) on subsequent foreign body responses is not totally understood, it is widely demonstrated that polymer surface properties can affect the amount and types of bound proteins [22]. In fact, functional groups on the surface of the device have a significant influence on the biomaterial-mediated fibrotic reaction in terms of fibrotic capsule thickness. For example, polypropylene microspheres functionalized with highly hydrophilic -OH groups trigger a strong inflammatory response and fibrotic capsule formation when implanted subcutaneously in Balb/C mice, with a high presence of inflammatory CD11b⁺ cells, and a fibrotic wall of 100-150 μm of thickness. In contrast, microspheres functionalized with less hydrophilic groups, such as -CH₂ and -COOH, elicit a moderate and mild capsule formation, with a lower presence of CD11b⁺ cells and a fibrotic wall thickness of 40-65 μm [32].

The surprisingly high L929 fibroblast cell adhesion shown in hydrophilic devices could affect negatively the future graft when implanted. In fact, the host's fibroblasts are

the major cells that adhere to the implanted devices thus, walling off the implant by a fibrotic capsule, potentially affecting the device function [34,35]. For example, implantable macroscopic devices used for glucose sensing or β -cell transplantation are generally affected by excessive fibrosis [36,37]. The thick fibrous wall that confines the device limits the diffusion of oxygen, nutrients and insulin, compromising the sensitivity to blood glucose levels changes and increasing the glucose response time. In addition, these diffusion problems affect negatively on cell viability, leading to the complete graft failure [36,37].

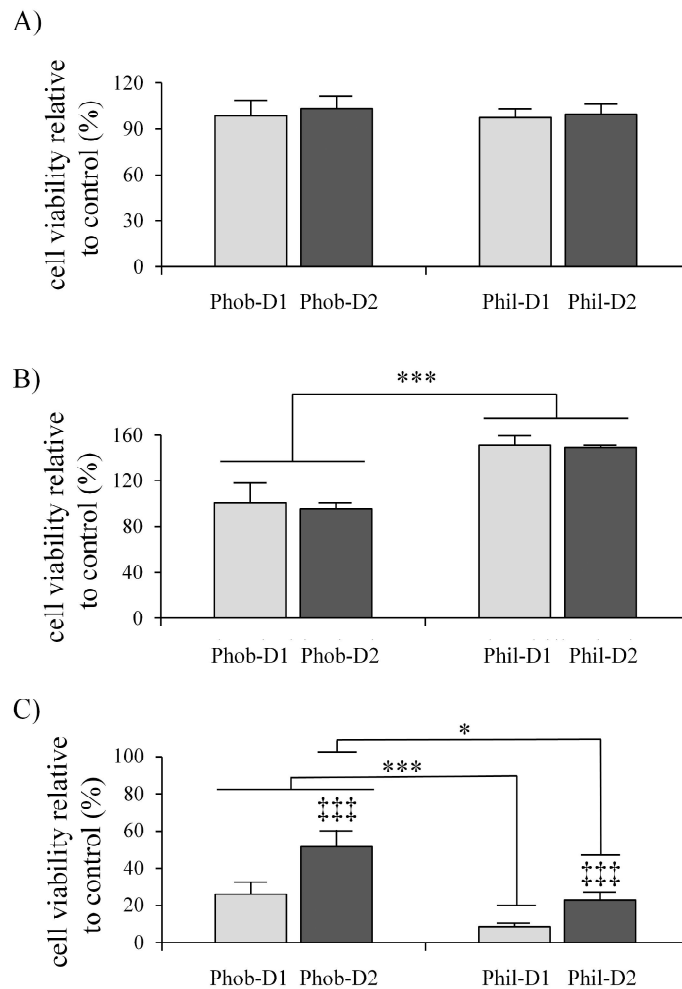


Figure 4. Biocompatibility evaluation of all devices following the ISO 10993-5. A) Indirect contact assay, B) adhesion assay, and C) direct contact assay. Values represent mean \pm SD. *: $p < 0.05$, ***: $p < 0.001$ in the comparison between the hydrophobic and hydrophilic devices, and ###: $p < 0.001$ in the comparison between the different pore sizes of each hydrophobic and hydrophilic devices.

In contrast with the obtained results, PEG coatings are expected to have high anti-fouling properties in accordance to their high hydrophilicity, and associated capacity to form a water layer close to the surface which acts as an energy barrier for protein adhesion

[21,38]. When hydrophilic polymers contact with bulk water, water molecules penetrate into the polymer film to form a hydrogen-bond network, responsible of the resistance to non-specific protein adsorption. However, since hydrogen bonds are relatively easily to break and reform, PEG can decompose in the presence of oxygen and transition metal ions found in most biochemically relevant solutions, and can experience the transition from non-fouling to fouling upon the change in surface hydration, graft density or temperature [21], which could explain the high cell adhesion found on our PEG-coated devices when immersed into the culture media. Besides this change in the anti-fouling properties of the PEG coating, the macrocapsule surface has -CO and -OH terminal groups generated with the plasma treatment that could promote cell adhesion after the dehydration of the PEG layer, resulting in the high adhesion values found experimentally.

On the other hand, the cell adhesion data regarding the hydrophobic devices are in agreement with the expected results when working with hydrophobic surfaces [38]. In fact, similar adhesion values have been described with human osteosarcoma cells MG63 that adhered onto hydrophobic siloxane-coated polystyrene surfaces with a contact angle of 103° [39]. Therefore, the lower L929 fibroblasts adhesion to our hydrophobic devices would indicate higher potential to avoid excessive fibrosis surrounding the device when implanted.

Regarding the direct contact assay, cell viability decreased in all devices compared to controls (Figure 4C). Hydrophilic devices displayed cell viability values of 8.3 % for Phil-D1 and 22.7 % for Phil-D2, while the hydrophobic devices showed significantly higher cell viability values with 25.9 % for Phob-D1 and 51.2 % for Phob-D2 ($p < 0.001$ for the Phil-D1 compared to both hydrophobic devices, and $p < 0.05$ for Phil-D2 compared to the Phob-D2). Considering the results from the previous cell adhesion assay, low cell viability values might be as well caused by the high cell adhesion capacity of all hydrophilic and hydrophobic devices. In fact, when cell monolayers were exposed to the devices, their high cell adhesion capacity promoted an elevated cell detachment from the cell monolayer towards the device. This was confirmed with the detection of blue-stained cells on the devices surface after performing the MTT assay on the retrieved devices (data not shown). Consequently, the colorimetric signal from the remaining attached cells was lower than the one from the controls not exposed to the devices. Moreover, since hydrophilic devices demonstrated higher cell adhesion values than the hydrophobic ones, cell detachment was also higher for the hydrophilic macrocapsules, giving lower cell viability values. There were also differences between pore sizes, with lower cell viability values for both small pore size devices (Phob-D1 and Phil-D1) ($p < 0.001$). Such differences might be explained by the larger surface area of D1 devices, leading to higher cell detachment.

3.3. Biological evaluation of the encapsulated INS1E single-cells

First, we confirmed that pre-gelled alginate hydrogels were able to flow through the loading inlet of the macrocapsules without obstruction allowing a controlled hydrogel deposition. Ten minutes later, devices were opened, confirming that alginate hydrogels were gelled and molded within the inner chamber. Then, the preliminary studies related to cell membrane integrity, viability and functionality were conducted with the rat insulinoma INS1E cell line, one of the most often used insulin-secreting cell line in the field of diabetes research because of their very stable differentiated β -cell phenotype and their capacity to secrete insulin and respond to glucose stimulation [40].

Then, the membrane integrity of the INS1E cells was evaluated (Figure 5A). At day 1, cells showed high membrane damage levels with no statistical differences between each studied device and the alginate control. This damage probably was caused by the cell embedding process, where cells are affected by the high shear forces during the mixing with the high viscosity alginate solution [41]. After 3 weeks, both hydrophilic devices showed significantly higher membrane damage ($p < 0.001$) (54.5 % for Phil-D1 and 69.5 % for Phil-D2) compared to the alginate control (21.4 %). In contrast, the hydrophobic devices showed similar values to the alginate control (26.7 % for Phob-D1 and 24.5 % for Phob-D2).

Regarding the cell viability results obtained by flow cytometry (Figure 5B), at day 1, cell death values were almost undetectable in all conditions, with values under 2 % and no statistical differences among groups. Although cell membranes were damaged, cells remained viable similarly to the alginate hydrogel group. Therefore, the hydrogel loading process within the devices did not suppose an extra stressing step for the cells, as they showed similar values of membrane damage and viability than the alginate control. These results were corroborated by fluorescence microscopy, where no dead cells were detected (Figure 5C). One week after encapsulation, the cell death percentages slightly increased in all conditions with values of dead cells under 5 %. The alginate control group showed the lowest values (around 1 %).

After 3 weeks, cell death percentages significantly increased in all the devices compared to the alginate control group (5.4 % for Phob-D1, 5.6 % for Phob-D2, 8.6 % for Phil-D1 and 17.3 % for Phil-D2, and 2.2 % for the control) (Figure 5B). These results were also corroborated by fluorescence microscopy (Figure 5C). Under the microscope, higher number of dead cells were detected in both hydrophilic devices, demonstrating that at day 21, INS1E single-cells recovered in both hydrophobic devices as well as in the alginate control group, with an important reduction of the cell membrane damage and high cell viability. Moreover, in the calcein/ethidium staining, at day 21 small cell aggregates were observed

in some regions of the alginate hydrogels in all conditions. However, in the Phil-D1 and Phil-D2 devices, a lower number of aggregates were observed and their size was smaller (Figure 5C). The formation of such cell aggregates indicates that INS1E single-cells were able to grow within the alginate matrix forming islet-like structures.

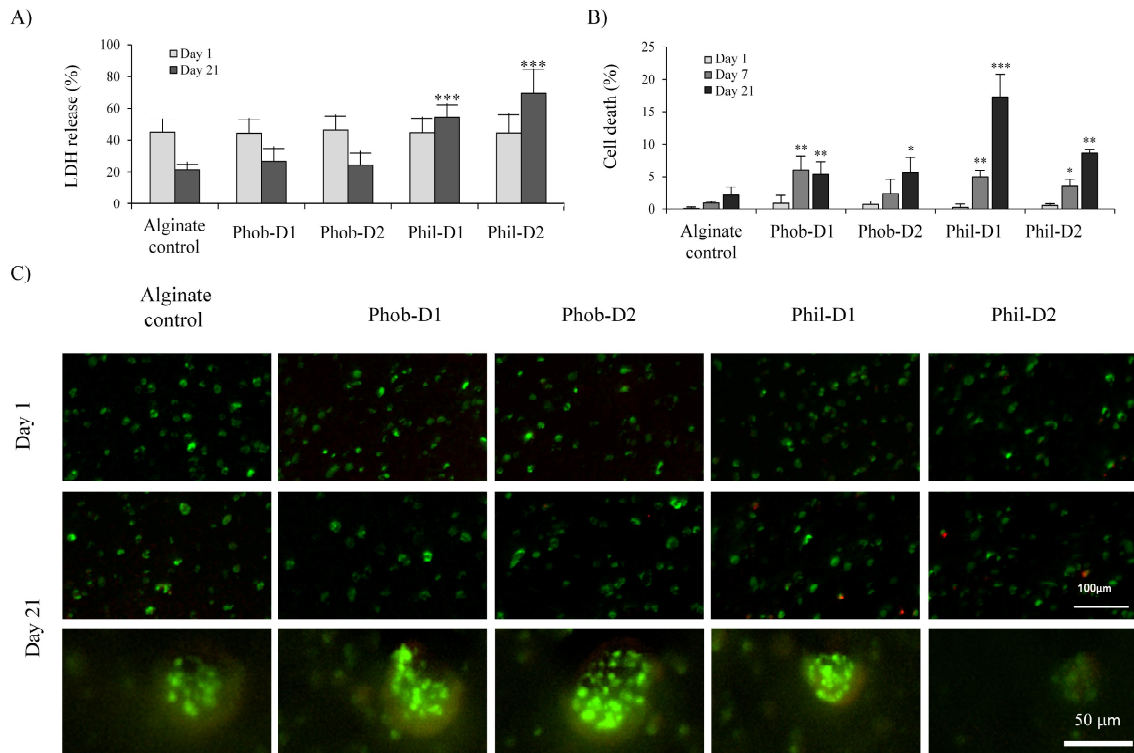


Figure 5. Biological evaluation of the INS1E single-cells within the different devices. A) Cell membrane damage assessment, B) cell viability quantification, and C) fluorescence microscopy of live/dead staining. Scale bar 100 μm . Values represent mean \pm SD. *: $p < 0.05$, **: $p < 0.01$ and ***: $p < 0.001$ compared to alginate control.

The results above could be explained by potential differences in the protein adsorption capacity between hydrophobic and hydrophilic surfaces that could affect the bioavailability of essential proteins of the culture media. In fact, the comparison between the adsorption of albumin and fetal calf serum (FCS) onto polyethylene terephthalate (PET) disks treated with oxygen plasma (hydrophilic surface) or treated with tetrafluoromethane CF₄ plasma (hydrophobic surface), showed that hydrophilic surfaces adsorb higher amounts of proteins from the culture media than hydrophobic surfaces [42]. In this regard, the higher adsorption of proteins onto the hydrophilic surface of our devices might deprive the encapsulated INS1E single-cells from part of these proteins, impeding an appropriate cell recovery after the stress suffered during the encapsulation process. This might be the reason why the high membrane damage values were maintained, and the cell death percentage increased in comparison to the

hydrophobic devices and the alginate control. However, all cell death levels were still low and, therefore, even though there were differences among the devices, all of them allowed an adequate cell survival over time.

3.4. Biosafety evaluation

Most conventional alginate hydrogel-based encapsulation systems are associated with fragility that potentially provokes cell protrusion and escape [11,43]. Therefore, when the encapsulated cells are implanted, individual cells can get out from the alginate matrix and, consequently, the host's immune response is enhanced leading to graft rejection [44]. An important advantage of the encapsulation of hydrogel-like biosystems within macroencapsulation devices is that it allows the confinement of the hydrogel, improving the mechanical protection of the inner hydrogel [6,12]. In this regard, it is crucial to control the outer pore size of the macrocapsule, since too large pore sizes may allow the spreading of the encapsulated cells from the inner hydrogel towards the outside of the device leading again to graft failure [45]. Therefore, we evaluated the biosafety of all the devices under microscope by observing the cells that escaped from the encapsulation system and attached to the culture plate (data not shown).

Results showed that 1 day after encapsulation, a few INS1E cells escaped from the control alginate hydrogel and grown after attaching to the culture plate. Similarly, the murine D3 embryonic stem cell line within 1.5 % alginate hydrogel starts getting out the matrix 4 days post-encapsulation and, more frequently after 14 days in culture [46]. This confirms the low biosafety of the naked alginate hydrogels for cell therapies where cell confinement is required. This biosafety issue is very important for pancreatic islet transplantation, where the hydrogel matrix needs to hold physical stress to avoid any cell exposure that might lead to graft failure [47].

In contrast to the alginate controls, no evidence of cell escaping was observed from the devices even 21 days post-encapsulation. Other devices for pancreatic islets transplantation have smaller outer pore size to ensure high biosafety. For instance, the commercial macroencapsulation device called Theracyte is composed of an inner membrane of 400 nm pore size, and an external membrane with a pore size of 5 μm that promotes neovascularization [45]. However, unlike our approach, cells are freely floating inside the Theracyte chamber, which sometimes results in cell aggregation that leads to loss of cell function or even cell death [11].

Some authors have studied by Atomic Force Microscopy (AFM) the pore size of hydrated alginate hydrogels with similar MW than ours (50-200 KDa), and have determined

that at a concentration of 1.5 % (w/v) the pore size is ranged between 10 and 40 nm [48,49]. In this sense, our macroencapsulation devices could also be considered as a double encapsulation system; where the outer microporous membrane could promote vascularization inside the chamber, and the inner alginate-based nanoporous hydrogel would contain the INS1E single-cells with higher degree of biosafety. In addition, our encapsulation system was able to overcome the aggregation between single cells, which is the problem in the Theracyte device, by maintaining all cells separated within the alginate matrix, thus avoiding loss of β -cell function and death. Hence, data suggest that this kind of double encapsulation systems hold great potential for safe β -cell replacement therapies.

3.5. Insulin secretion and diffusion

We also tested the ability of INS1E single-cells to secrete insulin from the inner alginate hydrogel by measuring the secreted insulin at 1, 7 and 21 days after encapsulation (Figure 6).

One day after encapsulation, insulin levels were under the detection limit of 0.15 $\mu\text{g/L}$, thus being undetectable. By contrast, at day 7 we detected insulin in the supernatant of all devices, thereby demonstrating that the secreted insulin from encapsulated INS1E single-cells was able to diffuse through the alginate hydrogel and the external microporous membrane. Moreover, the amount of insulin that was detected over the time progressively increased probably due to two main factors; on the one hand, cells regained their membrane integrity after suffering stressful conditions during the encapsulation process and, on the other hand, cells were able to grow properly inside the devices as cell aggregates were detected (Figure 5C). There were no statistical differences between D1 devices, but both D1 devices showed significantly higher insulin release than their counterpart Phob- and Phil-D2.

After 3 weeks, significant differences between D1 and D2 devices increased, and the Phil-D2 device showed the lowest insulin secretion profile, correlating with the highest cell membrane damage although its cell death values were similar to the rest of the devices. The lower insulin secretion from INS1E cells within Phob-D2 and Phil-D2 devices compared to their counterpart D1 device might be attributed to changes in the physicochemical properties of the inner alginate hydrogel. In this regard, in a previous study, we observed that the insulin secretion from INS1E single-cells within alginate hydrogels is susceptible to changes of the hydrogel stiffness. In fact, a decrease in the alginate hydrogel stiffness from 11.7 ± 2.0 KPa to 5.4 ± 1.2 KPa, diminishes the metabolic activity of the cells, which leads to a reduction in the insulin secretion [10]. Thus, a higher number of alive cells might not always imply a higher amount of secreted protein because this protein production and release would be dependent

of the metabolic activity of the cells. In this sense, the bigger pore size of the D2 devices supposes a higher exposure of the alginate hydrogel surface to the surrounding media, which might increase the osmotic stress on the hydrogel provoked by the exchange of Ca^{2+} ions from the alginate hydrogel with the Na^+ ions present in the media. Consequently, this ionic exchange would result in progressive loss of stiffness, leading to a reduction in the INS1E metabolic activity and, subsequently, in the insulin secretion [46,50,51]. In addition, the abovementioned higher nutrient deprivation in Phil-D2 device, due to the higher adsorption of essential proteins from the media onto the hydrophilic surface, might also explain that cells within such device displayed the lowest insulin secretion values as a consequence of lower metabolic activity. In contrast, the Phob-D1 device, with a reduction of the cell membrane damage and very low cell death percentages, showed the highest insulin secretion profile.

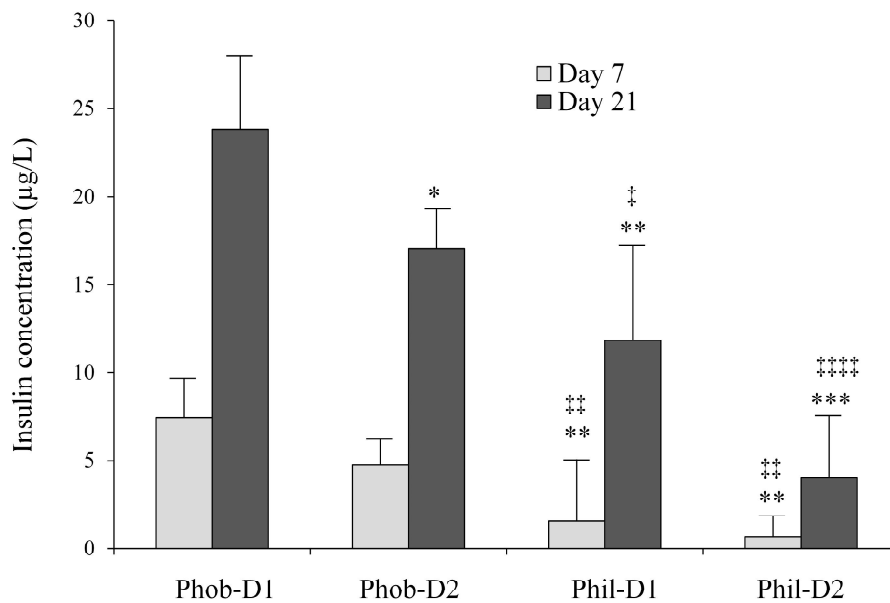


Figure 6. Insulin secretion profile from the encapsulated INS1E single-cells within the different devices. Values represent mean \pm SD. *:p<0.05, **:p<0.01 and ***:p<0.001 compared to Phob-D1 device and, †: p < 0.05, ††: p < 0.01, †††: p < 0.001 compared to Phil-D1 device.

Therefore, our data suggest that the Phob-D1 device is the best option to maintain high cell viability values of encapsulated INS1E single-cells without evidence of cell scraping and to preserve the mechanical integrity of the inner alginate hydrogel. Based on these results, we selected the Phob-D1 and Phil-D1 devices as the most suitable ones among all the studied devices to follow with further in vitro studies.

3.6. Biological evaluation of encapsulated INS1E pseudoislets

Next, we investigated the performance of the Phob-D1 and Phil-D1 devices to

encapsulate pancreatic islet-like cell aggregates. To that end, we generated and encapsulated INS1E pseudoislets of 150 μm of diameter, which is the correspondent size to one islet equivalent (IE) [52], and evaluated the cell viability, insulin secretion, and glucose responsiveness.

Pseudoislets viability was studied under a fluorescence microscope by using the calcein/ethidium staining (Figure 7A). At day 1, although pseudoislets were alive in both D1 devices, some dead cells were observed on the cell aggregates surface due to the mechanical stress suffered during the embedding process within the alginate. Importantly, one week after encapsulation, pseudoislets from both devices were recuperated from the suffered stress during the encapsulation process and no dead cells were observed, neither in the pseudoislets core nor on their surface. After 3 weeks, pseudoislets remained alive, although a few dead single-cells were again visible on the pseudoislets surface in both devices. This might be attributable to the mechanical pressure exerted by the alginate matrix as these cell-aggregates increase their volume. In addition, in both devices we also observed cells from the pseudoislets surface that, in an attempt to continue growing, started to migrate through the hydrogel matrix.

Other macroencapsulation devices lack any physical separation of the islets inside the chamber, resulting in a random islets distribution that favors their aggregation. This aggregation can lead to graft failure, since it supposes a limited diffusion of nutrients and oxygen, the loss of islet functionality and apoptosis [11]. As mentioned above, in other macroencapsulation devices, the encapsulated pancreatic islets are free floating inside a porous chamber with a random spatial distribution, which is unable to maintain them separated becoming closely packed together [53]. In contrast, our encapsulating system with the alginate hydrogel kept the pseudoislets separated, while maintaining their spherical structure without aggregation among them. Therefore, our system was able to prevent the clustering of the pseudoislets, thereby allowing to increase the viable β -cell number. When we quantified the insulin secretion after encapsulation (Figure 7B), both devices showed an increase in the insulin levels over the time. However, comparing these results to the insulin values obtained from encapsulated single-cells (Figure 6), we observed lower insulin values for encapsulated pseudoislets due to the lower number of β -cells forming the embedded pseudoislets. This might be also explained by the difference in the number of encapsulated β -cells; in fact, in the single-cells experiments, there were 5 times higher number of cells compared to pseudoislets. Besides, we did not detected differences in the insulin secretion levels between Phob-D1 and Phil-D1.

Finally, we evaluated the capacity of the encapsulated pseudoislets to respond to glucose challenges exposing pseudoislets to 3.3 mM and 16.7 mM glucose concentrations

(Figure 7C). Results showed that pseudoislets increased insulin secretion when exposed to high glucose, thereby confirming that the encapsulated pseudoislets maintained their biological function.

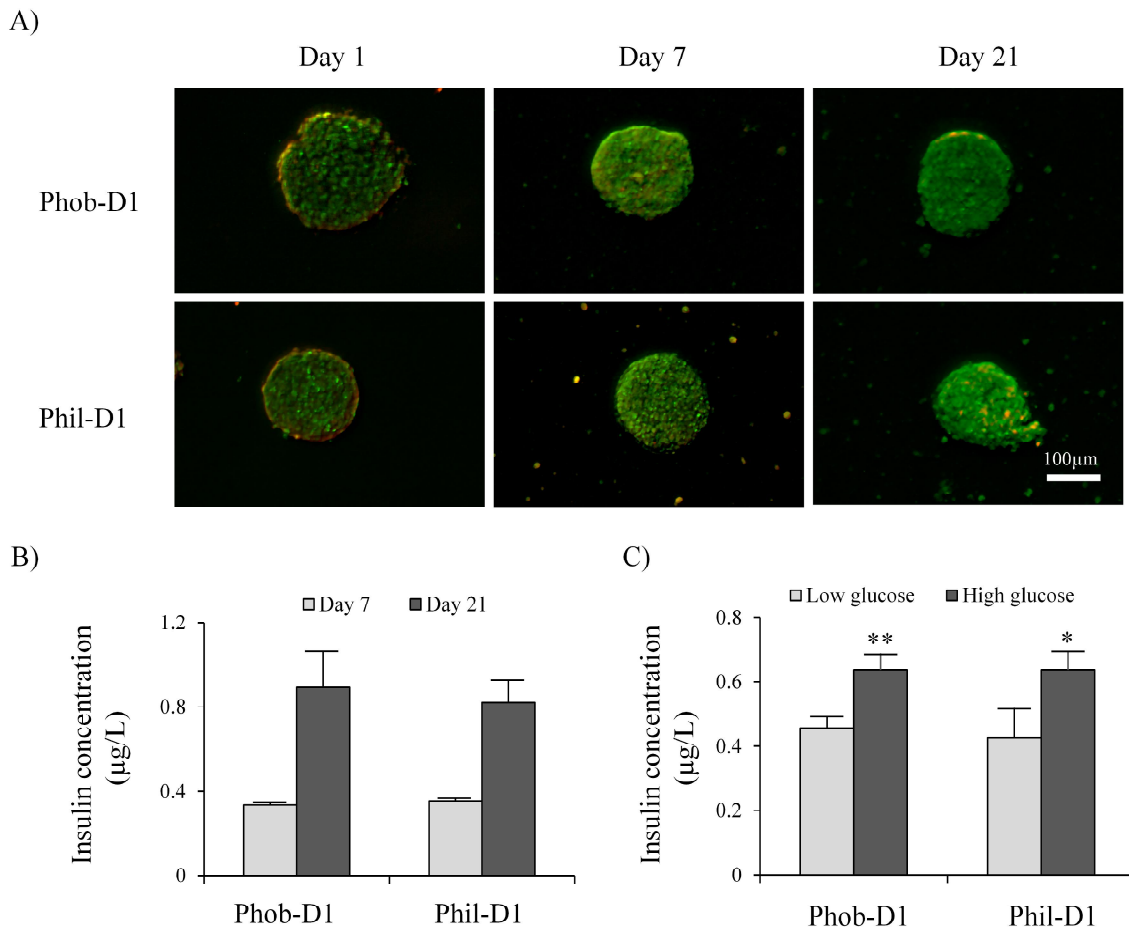


Figure 7. Evaluation of biological parameters of the encapsulated INS1E pseudoislets within the Phob-D1 and Phil-D1 devices. A) Pseudoislets viability by fluorescence microscopy (live/dead staining). Scale bar 100 μm. B) Insulin secretion. C) Glucose-stimulated insulin secretion assay. Values represent mean ± SD. *: $p < 0.05$ and **: $p < 0.01$ between the low and the high glucose conditions.

4. CONCLUSIONS

We can conclude that a double encapsulating system with an alginate-based hydrogel and a 3D printed polyamide macroencapsulation device increases the confinement of single-β-cells and islet-like cell aggregates. In addition, despite the great biocompatibility of all the studied devices, the hydrophobic ones could avoid better an excessive fibrotic response, and devices with smaller pore size provide higher stability to the inner alginate hydrogel, what in

the end translates into an improved insulin secretion from encapsulated INS1E cells. Hence, results suggest that the hydrophobic macroencapsulation system with a $12 \pm 4 \mu\text{m}$ pore size (Phob-D1) might represent a promising approach for safe β -cell replacement therapies in Type 1 Diabetes Mellitus.

ACKNOWLEDGMENTS

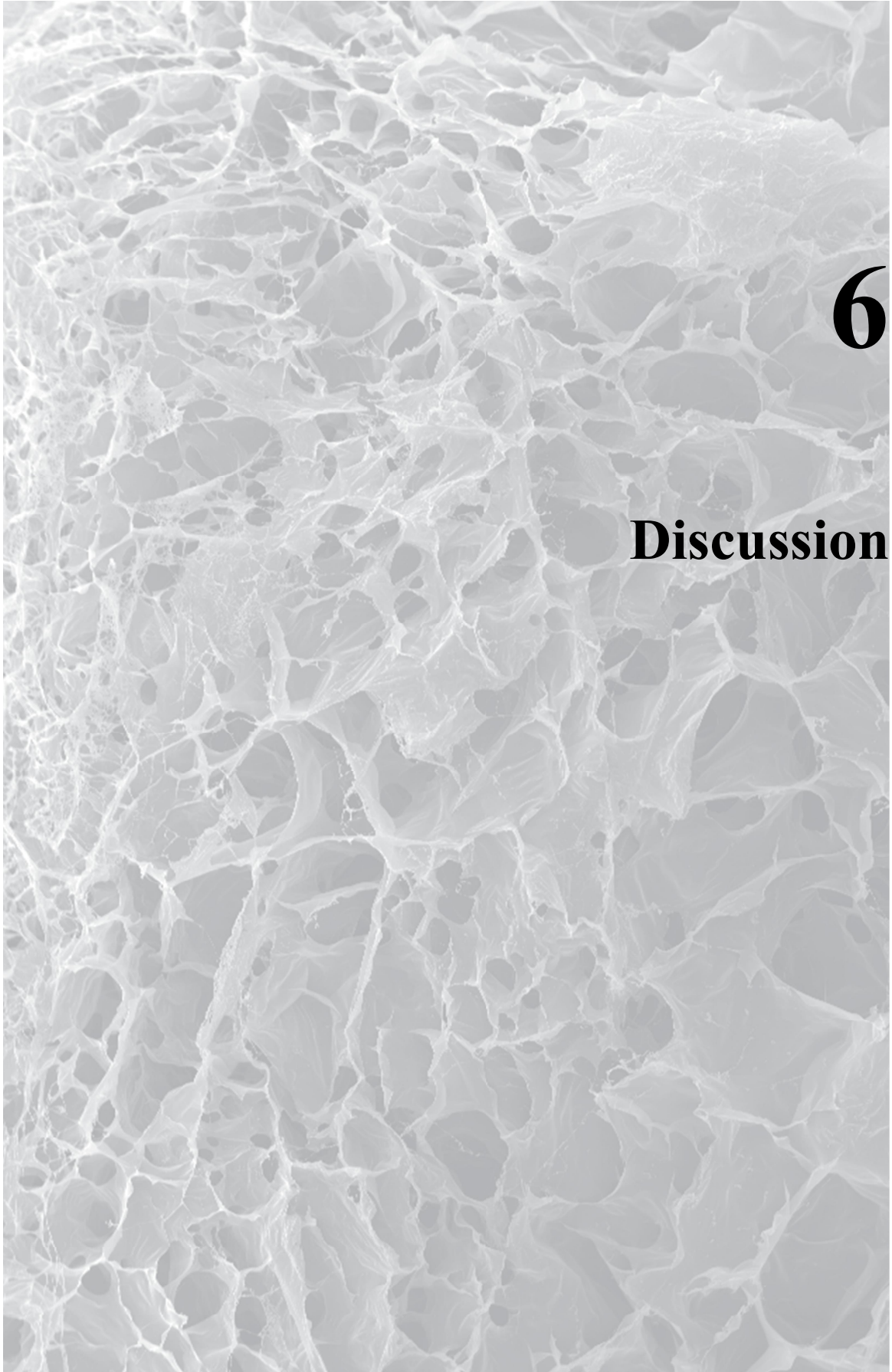
This work was done under the BIOPAN project (CIBER-BBN). Authors wish to thank the ICTS “MICRONANOFABS”, the ICTS “NANBIOSIS” and the Drug Formulation Unit (U10) of the CIBER-BBN. Also, they thank the support from the University of the Basque Country UPV/EHU, the Basque Country Government (Grupos Consolidados, No ref: IT907-16 to JLP), and the financial support from the Ministerio de Economía y Competitividad (MINECO) (Spain) through Ramon y Cajal program (RYC-2013-14479). Finally, the authors acknowledge Professor Maechler from the University of Geneva Medical Center for providing the INS1E cell line.

REFERENCES

- [1] Atkinson MA, Eisenbarth GS and Michels AW. Type 1 diabetes. *Lancet* 2014.
- [2] American Diabetes Association. Diagnosis and classification of diabetes mellitus. *Diabetes Care* 2009.
- [3] Zamboni F and Collins MN. Cell based therapeutics in type 1 diabetes mellitus. *Int J Pharm* 2017.
- [4] Orive G, Emerich D, Khademhosseini A, et al. Engineering a Clinically Translatable Bioartificial Pancreas to Treat Type I Diabetes. *Trends Biotechnol* 2018.
- [5] Sakata N, Sumi S, Yoshimatsu G, et al. Encapsulated islets transplantation: Past, present and future. *World J Gastrointest Pathophysiol* 2012.
- [6] Lathuilière A, Cosson S, Lutolf MP, et al. A high-capacity cell macroencapsulation system supporting the long-term survival of genetically engineered allogeneic cells. *Biomaterials* 2014.
- [7] de Vos P, Hamel AF and Tatarkiewicz K. Considerations for successful transplantation of encapsulated pancreatic islets. *Diabetologia* 2002.
- [8] Singh A and Peppas NA. Hydrogels and scaffolds for immunomodulation. *Adv Mater* 2014.
- [9] Zhu J and Marchant RE. Design properties of hydrogel tissue-engineering scaffolds. *Expert Rev Med Devices* 2011.
- [10] Espona-Noguera A, Ciriza J, Canibano-Hernandez A, et al. Tunable injectable alginate-based hydrogel for cell therapy in Type 1 Diabetes Mellitus. *Int J Biol Macromol* 2018.
- [11] Skrzypek K, Groot Nibbelink M, van Lente J, et al. Pancreatic islet macroencapsulation using microwell porous membranes. *Sci Rep* 2017.
- [12] Kepsutlu B, Nazli C, Bal T, et al. Design of bioartificial pancreas with functional micro/nano-based encapsulation of islets. *Curr Pharm Biotechnol* 2014.
- [13] Cahill D, Zamboni F and Collins MN. Radiological Advances in Pancreatic Islet Transplantation. *Academic Radiology* 2019.
- [14] Schweicher J, Nyitray C and Desai TA. Membranes to achieve immunoprotection of transplanted islets. *Front Biosci (Landmark Ed)* 2014.

- [15] Saenz Del Burgo L, Ciriza J, Espona-Noguera A, et al. 3D Printed porous polyamide macrocapsule combined with alginate microcapsules for safer cell-based therapies. *Sci Rep* 2018.
- [16] Maitz MF. Applications of synthetic polymers in clinical medicine. *Biosurface and Biotribology* 2015; 1: 161-176.
- [17] Teo AJT, Mishra A, Park I, et al. Polymeric biomaterials for medical implants and devices. *ACS Biomaterials Science & Engineering* 2016; 2: 454-472.
- [18] Winnacker M. Polyamides and their functionalization: recent concepts for their applications as biomaterials. *Biomater Sci* 2017.
- [19] Weng X, Ji Y, Zhao F, et al. Tailoring the structure of polyamide thin film composite membrane with zwitterions to achieve high water permeability and antifouling property. *RSC Advances* 2015.
- [20] Ostuni E, Chapman RG, Holmlin RE, et al. A survey of structure-property relationships of surfaces that resist the adsorption of protein. *Langmuir* 2001; 17: 5605-5620.
- [21] Chen S, Li L, Zhao C, et al. Surface hydration: Principles and applications toward low-fouling/nonfouling biomaterials. *Polymer* 2010.
- [22] Thevenot P, Hu W and Tang L. Surface chemistry influences implant biocompatibility. *Current topics in medicinal chemistry* 2008.
- [23] Zamboni F, Vieira S, Reis RL, et al. The potential of hyaluronic acid in immunoprotection and immunomodulation: Chemistry, processing and function. *Progress in Materials Science* 2018.
- [24] Merglen A, Theander S, Rubi B, et al. Glucose Sensitivity and Metabolism-Secretion Coupling Studied during Two-Year Continuous Culture in INS-1E Insulinoma Cells. *Endocrinology* 2004.
- [25] Nuhiji E, Wong CS, Sutti A, et al. Biofunctionalization of 3D nylon 6,6 scaffolds using a two-step surface modification. *ACS Appl Mater Interfaces* 2012.
- [26] Kenan DJ, Walsh EB, Meyers SR, et al. Peptide-PEG amphiphiles as cytophobic coatings for mammalian and bacterial cells. *Chem Biol* 2006.
- [27] Young T. III. An essay on the cohesion of fluids. *Philosophical Transactions of the Royal Society of London* 1805.
- [28] Wu J, Xu X, Zhao Z, et al. Study in performance and morphology of polyamide 12 produced by selective laser sintering technology. *Rapid Prototyping Journal* 2018.
- [29] Extrand CW. Water Contact Angles and Hysteresis of Polyamide Surfaces. *Journal of Colloid And Interface Science* 2002.
- [30] Moses (Varin) KJ, Kim S, Bilal M, et al. Tethered hydrophilic polymers layers on a polyamide surface. *Journal of Applied Polymer Science* 2018.
- [31] Srivastava GK, Alonso-Alonso ML, Fernandez-Bueno I, et al. Comparison between direct contact and extract exposure methods for PFO cytotoxicity evaluation. *Sci Rep* 2018.
- [32] Chandorkar Y, K R and Basu B. The Foreign Body Response Demystified. *ACS Biomaterials Science & Engineering* 2018.
- [33] Nair A, Zou L, Bhattacharyya D, et al. Species and density of implant surface chemistry affect the extent of foreign body reactions. *Langmuir* 2008.
- [34] Morais JM, Papadimitrakopoulos F and Burgess DJ. Biomaterials/tissue interactions: possible solutions to overcome foreign body response. *AAPS J* 2010.
- [35] Damanik FF, Rothuizen TC, van Blitterswijk C, et al. Towards an in vitro model mimicking the foreign body response: tailoring the surface properties of biomaterials to modulate extracellular matrix. *Sci Rep* 2014.
- [36] Bridges AW and Garcia AJ. Anti-inflammatory polymeric coatings for implantable biomaterials and devices. *J Diabetes Sci Technol* 2008.
- [37] Ryan AJ, O'Neill HS, Duffy GP, et al. Advances in polymeric islet cell encapsulation technologies to limit the foreign body response and provide immunoisolation. *Curr Opin Pharmacol* 2017.
- [38] Lih E, Oh SH, Joung YK, et al. Polymers for cell/tissue anti-adhesion. *Progress in Polymer Science* 2015.

- [39] Dowling DP, Miller IS, Ardhaoui M, et al. Effect of surface wettability and topography on the adhesion of osteosarcoma cells on plasma-modified polystyrene. *J Biomater Appl* 2011.
- [40] Skelin M, Rupnik M and Cencic A. Pancreatic beta cell lines and their applications in diabetes mellitus research. ALTEX 2010.
- [41] Lee KY and Mooney DJ. Alginate: properties and biomedical applications. *Prog Polym Sci* 2012.
- [42] Recek N, Jaganjac M, Kolar M, et al. Protein adsorption on various plasma-treated polyethylene terephthalate substrates. *Molecules* 2013.
- [43] Bhujbal SV, de Haan B, Niclou SP, et al. A novel multilayer immunoisolating encapsulation system overcoming protrusion of cells. *Sci Rep* 2014.
- [44] Wilson JL and McDevitt TC. Stem cell microencapsulation for phenotypic control, bioprocessing, and transplantation. *Biotechnol Bioeng* 2013.
- [45] Krishnan R, Alexander M, Robles L, et al. Islet and stem cell encapsulation for clinical transplantation. *Rev Diabet Stud* 2014.
- [46] Wilson JL, Najia MA, Saeed R, et al. Alginate encapsulation parameters influence the differentiation of microencapsulated embryonic stem cell aggregates. *Biotechnol Bioeng* 2014.
- [47] Vaithilingam V and Tuch BE. Islet transplantation and encapsulation: an update on recent developments. *Rev Diabet Stud* 2011.
- [48] Simpliciano C, Clark L, Asi B, et al. Cross-Linked Alginate Film Pore Size Determination Using Atomic Force Microscopy and Validation Using Diffusivity Determinations. *Journal of Surface Engineered Materials and Advanced Technology* 2013.
- [49] Leal-Egana A, Braumann UD, Diaz-Cuenca A, et al. Determination of pore size distribution at the cell-hydrogel interface. *J Nanobiotechnology* 2011.
- [50] Kuo CK and Ma PX. Ionically crosslinked alginate hydrogels as scaffolds for tissue engineering: part 1. Structure, gelation rate and mechanical properties. *Biomaterials* 2001.
- [51] Kaklamani G, Cheneler D, Grover LM, et al. Mechanical properties of alginate hydrogels manufactured using external gelation. *J Mech Behav Biomed Mater* 2014.
- [52] Scharp DW, Marchetti P, Swanson C, et al. The effect of transplantation site and islet mass on long-term survival and metabolic and hormonal function of canine purified islet autografts. *Cell Transplant* 1992.
- [53] Jiang L, Liu J, Wang K, et al. Investigating design principles of micropatterned encapsulation systems containing high-density microtissue arrays. *Sci China Life Sci* 2014.



6

Discussion

CELL ENCAPSULATION: TOWARDS THE DEVELOPMENT OF ADVANCED B-CELL REPLACEMENT THERAPIES FOR TYPE I DIABETES MELLITUS

Currently, Diabetes Mellitus (DM) affects more than 400 million people across the world [1,2]. Type 1 DM (T1DM) represents the 10 % of the total cases and it is characterized by severe insulin deficiency, and the subsequent elevation of blood-glucose levels, that lead to devastating vascular complications (Figure 1) [3,4].

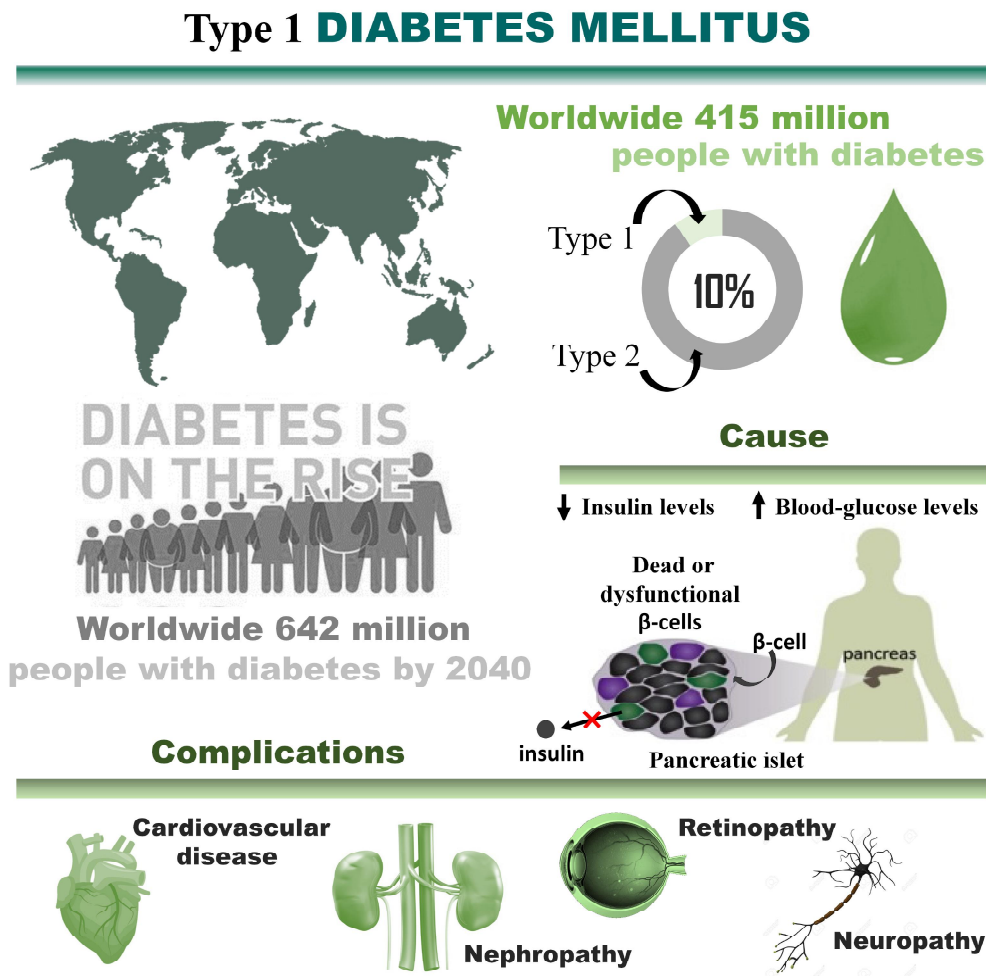


Figure 1. Infographic of worldwide incidence, cause, and complications of Type 1 Diabetes Mellitus

At present, the treatment through the administration of insulin fails in maintaining a stringent control of adequate blood-glucose levels [5,6]. Alternatively, pancreatic islet transplantation appears to be a promising approach for blood-glucose levels restoration, as it avoids complications associated with daily insulin administrations, and reduces the surgical risks associated with whole pancreas transplantation [7]. However, islet transplantation

treatment still possesses several limitations that hamper its widespread clinical application [8]. The most relevant obstacles include: loss of a large percentage of the transplanted islets after implantation (> 60 %), need for immunosuppression, and low islet survival in the long term [9,10]. Therefore, until the abovementioned deficiencies are not addressed, islet transplantation will remain as a treatment that will only be available for carefully selected cases of severe T1DM.

In order to overcome such limitations, cell encapsulation aims to encapsulate therapeutic cells within biocompatible materials that give mechanical support, mimic the islets' native biological micro- and macro-environment, and provide immunoisolation [8,11]. Nowadays, micro- and macroencapsulation of pancreatic islets are the most studied β -cell replacement strategies. In fact, several clinical trials have successfully achieved the restoration of the insulin secretory function. In both approaches, materials that are able to form hydrogels have been widely used for pancreatic islet encapsulation because of their great properties, such as excellent biocompatibility and physicochemical characteristics similar to the natural soft tissues. Moreover, hydrogels provide protection against immune cells and high molecular weight cytotoxic molecules, while allowing the diffusion of oxygen, nutrients, and hormones such as insulin [12-14].

Among these materials, alginate is the most commonly used biomaterial for both micro- and macroencapsulation of pancreatic islets, as it provides high biocompatibility, low cytotoxicity, and allows a fast and easy gelation under mild conditions [15]. However, both types of encapsulation approaches using alginate have got some obstacles that difficult their clinical translation. On the one hand, the elevated number of empty microcapsules that are generated during the encapsulation process limits the clinical application of the microencapsulation technology using alginate. Those empty microcapsules increase the therapeutic graft volume, which can result in an enhanced immune reaction after implantation. On the other hand, the macroencapsulation of cells using alginate is restricted due to the poor control over the alginate gelation process, and the fragility of the formed hydrogel. In this sense, the fast gelation of alginate makes difficult its manipulation when injected into the body or inside an implantable device. In addition, the fragility of the hydrogel does not ensure the long-term survival of the encapsulated islets.

In the present work, we have addressed several limitations of the β -cell micro- and macroencapsulation technologies with the goal of giving a boost to these advanced cellular therapies towards their widespread clinical application.

MICROENCAPSULATION TECHNOLOGY

A magnetic microcapsule-sorting device allows reducing the microencapsulated pseudoislets graft volume through an automatized purification process

One of the most important limitations of the microencapsulated islet-based therapy is the high number of empty microcapsules generated during the microencapsulation process. These non-therapeutic microcapsules considerably increase the graft volume, which can enhance the host immune reaction after implantation [16]. Currently, the reduction of the graft volume is accomplished by separating the microencapsulated islets from the empty microcapsules by hand selection. Therefore, this manual procedure is tedious and slow, which compromise its reproducibility [16,17].

In this context, we developed a magnetic sorting microfluidic device that allows separating the empty microcapsules from the microencapsulated islets. The aims of this study were: 1) to investigate the effect of the magnetic separation process itself on β -cell viability and biological function; 2) to reduce the therapeutic graft volume of microcapsules, and 3) to assess the therapeutic potential of purified microcapsules in Wistar rats with induced T1DM. In this study, we generated islet-like cell aggregates of 150 μm in diameter using the rat insulinoma INS1E cell line, that were used as a model of pancreatic islets.

To perform the magnetic purification, pseudoislets were magnetized with Fe_3O_4 /PEI-based nanoparticles (NPs) before microencapsulation to enable the magnetic separation of microcapsules within the microfluidic device. For this reason, we first studied the effect of Fe_3O_4 /PEI-based NPs used in the magnetization process of pseudoislets. After exposing pseudoislets to different Fe_3O_4 /PEI NPs concentrations, the 80 μg Fe_3O_4 /PEI NPs/mL was chosen as the optimal concentration for pseudoislets magnetization. At this concentration, cell viability was not affected, and pseudoislets showed the highest magnetic-derived mobility that allowed the displacement of the microcapsules inside the microfluidic device during the purification process. Afterwards, we encapsulated the magnetized pseudoislets within alginate (A) and alginate-poly-L-lysine-alginate (APA) microcapsules. These two types of microcapsules display different key physical properties that are crucial for the survival and the biological function of the microencapsulated pseudoislets. In particular, A microcapsules would provide better glucose and insulin diffusion, which is necessary for appropriate insulin secretion from microencapsulated pseudoislets *in vivo*; while APA microcapsules would confer higher mechanical strength, which is required to avoid their breakage during the mechanical stress generated in the magnetic purification process. [18,19]. After magnetic purification of A and APA microencapsulated pseudoislets, we confirmed that the magnetic separation was successfully performed, as many empty microcapsules were observed in the

non-purified sample while a higher presence of microencapsulated pseudoislets was noted in the purified sample (Figure 2).

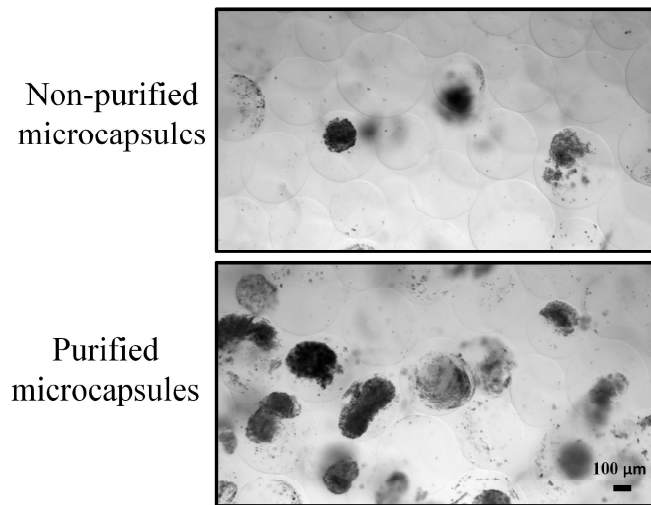


Figure 2. Representative brightfield microphotographs of microencapsulated pseudoislets directly after encapsulation (Non-purified microcapsules) and after 3 recircularized magnetic separations (Purified microcapsules). Scale bar: 100 μm .

Then, the physical integrity of the microcapsules and the pseudoislets viability of A and APA purified samples were evaluated. A microcapsules experienced progressive breakage as we detected increasing amounts of un-encapsulated fragmented pseudoislets in the culture plates (Figure 3A). The poor mechanical integrity of A microcapsules may be attributed to the low stability of the ionically cross-linked alginate hydrogels, where the exchange of Ca^{2+} ions from the hydrogel with the Na^{+} present in the media can lead to progressive degradation of the hydrogel [20]. In contrast, the higher mechanical strength provided by the PLL coating allowed APA microcapsules to endure the mechanical stress and avoid breakage. Thereby, with APA microcapsules we ensured the biosafety and functionality of the future graft, as pseudoislets remained alive and encapsulated through time (Figure 3B). At this point, we discarded A microcapsules because their massive breakage would enhance the host's immune reaction leading to graft failure. However, this type of microcapsules cannot be discarded for other biomedical applications such as regenerative medicine, where cells are required to escape from the capsules and regenerate the damaged tissue.

Finally, we estimated the purification efficiency and glucose responsiveness by measuring the secreted insulin. Results showed an insulin secretion ratio (purified/non-purified samples) of 4.67 ± 0.9 for APA microencapsulated pseudoislets, which would entail an important graft volume reduction of 78.6 %. Moreover, pseudoislets from purified APA samples displayed an adequate glucose responsiveness, as their insulin secretion under high-

glucose culture conditions increased almost 3 times (2.71 ± 0.16) compared to their insulin secretion at low-glucose conditions (Figure 3C).

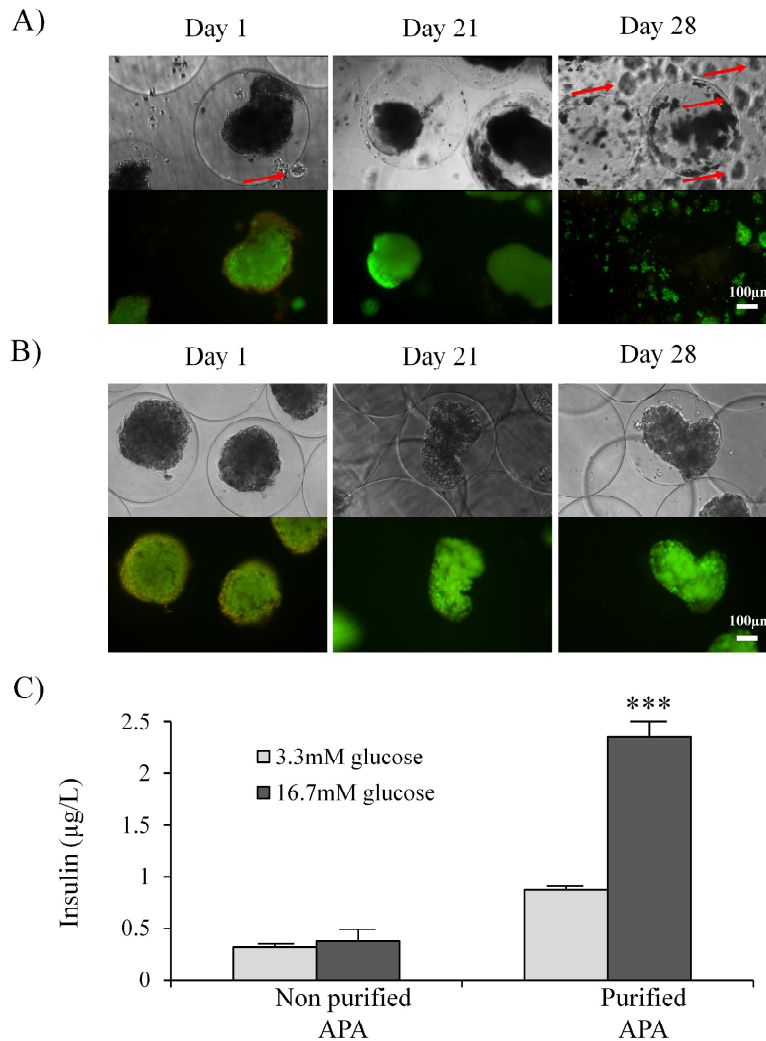


Figure 3. Brightfield microphotographs and fluorescence microscopy images of purified A) A, and B) APA microencapsulated INS1E pseudoislets. Red arrows identify fragmented INS1E cell aggregates. Scale bar: 100 µm. C) Glucose-stimulated insulin secretion of APA microencapsulated INS1E pseudoislets before and after 3 recircularized magnetic separations. Values represent mean \pm SD. ***: $p < 0.001$ compared to low glucose condition.

Overall, for a proper *in vivo* T1DM reversal, pseudoislets must remain viable within the microcapsule and display appropriate glucose responsiveness. Also, microcapsules must provide a high degree of biosafety, enduring physical and osmotic stress, to avoid any cell exposure, as their breakage might trigger the host's immune response against the exposed pseudoislets, implying the graft rejection [21,22]. For these reasons and based on our results, we considered APA microcapsules the most suitable microencapsulation approach to perform the *in vivo* study with diabetic Wistar rats. As shown in Figure 4A, blood-glucose levels

were monitored after diabetes induction in all the studied groups: rats implanted with empty microcapsules, purified and non-purified microencapsulated pseudoislets, as well as healthy and diabetic control rats.

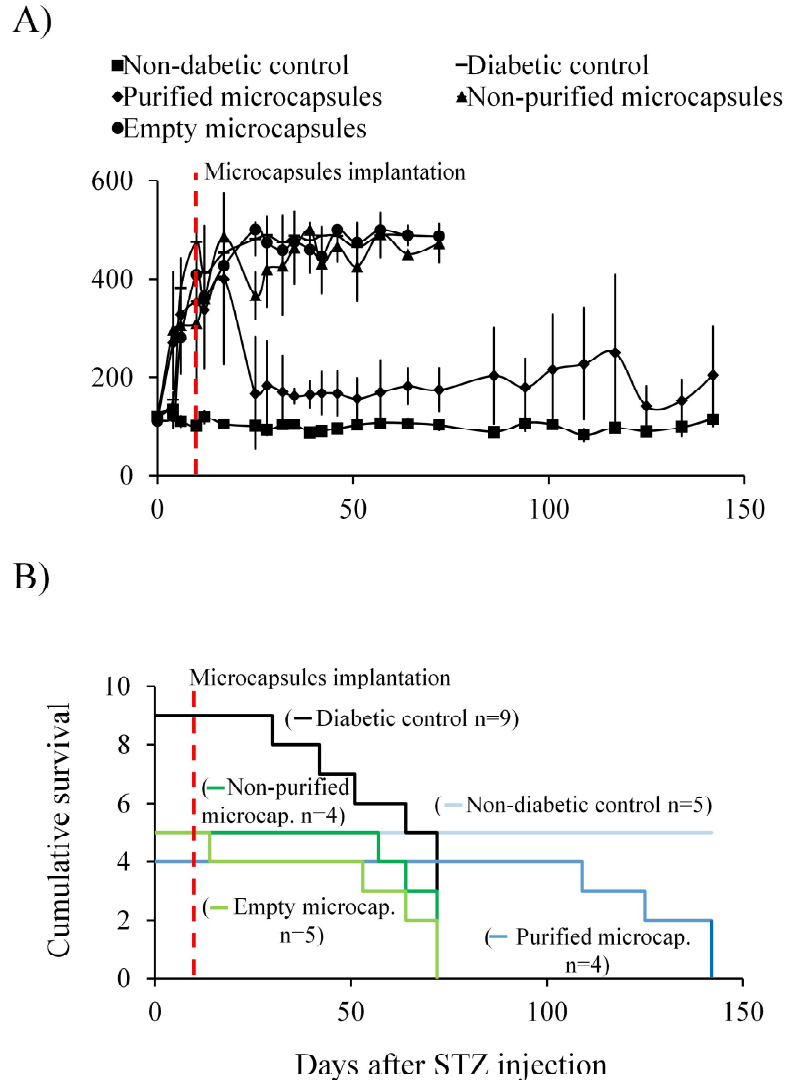


Figure 4. A) Long-term monitoring of blood-glucose levels of STZ-induced diabetic Wistar rats implanted with empty microcapsules, non-purified and purified microcapsules containing INS1E pseudoislets. Non-diabetic and non-implanted diabetic rats were used as controls. B) Kaplan-Meier analysis of rats from different groups. Dotted red lines identify the microcapsules implantation time point.

After 19 days, blood-glucose levels of rats implanted with purified microcapsules significantly decreased, reaching values within the normal glycemic range (< 200 mg/dL), very close to the non-diabetic control levels. In contrast, the rest of the STZ-treated groups remained diabetic, with blood-glucose levels between 350-500 mg/dL. These results correlated with the cumulative survival analysis data (Figure 5B), where diabetic animals

began to show discomfort early and were sacrificed. In contrast, animals with restored glycaemia showed higher survival rates. In this line, in a work published by de Vos and cols., Albino Oxford (AO) rats implanted with 2-2.5 mL of non-purified APA microencapsulated allogeneic Lewis-islets become normoglycemic within 5 days after implantation (< 200 mg/dL) [23]. Other authors have used a lower implantation volume of microencapsulated islets (1.7 mL), and animals also achieved normoglycemia 10 days after implantation [24]. Interestingly, although the therapeutic effect of our purified microencapsulated pseudoislets was detected later than in the mentioned studies, the reduced implantation volume that we used (0.4 mL) was also able to restore normoglycemia. These results show that we are able to achieve similar therapeutically relevant results implanting 4 to 6 times less volume of microcapsules [23-25].

Advances, limitations and future directions

The developed magnetic microcapsule sorting system boosts up the cell microencapsulation technology towards its translation to the clinics in the field of β -cell replacement for T1DM.

Although microcapsules can be implanted using a minimally invasive procedure, nowadays, the possible implantation sites are restricted to a few, due to the large volume of microcapsules that need to be implanted. Thus, the intraperitoneal cavity is the most used implantation site in clinical trials, as it has a high capacity to hold the entire therapeutic dose [26-28]. In this sense, the reduction of the therapeutic volume of microcapsules that we achieved with our purification system would add more flexibility to this β -cell replacement approach. In fact, as the volume of the graft is highly reduced, microcapsules could be implanted within other implantation compartments that have lower volumetric capacity such as the kidney capsule providing a more favorable environment.

In terms of biosafety, the implantation of microcapsules does not allow easy and complete removal of the transplanted microencapsulated islets since there is no control over the location of every single microencapsulated islet [29,30]. In this sense, the reduction of the implantation volume would open new strategies involving devices containing microcapsules, for example. This approach would combine the advantages of using microcapsules (suitable glucose sensing, adequate insulin diffusion, etc.) with the benefits of using larger devices holding the microcapsules, which would enable safer graft implanting/removal procedures. From another point of view, our technology allows the automatization of the purification process, avoiding manual steps and, consequently, minimizing technical errors. However, this system still has some limitations that need to be addressed before its clinical application. The primary issue resides in the long time required to process the total initial volume of

microcapsules through the system and, then, the time needed to perform the subsequent recircularization steps to achieve high yields of purification (several hours). This could be a problem when treating larger animals or humans. In fact, if higher volumes of microcapsules were required, the processing time to achieve a high purification performance would be considerably longer. Indeed, the processing of 12 mL of non-purified microcapsules requires around 4 hours to finally obtain the highly purified microcapsules pool. In clinical settings, the needed volume of microencapsulated islets increases up to 270-300 mL [31,32], which makes inviable the use of this technology at large-scale. In this sense, to reduce the processing time and make more efficient our technology, it would be interesting to develop a purification system involving several microfluidic devices in parallel. This would highly increase the capacity of processing the initial non-purified microcapsules. In addition, such parallel devices could be connected serially with more microfluidic devices, thereby performing the three recircularizations in one single step (Figure 5).

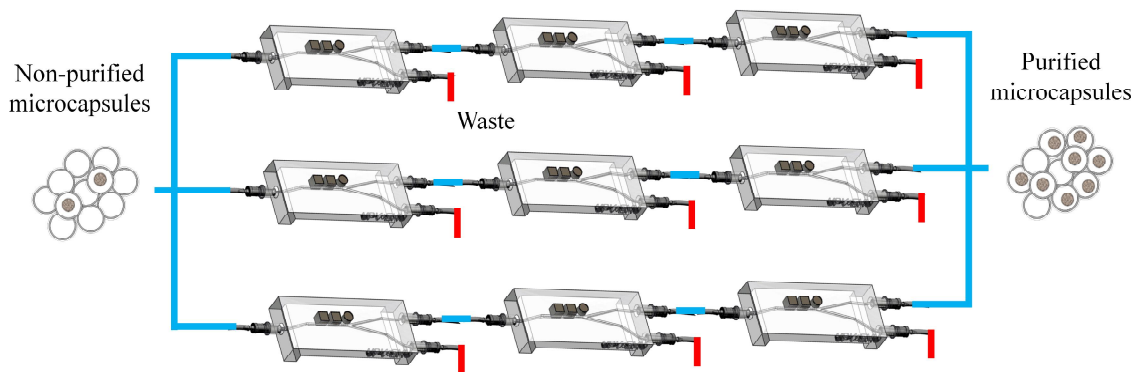


Figure 5. Schematics of a possible purification system involving serially and in parallel connected devices to increase the capacity of purification and to reduce the processing time.

Another aspect to take into account before the clinical application of this separation approach is that the validation of the system has been conducted with artificial pseudoislets that were homogenous in size (150 μm in diameter) without considering that pancreatic islets are highly variable in size [33]. In this sense, future experiments should focus on optimizing the magnetization process for the heterogeneous population of pancreatic islets, in order to achieve the appropriate magnetic-derived motion that allows their accurate purification through the microfluidic device.

MACROENCAPSULATION TECHNOLOGY

The addition of phosphate salts (Na_2HPO_4) allows modifying the physicochemical properties of alginate hydrogels while maintaining β -cells viable and functional. Hydrogel-based cell therapies usually allow delivering cells through minimally invasive techniques, such as simple hydrogel injection in the implantation site, or introduction of the hydrogel within an implantable device that enables easy implanting/retrieval procedures [34,35]. However, one of the most important limitations of islet macroencapsulation approaches using alginate is the fast and poorly controlled gelation process [36,37]. Nowadays, the lack of control over the alginate gelation rate forces clinicians to manage this technology very quickly under stressful working conditions. Alternatively, alginate hydrogels can also be made in molds outside the body and clinicians can implant the final gelled product by more invasive surgical procedures in comparison to a simple injection [38]. Therefore, the fast gelation of alginate affects the injectability of the therapeutic product, which restricts its clinical use for cell delivery [39-40]. In this context, the ideal gelation rate of a suitable hydrogel for cell delivery should be fast enough, in the order of minutes, but, at the same time, the hydrogel should remain in a viscous state long enough to facilitate its manipulation and injection [34,38].

In this work, with the objective of achieving a better control over the alginate gelation rate to facilitate its application for β -cell delivery in T1DM treatment, we explored the effect of the phosphate salt-based retardant agent Na_2HPO_4 in the alginate gelation reaction. The goal of this study was to establish the most adequate alginate/ Na_2HPO_4 formulation that could be used as an injectable hydrogel for β -cell delivery. To that end, we characterized the physicochemical properties of alginate hydrogels formed with varying Na_2HPO_4 concentrations, and we determined their biocompatibility with the embedded β -cells.

First, we determined the physicochemical properties of each alginate hydrogel formulation (Table 1). Results showed stronger elastic than viscous behavior, which is characteristic of a predominantly solid-like behavior, an important factor for the attachment of therapeutic cells. The elastic modulus (G') observed in hydrogels with 0.1 and 0.3 M Na_2HPO_4 was higher than in the control hydrogel. We might think that the slower alginate gelation in the presence of Na_2HPO_4 resulted in a more uniform distribution of Ca^{2+} throughout the hydrogel; thus, achieving a more homogeneous cross-linking degree that could explain the higher G' values compared to the control [36]. However, when the Na_2HPO_4 concentration was increased over 0.3 M, the elastic properties of the resultant hydrogels diminished significantly. We hypothesize that at high Na_2HPO_4 concentrations, a part of the Ca^{2+} ions could be retained as CaHPO_4 , resulting in a lower degree of cross-linking between alginate

molecules and, consequently, leading to a reduction of the elastic properties of the hydrogel. This hypothesis is also reflected on the gelation time values, since hydrogels with higher elastic properties (low Na₂HPO₄ concentrations) showed shorter gelation times (in the range of minutes), while hydrogels with lower elastic properties (high Na₂HPO₄ concentrations) demonstrated longer gelation times (in the range of hours).

Table 1. Rheological properties (G' and G'' moduli), gelation time, homogeneity, water content and Young's modulus of alginate hydrogels containing different concentrations of Na₂HPO₄ and control without Na₂HPO₄. Values represent mean ± SD. *: p < 0.05, **: p < 0.01 and ***: p < 0.001 compared to control hydrogel.

	[Na ₂ HPO ₄]					
	Control	0.1 M	0.3 M	0.5 M	0.6 M	0.9 M
Elastic modulus G' (Pa)	853.2 ± 110.2	1165.5 ± 177.8(*)	1445.6 ± 55.3(*)	468.6 ± 73.9(*)	483.8 ± 97.2(*)	27.9 ± 6.4(*)
Viscous modulus G'' (Pa)	87.4±9.1	108.1±15.7	120.9±4.5(*)	31.2±2.8(*)	30.5±4.8(*)	6.8±1.2(*)
Gelation time (min)	4.2±0.2	7.7±0.4(**)	9.9±0.2(**)	73.3±7.6(**)	148.5±13.1(**)	253.3±25.2(**)
Homogeneity	0.3±0.014	0.3±0.007	0.3±0.014	0.3±0.002	0.3±0.014	0.3±0.010
Water content (%)	97.2±0.7	97.5±0.7	97.2±0.5	97.1±0.6	97.5±0.1	96.1±0.5
Young modulus (KPa)	10.1±1.3	9.8±1.0	11.7±2.0	7.6±0.7(***)	7.9±0.9(***)	5.4±1.2(***)

The different degree of cross-linking due to changes in the internal hydrogel structure promoted by the addition of different Na₂HPO₄ concentrations, were visualized in the SEM analysis (Figure 6). Hydrogels without Na₂HPO₄ or with low Na₂HPO₄ content showed a similar degree of cross-linking, with pores of small size in the internal structure, which can explain their similar rheological properties. Besides, the small size of those pores also explained the compressive properties values. In fact, hydrogels containing low Na₂HPO₄ concentrations demonstrated the highest Young's modulus (Es) due to the higher cross-linking degree (Table 1).

On the contrary, hydrogels containing higher amounts of Na₂HPO₄ demonstrated a lower degree of cross-linking with bigger pores, resulting in softer hydrogels with lower Es values (Table 1). Importantly, the stiffness of all tested alginate hydrogels was within the range of Es values of native soft tissues; thus, validating the studied alginate hydrogels as adequate scaffolds able to mimic the mechanical characteristics of soft tissues [41,42]. Altogether, these results confirmed the hypothesis that Ca²⁺ ions remain as CaHPO₄ providing a lower cross-linking degree.

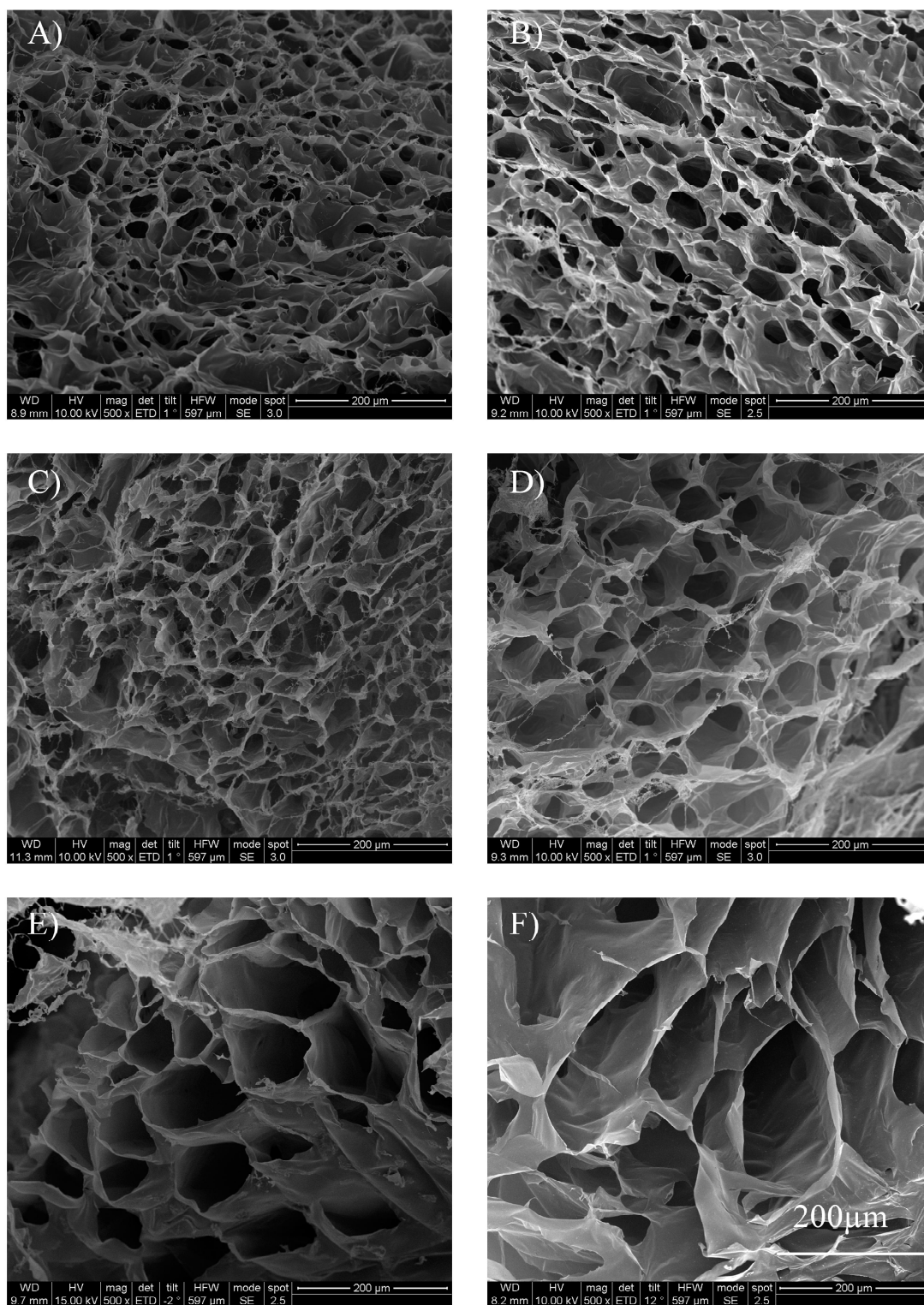


Figure 6. Scanning electron microscopy (SEM) images from the cross-section of alginate hydrogels. A) Control hydrogel without Na_2HPO_4 . Alginate hydrogels containing different Na_2HPO_4 concentrations: B) 0.1 M, C) 0.3 M, D) 0.5 M, E) 0.6 M and F) 0.9 M. Scale bar: 200 μm

After performing the physicochemical characterization, we evaluated the biocompatibility of all the studied alginate hydrogels with embedded INS1E rat β -cells (Figure 7A-C).

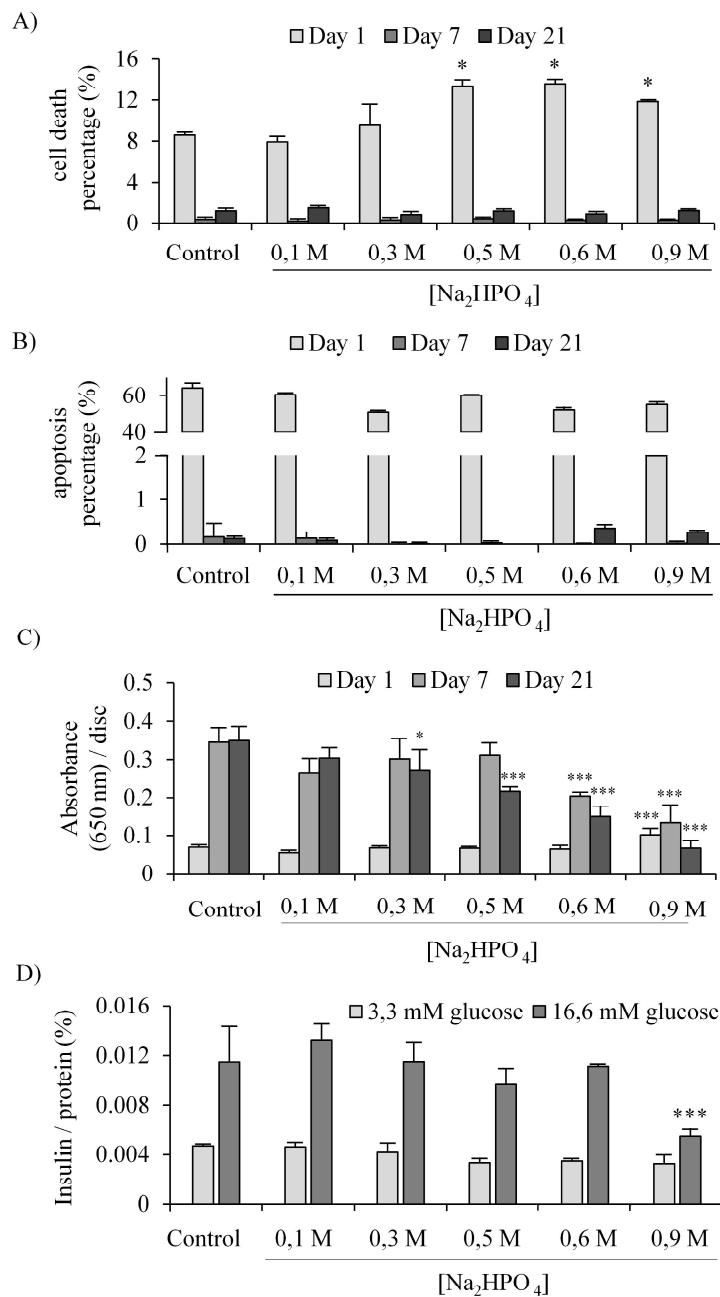


Figure 7. Effect of different Na₂HPO₄ concentrations on the viability, apoptosis, metabolic activity and insulin secretory response of INS1E embedded within different alginate hydrogels compared to control without Na₂HPO₄. A) Live/dead, B) apoptosis and C) metabolic activity analysis. D) Glucose-stimulated insulin secretion assay. Values represent mean \pm SD. *: $p < 0.05$ compared to control hydrogel.

One day after encapsulation, because of the mechanical stress generated during the embedding process itself [43], cells displayed the lowest metabolic activity and highest

percentages of death and apoptotic cells of the whole study. After a week, cells experienced an increase in the metabolic activity together with a decrease on cell death and apoptosis percentages, thereby denoting cell recovery after the stress suffered during the hydrogel formation. Among all the tested conditions, cell viability and metabolic activity values were higher in hydrogels formed with low Na_2HPO_4 concentrations, which can be attributed to the physicochemical properties of the hydrogels, in particular, the porosity and the stiffness. The porosity of such hydrogels allowed appropriate nutrient and oxygen diffusion, while stiffness provided adequate mechanical signals to promote cell proliferation and functionality. In fact, when we evaluated the insulin secretory response (Figure 7D), INS1E cells within alginate hydrogels formed with low Na_2HPO_4 concentrations were able to secrete insulin in response to glucose stimuli. However, in the hydrogel formed with the highest Na_2HPO_4 concentration, cells were not able to secrete insulin in a glucose-dependent manner. Therefore, hydrogels with low Na_2HPO_4 content provided appropriate mechanical signals to maintain the β -cell function and by contrast, softer hydrogels resulted in the loss of β -cells biological function. Hence, it can be concluded that the alginate gelation process and its physicochemical properties are modulated with the addition of Na_2HPO_4 within the formulation. Moreover, hydrogels containing 0.1 and 0.3 M Na_2HPO_4 showed the ideal injectable properties for their application in the clinics as well as good biocompatibility with the INS1E cells that maintained their functionality. In this sense, their great biocompatibility and injectability make our alginate- Na_2HPO_4 formulations a suitable approach for not only β -cell delivery in T1DM treatment, but also for other biomedical applications. The easy preparation of our hydrogels would allow them to be combined with other bioactive compounds to obtain specific biofunctional formulations. For example, our formulations could be mixed with calcium phosphate, a bioceramic that is widely used for orthopedic and dental applications, to obtain an injectable hydrogel for the regeneration of bone defects [44]. In addition, they could be combined with other cell types, such as chondrocytes, for cartilage regeneration [45]; or mixed with conductive nanoparticles, such as gold or carbon nanotubes, to be applied in cardiac regeneration, where the electrically conductive hydrogels would be more suitable to support the electrical signaling of cardiomyocytes [46]. Thus, using our hydrogels for the delivery of therapeutic agents (drugs, cells or inorganic substances for instance) would convert such hydrogels useful tools for the treatment of inflammatory processes, infectious diseases and cancer, and for the repair and regeneration of different tissues, such as bone, cartilage and heart, among others [47]. Therefore, our alginate- Na_2HPO_4 formulations can be considered as excellent candidates to be used as injectable biomaterials for a wide range of biomedical applications.

The combination of a Na₂HPO₄-modified alginate hydrogel with a 3D printed macroencapsulation device provides high mechanical protection while allowing the confinement of viable and functional β-cells and pseudoislets without cell spreading

In the previous work, we studied the modulation of the physicochemical properties of alginate-based hydrogels by adding Na₂HPO₄ and its effect on embedded rat INS1E β-cells. Alginate formulations containing low Na₂HPO₄ concentrations provided a feasible gelation time around 8-10 minutes, which would facilitate its manipulation when injected directly into the body or introduced in any kind of mold or device. However, in most cases, hydrogels are fragile and not stable enough to support the transplanted islets over a long period and, therefore, the long-term islet survival cannot be guaranteed [48]. In order to overcome this issue, hydrogel-islet biosystems can be confined within macroencapsulation devices, which confer strong mechanical protection improving the integrity of the inner hydrogel [49]. Moreover, this approach usually allows the implantation of the therapeutic graft in a specific location in the body avoiding the loss of transplanted islets, and permitting an easy graft retrieval and islet replenishment if required [50].

Importantly, the way that an implantable device interacts with the biological environment in the grafting site determines the success of the therapy. This interaction depends on its surface properties, such as roughness, morphology, pore size, surface hydrophilicity, and its chemical composition [51]. In this context, we developed a retrievable and straightforward β-cell encapsulation system, which involved the mentioned tunable alginate hydrogel and a 3D printed semipermeable macroencapsulation device made of polyamide (PA). In this system, the alginate hydrogel acts as a supportive matrix where the β-cells remain embedded, while the semipermeable macroencapsulation device confers mechanical protection as well as easy handling and retrieval.

Our aim was to achieve a non-degradable macroencapsulation device with a biocompatible surface that stabilizes the inner alginate hydrogel ensuring the biosafety of the system, and confers immunoprotection. Besides, in order to maintain the viability and biological function of the encapsulated β-cells, we looked for the appropriate oxygen, nutrients and insulin diffusion of this macroencapsulation system. To that end, we generated and characterized four devices following distinct fabrication processes to obtain different surface hydrophilicity and porosity. Afterwards, we evaluated the external surface of the different macroencapsulation devices (the side that would be in contact with the surrounding tissue when implanted) in terms of biocompatibility and biosafety. Finally, we assessed the biocompatibility of the whole system with the β-cells embedded within the inner hydrogel. First, we fabricated two macrocapsule devices (D1 and D2 devices) by selective laser

sintering with different printing patterns, resulting in a pore mean length of $12 \pm 4 \mu\text{m}$ for D1 devices (maximum length of $30 \mu\text{m}$), and $40 \pm 26 \mu\text{m}$ for D2 devices (maximum length of $170 \mu\text{m}$) (Figure 8A-B). Then, to obtain different degrees of hydrophilicity, we modified the devices' surface with a plasma treatment followed by PEG immersion to provide a higher degree of hydrophilicity. In this way, we obtained four different devices: two non-treated hydrophobic D1 and D2 devices (Phob-D1 and Phob-D2), and two treated hydrophilic D1 and D2 devices (Phil-D1 and Phil-D2).

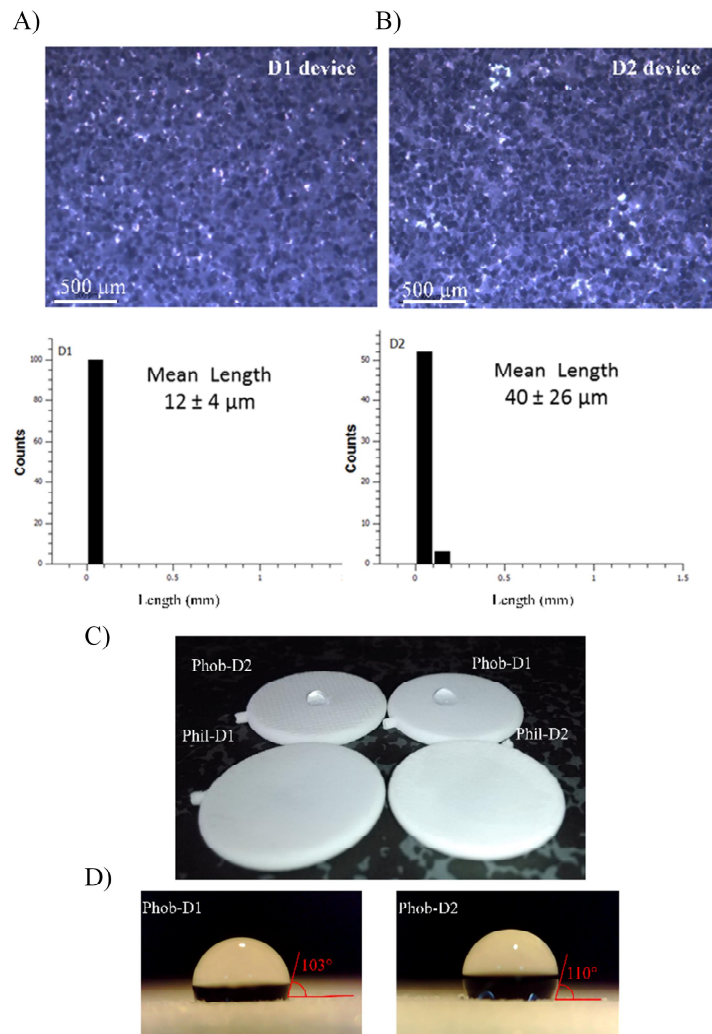


Figure 8. A) Optical images of the surface of D1 and D2 devices with their corresponding pore length histogram. Scale bar $500\mu\text{m}$. B) Photograph of the hydrophobic and hydrophilic devices with a water drop on top. C) Closer view of the water droplet on top of the Phob-D1 and Phob-D2 devices.

To characterize the surface hydrophilicity of the different devices, we evaluated the wettability by measuring the contact angle (θ_w) formed by a water droplet on top of each device surface (Figure 8C). The untreated devices showed a high hydrophobicity, with a

contact angle of $103 \pm 3^\circ$ for Phob-D1 devices and $110 \pm 3^\circ$ for Phob-D2 devices, as shown in Figure 8D. After the surface coating, both hydrophilic devices (Phil-D1 and Phil-D2) showed a contact angle below 5° (water spread into the surface).

After this physical characterization, the biocompatibility of the devices was studied on the L929 fibroblast cell line following the ISO 10993-5 “Tests for in vitro cytotoxicity: indirect contact, adhesion, and direct contact”. We confirmed that all the studied devices demonstrated high cell viabilities as well as high cell adhesion capacity without releasing cytotoxic leachable substances (Figure 9A-B).

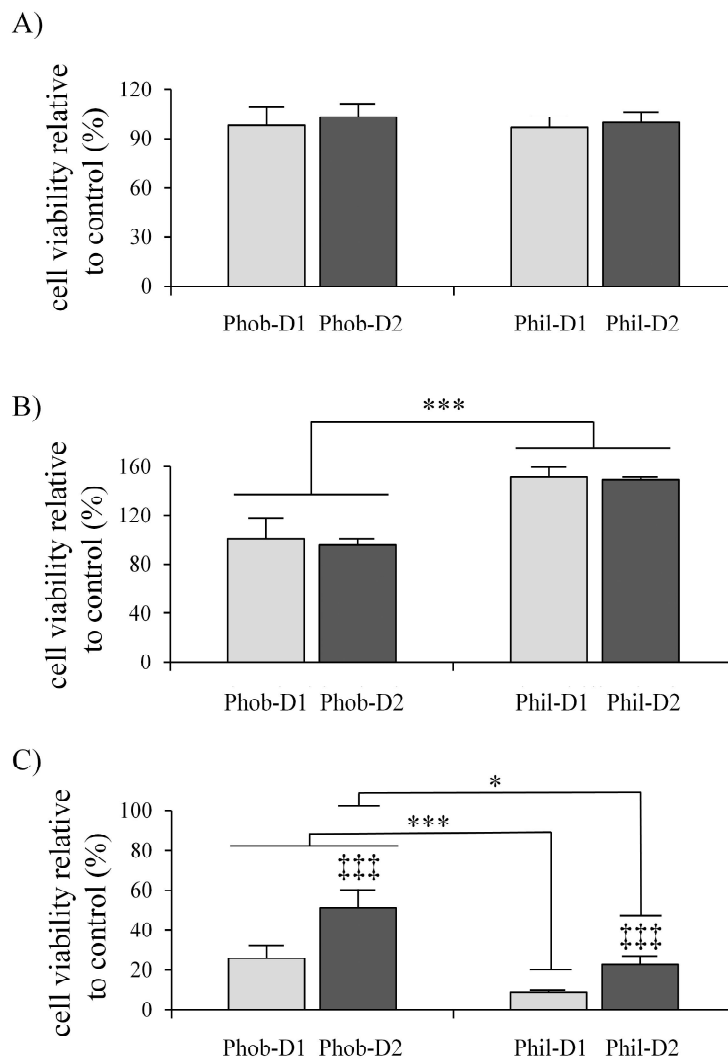


Figure 9. Biocompatibility evaluation of all devices following the ISO 10993-5. A) Indirect contact assay, B) adhesion assay, and C) direct contact assay. Values represent mean \pm SD. *: $p < 0.05$, ***: $p < 0.001$ in the comparison between the hydrophobic and hydrophilic devices, and ‡‡‡: $p < 0.001$ in the comparison between the different pore sizes of each hydrophobic and hydrophilic device.

However, the surprisingly higher cell adhesion of L929 fibroblasts to the hydrophilic devices could affect negatively the future success of the implanted graft. In fact, the host's fibroblasts are the major cells that might adhere to the implanted devices, walling off the implant by a fibrotic capsule. In this sense, since it has been shown that too thick fibrotic walls limit the diffusion of oxygen, nutrients, and insulin, an excessive fibrosis surrounding the implant could affect the device function [52,53]. In addition, the sensitivity to blood-glucose levels changes would be compromised, and the glucose response time would increase. Moreover, the reduced oxygen and nutrient supply would affect negatively on cell viability, leading to the complete graft failure [53,54]. Therefore, the lower L929 fibroblasts adhesion to our hydrophobic devices would indicate a higher potential to avoid excessive fibrosis surrounding these devices when implanted.

Regarding the direct contact assay, cell viability decreased in all the devices compared to controls (Figure 9C). Hydrophilic devices displayed cell viability values of 8.3 % for Phil-D1 and 22.7 % for Phil-D2, while the hydrophobic devices showed higher cell viability values, with 25.9 % for Phob-D1 and 51.2% for Phob-D2. In accordance with ISO 10993-5, viability values under 70 % are associated with a potential cytotoxic effect of the tested material [55]. However, we attributed this reduction in cell viability to the high cell adhesion properties of the devices instead of to cytotoxicity issues. In this sense, this high cell adhesion capacity provoked an elevated cell detachment of the cell monolayer that was in contact with the devices. In this way, when we evaluated the viability on the cell monolayer, we only detected the viability signal from the remaining low number of attached cells to the culture plates, without taking into account the missing cells that had attached to the device surface.

Then, before working with pseudoislets, we studied the biological behavior of encapsulated INS1E single-cells to validate the feasibility of β -cell confinement within the combined hydrogel-macrocapsule system. The analysis of cell membrane damage, cell viability and insulin production determined that the Phob-D1 device was the best option to maintain high cell viability of encapsulated INS1E single-cells (Figure 10A-C). Besides, we evaluated the biosafety of the devices by observing under the microscope the number of INS1E cells that escaped from the encapsulation systems and attached to the culture plate. Cells escaped from the control alginate hydrogel. In contrast, all the studied devices demonstrated a high degree of cell confinement, without evidence of cell spreading throughout the porous surface.

Based on these results, we selected the Phob-D1 and its complementary device, the Phil-D1 device, as the most suitable approaches among all the studied devices to follow with the in vitro studies with pseudoislets, evaluating their viability and biological function.

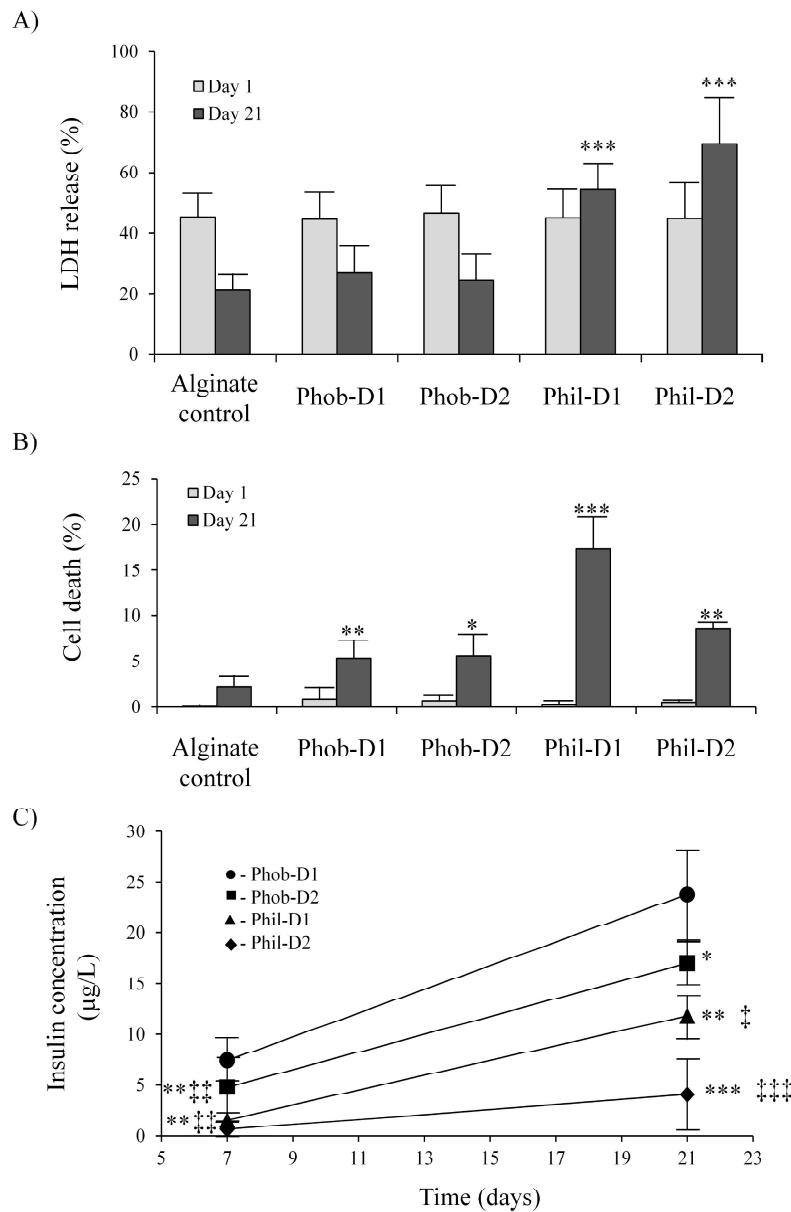


Figure 10. Biological evaluation of the INS1E single-cells within the different devices. A) Cell membrane damage assessment, B) cell viability quantification. Values represent mean \pm SD. *: $p < 0.05$, **: $p < 0.01$ and ***: $p < 0.001$ compared to alginate control. C) Insulin secretion profile from the encapsulated INS1E single-cells within the different devices. Values represent mean \pm SD. *: $p < 0.05$, **: $p < 0.01$ and ***: $p < 0.001$ compared to Phob-D1 device and, †: $p < 0.05$, ††: $p < 0.01$, †††: $p < 0.001$ compared to Phil-D1 device.

One day after encapsulation, some dead cells were observed on the cell-aggregates surface due to the mechanical stress suffered during the embedding process within the alginate (Figure 11A). Importantly, at day 7, pseudoislets within both selected devices recovered, as no dead cells were detected, and pseudoislets maintained their capacity to secrete insulin and respond to glucose stimuli (Figure 11B-C).

In contrast, other macroencapsulation devices lack physical separation of the islets inside the contention chamber, resulting in a random islets distribution that favors their aggregation. Such clustering limits the diffusion of nutrients and oxygen to the more internally located cells, leading to loss of islet function and death [49]. Therefore, our system was able to prevent pseudoislets aggregation, thereby, allowing an enhancement of the viable and functional β -cell number.

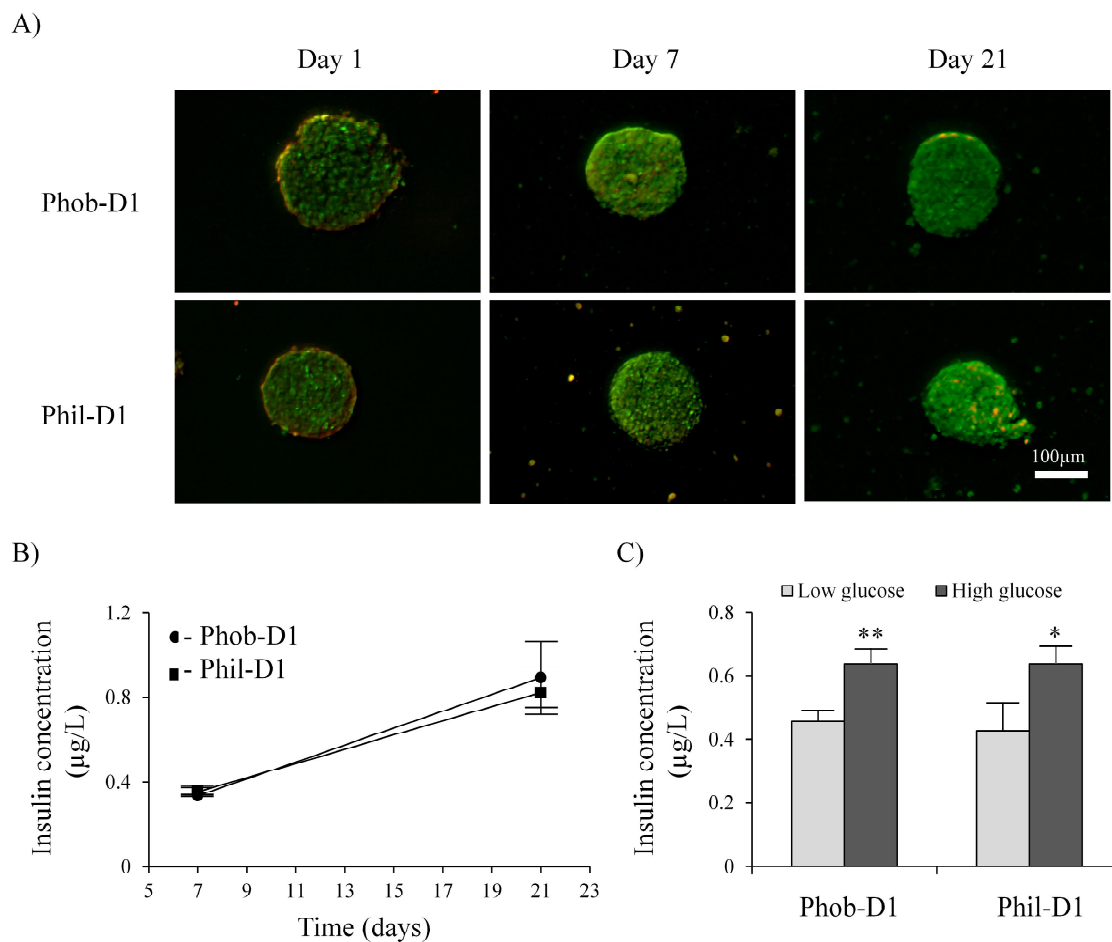


Figure 11. Evaluation of biological parameters of the encapsulated INS1E pseudoislets within the Phob-D1 and Phil-D1 devices. A) Pseudoislets viability by fluorescence microscopy (live/dead staining). Scale bar 100 μ m. B) Insulin secretion. C) Glucose-stimulated insulin secretion assay. Values represent mean \pm SD. *: $p < 0.05$ and **: $p < 0.01$ between the low and the high glucose conditions.

Advances, limitations and future directions

The developed dual encapsulating system shows a high potential to be applied in the clinics for T1DM treatment as it offers a high degree of biosafety. In addition, its shape would allow an easy and precise implanting with the possibility of retrieval in case of graft

failure or other complications, thus minimizing surgical risks [56]. Besides, single β -cells and islet-like cell aggregates are fully contained within the device, which will reduce the host's immune reaction [57]. Thus, this device would overcome one of the most critical limitations of pancreatic islet transplantation, the lack of pancreas donors [58,59]. The high degree of cell confinement would allow the use of alternative β -cells sources such as xenogeneic islets or β -cells derived from stem cells. This would suppose an increase in the number of diabetic patients that could be treated with β -cell replacement therapies, as currently, islet transplantation remains being a treatment available only for carefully selected cases of severe T1DM.

Apart from donor scarcity, another fact that limits the widespread application of islets transplantation is the graft failure due to the host's immune reaction against the implant. In this sense, we have proved that controlling the degree of hydrophilicity of the device surface we can modulate the fibroblasts adhesion onto the device. In this sense, controlling the properties of the surface, we could prevent the fibrotic growth, thus, avoiding the graft failure derived from excessive fibrosis. However, these studies have been performed *in vitro*; therefore, in future experiments, our devices should be implanted in animals. In this way, we could truly study how they interact with the surrounding tissues and evaluate the magnitude of the resultant immune reaction *in vivo*.

However, there are still some aspects that might limit this approach from being used as a β -cell replacement strategy. The primary limitation of the macroencapsulation devices is the reduced diffusion of oxygen, nutrients and insulin due to large diffusional distances between the encapsulated islets and the outside of the macroencapsulation device that can lead to graft failure [60]. In fact, comparing the glucose challenge assay that we performed in chapter 3 with 50 μ L of non-purified microcapsules (Figure 3C) and the one performed with 500 μ L of alginate hydrogel within the macroencapsulation device (Figure 11C) at the same density of 2000 pseudoislet/mL, we can see similar secreted insulin levels in both approaches (around 0.5 μ g/L). Therefore, the lower glucose and insulin diffusion within the macroencapsulation devices led to a 10 times reduction of the secreted insulin compared to microcapsules that have shorter diffusional distances.

To overcome this problem, the device diffusion properties should be enhanced by increasing the surface area of the device, while promoting its vascularization. The wide flexibility of designing, developing and fabricating this type of macroencapsulation devices will allow optimizing their configuration to improve their functionality. In this sense, as we confirmed the polyamide as a biocompatible material for the fabrication of the devices, we could keep working with the same material. However, we should change the design of the devices in order to enhance their diffusion properties. For example, as some encapsulation

systems involve hollow fiber structures to increase the oxygen and nutrients supply [61], we could generate a large-scale hollow fiber-like structure on the device to increase its surface area and promote its vascularization through the hollow fibers (Figure 12). Other encapsulation systems, such as the TRAFFIC, seek to generate tubular structures to overcome the diffusion limitations [62]. In this sense, we could also modify the design of our devices forming parallel tubular structures to enhance the diffusional properties. With these alternative designs, the distance between pseudoislets and the device surface would be reduced, increasing the exit of insulin from the inner hydrogel, while the neovascularization would enhance the glucose detection and nutrients supply.

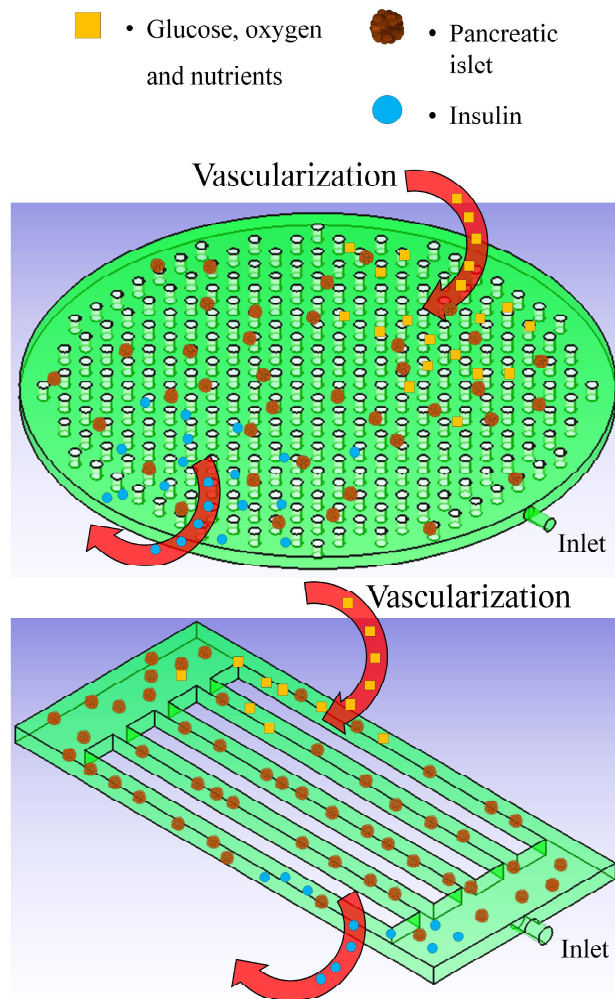


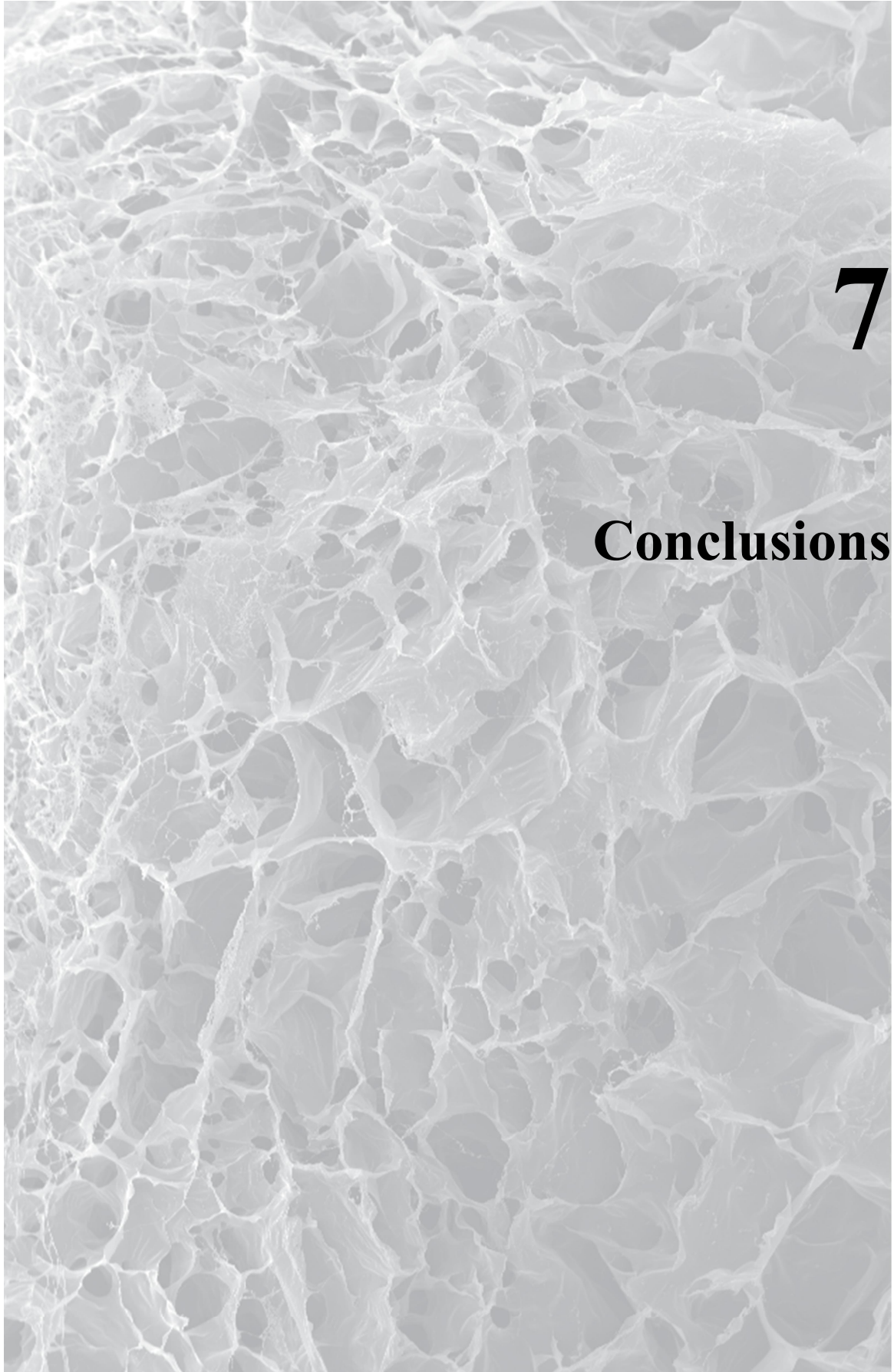
Figure 12. Schematics of the design of two prototypes for pancreatic islets macroencapsulation that would enhance the diffusion properties as well as the vascularization.

REFERENCES

- [1] Vieira A, Druelle N, Avolio F, et al. beta-Cell Replacement Strategies: The Increasing Need for a “beta-Cell Dogma”. *Front Genet* 2017.
- [2] Yoon JW and Jun HS. Autoimmune destruction of pancreatic beta cells. *Am J Ther* 2005.
- [3] Montanya E. Islet- and stem-cell-based tissue engineering in diabetes. *Curr Opin Biotechnol* 2004.
- [4] Amer LD, Mahoney MJ and Bryant SJ. Tissue engineering approaches to cell-based type 1 diabetes therapy. *Tissue Eng Part B Rev* 2014.
- [5] Li W, Zhao R, Liu J, et al. Small islets transplantation superiority to large ones: implications from islet microcirculation and revascularization. *J Diabetes Res* 2014.
- [6] Skrzypek K, Groot Nibbelink M, van Lente J, et al. Pancreatic islet macroencapsulation using microwell porous membranes. *Sci Rep* 2017.
- [7] Figliuzzi M, Bonandrini B, Silvani S, et al. Mesenchymal stem cells help pancreatic islet transplantation to control type 1 diabetes. *World J Stem Cells* 2014.
- [8] Desai T and Shea LD. Advances in islet encapsulation technologies. *Nat Rev Drug Discov* 2017.
- [9] Sakata N, Tan A, Chan N, et al. Efficacy comparison between intraportal and subcapsular islet transplants in a murine diabetic model. *Transplant Proc* 2009.
- [10] Schuetz C, Anazawa T, Cross SE, et al. beta Cell Replacement Therapy: The Next 10 Years. *Transplantation* 2018.
- [11] Korsgren O. Islet encapsulation: Physiological possibilities and limitations. *Diabetes* 2017; 66: 1748-1754.
- [12] Burcu Kepsutlu, Caner Nazli, Tugba Bal Bal, et al. Design of Bioartificial Pancreas with Functional Micro/Nano-Based Encapsulation of Islets. *Current Pharmaceutical Biotechnology* 2014.
- [13] Ahmed EM. Hydrogel: Preparation, characterization, and applications: A review. *J Adv Res* 2015.
- [14] Knobloch T, Abadi SEM, Bruns J, et al. Injectable Polyethylene Glycol Hydrogel for Islet Encapsulation: an in vitro and in vivo Characterization. *Biomed Phys Eng Express* 2017.
- [15] Gasperini L, Mano JF and Reis RL. Natural polymers for the microencapsulation of cells. *J R Soc Interface* 2014.
- [16] Buder B, Alexander M, Krishnan R, et al. Encapsulated islet transplantation: strategies and clinical trials. *Immune Netw* 2013.
- [17] Lee KY and Mooney DJ. Alginate: properties and biomedical applications. *Prog Polym Sci* 2012.
- [18] Tendulkar S, Mirmalek-Sani SH, Childers C, et al. A three-dimensional microfluidic approach to scaling up microencapsulation of cells. *Biomed Microdevices* 2012.
- [19] Kim HS, Kim H, Park KS, et al. Evaluation of porcine pancreatic islets transplanted in the kidney capsules of diabetic mice using a clinically approved superparamagnetic iron oxide (SPIO) and a 1.5T MR scanner. *Korean J Radiol* 2010.
- [20] Wilson JL, Najia MA, Saeed R, et al. Alginate encapsulation parameters influence the differentiation of microencapsulated embryonic stem cell aggregates. *Biotechnol Bioeng* 2014.
- [21] Opara EC, Mirmalek-Sani SH, Khanna O, et al. Design of a bioartificial pancreas (+). *J Investig Med* 2010.
- [22] Vaithilingam V and Tuch BE. Islet transplantation and encapsulation: an update on recent developments. *Rev Diabet Stud* 2011.
- [23] de Vos P, van Hoogmoed CG, van Zanten J, et al. Long-term biocompatibility, chemistry, and function of microencapsulated pancreatic islets. *Biomaterials* 2003; 24: 305-312.
- [24] Abdulkadir Omer, Valerie Duvivier-Kali, Justin Fernandes, et al. Long-Term Normoglycemia in Rats Receiving Transplants with Encapsulated Islets. *Transplantation* 2005; 79:1.
- [25] De Vos P, Van Straaten JF, Nieuwenhuizen AG, et al. Why do microencapsulated islet grafts fail in the absence of fibrotic overgrowth?. *Diabetes* 1999.
- [26] Calafiore R, Basta G, Luca G, et al. Microencapsulated Pancreatic Islet Allografts Into Nonimmunosuppressed Patients With Type 1 Diabetes: First two cases. *Diabetes care* 2006.

- [27] Bernard E. Tuch, Gregory W. Keogh, Lindy J. Williams, et al. Safety and Viability of Microencapsulated Human Islets Transplanted Into Diabetic Humans. *Diabetes Care* 2009.
- [28] Tan PL. Company Profile: Tissue regeneration for diabetes and neurological diseases at Living Cell Technologies. *Regenerative Medicine* 2010.
- [29] Weir GC and Bonner-Weir S. Scientific and Political Impediments to Successful Islet Transplantation. *Diabetes* 1997.
- [30] Jacobs-Tulleneers-Thevissen D, Chintinne M, Ling Z, et al. Sustained function of alginate-encapsulated human islet cell implants in the peritoneal cavity of mice leading to a pilot study in a type 1 diabetic patient. *Diabetologia* 2013.
- [31] Dufrane D, Gianello P. Macro- or microencapsulation of pig islets to cure type 1 diabetes. *World J Gastroenterol.* 2012 Dec 21; 18(47): 6885–6893.
- [32] Kührtreiber Willem M. *Cell Encapsulation Technology and Therapeutics* 1999.
- [33] Zorzi D, Phan T, Sequi M, et al. Impact of islet size on pancreatic islet transplantation and potential interventions to improve outcome. *Cell Transplant* 2015.
- [34] Lee KY, Mooney DJ. Hydrogels for tissue engineering. *Chem Rev* 2001 Jul;101(7):1869-1879
- [35] Heo EY, Ko NR, Bae MS, Lee SJ, Choi B, Kim JH, et al. Novel 3D printed alginate–BFP1 hybrid scaffolds for enhanced bone regeneration. *Journal of Industrial and Engineering Chemistry* 2017;45:61-67
- [36] Kuo CK, Ma PX. Ionically crosslinked alginate hydrogels as scaffolds for tissue engineering: part 1. Structure, gelation rate and mechanical properties. *Biomaterials* 2001 Mar;22(6):511-521
- [37] Nandini VV, Venkatesh KV, Nair KC. Alginate impressions: A practical perspective. *J Conserv Dent* 2008 January 01;11(1):37-41
- [38] Hoare TR, Kohane DS. Hydrogels in drug delivery: Progress and challenges. *Polymer* 2008;49(8):1993-2007
- [39] Kuo CK, Ma PX. Ionically crosslinked alginate hydrogels as scaffolds for tissue engineering: part 1. Structure, gelation rate and mechanical properties. *Biomaterials* 2001 Mar;22(6):511-521
- [40] Nandini VV, Venkatesh KV, Nair KC. Alginate impressions: A practical perspective. *J Conserv Dent* 2008 January 01;11(1):37-41
- [41] Huang G, Wang L, Wang S, Han Y, Wu J, Zhang Q, et al. Engineering three-dimensional cell mechanical microenvironment with hydrogels. *Biofabrication* 2012 Dec;4(4):042001
- [42] Tibbitt MW, Anseth KS. Hydrogels as extracellular matrix mimics for 3D cell culture. *Biotechnology and bioengineering* 2009 Jul 1;103(4):655-663
- [43] Marchioli G, Gurr v, L, Krieken v, P.P, Stamatialis D, Engelse M, Blitterswijk v, C.A, et al. Fabrication of three-dimensional bioplotting hydrogel scaffolds for islets of Langerhans transplantation. *Biofabrication* 2015;7(2):025009
- [44] Barrère F, A van Blitterswijk C, de Groot K. Bone regeneration: molecular and cellular interactions with calcium phosphate ceramics. *Int J Nanomedicine.* 2006 Sep; 1(3): 317–332.
- [45] Liu M, Zeng X, Ma C, et al. Injectable hydrogels for cartilage and bone tissue engineering. *Bone Res.* 2017; 5: 17014.
- [46] Peña B, Jett S, Teisha J, et al. Injectable hydrogels for Cardiac Tissue Engineering. *Macromol Biosci.* 2018 Jun; 18(6): e1800079.
- [47] Hyun Lee J. Injectable hydrogels delivering therapeutic agents for disease treatment and tissue engineering. *Biomater Res.* 2018; 22: 27.
- [48] Skrzypek K, Groot Nibbelink M, van Lente J, et al. Pancreatic islet macroencapsulation using microwell porous membranes. *Sci Rep* 2017.
- [49] Kepsutlu B, Nazli C, Bal T, et al. Design of bioartificial pancreas with functional micro/nano-based encapsulation of islets. *Curr Pharm Biotechnol* 2014.
- [50] Orive G, Emerich D, Khademhosseini A, et al. Engineering a Clinically Translatable Bioartificial Pancreas to Treat Type I Diabetes. *Trends Biotechnol* 2018.
- [51] Teo AJT, Mishra A, Park I, et al. Polymeric biomaterials for medical implants and devices. *ACS Biomaterials Science & Engineering* 2016; 2: 454-472.

- [52] Morais JM, Papadimitrakopoulos F and Burgess DJ. Biomaterials/tissue interactions: possible solutions to overcome foreign body response. *AAPS J* 2010.
- [53] Damanik FF, Rothuizen TC, van Blitterswijk C, et al. Towards an in vitro model mimicking the foreign body response: tailoring the surface properties of biomaterials to modulate extracellular matrix. *Sci Rep* 2014.
- [54] Bridges AW and Garcia AJ. Anti-inflammatory polymeric coatings for implantable biomaterials and devices. *J Diabetes Sci Technol* 2008.
- [55] Srivastava GK, Alonso-Alonso ML, Fernandez-Bueno I, et al. Comparison between direct contact and extract exposure methods for PFO cytotoxicity evaluation. *Sci Rep* 2018.
- [56] Dufrane D, Goebbels R and Gianello P. Alginate Macroencapsulation of Pig Islets Allows Correction of Streptozotocin-Induced Diabetes in Primates up to 6 Months Without Immunosuppression. *Transplantation* 2010.
- [57] Skrzypek K, Groot Nibbelink M, van Lente J, et al. Pancreatic islet macroencapsulation using microwell porous membranes. *Sci Rep* 2017.
- [58] Desai T and Shea LD. Advances in islet encapsulation technologies. *Nat Rev Drug Discov* 2017.
- [59] Korsgren O. Islet encapsulation: Physiological possibilities and limitations. *Diabetes* 2017; 66: 1748-1754.
- [60] Alejandro R. Allogeneic Islet Cells Transplanted Onto the Omentum 2014.
- [61] Teotia RS, Kadam S, Singh AK, et al. Islet encapsulated implantable composite hollow fiber membrane based device: A bioartificial pancreas. *Mater Sci Eng C Mater Biol Appl.* 2017 Aug 1;77:857-866.
- [62] An D, Chiu A, Flanders JA, et al. Designing a retrievable and scalable cell encapsulation device for potential treatment of type 1 diabetes. *Proc Natl Acad Sci U S A* 2018.



7

Conclusions

7. CONCLUSIONS

According with the results obtained in the previously described experiments, we can conclude that:

- 1) $\text{Fe}_3\text{O}_4/\text{PEI}$ NPs do not affect the viability of pseudoislets up to a concentration of $80\mu\text{g}$ NPs/mL, being this the optimal concentration that enables the displacement of the magnetized microencapsulated pseudoislets through the whole microfluidic device towards the magnetic channel.
- 2) The developed magnetic sorting system allows the purification of magnetically labeled microencapsulated pseudoislets with high purification yields, while enabling the monitorization of the process. It also avoids manual steps, thus, minimizing technical errors along the purification process.
- 3) The purified therapeutic graft of microencapsulated pseudoislets obtained after performing the magnetic purification procedure is able to reduce the blood-glucose levels within the normoglycemic range in diabetic rats.
- 4) The physicochemical properties of alginate hydrogels can be modulated through the addition of Na_2HPO_4 within the formulation, being the hydrogels containing $0.3\text{ M Na}_2\text{HPO}_4$ the ones that showed ideal injectable properties for their application in the clinic. In addition, they showed good biocompatibility and preservation of the INS1E β -cells functionality.
- 5) Our dual encapsulation system involving an alginate-based hydrogel and a 3D printed polyamide macroencapsulation device increases the confinement of single β -cells and islet-like cell aggregates enhancing the biosafety of the graft when implanted.
- 6) Macroencapsulation devices with a hydrophobic surface demonstrate higher potential to avoid an excessive fibrotic response. In addition, devices with smaller pore size provide higher stability to the inner alginate hydrogel. Thus, the hydrophobic macroencapsulation device with a $12\mu\text{m}$ pore size (Phob-D1) is the most suitable option among all the studied devices for future safer β -cell replacement therapies.





ANNEX I

Immobilization of INS1E insulin-producing cells within injectable alginate hydrogels

Immobilization of INS1E insulin-producing cells within injectable alginate hydrogels

A. Espona-Noguera^{1,2}, J. Ciriza^{1,2}, A. Cañibano-Hernández^{1,2}, L. Saenz del Burgo^{1,2*} and J.L. Pedraz^{1,2*}

¹ NanoBioCel Group, Laboratory of Pharmaceutics, School of Pharmacy, University of the Basque Country (UPV/EHU), Paseo de la Universidad 7, 01006, Vitoria-Gasteiz, Spain.

² Biomedical Research Networking Center in Bioengineering, Biomaterials, and Nanomedicine (CIBER-BBN), Vitoria-Gasteiz, Spain.

* Corresponding authors

ABSTRACT

Alginate has demonstrated high applicability as a matrix-forming biomaterial for cell immobilization due to its ability to make hydrogels combined with cells in a rapid and non-toxic manner in physiological conditions, while showing excellent biocompatibility, preserving immobilized cell viability and function. Moreover, depending on its application, alginate hydrogel physicochemical properties can be tuned such as porosity, stiffness, gelation time and injectability. This technology has been applied to several cell types that are able to produce therapeutic factors. In particular, alginate has been the most commonly used material in pancreatic islet entrapment for Type 1 Diabetes Mellitus treatment. This chapter compiles information regarding the alginate handling, and we describe the most important steps and recommendations to immobilize insulin-producing cells within an tuned injectable alginate hydrogel using a syringe-based mixing system, detailing how to assess the viability and the biological functionality of the embedded cells.

Key words: Alginate, hydrogel, tissue engineering, Diabetes Mellitus, controlled drug delivery system, insulin-producing cells.

Accepted for publication in the book "*Immobilization of Enzymes and Cells: Methods and Protocols*". Series: Methods in Molecular Biology published by Springer Nature



1. INTRODUCTION

In the last years, tissue engineering has been focused on the searching of biomaterials that mimic structural and mechanical properties and biological functions of the extracellular matrix of body tissues [1-3]. Some polymeric biomaterials possess the capacity to form hydrogels, a multicomponent system consisting of a three-dimensional (3D) network of polymer chains and water that fills the space between macromolecules. Hydrogels have received significant attention due to their similarity to soft tissues in terms of mechanical properties (stiffness, flexibility, etc.) and high-water content [4, 5]. These biomaterials are highly biocompatible, allowing immobilizing therapeutic cells within the hydrogel matrix, thus obtaining an effective long-term drug delivery system. Furthermore, hydrogels can be easily tuned with the addition of extracellular matrix proteins, peptides, growth factors, inorganic components, etc. that can help to the therapeutic cell development [6, 7]. Regarding their biophysical properties, the porous structure of the hydrogels enables the diffusion of nutrients and gases (O_2 and CO_2), as well as the sustained release of therapeutic molecules produced de novo by the immobilized cells. Such structure protects the entrapped cells from the host immune system keeping high molecular weight immune system components out [8-10]. All mentioned properties make hydrogels a suitable microenvironment that promotes and controls cell viability and proliferation. For that reason, the combination of these biomaterials with therapeutic cells like primary cells, transfected cells, mesenchymal stem cells, etc., provide a biosystem with great potential for cell-based therapies that restore, maintain and improve an affected tissue function [11].

Several biomaterials that can form hydrogel-like structures have been used for cell embedding; such as alginate, collagen, agarose, gelatin or hyaluronic acid. [12-15]. Among all different hydrogel formulations, alginate is recognized for properties and characteristics such as its ability to make hydrogels combined with cells in a rapid and non-toxic manner at physiological conditions, excellent biocompatibility, great physicochemical properties and ease crosslinking [16, 17]. Moreover, alginate hydrogel physicochemical properties such as porosity, stiffness, gelation time and injectability can be tuned as required. For example, in case of an injectable alginate-based hydrogel, gelation time as well as injectability can be controlled with the addition of phosphate salts-based retardant agents, until reach the desired injectable properties [4].

Alginate is commonly used in pancreatic islet entrapment for Type 1 Diabetes Mellitus treatment [18]. In Type 1 Diabetes Mellitus, pancreatic islets are destroyed by the immune system resulting in inadequate glucose homeostasis. Islet transplantation represents an alternative to daily insulin injections; but, the efficiency of this procedure is limited. A

large proportion of transplanted islets is destroyed by the host's immune system, requiring long-term immunosuppressive drug administration [19, 20]. To overcome this problem, islets can be immobilized within an alginate matrix that provides immunoprotection from antibodies and host's immune cells, resulting in a significant increase of islet survival. Several strategies to transplant immobilized pancreatic islets within alginate hydrogels have shown promising results. Thus, islets are usually entrapped in a bulk alginate hydrogel that can be directly injected subcutaneously or into the peritoneal cavity [21], or introduced inside an implantable device which is subsequently implanted [22, 23].

Our group has previously studied the immobilization of the insulin-producing cell line INS1E within an injectable alginate hydrogel, allowing the secretion of insulin in a controlled manner, for the treatment of Type I Diabetes Mellitus. Currently, alginate hydrogels are commonly formed by ionic crosslinking, where the aqueous sodium alginate solution is combined with ionic crosslinking agents, such as divalent cations (for example Ca^{2+} from CaSO_4). This type of crosslinking method is highly reproducible and easy to use under sterile conditions. However, alginate gelation occurs quite fast (around 1-2 minutes) and, subsequently, hydrogel formation is poorly controlled affecting its injectability. Recently, we have demonstrated that incorporating different concentrations of the phosphate salt Na_2HPO_4 in alginate hydrogels formulation; we can modulate the gelation time thus modifying the injectability, as well as tuning their physicochemical properties like stiffness and porosity. After evaluating different formulations, we observed that hydrogels formulations with 0.3 M Na_2HPO_4 showed an ideal injectability with a gelation time of around 8-10 minutes, thus providing longer working time that facilitates alginate manipulation during hydrogel formation [4]. In this chapter, we will describe our insulin-producing cells INS1E immobilization protocol within the tuned injectable alginate hydrogel formed by ionic crosslinking. The technique consists of a syringe-based mixing system that allows the mixture of a cell-sodium alginate suspension, the crosslinking agent, and the Na_2HPO_4 , obtaining a final homogeneous alginate hydrogel containing cells. Besides, we will also describe the subsequent assessment of embedded cells viability and biological function.

2. MATERIAL

2.1 INS1E cell line

Complete culture medium: Roswell Park Memorial Institute (RPMI) 1640 supplemented with 10 % heat-inactivated fetal bovine serum, 2 mM L-glutamine, 100 U/mL penicillin, 100 $\mu\text{g}/\text{mL}$ 1 % streptomycin, 1 mM sodium pyruvate, 10 mM HEPES buffer and 50 μM 2-mercaptoethanol.



2.2 Cell immobilization within alginate hydrogels

The following specific sterile material is required: 3 mL LuerLock syringes (BS syringes), Fluid dispensing connectors (Braun), glass plates with 2mm spacers and a circular punch. All the chemical solutions are dissolved in 1 % (w/v) mannitol and subsequently sterilized under a laminar flow cabinet by filtering through a 0.22 μm to avoid contaminations. All solutions can be stored at 4 °C until cell immobilization (see Note 1).

1. 1 % (w/v) mannitol solution: dissolve 1 g of mannitol into 100 mL of distilled water or scale up to the required volume. Stir until the solution is clear indicating that mannitol is completely dissolved. Next, filter the solution through a 0.22 μm filter (see Note 2).
2. Crosslinking solution: 1.22 M calcium sulfate (CaSO_4) solution; dissolve 2.1 g of CaSO_4 (99 % purity) into 10 mL of 1 % sterile mannitol solution (Figure 1A). After dissolution, CaSO_4 precipitates in few seconds (Figure 1B) (see Note 3). Scale up the amounts of calcium sulfate as needed.
3. Retardant agent solution: 0.3 M Na_2HPO_4 ; dissolve 0.54 g of Na_2HPO_4 powder (Panreac) into 10 mL of 1 % mannitol. Ensure complete dissolution using a vortex (see Note 4). Next, filter the solution through a 0.22 μm filter.
4. 1.5 % (w/v) low-viscosity sodium alginate (LGV) solution: for 10 mL, dissolve 0.15 g of ultrapure sodium alginate with a molecular weight of 75-200 kDa and guluronate/mannuronate ratio ≥ 1.5 (FMC Biopolymer) into 10 mL of previously prepared 1 % mannitol solution and, stir until alginate agglomerates (Figure 1C) are dissolved, and the solution is transparent (Figure 1D) (see Note 5). Scale up for higher volumes of alginate solution (see Note 6). Once alginate is completely dissolved, sterilize by filtration through a 0.22 μm syringe filter under laminar flow cabinet (see Note 7). Alginate can be stored at 4°C until needed.

2.3 Viability and biological function evaluation of immobilized cells

All reagents must be prepared just before performing the assay, not requiring to be sterilized as the experiments will last for just a few hours.

1. Calcein/ethidium staining solution: add 2.5 μL of 2 mM ethidium and 1.25 μL of 4 mM calcein provided in the LIVE/DEAD® Viability/Cytotoxicity Kit for mammalian cells (Life-Technologies) into 10 mL of DPBS with calcium and magnesium. For higher volumes, scale up as required (see Note 8).
2. Solution for cell viability quantification: all reagents are provided in the Cell Counting Kit-8 (CCK-8) (Sigma-Aldrich).

3. Solutions for insulin quantification: all reagents are provided in the rat insulin ELISA kit (Merckodia AB).

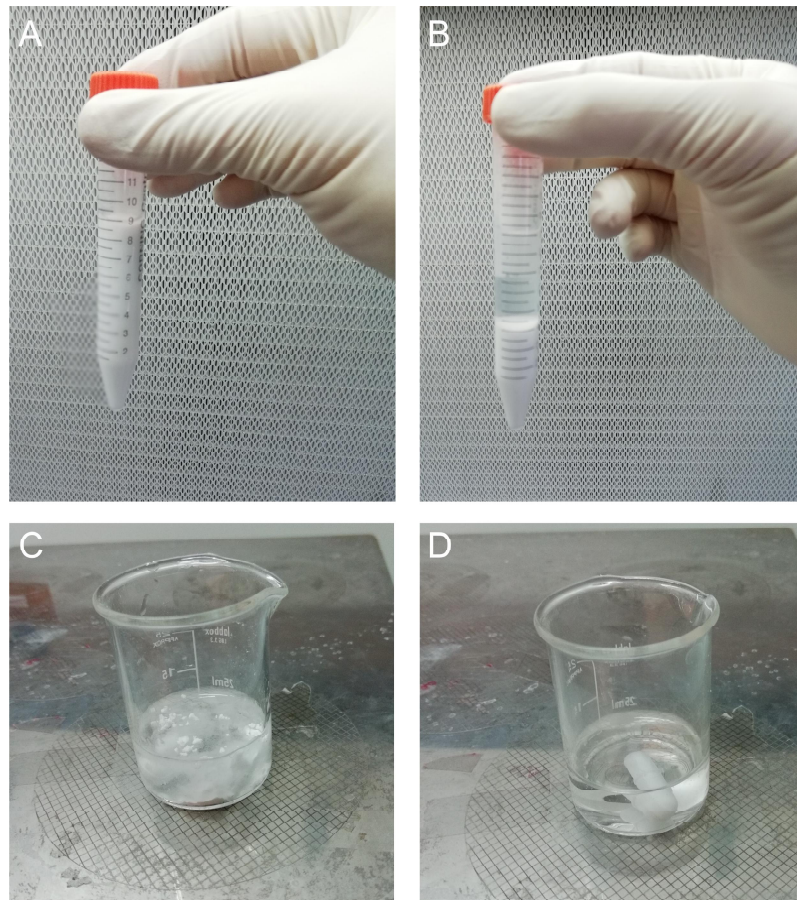


Figure 1. CaSO_4 and alginate preparation for hydrogel formation procedure. A.- Homogeneous 1.22 M CaSO_4 in 1 % mannitol. B.- precipitated 1.22 M CaSO_4 in 1 % mannitol. C.- Undissolved alginate in 1 % mannitol. D.- dissolved alginate in 1 % mannitol after stirring for 1 hour.

3. METHODS

All the steps are carried out at room temperature under aseptic conditions inside a flow laminar cabinet and using disposable sterile material. Otherwise, reusable material needs to be previously sterilized by autoclave.

3.1 INS1E cell culture

1. INS1E cells are stored in liquid nitrogen in 2 mL cryovial tubes. Cryovials are thawed quickly at 37 °C in a water bath, adding rapidly to a 15 mL conical centrifuge tube with 10 mL of complete culture media, to remove cytotoxic cryoprotectants from the freezing media, such as DMSO.

A

2. Spin cell suspension and resuspend the cell pellet into 10 mL of complete culture medium. Place the suspension in a T-75 flask and incubate at 37 °C in humidified 5 % CO₂/ 95 % air atmosphere.
3. Cells should be passaged every 4–5 days by detaching them with trypsin-EDTA 0.25 % and plating them with a 1:4 dilution. Cells are expanded in T-175 flasks as needed depending on the cell density and the final hydrogel volume that will be used.

3.2 Preparation of the cell suspension in the alginate solution

1. Remove medium from the T-175 flask and rinse the cells with 15 mL of PBS. Add 10 mL of trypsin-EDTA 0.25 % to the flask and incubate at 37 °C for 5 minutes. Afterward, inactivate trypsin by adding 10 mL of complete culture medium and pipet the cell suspension up and down to obtain a single-cell suspension (see Note 9).
2. Collect the cell suspension into a 50 mL conical tube through a 40 µm filter in order to remove the remaining cell aggregates and count the cell density under the microscope with a Neubauer chamber or by using an automatic counter (TC20™ cell counter, Bio-Rad, or similar).
3. Collect the volume of cell suspension to get the required number of cells for cell immobilization within the alginate hydrogel. We usually use a cell density of 5 x 10⁶ cells/mL of alginate; for example, to prepare a 3 mL hydrogel, 15 x 10⁶ cells are needed.
4. Centrifuge the cell suspension at 1500 rpm for 5 minutes and discard the supernatant by pipetting without aspirating the cell pellet.
5. Add 1.5 % sterile alginate solution to get the desired cell/alginate concentration. We usually add 3 mL of alginate to 15 x 10⁶ cell pellet to finally obtain the cell density of 5 x 10⁶ cell/mL of alginate. Carefully resuspend the cells in the alginate solution using a sterile spatula to homogenize the cells suspension (see Note 10).

3.3 INS1E cell immobilization within alginate hydrogel

1. Transfer 2.7 mL of the alginate cell suspension into a 3 mL LuerLock syringe avoiding the formation of bubbles. Collect in another 3 mL syringe 180 µL of 1 % mannitol, 60 µL of crosslinking solution and 60 µL of retardant agent solution, also preventing the formation of bubbles (Figure 2A) (see Note 11).
2. Connect both syringes through the Fluid dispensing connector (remove the air inside the connector to avoid bubbles formation by filling the connector with the cell-alginate suspension). Start the crosslinking reaction by mixing the cell-alginate suspension and the manitol-crosslinking solution-retardant agent solution mixture by passing the content of one

syringe to the other at least 10 times (Figure 2B) (see Note 12).

3. Dispense the mixed solution onto a glass plate with 2 mm spacers and quickly cover the plate with another glass plate without spacers. Leave the solution between the glasses for 45 minutes to ensure alginate is entirely crosslinked (Figure 2C).

4. Carefully, remove the upper glass plate with the help of a spatula leaving the crosslinked alginate hydrogel on the glass plate below. Cut disks with the desired diameter of the hydrogel using a circular punch. We usually cut hydrogel discs of 14 mm of diameter (Figure 2D).

5. Place the hydrogel disks in 12 well-plates and add 3 mL of complete culture medium. Change medium every 2-3 days. Observe the sample under an inverted microscope to ensure a homogeneous cell distribution through the hydrogel. Keep the samples in the incubator at 37 °C and 5 % CO₂/ 95 % air for further studies.

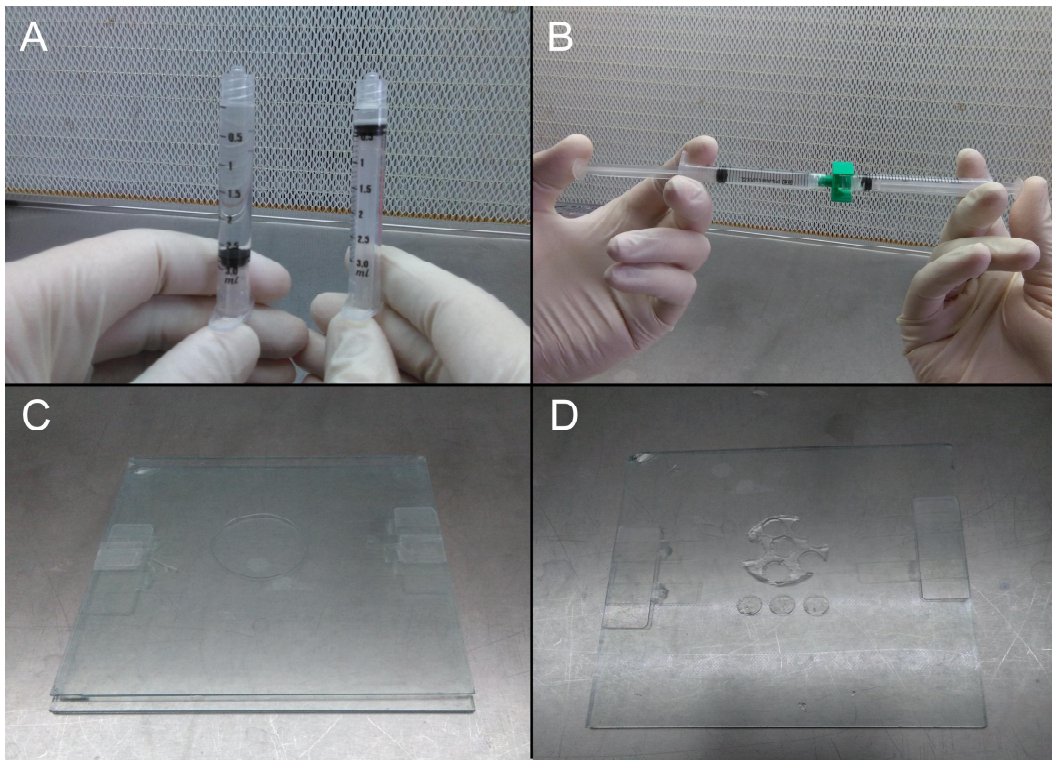


Figure 2. Detailed procedure of alginate hydrogels preparation. A.- 1.5 % Alginate solution and CaSO₄-Na₂HPO₄ placed in independent syringes. B.- Syringes connected and content mixed. C.- The resultant mixture spread between two glasses with 2 mm spacer. D.- Disk punched from the hydrogel.

3.4 Qualitative assessment by calcein/ethidium staining

1. Remove the medium from the well and rinse the hydrogel twice with DPBS containing Ca²⁺ and Mg²⁺.

2. Add 1 mL of the calcein/ethidium staining solution and incubate for 45 minutes at room temperature protected from light.

3. Assess under a fluorescence or confocal microscope the viability of immobilized cells. Calcein and ethidium staining can be viewed simultaneously with a conventional fluorescein longpass filter at the following excitation settings: for calcein AM excitation wavelength at 495 nm, and ethidium homodimer excitation wavelength at 495 nm (Figure 3) (see Note 13).

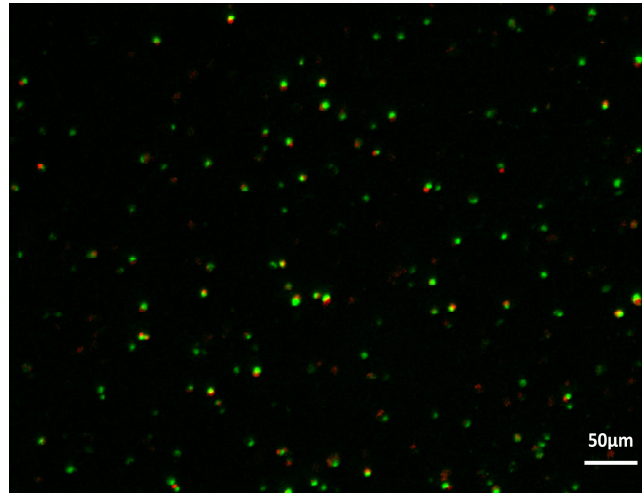


Figure 3. Viability assessment under confocal microscope of INS1E cells immobilized within alginate hydrogel. Green color indicates calcein staining (alive cells) while red color indicates ethidium staining (dead cells). Scale bar: 50 μm .

3.5 Viability quantification of immobilized cells

1. Remove the medium from the well and rinse the hydrogel twice with DPBS containing Ca^{2+} and Mg^{2+} .
2. Add 1 mL of complete culture medium containing 10 % of the CCK-8 assay reagent to the samples and incubate in the incubator for 4 hours at 37 °C (see Note 14).
3. Collect 100 μL of the medium from all samples and controls and transfer to a 96 well-plate at least in triplicates. Measure the absorbance at 450 nm with a reference wavelength at 650 nm using a microplate reader (Figure 4A). Determine the average values from readings of the samples and subtract the average value from the blank.

3.6 Insulin secretion quantification

1. At selected time points, remove the medium and add 1 mL of fresh complete culture medium and incubate in the incubator at 37 °C for 24 hours.
2. Collect the medium, transfer to a 1 mL conical tube and place it on ice.
4. Prepare sufficient microplate wells to accommodate calibrators, controls and samples in duplicate. Then, pipette 10 μL each of calibrators and samples in the corresponding well.
5. Add 50 μL of enzyme conjugate 1X solution into each well and incubate on a plate shaker

at 700-900 rpm for two hours at room temperature.

6. Discard the reaction volume by inverting the microplate over a sink and wash 6 times with 300 μ L of washing buffer 1X solution per well (see Note 15).

7. Add 200 μ L of substrate TMB into each well, incubate for 15 minutes at room temperature and next add 50 μ L of the stop solution.

8. Shake in a plate shaker for 5 seconds to ensure mixing and read the absorbance at 450 nm using a microplate reader (Figure 4B).

9. Plot the absorbance values obtained for the calibrators against insulin concentration and construct a calibration curve. Finally, read the concentration of the samples from the calibration curve to determine the insulin concentration.

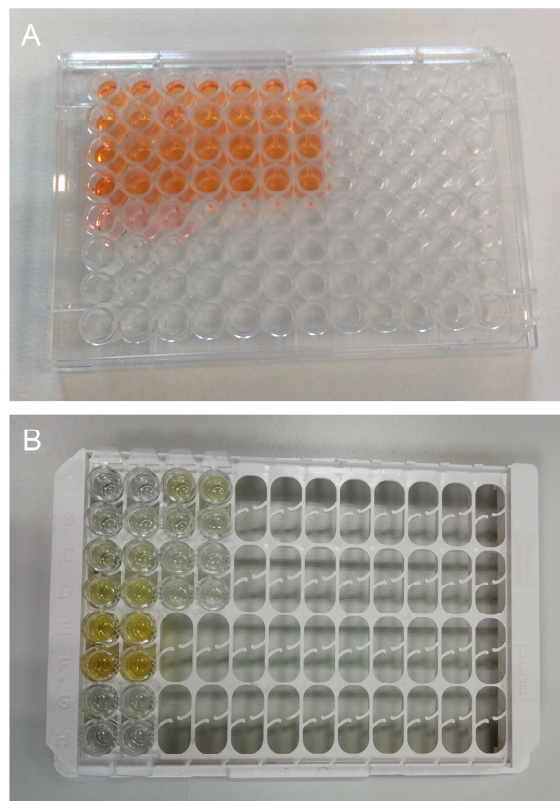


Figure 4. A) Viability quantification of encapsulated cells: 96-well plate with a CCK-8 quantification assay. B) Insulin quantification with Rat insulin ELISA kit.

4. NOTES

1. All the chemical solutions used for cell immobilization within alginate hydrogels can be prepared the day before the procedure.
2. High volumes of 1 % mannitol are easily and quickly filtered using a Stericup® vacuum system with 0.22 μ m filter.



3. CaSO_4 is not soluble and it must be shaken just before use.
4. Na_2HPO_4 requires 8-10 minutes of vortexing to get completely dissolved.
5. Alginate needs several hours stirring for getting dissolved, because of its high viscosity. Sometimes undissolved alginate gets stuck on the bottom or the walls of the beaker and needs to be detached using a spatula. Other times alginate gets agglomerated on the top of the solution, being difficult to dissolve. To facilitate agglomerates dissolution, they must be broken using a spatula.
6. It is highly recommended to prepare a higher alginate solution volume because some proportion is lost during the entire procedure. Alginate gets stuck on the handling material such as beaker, spatula, pipette, etc. and, besides, during the sterilizing filtration some alginate remain within the syringe and the $0.22\ \mu\text{m}$ filter. For example, to prepare a 3 mL hydrogel, 10 mL of alginate solution should be enough.
7. We recommend filtering the alginate solution using a 3 mL syringe connected to a $0.22\ \mu\text{m}$ syringe filter (Minisart Plus, Sigma), since syringes with higher volumes require higher strength due to the high viscosity of alginate solution. When filtering volumes higher than 10 mL, it is recommended to change the $0.22\ \mu\text{m}$ filter after filtering 15 mL before it gets obturated.
8. Calcein/ethidium staining solution for confocal microscopy must be freshly prepared, and light protected.
9. It is important to avoid generation of bubbles to avoid the collection of foam from the cell suspension.
10. Cell suspension in alginate should be completely homogeneous without presence of bubbles. Try to remove any bubble in the new solution with a micropipette.
11. When cell-alginate suspension is transferred to the 3 mL LuerLock syringes, bubbles can be generated due to the pipetting. Remove the bubbles inside the syringe by going up and down with the plunger. The presence of bubbles and the presence of cell aggregation imply the formation of a non-homogeneous hydrogel that can lead to errors in the biological assays. CaSO_4 is not soluble; shake the conical tube 10 times before taking the desired volume.
12. This step needs to be performed gently to ensure complete homogenization of the mixture.
13. We usually observe samples under a Nikon TMS confocal microscope and subsequent image analysis with NIS-elements software.
14. Include three control wells of medium alone to provide the blanks for absorbance readings.
15. Tap firmly several times against absorbent paper to remove excess of liquid and bubbles.

REFERENCES

- [1] O'Brien FJ (2011) Biomaterials & scaffolds for tissue engineering. *Materials Today* 14(3):88-95.
- [2] Chen F, Liu X (2016) Advancing biomaterials of human origin for tissue engineering. *Progress in Polymer Science* 53:86-168.
- [3] Kubinova S (2017) Extracellular matrix based biomaterials for central nervous system tissue repair: the benefits and drawbacks. *Neural Regen Res* 12(9):1430-1432.
- [4] Espona-Noguera A, Ciriza J, Cañibano-Hernández A et al (2018) Tunable injectable alginate-based hydrogel for cell therapy in Type 1 Diabetes Mellitus. *International Journal of Biological Macromolecules* 107:1261-1269.
- [5] Ahmed EM (2015) Hydrogel: Preparation, characterization, and applications: A review. *Journal of Advanced Research* 6(2):105-121.
- [6] Hoffman AS (2002) Hydrogels for biomedical applications. *Advanced Drug Delivery Reviews* 54(1):3-12.
- [7] Buwalda SJ, Vermonden T, Hennink WE (2017) Hydrogels for Therapeutic Delivery: Current Developments and Future Directions. *Biomacromolecules* 18(2):316-330.
- [8] El-Sherbiny IM, Yacoub MH (2013) Hydrogel scaffolds for tissue engineering: Progress and challenges. *Glob Cardiol Sci Pract* 2013(3):316-342.
- [9] McMurtrey RJ (2016) Analytic Models of Oxygen and Nutrient Diffusion, Metabolism Dynamics, and Architecture Optimization in Three-Dimensional Tissue Constructs with Applications and Insights in Cerebral Organoids. *Tissue Eng Part C Methods* 22(3):221-249.
- [10] Zhu J, Marchant RE (2011) Design properties of hydrogel tissue-engineering scaffolds. *Expert Rev Med Devices* 8(5):607-626.
- [11] Howard D, BATTERY LD, Shakesheff KM et al (2008) Tissue engineering: strategies, stem cells and scaffolds. *J Anat* 213(1):66-72.
- [12] O'Connor SM, Stenger DA, Shaffer KM et al (2001) Survival and neurite outgrowth of rat cortical neurons in three-dimensional agarose and collagen gel matrices. *Neurosci Lett* 304(3):189-193. S0304394001017694
- [13] Szot CS, Buchanan CF, Freeman JW et al (2011) 3D in vitro bioengineered tumors based on collagen I hydrogels. *Biomaterials* 32(31):7905-7912.
- [14] Allison DD, Grande-Allen KJ (2006) Review. Hyaluronan: a powerful tissue engineering tool. *Tissue Eng* 12(8):2131-2140.
- [15] Tsou Y, Khoneisser J, Huang P et al (2016) Hydrogel as a bioactive material to regulate stem cell fate. *Bioactive Materials* 1(1):39-55.
- [16] Andersen T, Auk-Emblem P, Dornish M (2015) 3D Cell Culture in Alginate Hydrogels. *Microarrays (Basel)* 4(2):133-161.
- [17] Lee KY, Mooney DJ (2012) Alginate: Properties and biomedical applications. *Progress in Polymer Science* 37(1):106-126.
- [18] Qi M (2014) Transplantation of Encapsulated Pancreatic Islets as a Treatment for Patients with Type 1 Diabetes Mellitus. *Adv Med* 2014:429710.
- [19] Marchioli G, van Gorp L, van Krieken PP et al (2015) Fabrication of three-dimensional bioplotting hydrogel scaffolds for islets of Langerhans transplantation. *Biofabrication* 7(2):5090/7/2/025009.
- [20] Bottino R, Trucco M (2015) Clinical implementation of islet transplantation: A current assessment. *Pediatr Diabetes* 16(6):393-401.
- [21] Dimatteo R, Darling NJ, Segura T (2018) In situ forming injectable hydrogels for drug delivery and wound repair. *Advanced Drug Delivery Reviews*.
- [22] O'Sullivan ES, Vegas A, Anderson DG et al (2011) Islets transplanted in immunoisolation devices: a review of the progress and the challenges that remain. *Endocr Rev* 32(6):827-844.
- [23] Krishnan R, Alexander M, Robles L et al (2014) Islet and stem cell encapsulation for clinical transplantation. *Rev Diabet Stud* 11(1):84-101.



